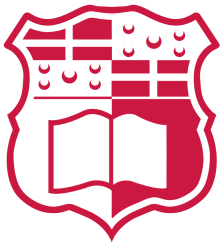

L-Università ta' Malta

A Portable In-Shoe Measurement System to Acquire Dense Continuous Foot Temperature Maps

JOSEF GRECH

Supervised by:

DR. OWEN FALZON

Co-supervised by:

DR. STEPHEN MIZZI

A dissertation submitted in partial fulfilment of the requirements

for the degree of

Master of Science in Biomedical Cybernetics

within the

Centre of Biomedical Cybernetics

December 2019

Copyright Notice

Abstract

People suffering from diabetes are at risk of developing ulcerations, which, if left untreated, could also lead to amputation. Monitoring of the foot temperature can help identify ulcerations sites before there are any visible signs on the skin. Various studies have shown that elevated temperatures in the foot may be indicative of ulceration. Over the years there have been numerous devices that were designed for foot temperature monitoring, both for clinical and home use. The technologies used vary from infrared (IR) thermometry, liquid crystal thermography (LCT), IR thermography and a vast range of analogue and digital temperature sensors that were incorporated in different measurement platforms. The aim of this thesis is to design an in-shoe portable system that utilises a high-density sensing array to record temperature data from the foot. Software was designed to visualise the recorded temperature data, representing it in format suitable to both clinical and non-clinical users. Various testing was done to validate the system performance, and eventually carried out trial walks with healthy subjects for the analysis of temperature data. The system was able to record temperatures continuously, with the analysed results in line with findings from previous studies. With the systems currently available for in-shoe temperature monitoring, the device designed in this project enable more in-depth analysis of the temperature variations of the foot within the shoe.

Acknowledgements

I would like to thank my supervisor Dr Owen Falzon and my co-supervisor Dr Stephen Mizzi, who have provided the guidance and support required to carry out the work in this thesis.

I would also like to thank my soon-to-be wife Martha for her constant support through this journey, and for pushing me when it seemed impossible to go on. I extend my gratitude to my parents, Carmen and John, my in-laws, family and friends.

Contents

List of Figures

List of Tables

Glossary

ADC	analogue-to-digital converter.
BGA	ball grid array.
BLE	Bluetooth low-energy.
BMI	body mass index.
CI	confidence interval.
DAC	digital-to-analogue converter.
DFU	diabetic foot ulceration.
DIP	dual in-line package.
FBG	fibre Bragg gratings.
GATT	Generic Attribute.
GPIO	general-purpose input/output.
I^2C	inter-integrated circuit.
IC	integrated circuit.
ICC	intraclass correlation coefficient.
IMU	inertial measurement unit.
IR	infrared.
LB	lower boundary.

LCT liquid crystal thermography.
LoA limits of agreement.

MCU microcontroller unit.
MISO master-in slave-out.
MOSI master-out slave-in.
MTH metatarsal head.

NTC negative temperature coefficient.

PCB printed circuit board.
PRT platinum resistance thermometer.
PTC positive temperature coefficient.

RF radio frequency.
RFID radio frequency identification.
RH relative humidity.
RPE rate perceived exertion.
RTD resistance temperature detector.

SCLK serial clock.
SOC System-On-Chip.
SPI serial peripheral interface.
SS slave select.

T2DM Type 2 Diabetes Mellitus.

UART universal asynchronous receiver/transmitter.
UB upper boundary.
UUID Universally Unique ID.

Chapter 1

Introduction

1.1 Definition of the Problem

Type 2 Diabetes Mellitus (T2DM) is a global concern, and its prevalence is constantly on the increase. Back in 2013, the prevalence of T2DM in Europe was approximately 8.5%, resulting in an overall healthcare expenditure of 56.3 million Euro throughout the year [1]. Malta and its population are in no way an exception; back in 1981 a cross-sectional study was conducted using a nationally representative sample and it was found that 7.7% of the population suffered from T2DM [2]. A pilot European Health Examination Survey (EHES) was conducted in 2010, which showed that the prevalence of T2DM was estimated at 9.8% [3]. In 2013, this increased once again; with the International Diabetes Federation stating that 10.1% of the population aged between 20-79 years suffers from Diabetes, placing Malta in the first quartile within the European region [1]. The mean diabetes-related expenditure was quoted at 1,535 USD per diabetic patient [1], with local excess costs estimated at 9 million Euro for hospital, primary care and specialist visits for diabetic patients when compared to non-diabetic patients (European Health Interview Survey 2008).

Diabetes can have a vast range of health impacts, including cardiovascular disease, kidney disease, peripheral arterial disease and peripheral neuropathy. The poor blood supply caused by peripheral arterial disease could lead to gangrene; the damage

and possibly death of tissue due to lack of oxygen and nutrients to the affected area [4]. With conditions such as neuropathy, tissue damage and injuries could go unnoticed due to the lack of sensation caused by damage the nerves. With neuropathy affecting up to 50% of patients [5] there is a high occurrence of ulcerations that go unnoticed, which left untreated will lead to amputation. This not only greatly affects the quality of life of the patients, but also leads to high costs of procedures, hospital stays and post-op care on the healthcare system.

Monitoring the temperature of the foot is a highly recommended method for determining the state of health of the foot [6], and its importance has been stressed in order to reduce the occurrence of diabetic foot syndrome [7]. A range of foot complications can be included in the term diabetic foot syndrome, which, as defined by the World Health Organisation (WHO), is the ulceration of the foot in association with neuropathy and varying levels of ischemia and infection [8]. Studies have shown that temperature differences greater than 2.2 °C between contralateral sites in the feet are an indication of possible ulcerations [9], with ulceration sites experiencing temperature elevations greater than 4.0°C [10]. These findings highlighted the need to start exploring more precise methods of temperature measurements to assist clinicians in diagnosing foot problems at an earlier stage. The system proposed in this study aims to provide a means of analysing the temperature of the foot during normal daily activities with minimal intrusion, to help in the prevention of occurrence/reoccurrence of foot ulcerations. In this manner, the patients will avoid the need of costly treatments and the resulting effects that the healing process has on the their daily routines. With such technologies in place, it would be more feasible to focus on preventive care, which in turn will reduce the need of tissue damage treatment and amputations. This will not only improve the patient's quality of life with regards to lower limb alterations, mobility, pain and emotional repercussions [9], [11], but also reduce healthcare costs in this sector. Between 2014 and 2015, the expenditure in England for diabetic foot care was estimated between £837.01 million and £962.38 million. With 35% of this expenditure going to impatient care for ulcerations (28%), impatient care for amputations (5%), and post-amputation care (2%); focusing on the prevention of ulcerations and further complications can greatly reduce healthcare costs [12].

1.2 Aims and Objectives

Monitoring of the foot temperature has been found to be an effective method in detecting inflammation and soft tissue injury, for both healthy patients and those suffering from diabetes [13], [14], [15]. Nowadays, thermography can be used by clinicians to capture high-density temperature data from the bare foot. However, in-shoe temperature data can also provide vital information on the temperature development during ambulation. Since IR cameras cannot be used in such applications, alternative temperature measurement methods are required.

There have been various studies that proposed or developed in-shoe temperature measurement systems [16], [17]. These vary in the type and number of sensors used, but none have aimed to measure temperatures beyond the conventional sites of interest along the sole of the foot; namely the toes, metatarsal region, lateral midfoot, arch, and heel. Temperature measurements from single points along the foot can be limiting and do not necessarily provide a comprehensive temperature assessment of the foot. Having a system able to capture high-density temperature data from within the shoe can be a vital tool is improving the level of monitoring for patients suffering from diabetes mellitus or any other condition affecting the lower limb perfusion.

1.3 Contributions

In this study, an in-depth review of the technologies used for foot temperature monitoring was carried out. Various system designs have been used by researchers exclusively as research tools [18], [19], [20], whereas others have been made commercially available to be bought as clinical tools and consumer products [7], [21], [22]. These systems were analysed from a a design perspective, taking a comprehensive look at the technologies used in determining the temperatures of the foot and how well these perform. By taking into consideration their strengths and shortcomings, the system built in this project has a more robust design and aims to be

innovative when looking at the gaps in the present technology.

The objective of this project was to design and develop a portable system using a high-density temperature sensing array for the continuous measurement of temperature data of the foot from within the shoe. The system enables long-term foot temperature monitoring and recording during the user's daily activities. The system also includes software for the analysis of the recorded data, assisting the patients in preventing damage to their feet and providing the clinicians with the necessary information to adapt the treatment plan required for a particular patient.

The system and its components were tested in various testing arrangements, ensuring that the performance of the system as a whole provided the required level of temperature monitoring. The chosen temperature sensors were tested using calibrated equipment within static test setups, certifying their operation and providing a means of sensor calibration. Furthermore, the complete system was also tested in dynamic conditions, making sure that the sensors within the shoe environment during ambulation still performed correctly and the circuitry was able to process the sensor data throughout. Once the system design was finalised, ironing out any issues noted during testing, a series of walk trials with 10 healthy subjects was conducted. Other than extensively testing the robustness of the system in real-life conditions, the collected data was used to evaluate the performance of the system. The collected data was compared to temperature measurements using thermal imagery where possible, but also compared to previous studies that have also investigated the in-shoe foot temperatures during walking.

1.4 Structure of the Thesis

There are a total of six chapters, with Chapter 1 having introduced the impact of diabetes on the health status of the foot, and analysed the benefits of monitoring the temperature of the foot. Moreover, it outlined the objectives of the project and gave a brief overview of the work presented throughout the work.

Chapter 2 presents a review of the literature found in conjunction with foot temperature measurement systems. The variety of systems present multiple approaches in monitoring of the foot temperatures, and the technologies used are examined in detail to determine the best design method for the system being designed.

Chapter 3 outlines the design process undertaken in this project, including sensor selection, sensory platform designs, circuit design as well as the software development that was done.

Chapter 4 outlines the testing carried out on the system throughout the design process. This includes the testing done on the sensors, the sensory platforms as well as the system as a whole. The results at every stage are also presented in this chapter.

Chapter 5 includes the discussion of the testing and the obtained results presented in the previous section. It also outlines the limitations that were observed when testing the designed system.

Chapter 6 summarises the work done in this study and reviews the possible improvements in the system and any further development on both the hardware and the software.

Chapter 2

Literature Review

2.1 Introduction

Foot and in-shoe temperature analysis have been used in various studies with aims ranging from testing the thermal comfort within shoes [23], [24] to testing the quality of insoles within fire-fighter boots [25], not to mention the various systems designed for diabetic foot care. Monitoring of skin foot temperature is a highly recommended method for determining the state of health of the foot [6], and its importance has been stressed in order to reduce the occurrence of ulceration in individuals with diabetic foot syndrome [7]. Clinically, manual palpation is used to check for temperature variations in the feet; however these are generally too subtle to be determined reliably using this approach [26]. Since temperature differences greater than 2.2°C between contralateral sites in the feet are an indication of possible ulcerations [9], more precise methods of temperature measurements are required to assist clinicians in diagnosing foot problems at an earlier stage.

Ever since the 1970s, there have been indications that IR thermography was found to be useful in the management of limbs suffering from insensitivity problems [27]. This imaging modality provides the clinician with a dense temperature map of the foot, which helps pinpoint any areas with elevated temperatures that could be at risk of complications [28], [29], [30]. Thermal imaging is very advantageous

since it is unaffected by the level of light within the room, requires no direct contact to the surface being analysed, and the data is obtained in real time for viewing and processing [31]. One study [31] utilised IR thermography to analyse the thermodynamics in sports footwear by recording images of the shod feet post-workout. It was found that the greatest temperature increase is towards the front end of the shoe, in the toe area, but varying material thicknesses within the shoe could have influenced the results. Heat generated in other areas of the foot which were covered by thicker materials may have not been captured by the IR thermal camera. Thermal imaging has also been used to detect diabetic foot problems; linking plantar foot temperatures to diabetic polyneuropathy while attempting to prevent the occurrence and recurrence of ulcerations [32], [33]. One major disadvantage in using this method is that only static readings of the feet can be recorded. Therefore, since no temperature data can be collected from the foot in motion, one cannot analyse the temperature fluctuations in the foot during ambulation. In such cases, an in-shoe temperature monitoring system surpasses any thermal camera since temperature readings are taken directly from the skin surface.

Even though IR thermal cameras can achieve high resolution and dense temperature measurements of a surface, it is not ideal for home monitoring of neuropathic patients. Unassisted, it could prove difficult to capture images of one's own feet using a thermal camera. Hence, there have been various studies and innovations over the years with the aim of facilitating self-monitoring of diabetic patients. These are discussed in depth in Section 2.2, where both static and dynamic measuring systems are reviewed, comparing the different technologies used and how well each one performs. Since the aim of this study was to design an in-shoe temperature monitoring system, special attention was given to the sensors used, which will be reviewed in Section 3.2.1 along with other sensing technologies.

2.2 Current Systems and Studies

A variety of devices, ranging from IR thermometers to sensory socks and insoles, have been designed in order to measure foot temperatures. Some of these are able to measure temperatures of the foot at rest, whereas others can be used to analyse the foot temperatures during ambulation. There have been various studies that used such systems, analysing foot temperatures in different experimental setups.

2.2.1 Static Measurement Systems

Static measurement systems are designed with the purpose of measuring single temperature readings from the foot while at rest. Both the structure and sensory technology used hinders the use of these systems inside the shoe during ambulatory activities.

For example a digital infrared thermometer utilises a lens to focus the radiated heat from objects onto a detector, as shown in Figure 2.1(a). This detector, or thermopile, translates the infrared radiation into electrical signals that can then be converted into a quantifiable temperature reading. Such a system is bulky and cannot be fitted underneath the foot sole and within the shoe, which is why it can only be used to measure the temperature of the foot while at rest. One such device is the Xilas Medical (San Antonio, Texas, USA) TempTouch® Dermal Thermometer shown in Figure 2.1(b), a digital infrared thermometer that could be used as a self-monitoring tool by diabetic patients . The accuracy of infrared thermometers is determined by their distance-to-spot ratio, which determines the maximum measure distance depending on the target size to be measured [34]. Thus, the structure of the TempTouch® ensures that readings are always taken at the same distance so as to measure a constant target area. Other than that, the dimensions of the TempTouch® allows for easy self-assessment even by patients who may have difficulty reaching their feet.

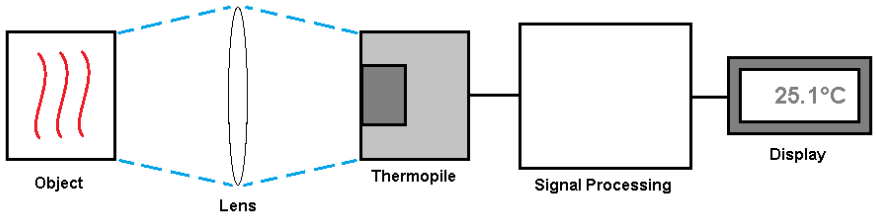

(a) The principle of operation of an IR thermometer

(b) TempTouch® Dermal Thermometer (adapted from [35])

Figure 2.1: (a) Image illustrating the principle of operation of an IR thermometer. (b) The TempTouch® Dermal Thermometer by Xilas Medical.

The TempTouch® was used in two separate studies [7], [14] as a tool to measure foot temperatures, included in the therapy assigned to parts of the study groups. In one study [7] conducted over a period of 15 months, 173 subjects with a history of diabetic foot ulceration (DFU) were split into three groups: a group that underwent only standard therapy, a group that underwent structured foot examinations and a group that underwent enhanced therapy. All subjects were given therapeutic footwear, basic diabetic foot education and provided with regular foot care. In addition to this, the structured foot examination group was instructed to carry out visual foot examinations each day and note any redness, discolouration or swelling. Moreover, the enhanced therapy group was provided with a dermal thermometer to record the temperatures of six specific sites on the foot: the big toe, the first, third and fifth metatarsal heads, the mid-foot and the heel. In the event of temperature differences greater than 2.2°C between contralateral sites on the feet for two consecutive days, the patients were asked to reach out to the study nurse and reduce their physical activity until the temperatures normalised. Similarly, all the study groups were asked to contact the study nurse in the event of any visible foot abnormalities to take the required actions. Results showed that the enhanced therapy

group only had an 8.9% occurrence of foot ulcers, almost 3.5 times less than both the standard therapy (29.3%) and the structured foot examination (30.4%) groups.

Similarly, in the other study [14], 225 subjects at high risk of DFU were recruited in an 18 month long study. The subjects were divided into two groups, each provided with the same elements (therapeutic footwear, diabetic foot education and regular foot care) and all asked to assess their feet daily. One of the groups was asked to use a dermal thermometer to measure the temperature twice daily at six specific sites on the sole of the foot. The subjects were also asked to report any temperature differences greater than 2.2°C between corresponding sites on their feet to the study nurse. The study yielded similar results, with the occurrence of ulcers being 3 times less in subjects in the dermal thermometry group than those within the standard therapy group.

Even though the results obtained from these studies were promising, a dermal thermometer cannot be used to obtain a temperature map of the entire sole of the foot. In both these studies, only 6 points were being analysed either once or twice daily. If the density of monitored points and the frequency of readings were to be increased, the additional information from such a system could help reduce the rate of recurring ulcers further and potentially detect them earlier on. Moreover, the 2.2°C difference in temperature between contra-lateral foot sites is an indication of the required resolution of temperature sensors to be used to be able to sense these temperature fluctuations.

Liquid crystal thermography is one alternative technology that can be used to obtain a dense picture of foot temperatures. One commercially available system is the SpectraSole (Linköping, Sweden) Pro 1000, designed for the acquisition of thermographic images of the feet. This device consists of two rectangular plates of liquid crystal layers, with each layer sensitive to different temperatures and changing colour accordingly as shown in Figure 2.2. Upon placing the feet for one minute on the plates (with the patient either in the standing or sitting position), a thermographic image of the temperature distribution of the sole of the feet is obtained. The image can then be stored digitally using a camera or have the clinician/home-user manually

document any temperature abnormalities on a foot diagram before the image fades away.

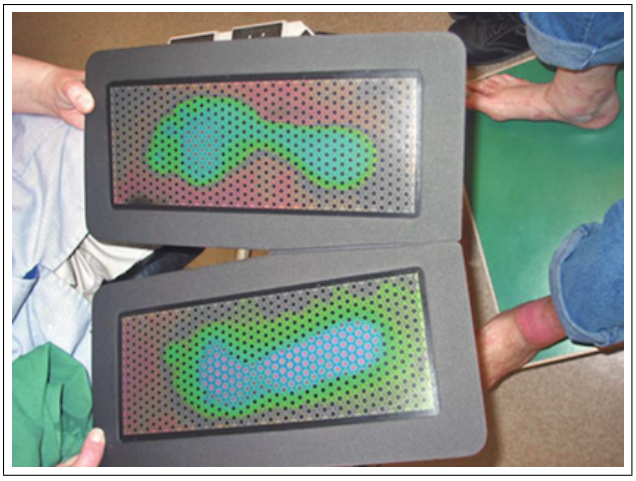

Figure 2.2: SpectraSole Pro 1000 (adapted from [36])

A study was conducted in Sweden using the SpectraSole Pro 1000 [36], where 65 patients who came in for scheduled or self-imposed visits were also examined using this foot detector on top of the standard examination. A total of 65 test subjects diagnosed with diabetes were recruited, aged between 22 and 93 years. The standard examinations were conducted according to Swedish guidelines that outline the frequency of inspection depending on the severity of the foot condition and the signs to look out for, such as deformities, inflammation and wounds. All the data from these examinations were noted down in a study protocol containing also a foot diagram on which problematic areas were highlighted. Then, using the SpectraSole Pro 1000, the clinicians investigated whether the same areas were tagged as precarious and as a result, required any alterations in treatment or self-care guidelines. From the 65 patients, temperature differences between the two feet were found in 31 cases, six of which were not detected without the use of the foot indicator. These six patients, from which five were categorised as requiring primary care and one needing specialised care, were given prescriptions and self-care advice with the required amendments. Upon their respective follow-up examinations, these patients showed no or minor changes in temperature between their two feet. During this study, the temperature differences between the two feet were classified in three different levels of severity (no temperature values were given in relation to these differences):

1. a mild temperature difference, based on visual assessment of the plates
2. a temperature difference requiring follow-up, based on visual assessment of the plates
3. a temperature difference requiring follow-up, based on a temperature difference greater than 1.5°C when measured with an infra-red thermometer

The images obtained by the SpectraSole were compared to a template so as to be able to interpret them, getting a rough idea of the temperatures recorded throughout the foot. One major setback of this system is that the readings are highly subjective since they are based on the personal interpretation of the shades of colour and do not give a precise temperature value. Thus, it is still required to have a measuring device that outputs a precise temperature reading to be able to fully assess the status of the foot.

In fact, in similar research [37] using a different LCT system, the clinician also used a dermal thermometer to assess the study participants. The TempStat™ (Visual Footcare Technologies, LLC, South Salem, New York) LCT system that was used in this study had a similar build structure to the SpectraSole Pro 1000, consisting of two polycarbonate plastic plates made of liquid crystalline cholesteric esters that change colour according to the skin surface temperature. The only difference in the TempStat™ is that rather than having two separate plates, they are built into a single unit similar to a bathroom weighing scales as shown in Figure 2.3, with a convex mirror in between the two plates to be able to analyse the sole of the foot through the reflection when conducting home self-examinations.

In this study [37], the subjects were asked to perform visual self-examinations with and without the TempStat™ . This was done in conjunction with clinical examinations performed by a podiatrist, using also an infrared thermometer to measure the temperature at specific points of interest along the sole of the foot. This was done so as to assess the abilities of the TempStat™ in locating heightened temperature points while at the same time validating its ease of use for

Figure 2.3: TempStat™ - Visual Footcare Technologies (adapted from [37])

self-examination of one's foot. In total, 45 subjects took part in this study, ranging from healthy patients to ones suffering from Type 2 diabetes.

In the case of one of the subjects who was suffering from a chronic ulcer in his right foot, the left foot temperature was in the 25-28°C region whereas the right foot was close to 29°C, with a 31.7°C temperature recorded at the ulcer site. The TempStat™ represented the left foot status as a green/blue footprint, whereas the right foot was a darker shade of blue with a red spot at the ulceration site as as shown in Figure 2.4(a). Another subject, one who was not suffering from any ulceration, had the temperatures of both his feet in the 30°C region with a 33.3°C temperature recorded at the heels. On analysing the foot with the Tempstat™ it generated a generally blue coloured footprint with a red tint at the heel as shown Figure 2.4(b). In both these cases, the actual temperatures of the feet were clearly represented by the different hues in the foot pattern and it was shown that it is easy for the subjects themselves to make basic conclusions about their foot status.

(a) Thermal image of subject with ulceration

(b) Thermal image of subject with healthy feet

Figure 2.4: TempStat™ Results - Subject with ulceration under right first metatarsal head, circled in red (a) and subject with healthy feet (b) (adapted from [37]).

Another device in a weighing scales form factor was the ThermoScale® (Manichand Healthcare, Taiwan) depicted in Figure 2.5. The innovation in this product is its capacity to measure and track a person's weight, body mass index (BMI), as well as the variance in temperature of the foot soles. It is capable of having 4 different user profiles where each can store up to 14 previous readings. In this way, the user can monitor his/her foot status by checking for any temperature differences between their feet over a period of time. This device uses an array of temperature sensing points under each foot sole to obtain the foot temperatures, from which it can then point out any variances that might need to be referred to the clinician. While literature regarding this device is limited, from the documentation available it seems that the unit uses multiple sensing points, going beyond the six sensors at the particular points of interest that were monitored in previous studies [7], [14]. This is a significant step forward in obtaining more dense temperature readings while reducing the amount of unmonitored areas of the foot. Nevertheless, it is unclear whether the unit compares contralateral points on both feet and flags any major temperature differences or if foot status is determined from the average foot temperature.

Figure 2.5: ThermoScale® (Manichand Healthcare, Taiwan) (adapted from [38]).

A similar device also using temperature sensors was the Remote Temperature Monitoring System Podimetrics Mat (Podimetrics, Inc., Somerville, MA) shown in Figure 2.6(a). This mat measures approximately 30 cm by 43 cm, and contains an array of 2,000 thermistors. The thermistors provided an accuracy of ± 0.6 °C and a precision of 0.1°C for the range of temperatures between 15 and 40 °C. The device was designed as a home-monitoring tool, enabling patients to assess the

temperatures of their feet and highlight any asymmetries in their thermal distribution. The device automatically switches on when a person steps onto it, and requires him/her to remain stationary for approximately 20 seconds to finish the scan. The data is then wirelessly transmitted back to the manufacturer for the analysis and processing of the data, sending back a report with the generated thermograms as shown in Figure 2.6(b).

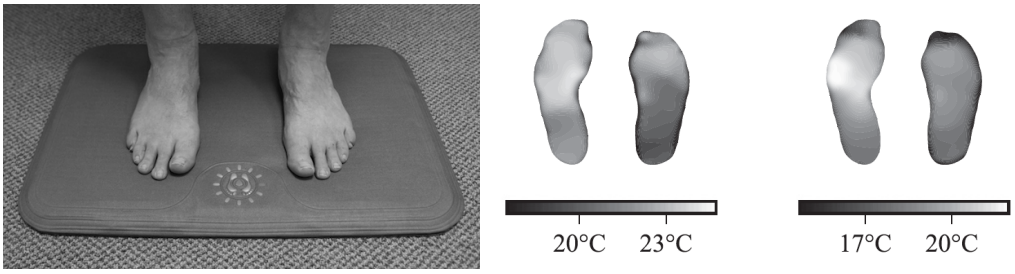

Figure 2.6: Remote Temperature Monitoring System Podimetrics Mat: (a) The sensory mat on which the user stands to get his/her foot temperatures measured; (b) Foot temperature maps extracted from the data collected by the system [39].

This device was used in a study with 132 subjects suffering from diabetes mellitus. Each of these participants were given a Podimetrics Mat to carry out daily scans of their feet for a period of two months. They were instructed to carry out daily foot inspections and asked to visit their physician in the event that they notice any new lesions in their feet. When analysing the collected data, and using a 2.22 °C asymmetry threshold, the system was found to detect 97% of non-traumatic ulcerations approximately five weeks before any visible signs. These results continued to prove the importance of daily temperature analysis of the feet in order to detect and prevent ulcer formation.

The static measurement systems reviewed in this section all possess their respective strengths and limitations which are to be considered in the design of the system being built. The liquid crystal thermography systems showed the importance of a dense temperature map in order to get the full picture of the temperature status of the foot, but they lacked the capacity to save information/readings. Other than that, assessments of the thermographic images obtained by such systems are too subjective

and may vary from one person to another due to distinct colour interpretation. Thus, systems based on temperature sensors are deemed more precise since they output quantifiable results from digital or analogue sensors. Even though dermal thermometry uses such sensors, there are various drawbacks to these systems. Firstly, the measurements need to be taken directly from the foot sole while the foot is at rest and it would be time consuming to get the separate readings required for a dense temperature map. The Thermoscale™ and Podimetrics Mat systems solve this problem by increasing the number of sensing points to monitor as much of the plantar area as possible. It is thus the aim of the system developed here to have numerous sensors forming a dense sensing array to monitor the temperature fluctuations across the foot sole. In addition to increasing the sensor count, the frequency of readings is to be incremented as well. When using a static measurement system, it is only capturing a momentary snapshot of the foot temperatures and more frequent readings are required in order to properly diagnose the foot. Dynamic measurement systems aim to do just that, to provide continuous temperature readings while the foot is in motion.

2.2.2 Dynamic Measurement Systems

The development of in-shoe systems not only gave researchers the possibility to investigate health related issues, but also delved into other parameters such as shoe comfort and performance, as well as effectiveness of specialized shoes such as those worn by athletes and fire-fighting boots. This could only be done with the collection of data from within the shoe while a person is in motion. Various systems were analysed in this section, some measuring solely temperature [18], [25], [40], [41] while others measured a vast range of parameters including humidity, pressure, bio-impedance and acceleration [16], [18], [19], [20], [24], [42], [43].

2.2.2.1 Single-Sensor Temperature Measuring Systems

One of the first in-shoe temperature measuring systems to be designed used a thermocouple-based temperature logger, the TC4000 (MadgeTech, New Hampshire, USA) illustrated in Figure 2.7, combined with a T-type thermocouple for skin temperature monitoring. This unit was an off-the-shelf product designed for temperature monitoring for various applications. This system was used in a study [40] with the aim of analysing the differences in foot temperature fluctuations between healthy individuals and ones suffering from polyneuropathy.

Figure 2.7: The MadgeTech TC4000 Thermocouple Recorder (adapted from [44]).

The temperature logger's internal temperature sensor was used to monitor the ambient temperature of the subject whereas the thermocouple was used to record their foot temperature from within the shoe. The internal channel had a resolution of 0.1°C with a precision of 0.5°C, able to read temperatures between -40°C to 80°C. The

T-type thermocouple used also had a 0.1°C resolution with a 0.5°C precision, but could read a much wider range of temperatures; from -200°C to 1190°C. Using the ERTCO Data Recording Software (Eveready Thermometer Company, New Jersey, USA), the unit's frequency and time of recording could be set accordingly. The frequency could range anywhere between 30 recordings per minute to 2 recordings per day, able to save up to 16,383 internal and 16,383 external records; but this was set to 1 recording per minute, with a typical recording duration of 24-36 hours.

The TC4000 came in two different configurations; either with a permanently attached thermocouple of relatively short length or with an adapter to which one can attach his/her own choice of thermocouple. Both modalities were used in the study, attaching the recorder to the participant's calf when using the short thermocouple, or attaching it to their belt and using a longer thermocouple plugged into the adapter. The thermocouple itself was affixed to the dorsal area of the foot or in the webspace between the 1st and 2nd toes. Nevertheless, there were issues with the thermocouples in both cases, with damage caused by excess strain within the shoes as well as moisture caused by perspiration.

A total of 21 subjects signed up for this study [40], with 16 of them suffering from polyneuropathy as a result of diabetes mellitus (7), celiac disease (1), autoimmune demyelinating disease (1), axonal polyneuropathy (1) and idiopathy (2). During data collection, some technical difficulties were encountered which resulted in one normal subject and four polyneuropathy patients being unable to complete the entire recording period. The main cause for this disruption was the failure of the circuit due to damage incurred to the thermocouple. The authors assumed that the excessive strain due to torsion or pressure, and possibly sweat from the skin interfering with the connection between the 2 metals in the thermocouple, all contributed to the failure of the system. Even though more robust sensors seem to be required for such an application, it must be made sure that the system does not cause skin irritation or even worse, ulceration, in the process of trying to prevent these to begin with.

Following this first attempt in capturing temperature data from within the

shoe, many variations of the same principle system were developed. In one study [41], a system was developed to measure the skin temperature of the foot using also a single sensor. It was built in collaboration with the Centre of Biomedical Technology (Danube University, Krems, Austria) and Digilog Inc. (Perg, Austria). The system was made up of a base station connected to a computer to which the ultra-low-power microcontroller (MSP430F149, Texas Instruments Inc, USA) sent the temperature data. The microcontroller, which was encapsulated in a two-component epoxy resin, also contained the temperature sensor. The voltage drop measured across a silicone diode within the microcontroller was used to evaluate the change in temperature of the surface in contact with it. The voltage-temperature relationship of the sensor was found to be linear when measuring the temperatures of a water bath. The microcontroller could store up to 57,000 readings and was able to run on battery for 2-3 years. The sensor activation frequency could be programmed according to the study's requirements. In this case, the frequency was set at an interval of 5 minutes for healthy subjects and 1 minute for subjects with problematic feet. The temperature readings were then downloaded to the computer via the wireless radio frequency identification (RFID) interface incorporated in the system.

Temperatures were recorded for two healthy male subjects aged 45 and 46 years. Both feet were being monitored, with the sensors placed on the dorsal area of the foot as illustrated in Figure 2.8. In that position, the sensors were outside of the shoes and only covered up with socks. This, in turn, resulted in temperature fluctuations due to the varying ambient temperatures during the winter period, with outside temperatures ranging between -12°C and 10°C and room temperatures between 22°C and 25°C. During this study the ambient temperature was not recorded and thus no indication was given of its effect on the range of skin temperatures recorded (28-36°C). Even though Kang et al. [40] proved that the temperature of the foot in a healthy adult is independent of the ambient temperature, that study was done with warmer ambient temperatures ranging from 12-34°C. From the results collected, it was found that there were minor temperature changes between the two feet, with a maximal mean value of 1.4 ± 0.93°C recorded between 02:00 and 03:00 during the night. As suggested in the study, given the time of recording, there is a high probability that this difference in temperature occurred due to one foot not being

covered by the blanket during sleep. Even though this system included wireless communication and the capability of recording for long periods of time, without incurring any skin irritations from the epoxy resin, it gave no indication of the temperatures of the foot sole from within the shoe during physical activity and thus only gave a vague idea of the health status of the foot.

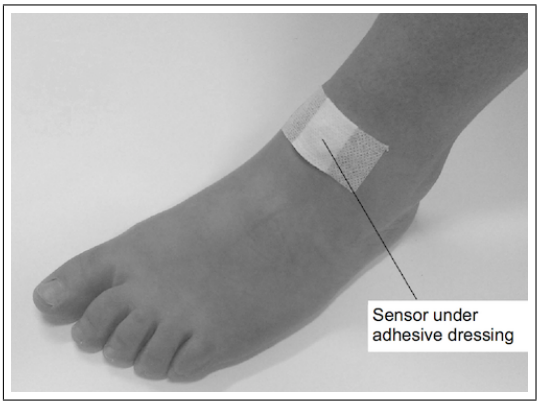

Figure 2.8: Sensor placement on a subject's foot in Foltynsky et al.'s study (adapted from [41]).

Similarly, another study [45] used the iButton® technology (Maxim Integrated, Inc., California, USA) which is also a small microcontroller device, capable of storing temperature readings of surfaces in contact with it. Unlike the previous study, not only was the foot temperature sensor placed within the shoe, but a separate sensor was used to monitor the ambient temperature. The in-shoe sensor (DS1921H-F5#) had a range of +15°C to +46°C with a resolution of 0.125°C and accuracy of 1.0°C whereas the ambient sensor (DS1921G-F5#) had a wider range from -40°C to +85°C with a precision rating of 1.0°C from -30°C to +70°C. The in-shoe sensor was placed on the dorsal area of the foot, in the webspace just before the first and second toes, whereas the ambient temperature sensor was to be affixed to the top layer of the subject's clothing using the key ring as shown in Figure 2.9. In addition to the temperature sensors, an actigraphy monitor (Actiwatch 16, Mini Mitter Company Inc., Oregon, USA) was placed around the ankle of the test subjects (Figure 2.9) to be able to record the motion of the foot. The target recording period for every subject was 48 hours, with temperature readings set at a period of 2 minutes and the activity monitor set to record short periods of 15 seconds each (the frequency of these readings was not specified). The subjects were also asked to keep an activity journal

so that it would be easier to link any changes in temperature and actigraphy readings with the respective activity during that period; e.g. sitting at a desk, walking, sleeping, etc. This was also used to note down the times when the subjects showered and removed the sensors, so as to crop out that period of recording from the saved readings.

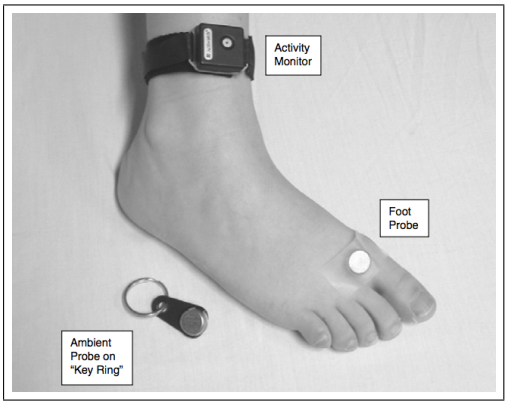

Figure 2.9: Placement of two iButton® probes and activity monitor (adapted from [45]).

In this study [45] there was a total of 20 subjects, with 13 women and 7 men, all of whom suffered from diabetes but only 4 of the total 20 had clinical polyneuropathy. Their ages varied from 22.4 to 66.6 years, with a mean age of 47.4 years. They were given identical socks and asked to wear non-insulated footwear throughout the study. During the recording period, none of the patients reported any injurious reactions to having the sensors directly attached to their feet and none of them needed to remove the sensor due to discomfort. Upon analysing the results, the mean foot temperature recorded from all 20 subjects was 31.6°C, with temperatures ranging from 27.5°C to 33.8°C. These results were consistent with Kang et al.'s study [40] where the mean foot temperature was found to be 32.1°C, ranging from 29.0°C to 33.8°C. The fluctuations in foot temperature were as expected when considering the changes in ambient temperature between indoor and outdoor activities, and temperatures were relatively steady during the sleeping period. With regards to the ambient temperature, in 15 of the subjects these corresponded well to the activities logged in the journal, but 2 of the remaining varied inconsistently whilst the rest didn't seem to vary at all between indoors and outdoors. It is worth noting that in studies that are conducted outside the clinic and dependent on the subjects' input,

such errors cannot be justified confidently as they could be due to equipment malfunction or erroneous logging by the subject or both.

Having only a single sensor, these systems could only give a general indication of the temperature conditions within the shoe based on the temperature of the dorsal area of the foot. Even though this was a step forward from the static measurements systems that required the foot to be outside of the shoe, still no information was being gathered from the sole of the foot. With an increase in the number of sensors, a system could monitor multiple points of interest from the sole of the foot and give a more complete idea of the status of the foot.

2.2.2.2 Direct Contact Multiple-Sensor Systems

Shimazaki et al. aimed to investigate the effects of gait on the thermal environment within the shoe [42] by using a number of sensors to measure a varied range of variables. These included plantar pressure, foot motion, foot temperature, ambient weather conditions, metabolism through breath analysis, and body weight. J-type thermocouples were used to monitor the temperatures at the big toe, small toe, arch, heel, medial malleolus, lateral malleolus and instep; as shown in Figure 2.10 but no further information was given on the data-logging system used. The Tekscan F-Scan (Tekscan Inc., Massachusetts, USA) was used to analyse the in-shoe plantar pressures and the ZMP IMU-Z2 (ZMP Inc., Tokyo, Japan) inertial measurement unit (IMU) was used to track the foot's motion. The aim of this study was to analyse the pressures exerted on the sole of the foot and the resultant temperatures in response to changes in gait speed, specifically at 3.0, 6.0, 9.0 and 12.0 km/hr.

In total, 17 healthy males aged 19 to 23 years were chosen for this study, with a mean age of 21.1 years, mean height of 170.3 cm and a mean body weight of 60.1 kg. The subjects were fitted with the sensors 15 minutes prior to the testing period so as to give them time to acclimatise to the ambient conditions. After 10 minutes of rest, the subject performed 30 minutes of walking/running at one of the aforementioned gait speeds followed by a final 10 minutes of rest. In trying to verify

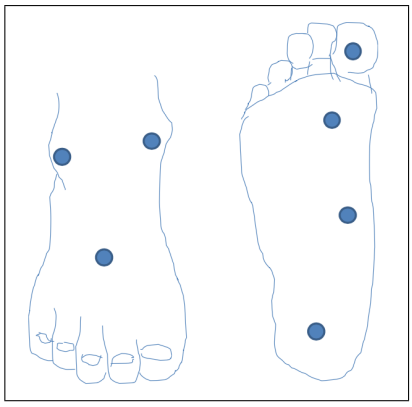

Figure 2.10: Temperature measurement points on the foot in Shimazaki et al.'s stidy (adapted from [42]).

the relationship between pressures exerted on the foot sole and temperature elevations in the monitored sites, it was vital to analyse the pressure variations during the gait cycle. From the data collected by the F-Scan, it was distinguishable that both contact force and contact area increased from the point of heel-strike up to the point where the whole foot is in contact with the ground, reaching a maximum. Beyond that, both the contact force and area start to decrease up to the point of toe-off, where they then become zero. When considering varying gait speeds, faster walking led to greater landing velocities and contact forces but the contact area grew only slightly. Also, with greater walking speeds the stance time became shorter thus decreasing the gait-motion cycle and resulting in more frequent foot-ground contact. All these factors had an adverse effect on the sole of the foot, with temperatures rising further, especially in the big toe and heel regions. This is because these 2 areas sustain the greatest contact forces at different stages throughout the gait cycle. At the point of initial contact of the foot with the ground, all the body weight is supported by the heel and thus a strong contact force is noted [46]. Similarly, during the final stage of the stance, the body weight is supported by a small area of the forefoot (mainly the big toe) which thus endures a significant contact force [47].

Similarly, another system [20] was designed measuring temperature, humidity, applied force, acceleration, rotation rate, galvanic skin response and skin inflammation using a capacitively coupled bioimpedance sensor. The array of sensors was attached directly to the foot as seen in Figure 2.11. Data from the foot sensors was transferred via Bluetooth to the main processing unit, which in turn was also

monitoring the ambient temperature and humidity levels. The Raspberry Pi 2 was chosen as the control unit because it is a low cost system with great software and hardware capabilities. Not only does it have multiple USB ports and a LAN connection, but its native operating system (Rasbian OS) supports python scripts and a very stable and lightweight platform for data acquisition and processing. The skin temperature sensors of choice were the ATC-Semitec (Northwich, UK) negative temperature coefficient (NTC) flexible thermistors 104JT-25. These were placed under the big toe, 1st metatarsal head and the calcaneus, coupled with force sensors. The temperature transducers used were calibrated using a PID controlled oven, setting the temperatures at approximately 22, 24, 28, 33 and 37°C. The gathered data from all the sensors was sampled at 20Hz by an Arduino Nano processor, which was then transmitted via Bluetooth to the Raspberry Pi for processing. With a 3.7V 900 mAh battery, the system was operational for approximately 2.5 hours. If low power electronic components were used in the circuit design, the operational time would have been increased. Even though no information on the temperature measurements was outlined in the study, various factors from the system design are worth noting, in particular the temperature transducers used which are both inexpensive and physically ideal for the project in this project.

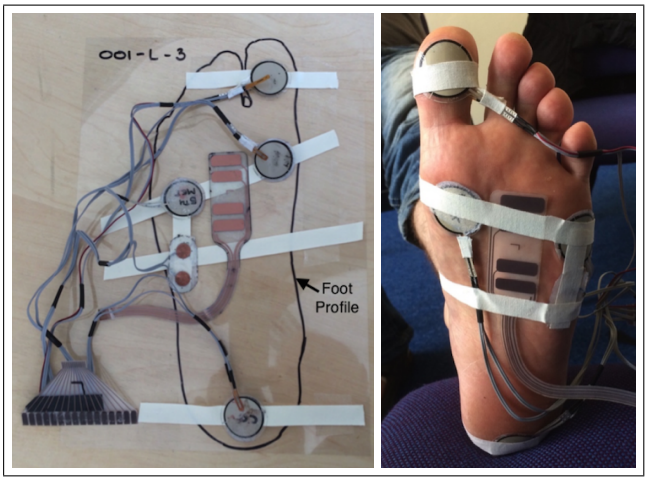

Figure 2.11: The system sensors and their location on the foot in Coates et al.'s study (adapated from [20]).

Focusing solely on temperature and relative humidity (RH), Mizzi [43] set up a system consisting of thermistors and humidity sensors to analyse the effect of

climate on micro-climate within the shoe during moderate exercise. The temperature transducers used were the Biopac® TSD202A (Biopac Systems Inc., California, USA) which were small sensors with a fast response time, ideal for in-shoe temperature measurements. The maximum operating temperature for these thermistors was 60 °C, with a precision of 0.2 °C and a response time of 0.6 seconds. The Honeywell HIH 4000 series (Honeywell International Inc., Minnesota, USA) were used to monitor the RH within the shoe. The thermistor and the RH sensor were coupled together as shown in Figure 2.12, with a total of two pairs used, located below the navicular and between the hallux and second digit.

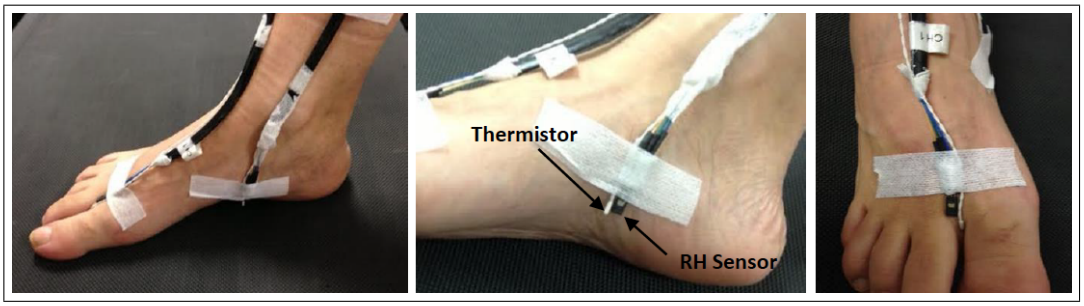

Figure 2.12: Sensor placement in Mizzi's study (adapted from [43]).

The sensors were connected to a PC via a Biopac® MP150A-CE system using SKT100C and HLT100C amplifiers for a direct connection to the temperature and RH sensors. The data was recorded by the Biopac® Acq*Knowledge* software at a sampling rate of 1kHz, which was then smoothened and down-sampled to one reading per minute. The sensors' accuracies were validated by comparing their readings against calibrated gold-standard equipment, where in the case of the temperature sensors, a calibrated platinum resistance thermometer (PRT) was used. A humidity chamber (Thunder Scientific 2500 Benchtop) was utilised to set the humidity and temperature levels at which the sensors would be tested. Readings were taken at a fixed RH of 50% and the temperature varied through 20 °C, 30 °C, 40 °C and 50 °C, getting four hours' worth of readings at every temperature. The adjustments done to the sensors were then validated at varying RH levels (50%, 65%, 80% and 95%) at 30 °C. With both types of sensors calibrated, two separate studies were done on healthy adults and patients suffering from diabetes mellitus, noting the differences in-shoe microclimate between summer and winter.

From the 14 healthy adults, there were 5 males and 9 females, with an average age of 49 years, a mean weight of 75kg and a mean height of 165.7cm. From the six patients suffering from diabetes mellitus, four were male and two were female, with an average age of 69 years, a mean weight of 75.4kg and a mean height of 166.1cm. The sensors were attached to the patients' feet by using medical adhesive tape (Mefix® self-adhesive fabric tape), making sure that no damage is incurred to the skin especially in the case of the diabetic patients. The trials were conducted indoors using a treadmill, with the walking speed selected by the subject so as to have all patients exerting the same level of physical activity. The level of physical exertion was measured using the Borg rate perceived exertion (RPE) scale [48], enabling each of the participants to determine the speed that is equivalent to low level exercise. In the cases where the indoor ambient temperature and RH were required to reflect those of the outdoors, the windows and doors were left open for the room to stabilise to atmospheric conditions. In this study, a portable system would have been beneficial in performing the trials outdoors in actual atmospheric conditions. Also, in this study no data was recorded from the sole of the foot, which could have given an indication of the effect of the microclimate within the shoe on the person's foot plantar area. This study gave indications that foot temperatures are higher in the summer period than in winter, for both the healthy and diabetic participants, whereas RH is unaffected by seasonal changes. Also, in accordance with previous studies, it was observed that the foot temperatures of the diabetic subjects were lower than those of the healthy participants, with this discrepancy being higher in the warmer season.

Another system using only temperature sensors was built to analyse the performance of different insole materials for fire-fighter boots [25]. Even though this system cannot be used to measure the temperature characteristics of the human foot, it uses the same principle concepts of these temperature monitoring systems. The LM35 (Texas Instruments Inc, USA) sensors, which provide an accuracy of 0.5 °C between -55 °C and 150 °C, were mounted between the bone structures of a 3D printed foot model. The printed foot was then surrounded by translucent polydimethylsiloxane to mimic the muscles and tissues, creating a temperature sensing foot model as shown in Figure 2.13. The ATMega328 was used as an interface between the sensors and the laptop running the controlling software developed for the system, capturing readings

every second from all three sensors. An additional sensor was used to monitor the temperature of the outsole, with an ambient thermometer monitoring the temperature of the surrounding environment. The boot was then placed on a controlled heating surface to analyse the temperature elevations experienced by the sensing foot when using different insoles.

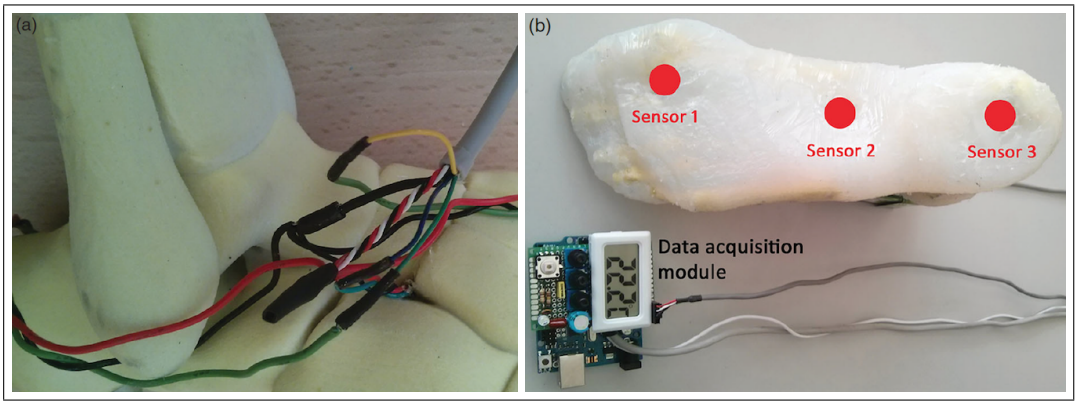

Figure 2.13: Sensor placement of data acquisition system

There are various advantages to having a system with loose sensors that are placed directly onto the patient's foot. Firstly, the system is adaptable from one patient to another since foot shape variations require different sensor placement. Secondly, such systems ensure good solid contact between the area of interest and the corresponding sensor. Nevertheless, with the aim of designing a system for self-monitoring of diabetic patients, a system without the need for attaching separate sensors to the foot would be appealing. One way to avoid this is to have a sensory platform with a number of sensors readily affixed to it, which is either worn on the foot or placed within the shoe.

2.2.2.3 Insole Temperature Measuring Systems

One approach to the suggested solution would be to have a system which utilises a sensory insole. The concept of designing a sensory insole system was very common in studies concerned with plantar pressure analysis [49], [50], [51], but it was a first to have a similar system measuring also temperature and humidity [16]. The system illustrated in Figure 2.14 used two types of sensors: four Paromed

0255-205 combined pressure and temperature sensors and a single Honeywell HIH series humidity sensor. The humidity sensor was placed at the toe end of the insole whereas the pressure and temperature sensors were placed under the medial, central and lateral metatarsal heads, and under the heel. The sensors were moulded between two plastazote layers, which would then be fitted on the insole and placed within the person's shoe. Even though all the Paromed sensors were capable of measuring both pressure and temperature, the latter was only sampled from the sensors under the heel and the central metatarsal head. Pressure data was gathered at 30Hz whereas temperature and humidity were measured every minute. The system used a Motorola 68HC912V32 microcontroller, coupled with an Atmel 16 megabit flash RAM (AT45DB161), enabling a total recording time of 4.5 hours. A LabView application designed specifically for this system allowed for viewing of the recorded data.

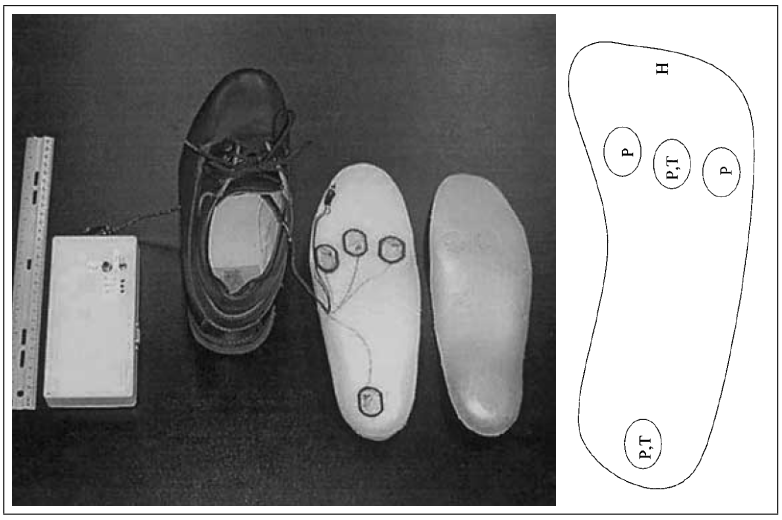

Figure 2.14: Sensor placement of the temperature measurement system used in Morley et al.'s study ([16]).

A separate study [17] was conducted to validate the performance of the designed system. The measurements from the pressure sensors during walking trials were compared to readings collected from the Tekscan F-Scan. The humidity sensors' performance was tested by placing the shoe inside environmental chambers set at specific humidity levels (75%, 60% and 23%) whereas the temperature sensors were validated by placing the shoe inside an incubator with temperatures varied in 5 steps, from 24 °C to 47 °C. The temperatures at the heel and toes area were noted using mercury thermometers after the temperatures within the incubator had stabilised for

30 minutes. On comparing the system's readings with the control values, it was found that there were some slight discrepancies in the readings (±5% in humidity readings, 0.96±1.56 °C in temperature readings and the correlation coefficient r for the pressure readings varied from 0.82 to 0.98). Due to the layer of plastazote between the sensors and the subject's foot, the authors suggested that the temperature variations detected could not be linked directly to localised skin temperature fluctuations. Instead, these temperature fluctuations were mostly indicative of the environmental temperatures within the shoe.

Another sensory insole system used to measure the temperatures of the foot was designed in Reddy et al.'s study [18]. The system depicted in Figure 2.15 could measure temperatures from four different locations under the foot, namely the hallux, between the 1st and 2nd metatarsal heads, the lateral side of the foot, and the heel. The TMP35 (Analog Devices, Massachusetts, USA) temperature sensors used were embedded within a 5mm thick hard foam insole and connected to a National Instruments (Texas, USA) myRIO for processing. These sensors provided measurements with an accuracy of ±2 °C for temperature ranges between -40 °C and +125 °C. Additionally, the system could also monitor the user's movement by accessing the data measured by the myRio's internal accelerometer. This battery powered system could be used for recording sessions of up to ten hours.

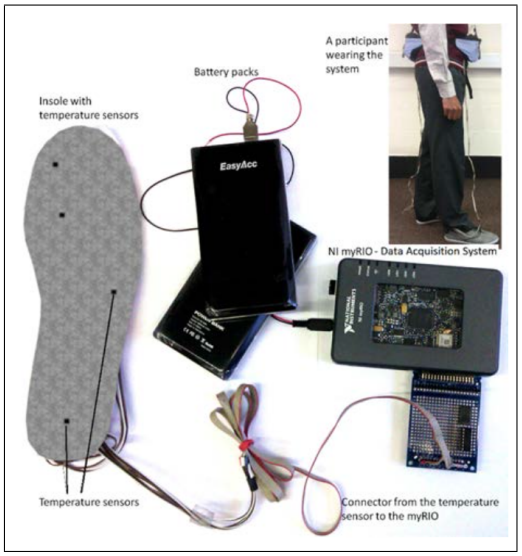

Figure 2.15: Components of the foot measurement system used in Reddy et al.'s study and a participant wearing the system (adapted from [18]).

In this study there were 14 participants (13 male and 1 female) with ages ranging between 21-40 years. None of the patients had a history of foot problems or deformities, and all participants were tested for loss of sensation by using the 10gm monofilament test. Standardised shoes were used all across the subjects, each fitted with sensor insoles of custom size. Each subject was called in for 3 separate sessions with varied walking speeds: 0.8 m/s [2.88 km/hr], 1.2 m/s [4.32 km/hr] and 1.6 m/s [5.76 km/hr]. Every session started with the subject sitting down for 10 minutes with their legs stretched out to let the feet return to their resting temperature. This was followed by another 5 minutes of sitting while wearing the shoes and finally by 10 minutes of standing before walking for 45 minutes on the treadmill. The session was then concluded with a final 15 minutes of sitting down while wearing the shoes to analyse temperature variations post-walking. Upon analysing the collected data, it was noted that the temperature elevations were affected by the walking speed as clearly pointed out in previously analysed studies, and similarly, no major discrepancies were noted between the two feet, as expected from healthy adults. Temperature at all 4 points on the foot was noted to rise instantly as soon as walking commenced, and eventually plateauing at different temperature levels. Table 2.1 illustrates the temperature changes at the 4 foot areas and how these varied with increasing walking speeds. When comparing these results to those of Shimazaki and Murata [42], the temperature at the hallux seems questionable. In fact, Reddy et al. pointed out the issues with insufficient contact between the big toe and the insole. Possibly, this was due to movement of the foot within the shoe and thus reducing contact between the toe and the sensor area. At times, this was also noted at the heel, having incidents where a temperature rise was noted after walking stopped and the subject was seated. Moreover, sensor placement in the insole was done by analysing the average foot and not custom made for each and every subject, thus anatomical differences in the subjects' feet resulted in erroneous sensor placement. Having a system with an array of sensors instead of single sensors placed at specific locations would solve such problems. This is due to the fact that there will be sensors located all throughout the insole and all areas of the foot will be analysed no matter the shape/deformities of the foot.

Temperature is not the only factor within the shoe having an adverse

Speed (m/s)	Temperature Elevations (°C)			
	Hallux	**Met. Heads**	**Lateral Side**	**Heel**
0.8	2.01±1.51	3.55±1.36	3.16±0.99	3.01±0.89
1.2	2.80±2.02	3.74±1.43	3.14±0.97	2.69±1.29
1.6	3.12±2.16	4.55±1.39	3.70±1.19	4.23±2.50

Table 2.1: Temperature elevations of feet area at varying walking speeds.

effect on the health of the foot. Previous studies have shown that sweating disorders may result in dry skin on the foot sole, causing the skin to bleed [52] and eventually leading to fissure formation and ulceration [53]. The combined effects of fluctuating temperature and relative humidity levels are responsible for the level of skin hydration on the foot [54], [55], [56], [57]. Thus, by monitoring the microclimate within the shoe, one may help maintain an optimally-hydrated foot to help prevent the formation of fissures and ulcerations [58], [59], [60]. A study was conducted [19] where both temperature and RH were monitored using a system specifically designed for the study using sensor-based insoles. This system was made up of 3 main modules: the portable module including the sensor insoles and control unit (M1), the communications module to the computer (M2) and the software run on the computer for data interpretation. A single insole contained 5 SHT15 temperature and humidity sensors (Sensirion AG, Säafa, Switzerland) capable of reading ranges of 100% RH $\pm$ 2% and temperatures within -40 °C to 123.8 °C $\pm$ 0.3 °C. The sensors were spread out beneath 3 areas of the foot; two under the forefoot area, two under the midfoot area and one under hindfoot area, as shown in Figure 2.16. The sensors were placed in holes drilled in the insole, deep enough to allow an air channel to be present between sensor and the plantar surface so as to be able to read the characteristics of the microclimate without problems. A PIC18F452 micro-controller (Microchip, Arizona, USA) was used to process the data from the sensors and save it to memory (AT24C256, Atmel, California, USA). The unit was capable of saving 500 records for an 8 hour recording period, with a display and buttons to be able to select the recording period and frequency. The sensors were physically connected to the

micro-controller board via a flexible cable with a 14-pin header connection. Similarly, module M1 was connected to M2 with an identical cable, where the PIC18F2550 in M2 took care of the communication to the computer. Readings were input into a MySQL database, from which a Matlab program plotted the data and enabled direct comparison between sensors and between recording sessions.

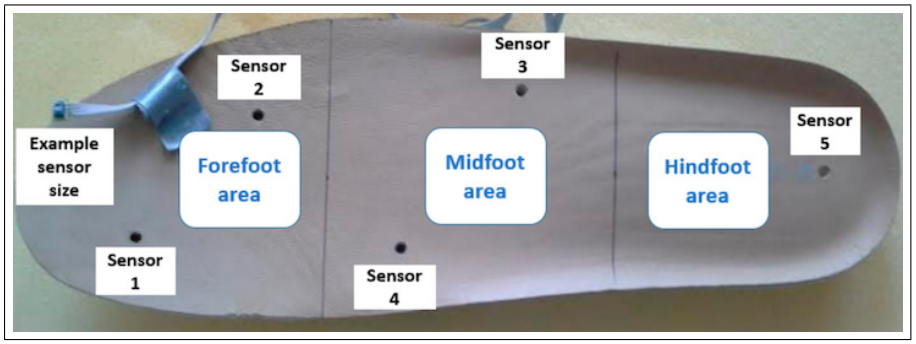

Figure 2.16: Sensor placement on the insole, part of module M1 in Sandoval-Palomares et al.'s system (adapted from [19]).

In Sandoval-Palomares et al.'s study [19], two healthy 45-year-old males were chosen to take part, both without any history of foot disease or deformities. 5 cycles of 60-minute readings were performed on each subject, with the first 5 minutes of every cycle used to get readings of the shoe microclimate without the subject's foot. The average temperature ranges per participant were found to be 24.37°C to 29.27°C and 23.44°C to 29.41°C. RH readings were found to be within 53.01% and 71.82% for one participant and 50.13% and 67.75% for the other. No technical problems were reported during the recording periods, except for slight temperature dips half-way through the recording which could be due to excess ventilation caused by foot posture changes. All in all, the system was deemed to be a useful in determining the microclimate of the shoe, which in turn could help prevent injury in patients suffering from diabetic foot syndrome.

One way of avoiding issues with foot movements within the shoe, as observed in the previous study, is by having sensors embedded into a sock rather than an insole. This will help to keep the sensors in constant contact with the foot during ambulation, and avoid recording any temperature dips due to loss of sensor contact.

2.2.2.4 Sock Temperature Measuring Systems

A study [61] was conducted using a smart sock prototype designed and built by Novinoor LLC (Wilmette, Illinois, USA) called SmartSox. The sock was embedded with FBG sensors which are single core fibres that are laterally exposed to intense ultra violet light patterns in order to alter the refractive index (grating) of parts of the fibre core [62]. With this process, the fibre core reflects light at a particular wavelength defined by the period of the gratings, but dependent also on the strain and temperature of the core. Therefore, the response to changes in strain and temperature makes the FBGs useful as sensors to be able to measure these parameters, as well as calculate plantar pressure readings. In this system, each FBG sensor was connected to an optical filter and IR detector, with a micro-controller processing the raw data and storing the angular strain and temperature fluctuations of the foot. The areas that were monitored were the big toe, the first metatarsal head (MTH), the fifth MTH, the midfoot and the heel, with the addition of a sixth sensor on the top side of the hallux to measure movement about its joint. A LabView application was utilised for the acquisition, presentation and storage of the data. Testing on the system was done in various stages; starting out with *in vitro* testing of the system characteristics, then *in vivo* testing on subjects with Type 2 diabetes with a high risk of DFU, and finally testing on a more generic population of diabetic subjects with a range of foot deformities. The initial testing on a smaller section of the diabetic population was done to validate the system rather than collect data for analysis. The subjects performed walking trials of approximately 30 metres, wearing the Smartsox as well as Tekscan F-Scan pressure insoles for comparison of pressure readings. Additionally, the subjects were assisted in taking off and putting on the Smartsox to be able to capture thermal images of the foot just before as well as immediately after the walk.

Even though testing was deemed successful, a few issues with the system were highlighted and eventually improved upon. The most prominent issue was the use of cabling between the system and the computer processing the data. Not only did the cable restrict movement, but the fact that is was made of fibre optics proved to be too fragile and was constantly getting damaged when pulled or stepped upon. The

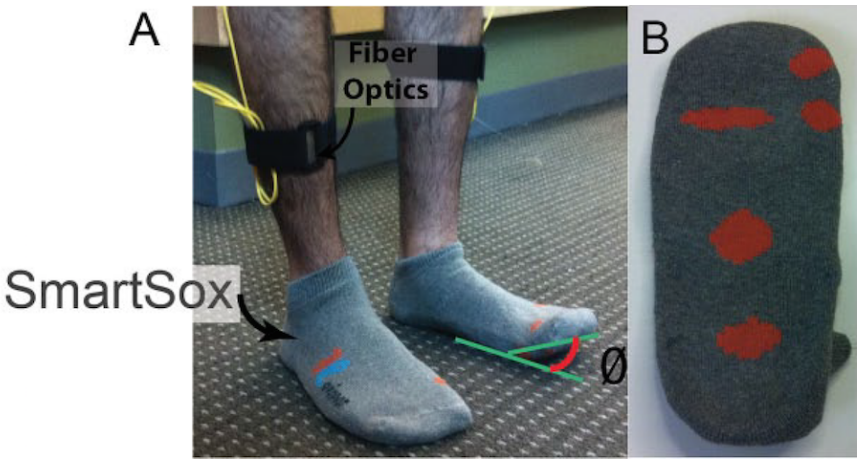

Figure 2.17: The SmartSox system: (a) the prototype composed of the socks embedded with FBG sensors and fibre optic cables going up to the processing unit; (b) sensor locations on the bottom of the sock (adapted from[61]).

connection between the cable and the sock was not ideal as fibre breakdowns were also occurring because of twisting of the cable during walking. Eventually, the prototype was improved, incorporating a thread latch lock for a more robust connection to the sock and eventually omitting the need for a cable altogether by having the system transfer data wirelessly to a computer. Alterations were also required for the actual sock design, as the fibres were getting damaged with excessive weight and uneven distribution of weight along the plantar surface for subjects with severe foot deformities. The addition of a thin layer of soft padding on the bottom side of the sock helped to preserve the integrity of the fibre cores while at the same time increasing the comfort of the socks themselves. This improved prototype was then used for further testing to verify the improvements in the system. At the time of the study [61], the SmartSox system was still a system used solely for clinical testing, and up to recently no further information was found as to whether the system prototype was then taken to market.

However, another sensory sock based system was designed and available for prescription by doctors. The Siren Diabetic Socks [63] (Siren Care Inc, San Francisco, CA) are integrated with six temperature sensors located at conventional sites of interest; the hallux, the first, third and fifth metatarsal head (MTH), the midfoot, and the heel. The micro-sensors are woven directly into the fabric, but no further information was given on the type of sensors used. These were connected to a

small processing unit integrated in the sock located above the ankle as shown in Figure 2.18. The unit consisted of a micro-controller and Bluetooth communication chip, along with the battery powering the sock. Temperature readings from the sensors are taken at 10-second intervals, with the data stored in the processing unit and sent to a smart-phone paired with each pair of socks. The software application offered with the system has the option to set up alerts when there are temperature fluctuations that could signify possible ulcerations. A pilot study [22] was conducted using this system in order to be able to assess the comfort of the socks as well as the integrity of the recorded temperature data, making sure it is in line with observations done clinically.

Figure 2.18: Siren Diabetic Socks: (a) image of socks showing (circled) processing unit location; (b) image of the bottom of the sock showing sensor locations (adapted from [22]).

Initial testing was done on the sensors themselves and then on the sensory sock, using a high-precision thermostatic water bath in both cases, verifying temperature readings with a precision of 0.01 °C. In both instances the sensors were seen to measure temperature values close to the reference standard, thus concluding that the socks were capable of getting precise temperature readings within a 10 second window. A total of 35 diabetic patients were then enrolled in the study, classifying them in three separate groups: one with no history of ulcers, another with a history of ulceration but having none at the time of the study and finally one with a pre-ulcer during the study as determined by the researcher. The subjects were given the Siren socks and an Android phone on their first visit to the clinic, where a board-certified podiatrist also carried out a general foot exam and inspection. The patients were

instructed to use the socks for a period of 6 hours where they would then return the system on their second and final visit to the clinic and give in their feedback.

From the questionnaires provided, all the subjects gave high ratings to the system in terms of comfort, and reported that there was no noticeable differences from ordinary socks. A few case studies were presented, and the data collected was in line with the initial foot exam; reading temperature differences between contralateral sites of the foot greater than 2.2 °C at the sites of concern. The pilot study was deemed a success as the system was seen to reach its goals; to monitor the temperatures of the foot without the user having his/her daily routine affected. Of course, since the testing period was a single session of a few hours, no long terms outcomes could be reported. No breakages or issues with the system performance were reported in the study, but long-term testing is required to be able to guarantee sensor and wiring resilience to the conditions within the shoe on a daily basis and for day-long periods. Additionally, even though the socks are washable, they need to be replaced every six months due to possible wear to the fabric that could compromise the fit of the sock [63]. In this way, the user never needs to replace the batteries since the button cell batteries that are fitted with the processor tag should last the whole 6-month period [64].

This novel method of foot temperature measurement using sensory socks is in line with the current trend of wearable devices. It provides a means of keeping the temperature sensor in continuous contact with the foot. From a design perspective, sensors and wiring need to be even more discrete than in sensory insole design in order to avoid harmful pressure points under the sole of the foot which could cause discomfort and tissue damage.

2.3 Summary

Various dynamic measuring systems have been reviewed, some of which have been specifically designed for the measurement of temperatures within the shoe while others sought to collect additional parameters over and above temperature. Nevertheless, all these systems pointed out design flaws and strengths to be

considered in the development of a new system, whereas similarities between systems help to confirm the benefits of certain design characteristics. Table 2.2 lists all the dynamic measuring systems that were created for research purposes that have been reviewed in this chapter, outlining the sensor type, sensor precision, sampling rates and recording durations amongst other characteristics.

The design process in this study will be discussed in detail in Chapter 3, with the aim of creating a system capable of analysing the temperature of the foot with sensor densities higher than any of the systems to date.

System	Sensor Type	Sensors/Foot	Temp. Range	Precision	Sampling Rate	Storage	Duration
Morley et al. (2001) [16]	RTD	2	-20°C to 80°C		1 reading/min	270 readings [16Mb]	4.5 hours
Kang et al. (2003) [40]	Thermocouple	1	-200°C to 1190°C	±0.5°C	1 reading/min	16,383 readings	24-36 hours
Foltyński et al. (2012) [41]	Digital Sensor	1	-40°C to 85°C		1 reading/min [1]	57,000 readings	2-3 years
Rutkove et al. (2007) [45]	Digital Sensor	1	15°C to 46°C	±1°C	1 reading/2 min	2048 readings [2Kb]	3.5 years
Shimazaki & Murata (2015) [42]	Thermocouple	8	-210°C to 1200°C [2]	±2.2°C	1 reading/min		50 mins [3]
Reddy et al. (2016 [18]	Digital Sensor	4	-40°C to 125°C	±2°C	100Hz	USB Storage [Unlimited]	10 hours
Sandoval-Palomares et al. (2016) [19]	Digital Sensor	5	-40°C to 123.8°C	±0.3°C	1 reading/min	500 readings	8 hours
Coates et al. (2016 [20]	Thermistor	3	-50°C to 125°C	±0.4°C	20Hz		2.5 hours
Mizzi (2016) [43]	Thermistor	2	max 60°C	±0.2°C	1kHz [4]	PC Memory [Unlimited]	50 mins [5]

[1] *The frequency was reduced to 1 reading/5 mins for healthy participants.*
[2] *Stated generic J-thermocouple specifications.*
[3] *Stated length of recordings, no information was given on portability of system.*
[4] *The data was down-sampled to 1 reading/min.*
[5] *Stated length of recordings, unit did not operate on batteries.*

Table 2.2: Dynamic In-shoe Temperature Measuring Systems.

Chapter 3

System Design

3.1 Introduction

As per several systems reviewed in Chapter 2, the system being designed in this project follows a similar system structure, composed of three main components:

- Sensor Module
- Data Collection/Transmission Module
- Software Module

These sub-systems form part of a single work-flow as shown in Figure 3.1; starting with the collection of temperature data from the sensory module and then having this data processed and transmitted to a device (PC/mobile/tablet) that is running the end-user software.

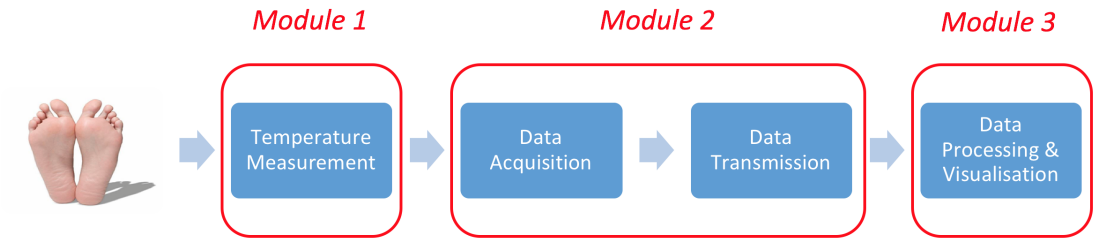

Figure 3.1: Block diagram of the different functional modules within a foot temperature analysis system.

The first steps in the design process are to:

- choose the type of temperature sensors to be used
- looking into the ideal sensor count and locations
- determining the medium upon which these need to be mounted

Based on the type of sensors that are chosen, the interfacing circuitry is designed in order to acquire the temperature readings. The acquisition module must also provide a means of transmitting the data to a PC or smart device that would be running the data processing and visualisation software. The data transmitted from the separate foot modules must be synchronised so as to make sure that the temperature readings reflect the actual temperatures of the feet at the same point in time. Since the system is required to monitor the temperatures of both feet, that same device should be able to receive data from two separate acquisition modules. Additionally, data logging onto a memory card is necessary so as to be able to operate the system even without the use of a smart device, and analyse the data post-recording.

The building of the acquisition module went beyond designing the physical circuit supporting the functions within the system. Embedded software programming was essential in enabling the microcontroller to manage the separate elements within the circuit. It is responsible for acquiring the data from the sensors and/or ADCs, as well as handling the transmission and logging of that data. The user

software which displays and processes the data, was designed at a much later stage since system functionality was not dependent on it.

In the following sections, the design approaches considered for each module are described, highlighting why the final design was deemed the best solution for the application at hand. Several design aspects will be discussed; including shape, dimensions, cost, and ergonomics amongst others.

3.2 Sensor Module

The systems analysed in Chapter 2 used a variety of temperature sensors, which will be described in more detail in Section 3.2.1. All the sensors performed well enough for the systems to be able to capture relevant data, but some sensors were better suited for this type of application and resulted in a better sensory platform design. The various sensor form factors offer a multitude of design approaches for the sensory module. The sensors' physical characteristics play a very important role in determining their suitability to be placed under the foot. Other than that, the type of sensor used will also determine the circuitry required for the collection of the temperature data.

3.2.1 Types of Temperature Sensors

The various systems that were reviewed in the literature used different kinds of sensors, ranging from analogue thermocouples to digital sensors as shown in Figure 3.2. In every case, a particular sensor was chosen because of its physical attributes as well as the precision of the temperature readings and its response time. When considering in-shoe systems, such as the one designed in this study, sensor form factor is of utmost importance. The sensors need to be small and thin if they are to be placed beneath the foot since they should not be felt, and more importantly should not cause discomfort and irritation. It is imperative that the sensors will not cause any injuries to the foot, especially if the system is to be used by diabetic and neuropathic patients. Nevertheless, the sensors need to be robust enough to withstand

the pressures exerted by the foot and small or flexible enough not be damaged with the movements of the foot. Additionally, the type of sensors used will also determine what circuitry is required. Digital sensors will generally be found in an integrated circuit (IC) form factor, and may only require some passive external components for the correct operation of their internal circuitry. No further signal conditioning circuitry would be required since the output is a readily converted digital signal that would be transmitted to the processing unit via communication protocols such as SPI or inter-integrated circuit (I^2C) [65]. On the other hand, when using analogue sensors, the output will be a voltage signal that will need to be conditioned and eventually converted into a digital signal using an analogue-to-digital converter (ADC).

(a) Thermocouple (adapted from [66])

(b) Thermistors (adapted from [67])

(c) RTD (adapted from [68])

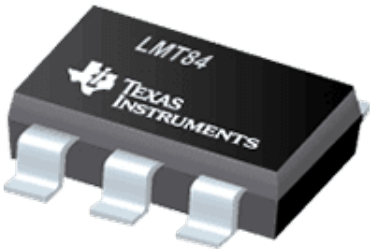

(d) IC Sensor (adapted from [69])

Figure 3.2: Types of temperature sensors

The sensor type will not only dictate what circuitry is required, but it will also have an impact on the number of sensors that can physically be placed on the module. With the currently available systems having no more than eight sensors, there is no indication of the ideal number of sensors required to have a high density recording system. For this study, the system will be designed with a maximal sensor count in order to obtain high density measurements. Upon analysing the testing results, the temperature variances along the foot sole can give an indication of the spatial sensor

density that is actually required for the system. At this stage of the project, the first step is to review the different types of sensors so as to choose the most adequate sensors to be used in the system being designed.

3.2.1.1 Thermocouples

Thermocouples are very robust, low-cost temperature sensors that can operate at wide temperature ranges with moderate margins of error. The principle of operation is based on the fact that when a junction of two dissimilar metals is heated or cooled, a voltage is created across that junction [66]. This is illustrated clearly in the schematic in Figure 3.3 below.

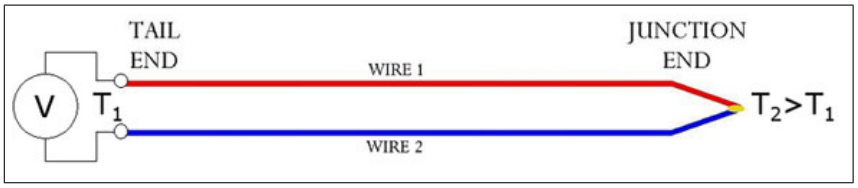

Figure 3.3: Schematic representation of a thermocouple [70].

There are various types of thermocouples depending on the metals used, each with their own range of operating temperatures and accuracies as listed in Table 3.1. There are other factors that affect the accuracy of a thermocouple, including the material and diameter of the sheath, the construction of the sensor (how well the two metals are bonded together) and the type of medium being measured (gas, liquid or solid).

Thermocouple Type	Composition	Temperature Range (°C)	Standard Error (°C)	Special Limits of Error (°C)
Type K	Nickel-Chromium / Nickel-Alumel	-270 to 1260°C	±2.2°C	±1.1°C
Type J	Iron / Constantan	-210 to 760°C	±2.2°C	±1.1°C
Type N	Nicrosil / Nisil	-270 to 392°C	±2.2°C	±1.1°C
Type E	Nickel-Chromium / Constantan	-270 to 870°C	±1.7°C	±1.0°C
Type S	Platinum Rhodium (10%) / Platinum	-50 to 1480°C	±1.5°C	±0.6°C
Type T	Copper / Contantan	-270 to 370°C	±1.0°C	±0.5°C

Table 3.1: Thermocouple types and characteristics [71].

For the purpose of analysing changes in the skin of the foot, thermocouples may not be the best suited sensors. Since temperature fluctuations in the foot during ambulation have been found to be below 5°C [18], [19], temperature sensors need to have high sensitivity. Thermocouple sensitivity is in the range of µV for every 1 °C of temperature change [72], being susceptible to electrical noise and requiring high precision ADCs to be able to sense small changes in temperature. Moreover, their rigid form factor is not ideal in such an application where movement is very frequent, possibly resulting in damage to the thermocouples or injury to the user.

3.2.1.2 Thermistors

A thermistor is an element whose resistance fluctuates in response to temperature changes. The relationship between resistance and temperature is dependent on the materials with which the thermistor is composed of. Negative temperature coefficient (NTC) thermistors, whose resistance decreases with an increase in temperature, are created from sintered metal oxides. On the other hand, positive temperature coefficient (PTC) thermistors are composed of doped polycrystalline ceramic and their resistance increases with an increase in temperature. Measurements are very stable and do not drift over temperature or time, thus providing precise repetitive results [73]. They respond quickly to temperature changes, with precisions ranging from $\pm$0.1 °C to $\pm$0.2 °C [74]. The coating used on the sensing tip is dependent on the temperature range being monitoring, using epoxy typically for measurement of -50 to 150°C and glass for temperature range up to 300°C. Thermistors are produced in various form factors, including film thermistors that are ideal for in-shoe applications due to their thin dimensions and flexibility.

The relationship between resistance and temperature is not linear for either type of thermistors. In order to extract a mathematical relationship between resistance and temperature, one can use linearisation circuitry to get a straight-line response. Alternatively, there is the Steinhart-Hart equation which is used to model a generic curve shape for thermistors, useful for getting the resistance values at specific temperatures, or vice versa. The relationship is defined as follows:

$$\frac{1}{T} = A + B\ln(R) + C(\ln(R))^3 \tag{3.1}$$

Where

- **T** is the temperature in Kelvin (K)
- **R** is the resistance at temperature T in Ohms(Ω)
- **A**, **B** and **C** are the Steinhart-Hart coefficients which vary between thermistor makes and models, and are generally defined by the manufacturer.

Certain manufacturers, as in the case of ATC-Semitec, do not provide all three of these coefficients, and will only give the β-value - describing how the thermistor resistance decreases with temperature - and a reference resistance value $\mathbf{R_0}$ at temperature $\mathbf{T_0}$. There is another, less accurate, equation that is based on these three values which may be used to extract the thermistors resistance $\mathbf{R_T}$ value for a given temperature **T**, and is defined as follows:

$$\frac{1}{T} = \frac{1}{T_0} + \frac{1}{\beta}\ln\left(\frac{R_T}{R_0}\right) \tag{3.2}$$

3.2.1.3 RTD

Resistance temperature detectors (RTDs) are very similar to thermistors but have a more linear response. They generally consist of a wire wound ceramic/glass core or a coil element which may be placed within a sheated probe as shown in Figure 3.4, enabling the use within more rugged applications. The element may be composed of platinum, nickel or copper; with platinum being the most accurate and stable [75]. There are two levels of resistance tolerances according to the IEC 751 standard:

- Class A - 100 ±0.06 Ω at 0 °C

- Class B - 100 $\pm$0.12 Ω at 0 °C

with operating temperatures of -200 to 850 °C. The precision of these sensors varies with temperature as follows [76]:

- Class A = $\pm(0.15 + [0.002 \times T])$ °C where T = -30 to 300 °C
- Class B = $\pm(0.30 + [0.005 \times T])$ °C where T = -50 to 500 °C

RTD elements may also be of the thin-film type, making them more suitable for surface temperature monitoring and space-restricting applications. These types of sensors would also be suitable for the system being designed here, but are a more expensive option than thermistors.

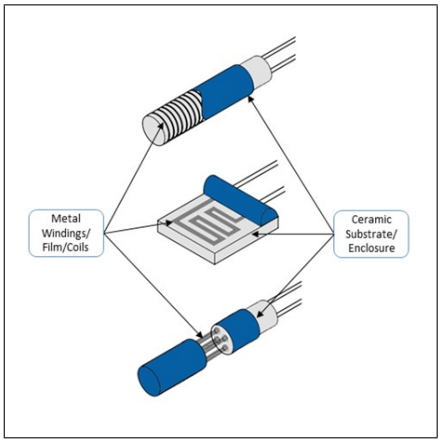

Figure 3.4: Structural view of an RTD [77].

3.2.1.4 Silicone Temperature Sensors

Digital IC temperature sensors work on the principle of temperature varying operational characteristics of transistors. Temperature measurements can either be proportional to voltage differences between the base-emitter voltages of two identical transistors operated at a constant ratio of collector currents or else proportional to the base-emitter voltage of a diode connected transistor [78]. In both cases, the voltages vary with the absolute ambient temperature, with the latter varying

inversely with the thermal characteristics of its surroundings. The base-emitter voltage is then amplified and converted to digital form via an analogue-to-digital converter (ADC). The accuracies of these sensors vary according to the range of temperatures they are designed to operate at. For small ranges between 0 and 70°C, accuracies may reach ±0.5 °C, but for wider ranges from -55 to 175 °C accuracies are closer to ±1.5 °C. Even though sensor ICs may be very small in size and would be unsensed under the foot, especially in high densities, there are issues of installation. These sensors are ideally mounted on printed circuit board (PCB)s and are difficult to have them installed onto insoles and wired to the sensing circuitry as with leaded sensors. Thus PCBs would have to be thin and flexible, while at the same time able to endure the pressures of the foot without damaging the PCB or ICs themselves.

Having analysed the different type of temperature sensors available, the sensory platforms attempted in this project were designed with the most ideal sensor form factor for each application.

3.2.2 PCB Insole

The initial concept design of the sensory interface was an insole composed of a flexible PCB, housing an array of temperature sensing ICs. In order to avoid single pressure points caused by the components underneath the foot, the sensors and other complementary circuitry components (mainly capacitors and resistors) needed to be as small as possible and mounted as densely as possible. Two designs were considered as illustrated in Figure 3.5; one using digital sensors that would not need any conditioning circuitry on the acquisition module, and another using analogue sensors that would require accompanying ADC circuitry (full-scale images of the insole sensory layouts can be found in Appendix A). When researching which sensors might be adequate for this design, there were two criteria that had to be met:

- The width and length of the IC package had to be within 2 - 4 mm.
- The accuracy of the sensor had to be 0.5 °C or better, to match precision of systems found in literature.

- Able to operate at 3.3 V and 5 V supply voltages.
- Measure temperatures over the range of 10 - 50 °C.

The LMT86 (Texas Instruments) analogue sensors fit the requirements, available in the 5-pin SOT package measuring 2.0±0.1 mm by 1.25±0.1 mm. They have a typical accuracy of ±0.4 °C within the operational range of -50 °C to 150 °C. The digital alternative that was found was the MCP9808 (Microchip) sensor, measuring 3.0±0.1 mm by 3.0±0.1 mm in the 8-pin MSOP package. It has a typical accuracy of ±0.25°C for temperatures between -40°C and +125°C, with a user selectable measurement resolution of 0.5°C, 0.25°C, 0.125°C, and 0.0625°C. Both variants are able to operate with supply voltages ranging from 2.7 V to 5.5 V.

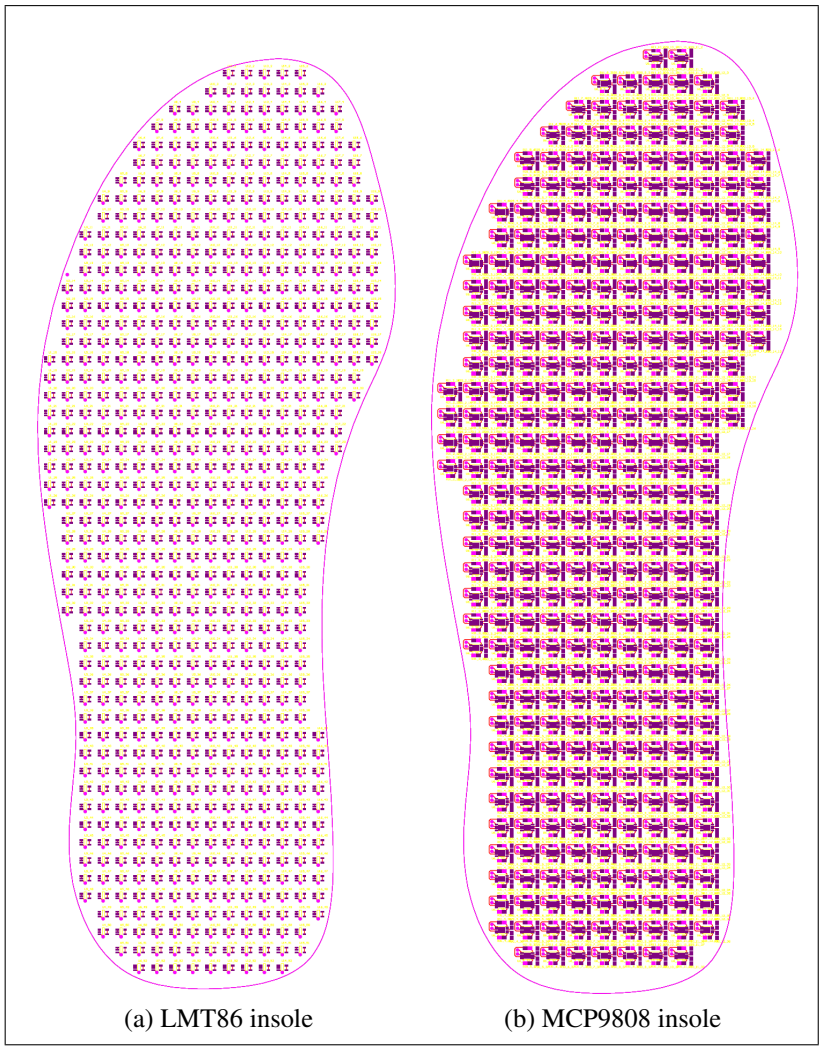

(a) LMT86 insole (b) MCP9808 insole

Figure 3.5: Component layout for the sensory PCB insoles: (a) insole using the LMT86 analogue sensors; (b) insole using the MCP9808 digital sensors.

When using analogue sensors, less components are required on the insole since the sensors do not need any accompanying components to function. This meant that more sensors would be fit onto the insole, which would greatly increase the density of the measurements. The required circuitry to convert these analogue signals into digital format for the microcontroller to process would be located on the acquisition module. However, with the digital sensors, the additional components required for the sensors' functionality must be kept within the sensors' proximity. This means that a greater circuit footprint is required per sensor, and hence results in a lower sensor density on the insole.

It is worth noting that even though the solution using the analogue sensors might seem to be the superior option due to the higher sensor density, it does have its downsides. By having a greater number of sensors on the insole, there will be more voltage readings to be converted and will thus result in more components on the PCB module. This will in turn have adverse effects on the size of the module as well as its power consumption, requiring a bigger power source which will also increase the module's weight. When considering the alternative with the digital sensors, there would be no need for signal conversion at the acquisition module. This keeps the acquisition module circuitry relatively simple since the data need only to be transmitted and no analogue signal processing is required.

With each design having its own benefits, there were a few concerns that were common to both and made this approach less feasible. When considering the insole's resilience to being exposed to the harsh physical environment underneath the foot, there were a few possible points of failure. Due to the continuous shear forces between the foot and the shoe, the soldering joints and component leads would be prone to breaking, causing loss of sensor function. Alternatively, the components themselves could get pulled off the PCB, tearing off any copper tracks that might still be soldered to the components and cause partial or full loss of function of the circuitry. Additionally, this approach was not very cost effective since the price to have the PCBs manufactured and assembled was rather substantial. The cost per PCB is broken down in Table 3.2, showing both options with the analogue and digital sensors. The fixed costs will not vary with the quantity of PCBs ordered, whereas the

other costs will be reduced depending on the quantity ordered.

Cost Type	Circuitry using analogue sensors LMT86	Circuitry using digital sensors MCP9808
Components	$209.80	$322.58
PCB	$15.00	$15.00
Assembly	$133.33	$197.34
Tooling (fixed)	$150.00	$150.00
Stencil (fixed)	$120.00	$120.00
Total	**$628.13**	**$804.82**

Table 3.2: Fabrication costs for the sensory PCB insoles.

When reviewing the costs entailed with this design, and the possible issues with the robustness of the insole, alternative approaches were researched instead. From the literature reviewed in Chapter 2, a number of the researchers opted for foam or fabric sensory insoles [16], [18], [19]. This option provides a more flexible sensor platform, not to mention being more cost effective for the design of the system.

3.2.3 Sensory Fabric Insole

With a sensory fabric insole design, the most important choices to be made are the types of sensors to be used and the wiring required to connect the sensors to the acquisition module. The sensors ideally must be thin and flexible so as not be damaged with the bending of the insole, while not causing any discomfort to the user. Similarly, the wiring must also be as thin as possible to avoid skin damage during walking, but it must be robust enough so as not to have disconnection due to the harsh conditions within the shoe.

One of the systems [20] reviewed in Chapter 2 used the ATC-Semitec (Northwick, UK) flexible thermistors shown in Figure 3.6. The JT thermistor series are less than 0.5 mm in thickness and are electrically insulated, making them ideal to

be used in various applications including medical devices. They have a wide operational temperature range between -50 °C and 125 °C with an approximate thermal time constant of 5 seconds.

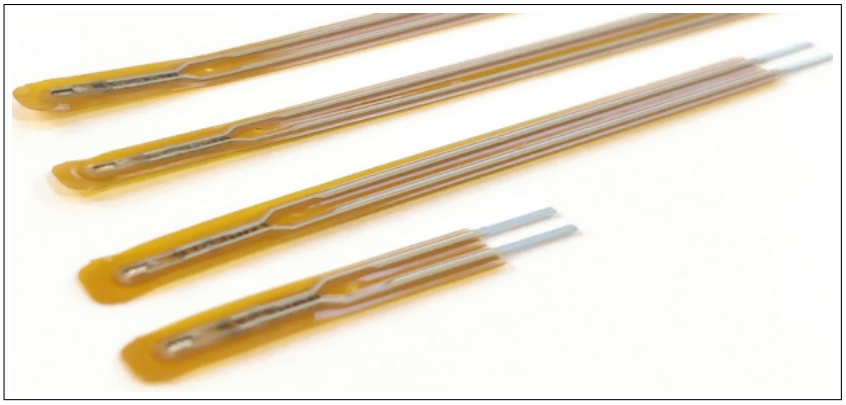

Figure 3.6: ATC Semitec JT Ultra-Thin Film NTC Thermistors.

The JT thermistors can be ordered in different lengths: 25 mm, 50 mm, 75 mm, and 100 mm, while still having the same 0.5 mm thickness and 3.6±0.5 mm width. In terms of performance specifications, there are two main variants of these sensors: the 103JT having a rated zero-power resistance value of 10 kΩ at 25 °C and the 104JT having a zero-power resistance value of 100 kΩ at 25 °C, both of which have a negative temperature coefficient (NTC). The main difference is that for a given range of temperatures, the thermistors will vary between a different range of resistances. For the temperature range of interest in this project, between 10 °C and 50 °C, the 103JT will vary from 18.07 kΩ to 4.417 kΩ whereas the 104JT will vary from 212.5 kΩ to 32.51 kΩ. Both types of sensors were tested using the climate chamber test setup described in Section 4.2. Repeated tests were performed whereby the resistance of the thermistors was measured at specific set temperatures. It was found that the repeatability of results with the 103JT series was slightly better, obtaining a higher correlation coefficient of 0.96 when compared to that of the 104JT series, calculated at 0.91. As can be seen in Figure 3.7, both sensors respond similarly to temperature, with a non-linear decrease in resistance as the temperature is increased. Additionally, the manufacturer provided the full resistance data for the 103JT series only, making them the preferred option to be used in this design.

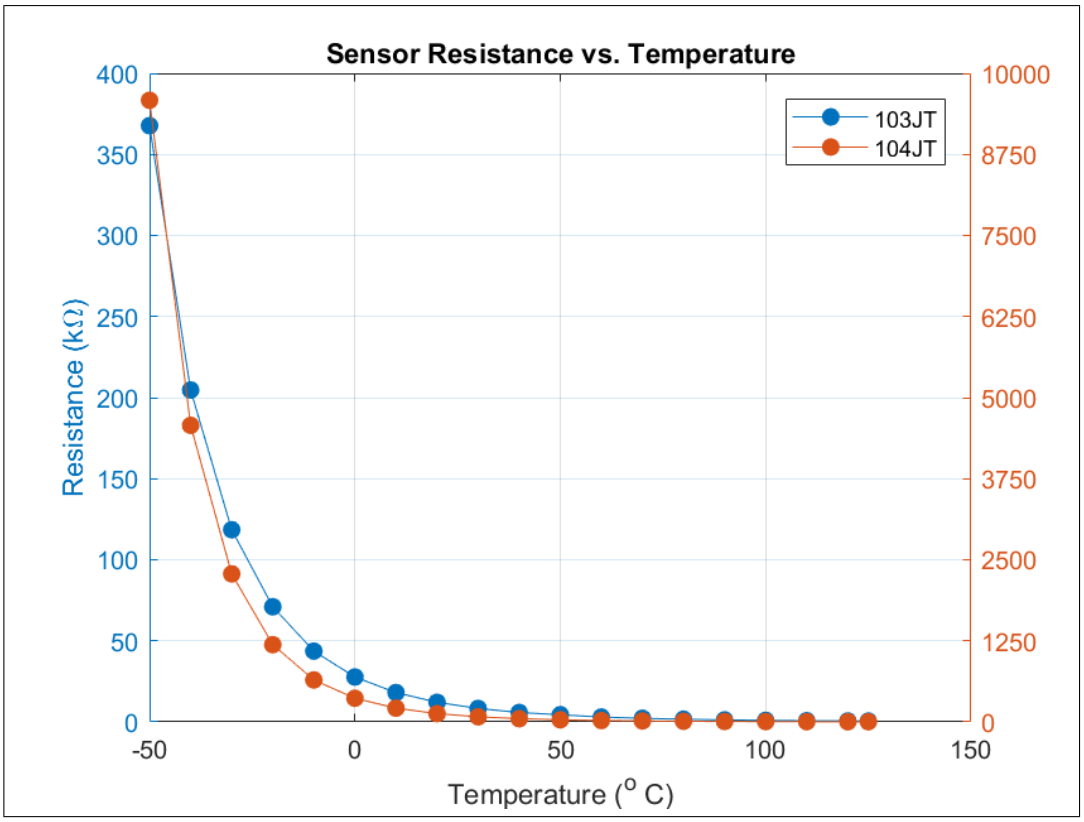

Figure 3.7: The two JT thermistor variants' resistance response to temperature.

The JT thermistors were incorporated into a thin, soft fabric insole that could be placed in any shoe without having to remove the shoe insole. The sensors were wired using flat IDC ribbon cables, since these were thin and flexible enough not to cause discomfort under the foot and would not break with the continuous bending during walking. A total of 30 sensors were placed on the insole, as shown in Figure 3.8, spread along the length of the insole so as to have sensory coverage under the whole sole of the foot. The sensors were sewn to the insole using regular sewing thread, and the cabling routed underneath the insole and out from the sides.

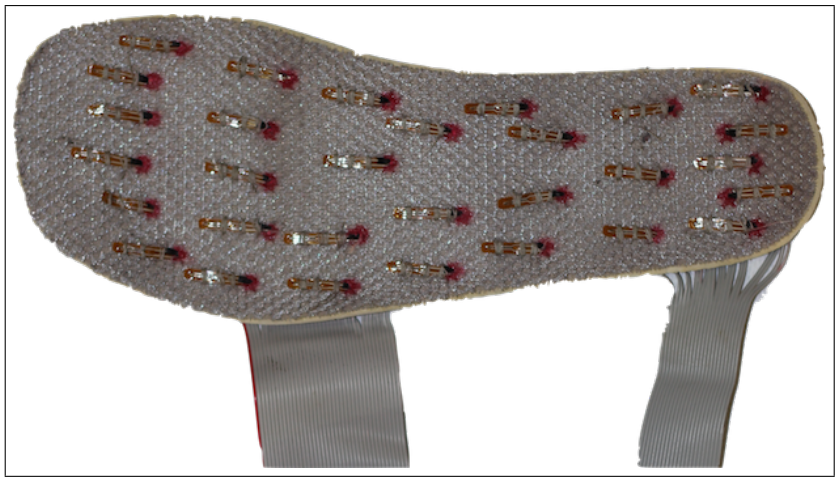

Figure 3.8: The sensory insole using the ATC-semitec JT thermistors.

The insole was tested in both static and dynamic setups. The static test was done with the aim of testing the performance of the sensors in response to different set temperatures, whereas the dynamic tests were more focused on checking the durability of the sensory insole when placed within the shoe during walking trials. At this point of the development stage, it was required to have a basic means of reading the voltages from the sensors and having these stored and transferred wirelessly for analysis. A circuit board was designed for evaluation purposes, where small dimensions and light weight were not a priority. The design of this circuit will be outlined in Section 3.3, and the testing procedures described in Chapter 4.

During the test walks using a single sensory insole, particular attention was given to the physical state of the sensors and their connections after every walk. Unfortunately, two sensors required re-soldering after 120 minutes of walking as the cable/s broke off. It is worth noting that the breakage occurred at the soldering point, where the cable is stiff due to the solder as shown in Figure 3.9 (a). This highlighted the need for an alternative soldering technique where the bending of the cables does not put excessive strain on the soldering connection. For this reason, the wiring of the sensors was updated, using the soldering technique illustrated in Figure 3.9 (b). In this way, the bending of the cable is not done at the soldering joint but rather on a section of the cable that is still insulated and not rigid due to soldering.

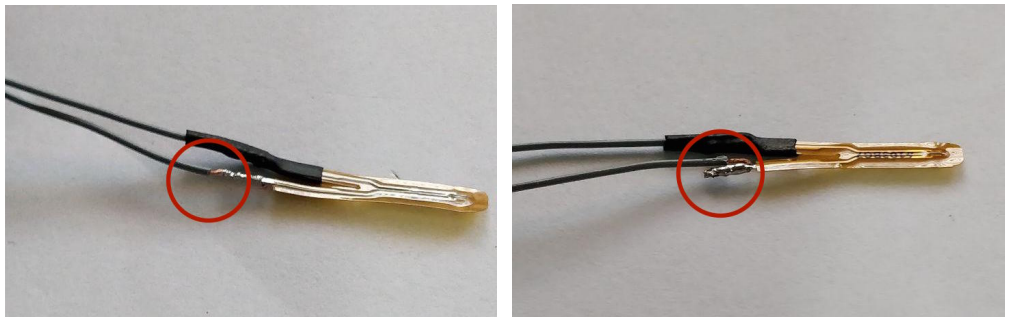

(a) Original soldering technique (b) Improved soldering technique

Figure 3.9: The soldering techniques used for the flexible sensors: (a) the image illustrates the bending point occurring at the soldering joint; (b) the alternate soldering technique that ensures bending is done on the insulated cable.

Since it was observed in other studies [18], [19] that there may be loss of contact between the sensors mounted on the insole and the surface of the foot, it was decided to test out an alternative sensory platform - the sensory sock.

3.2.4 Sensory Sock

There have been studies and systems that use socks with embedded temperature sensors [22], [61], but the number of sensors never exceeded ten. The aim here was to create a dense array of sensors within the sock, and monitor beyond the conventional points of interest on the foot sole. Even though the ribbon cable was thin and flexible enough for the insole, even thinner cable was required for the design of a soft sensory sock. A 0.03 mm^2 single-core cable with thinner insulation was used in the attempt to help avoid the sock being too stiff. Even though the cable used was much thinner, the multitude of cables encased in the sock and the accompanying sewing, as illustrated in Figure 3.10, resulted in a rigid sock structure. This compromised the ease of putting on and taking off the sock, which goes against one of the main aims of the systems; to be easy to use by anyone.

Figure 3.10: The sensory sock using the ATC-semitec JT thermistors.

When the sock was used during test walks, it was noted that the sensor wiring was more susceptible to breakage. During the walking trials there were multiple sensor breakages and thus a lot of the temperature data was not recorded. The main cause for this was the fact that a single core cable was not resilient to continuous bending as a multi-core cable. This caused breakages during walking, and at times even while taking off or putting on the sock. The lack of robustness of the sensor wiring within the sock structure also raised concerns with regards to the wash-ability of the socks for hygiene purposes. Even though sensor functionality is not affected by immersion in water, the wiring cannot sustain the harsh conditions of a washing machine or a rinsing process.

3.2.5 Sock with Integrated Sensory Insole

In trying to incorporate the benefits of both the insole and sock design into a single module, another sensory platform was designed. When comparing the two previous designs, it was found that the sensory insole was much easier to be placed into the shoe and was less susceptible to damage during use. On the other hand, the socks were found to keep the sensors closer to the foot and ensure continuous contact.

For these reasons, it was decided to create a sock with a false bottom, into which a sensory insole can be placed. This would avoid any issues when it comes to washing the socks, since the insole can simply be removed and the socks washed normally like any other regular item of clothing.

At first, it was thought to have the sensors embedded in a latex compound to form a custom made insole as shown in Figure 3.11(a). The fabrication process was done in two separate stages. First, the sensors would need to be laid out onto a smooth surface and stuck in position. This was done by using a piece of glass that had an outer frame that would encase the poured latex material. The insole shape was drawn on the glass and then covered with double sided tape, onto which the sensors and wiring were attached. Once this was done, the final task was to pour the latex material evenly over the whole area. The poured volume would have to be enough to immerse the sensors and wiring, but not too thick that would then affect the transmission of heat to the sensors. Unfortunately, during the curing process, some of the sensors and cables started to detach from the double sided tape and pierce through the surface of the latex compound. This resulted in a few of the sensors sticking out the insole as illustrated in Figure 3.11(b). In addition to that, since the insole was kept as thin as possible, the cured latex material started to tear when peeled off the double sided tape. Leaving the tape attached was not an option since it would add rigidity to the insole as well as hinder the insertion and removal of the insole from the sock due to the adhesive.

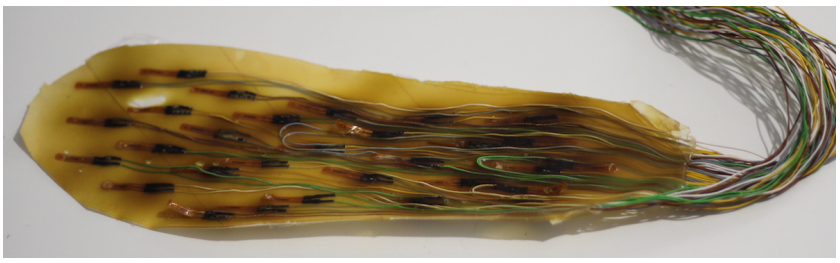

(a) Latex insole

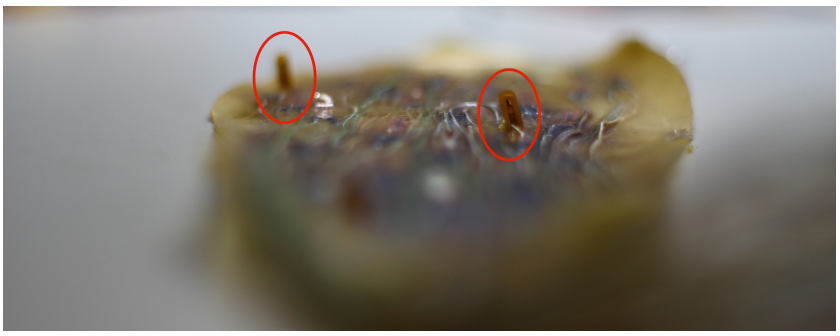

(b) Insole defects

Figure 3.11: (a) Latex insole with 30 encapsulated sensors and wiring. (b) Insole defects due to sensors piercing through the latex compound.

Given the shortcomings of this method, the previously used fabric insole was re-used in this design. In order to improve the flexibility slightly, the IDC ribbon cable along the insole was replaced with a thinner multi-core cable with a cross-sectional area of 0.05 mm^2. The IDC ribbon cable was still utilised to connect the insole to the PCB, but the thinner cable was better suited to be routed along the insole. The updated insole design is depicted in Figure 3.12(a), whereas Figure 3.12(b) shows the complete sock-insole design. Following some testing using the sock-insole module, it was decided to go ahead with this design for data collection purposes. During testing, no dips in temperatures were noted which proves that the contact between the foot and sensory insole was continuous. Moreover, putting on this sock proved much easier than the previously designed sock, and no sensor breakages were observed during the initial stages of testing.

(a) The updated insole design (b) The worn sock-insole module

Figure 3.12: The soldering techniques used for the flexible sensors: (a) the image illustrates the bending point occurring at the soldering joint; (b) the alternate soldering technique that ensures bending is done on the insulated cable.

3.3 Acquisition Module

As initially explained in Section 3.1, the sensory module is only a part of the whole system, and needs the other modules to be able to collect temperature data. The circuitry which makes up the acquisition module utilises the sensors as a means to convert temperature into electrical signals that can be processed and converted into digital temperature data. There are various components that make up the designed circuit, including: the micro-controller, the sensor interfacing circuitry, the wireless communication module and the memory card for data logging. In this section, each element will be discussed and the design choices explained.

3.3.1 Microcontroller

Within any device that requires some form of data processing, there must be a central processing unit handling all the operations that are required for its

functionality. In a computer, the main processor chip (CPU) is solely responsible for processing tasks, and other functions such as memory and input/output interfacing are supported by other dedicated chips. However, for embedded systems such as the one designed here, a single-chip microcontroller unit (MCU) is generally the preferred option. A single IC can store the application code that needs to be run and support all the required functionality within the device. It can interface with other devices using dedicated communication protocols, as well as process input and output signals. The MCU can only handle digital signals, but some have an internal analogue-to-digital converter (ADC) and digital-to-analogue converter (DAC) to be able to read and output analogue signals respectively. If these are not present, or do not meet the required performance specifications, external devices can be used instead. This was done in this case because of the numerous voltages signals to be read, since it is not common to find a microcontroller with a 30-channel internal ADC. Even though this will increase the footprint of the circuit, it provides added benefits such as being able to opt for a higher resolution ADC. The only requirement for the MCU would be to support the communication protocol used by the ADC, which are generally serial peripheral interface (SPI) or inter-integrated circuit (I^2C), both of which are commonly found in the majority of microcontrollers.

Having had prior experience with using the 8-bit Microchip ATmega328P, while also ticking all of the requirements, it was chosen for this project. The device comes in various footprints including the 28-pin SPDIP and the 32-pin TQFP packages illustrated in Figure 3.13. Both packages were used, the larger SPDIP utilised for the first circuit prototype and the smaller TQFP for the second board prototype. The ATmega328P has an operating voltage range of 1.8-5.5 V, which gives the option to have the entire circuit working at the conventional 3.3 V or 5.0 V supplies, dependent on the voltage of the chosen battery source. It also has a total of 23 general-purpose input/output (GPIO) lines, well in excess of the required amount.

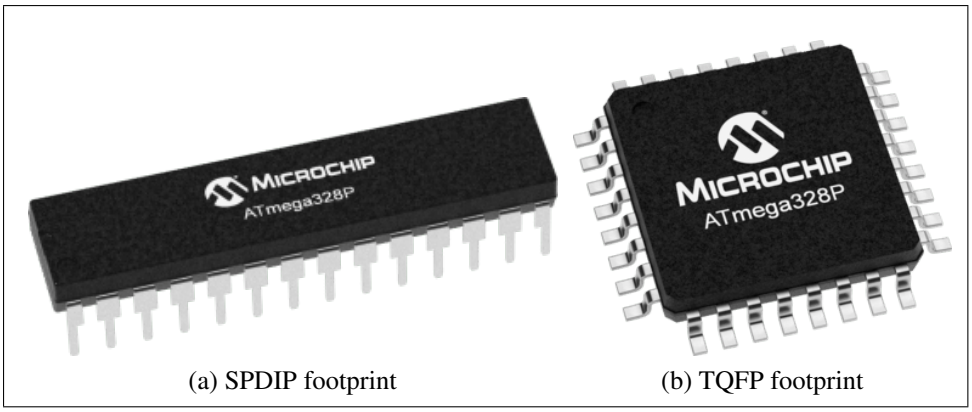

(a) SPDIP footprint (b) TQFP footprint

Figure 3.13: The ATmega328P microcontroller in 2 different footprints: (a) PDIP, and (b) TQFP.

3.3.2 Sensor Interfacing Circuitry

Since there is no way for the microcontroller to directly obtain the resistance values of thermistors, a thermistor-resistor circuit was required in order to get a voltage response to the resistance change in the thermistors. There were various circuit designs that would suit this application, including a constant current source powering the thermistor, the Wheatstone bridge and series-connected resistance circuits. The voltage responses of these circuit designs will be discussed in detail in the following sub-sections, outlining the strengths and weaknesses that they entail.

3.3.2.1 Constant Current Source

The simplest way to be able to acquire the resistance value of a thermistor is by passing a constant current of known value through it and reading the voltage across it. By then using Ohm's law, the resistance of the thermistor can be extracted as shown in Equation 3.4, and converted to temperature using the resistance-temperature data from the datasheet.

$$V_{out} = I_s \times R_T \tag{3.3}$$

Rearranging for R_T:

$$R_T = \frac{V_{out}}{I_S} \tag{3.4}$$

The most advantageous aspect of this circuit is that the only component in the circuit is the thermistor itself, as shown in Figure 3.14. Given that the circuit is composed solely of the current source and the thermistor, there will be no added errors as a result of component tolerances, and the voltage response will follow the non-linear resistance response of the thermistor, similar to what was previously shown in Section 3.2.3.

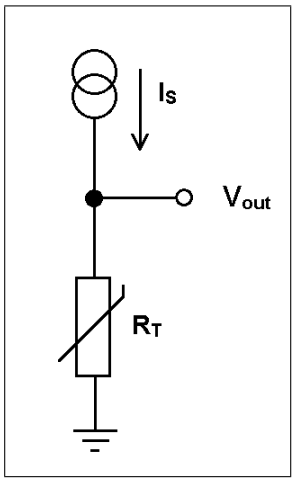

Figure 3.14: The measurement circuit using a constant current source.

In order to take advantage of the low component count of this circuit, the numerous thermistor sensors must be connected in series to a single current source. With such a configuration, a breakage in any part of the insole or sock circuitry would disconnect the entire circuit and no measurements would be taken. Therefore, in order to avoid a high component count and added cost to have dedicated current sources for each thermistor sensor, other circuit configurations using voltage sources were considered. In this way, the thermistor sensors are independent of each other, and if there is a disconnection of a single sensor, the remainder of the circuit is still functional.

3.3.2.2 Wheatstone Bridge

The Wheatsone Bridge circuit was originally designed in 1833 by Samuel Hunter Christie, but was later studied and improved by Charles Wheatstone in 1843. It was intended as a means of measuring resistance values, and even though in this day it has been replaced by the digital multimeter, it is still the method of choice to measure resistance values in the milli-ohm range. However, it is nowadays also very common as a means of interfacing sensors and transducers to amplifier and ADC circuits. The concept behind the Wheatstone bridge is that there are two series resistor branches connected in parallel – branches ACB and ADB in Figure 3.15. When the resistances in these two branches are equal, the voltage at points C and D are equal and hence no current would flow. A change in resistance in just one of the resistors will cause an imbalance and the voltage between these two points would fluctuate from 0 V. Originally, this circuit would have made use of a galvanometer to measure the flow of current between points C and D when the circuit in unbalanced. Alternatively, this circuit is now used as a bridge circuit and an output voltage $\mathbf{V_{out}}$ is measured instead. In this way, the circuit can be interfaced to ADC circuits to digitize the readings using a microcontroller.

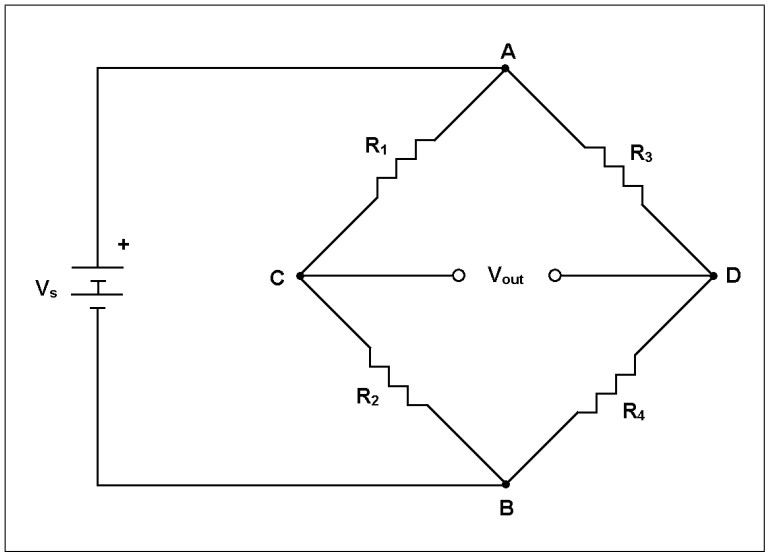

Figure 3.15: The circuit design for the Wheatstone Bridge.

Therefore, if resistor $\mathbf{R_4}$ were to be replaced by a thermistor $\mathbf{R_T}$, the change

in output voltage would be a result of the change in the thermistor's resistance as a result of temperature fluctuations. The relation between the output voltage $\mathbf{V_{out}}$ and the temperature **T** is as follows:

$$V_{out} = V_s\left(\frac{R_2}{R_1+R_2} - \frac{R_T}{R_3+R_T}\right) \tag{3.5}$$

Assuming R_1=R_3:

$$V_{out} = V_s\left(\frac{R_2}{R_1+R_2} - \frac{R_T}{R_1+R_T}\right) \tag{3.6}$$

Rearranging for R_T:

$$R_T = R_1\left(\frac{V_sR_2 - V_{out}(R_1+R_2)}{V_sR_1 + V_{out}(R_1+R_2)}\right) \tag{3.7}$$

As previously defined in Section 3.2.1.2:

$$\frac{1}{T} = \frac{1}{T_0} + \frac{1}{\beta}\ln\left(\frac{R_T}{R_0}\right) \tag{3.8}$$

Substituting for R_T:

$$\frac{1}{T} = \frac{1}{T_0} + \frac{1}{\beta}\ln\left(\frac{R_1}{R_0}\left(\frac{V_sR_2 - V_{out}(R_1+R_2)}{V_sR_1 + V_{out}(R_1+R_2)}\right)\right) \tag{3.9}$$

Setting R_1=R_2=R_3=R_b:

$$\frac{1}{T} = \frac{1}{T_0} + \frac{1}{\beta}\ln\left(\frac{R_b}{R_0}\left(\frac{V_s - 2V_{out}}{V_s + 2V_{out}}\right)\right) \tag{3.10}$$

By using the relationship defined in Equation 3.10, the voltage measured by the microcontroller can be translated into the temperature values that are sensed by the

thermistor. Alternatively, for the range of temperature of interest (in this project's case between 10 °C and 50 °C), a curve or straight line can be fitted to the Wheatstone circuit voltage response shown in Figure 3.16, and the respective equation used to convert voltage readings into temperature. Approximation errors will vary depending on the degree of the polynomial curve being fitted, with the greatest error being introduced when using a straight-line approximation.

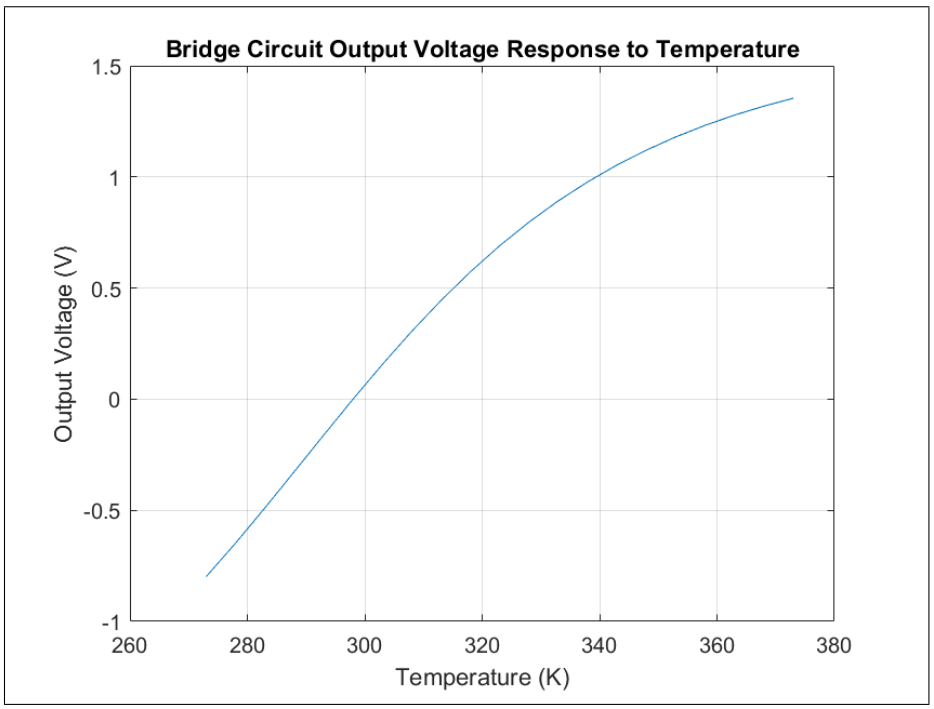

Figure 3.16: The Wheatstone Bridge voltage response to temperature.

There are various benefits to using the bridge circuit to interface resistive sensors with ADC circuitry. Not only does the Wheatstone bridge offer great precision in measuring the resistance change, but it is especially suited to sense the slightest change in resistance. This is essential for sensors whose resistance varies only slightly from the nominal value, as in the case of strain gauges. However thermistors' resistance varies highly with temperature, and the high sensitivity of the Wheatstone bridge is lost on such an application. Additionally, since the bridge circuit has a low amplitude output signal, an amplifier is necessary to boost the output signal. Therefore, other circuit configurations might be worth considering, as they might provide adequate sensitivity while keeping the circuit footprint to a minimum.

3.3.2.3 Series-Connected Resistance Circuit

The series-connected circuit, more commonly known as a potential divider circuit, requires only a single additional resistor to be able to acquire a voltage response from the thermistor, as illustrated in Figure 3.17.

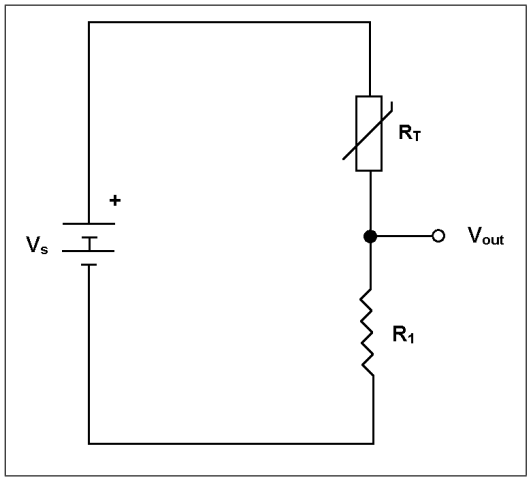

Figure 3.17: The circuit design for the voltage divider.

The circuit does not offer any linearisation of the thermistor's response to temperature, but as can be seen in Figure 3.18, the response is relatively linear close to the midpoint of the curve, around the 300 K (27 °C) point. Therefore, depending on the range of temperatures of interest, the response can be assumed to be linear, and a relationship between output voltage $\mathbf{V_{out}}$ and temperature $\mathbf{T}$ can be easily extracted for the conversion of readings.

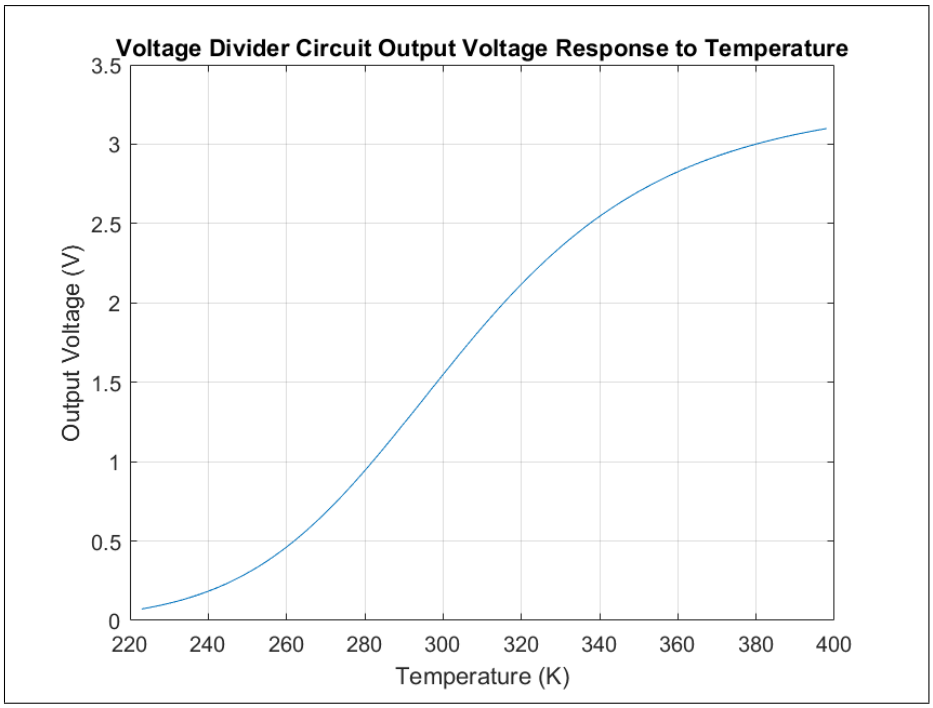

Figure 3.18: The voltage divider response to temperature.

Another option would be to use the voltage divider response function in Equation 3.11 and rearranging for the thermistor resistance $\mathbf{R_T}$ (Equation 3.12). In this way, the resistance values can then be converted into temperature by using the temperature-resistance data from the datasheet provided by the manufacturer.

$$V_{out} = V_s\left(\frac{R_1}{R_1 + R_T}\right) \tag{3.11}$$

Rearranging for R_T:

$$R_T = R_1\left(\frac{V_s}{V_{out}} - 1\right) \tag{3.12}$$

For the temperature range of interest for this application, the thermistor resistance will vary by approximately 13.7 kΩ across the scale, with 200 Ω being the smallest change in resistance over 1 °C. This makes the sensitivity of the Wheatstone bridge somewhat redundant, while making the series-parallel circuit, with its low component count, the more appealing option.

3.3.3 ADC Selection

Having established that the voltage divider is the most suited sensor interfacing circuit for this application, an external ADC was required to convert these output voltages. The built-in ADC of the ATMega328P microcontroller could not be used because it only has 8 input channels, with a 10-bit resolution. The ideal solution would be an ADC with 30 input channels, but unfortunately this is not a common specification. The 32-channel ADCs that were found were of the current-input type and would cost four times more than using four separate 8-channel ADCs. Additionally, they were only available in the ball grid array (BGA) package, which would limit soldering to be done only in a reflow oven. The alternative solution would be to have multiple ADC ICs, which would still be able to convert the 30 analogue signals from the thermistor sensors. Other than the number of input channels available, another criteria that must be considered when selecting the ADC is its resolution. This defines the minimum voltage change that can be detected, and in turn specifies the thermal resolution of the system. With a minimum ADC resolution of 10-bits, the MCU would be able to sense voltage changes in the interfacing circuitry of 0.003 V when powered by 3.3 V or 0.005 V when operating on 5.0 V. In terms of temperature, taking into consideration the resistance range of the thermistors between 10 °C and 50 °C, the device would be able to sense temperature changes of 0.107 °C and 0.118 °C for the 3.3 V and 5.0 V powered circuitry respectively. With this level of temperature sensitivity, the device would be able to measure temperature changes well within the range of 2.2 °C.

The ADC78H90 12-bit 8-channel ADC by Texas Instruments was chosen for this application. It is a low-power ADC with a successive approximation register architecture and having an integrated track-and-hold circuit. The IC can be powered with separate digital (DV_{DD}) and analogue (AV_{DD}) supplies, ranging from 2.7 V to 5.25 V. The range of the permissible analogue input voltages is within 0 V and AV_{DD}, which is thus set accordingly depending on the supply voltage of the circuitry. When using a 3.3 V supply, the input voltages are expected be within 1.03 - 2.15 V, and between 1.56 - 3.25 V for a 5 V supply, for the 10 - 50 °C temperature range. SPI communication is supported by the device, with an automatic power-down feature

when it is unused, reducing the overall power consumption. Even though the 16-channel ADCs were comparable in price and package type, it was decided to opt for the 8-channel to be able to distribute the components better when designing the PCB, utilising all the space on both sides of the board.

The chosen ADC utilises the SPI protocol for the transmission of data. This is a 4-wire communication protocol comprising of the serial clock (SCLK), master-out slave-in (MOSI), master-in slave-out (MISO) and slave select (SS) lines. The SPI data bus is synchronous, utilising a clock signal to keep all devices connected to the bus in sync and having a SS signal to trigger data transfer to/from the slave device. The latter is generally an ”active low” signal, meaning that its default state is ”logic high” and needs to be pulled low to initiate data transfer. Once in ”logic low”, the master outputs the clock signal and sends out data (generally a request command) to the slave via the MOSI line, and in turn the slave will return the requested data onto the MISO line. In the case where there are multiple slave devices, the clock and data lines are shared among all the devices, and separate SS signals are set up for each device, as illustrated in Figure 3.19.

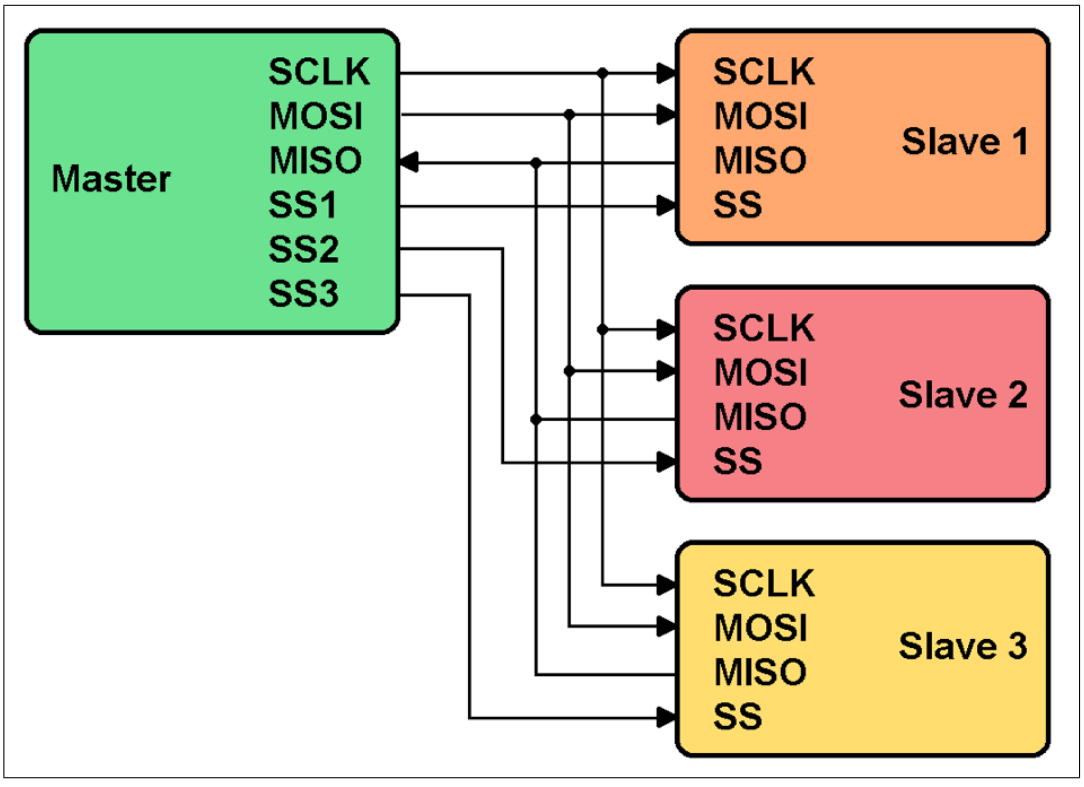

Figure 3.19: The SPI communication bus with a master and multiple slave devices.

This is the case in the circuit being designed here, except that there are four 8-channel ADCs connected to the bus. Data acquisition is initiated by the master pulling the SS signals low one at a time, and sending the channel addresses to the slaves for them to respond back with the converted voltages and reading them from the MISO line.

3.3.4 Signal Conditioning Circuitry

In order to get precise voltage measurements to the microcontroller, the voltage signals must be conditioned before being fed to the ADC. Unlike the Wheatstone Bridge, the output from voltage divider circuit does not require signal amplification to be measured. It is however essential to choose the correct value of the sensing resistor $\mathbf{R_1}$ so as to maximise the output voltage range. This is dependent on the minimum and maximum resistance values expected from the thermistor for the given temperature range of operation. The resistor value must be much larger than the thermistor's minimum resistance $\mathbf{R_{min}}$ but smaller than its maximum resistance $\mathbf{R_{max}}$ [79]. For temperatures ranging between 10 °C and 50 °C, $\mathbf{R_{min}}$ would be 4.417 kΩ and $\mathbf{R_{max}}$ would be 18.07 kΩ. Using Equation 3.13 [79] yields a resistance value of 8.93 k Ω for resistor $\mathbf{R_1}$.

$$R_{sense} = \sqrt{R_{min} \times R_{max}} \tag{3.13}$$

Theoretically, using this value for $\mathbf{R_1}$ yields an output voltage range of 1.17 V for the aforementioned temperature range. With the actual resistance value used of 8.2 kΩ, the output range was slightly reduced to 1.16 V. If the resistance value were closer to the limits of the thermistor resistance range, it would not only reduce this output voltage span further, but it will also shift the linear section of the curve. This is illustrated in Figure 3.20, where an increase or decrease in the resistance value of $\mathbf{R_1}$ is seen to shift the linear mid-section of the curve to a lower or higher temperature respectively. This would increase the margin of error of the voltage-to-temperature conversions when using a straight line approximation of the circuit output response curve.

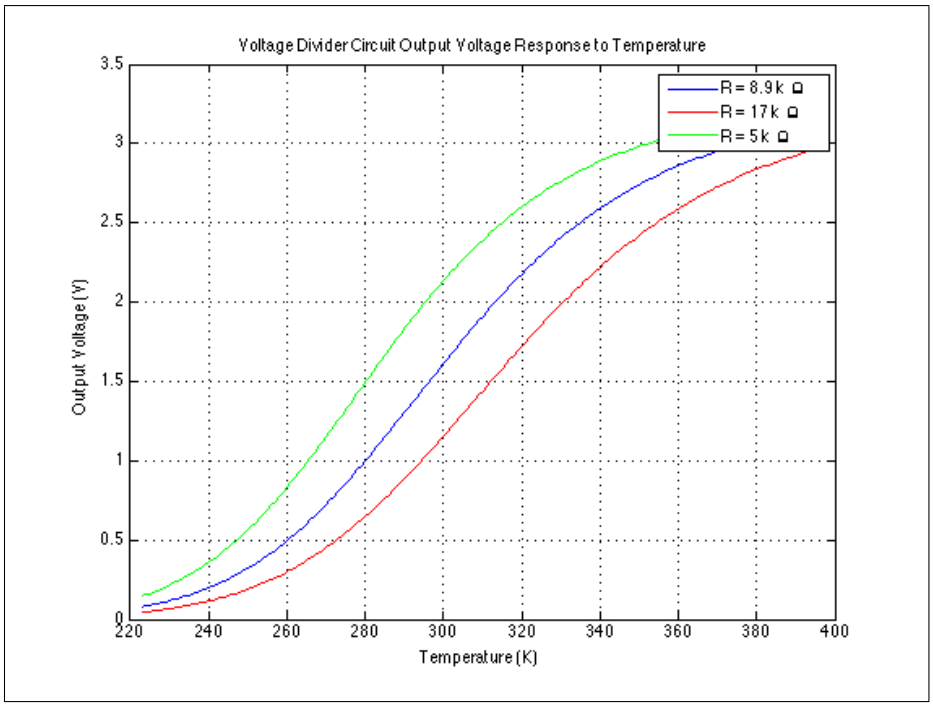

Figure 3.20: The effect of resistor value on the circuit output.

In the first circuit design, the output from the voltage divider circuit was fed directly to the ADC. During testing, it was found that further signal conditioning was required as noise components within the signals were causing erratic erroneous readings within the system. A first order active low-pass filter was included in the updated design so as to block out any high-frequency noise components induced onto the signal from the surrounding circuitry. Since the output from the voltage divider is a steady DC voltage signal which varies slowly over time, the filter was designed with a low corner frequency of 10 Hz. This low corner frequency also made sure that signal components at the Nyquist frequency and above are attenuated, so as to avoid aliased components from being sampled.

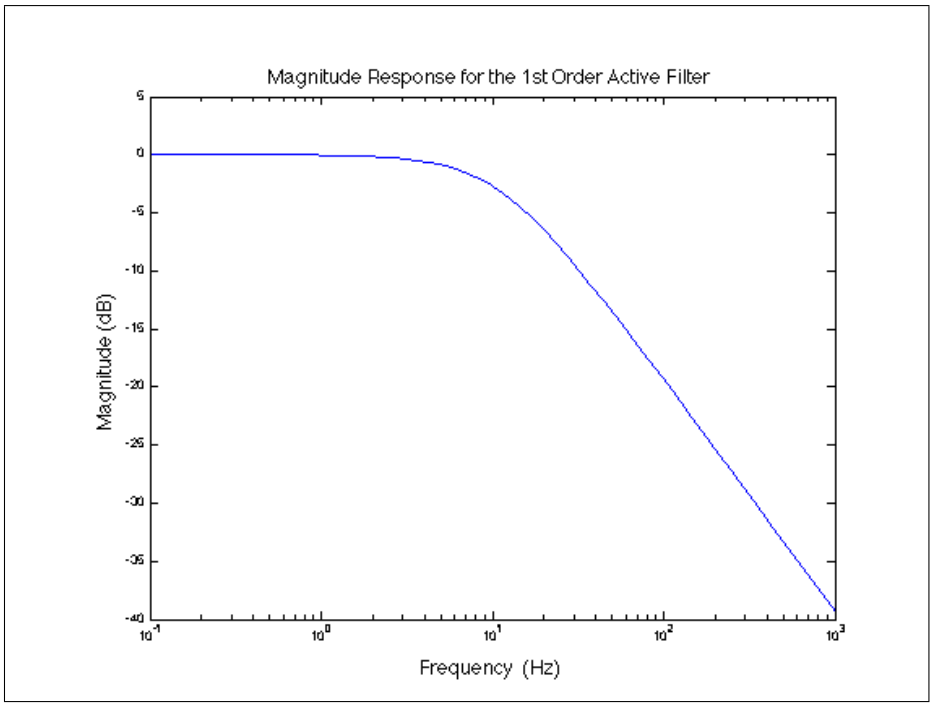

Figure 3.21: The magnitude response of the 1st order active filter.

In addition to filtering out noise, it is also beneficial to have the input signal buffered and coupled to the ADC input channel. In general, multi-channel ADCs simply multiplex numerous input channels to a single converter as shown in Figure 3.22. A sampling capacitor charges up to the voltage of a particular input channel and holds the charge for the period of time required for the conversion to take place and for the digital data to be clocked out. For the consecutive reading, that sampling capacitor must charge/discharge to the voltage of the next channel in a very short period of time. To do so, the input impedance to the ADC must be below a certain threshold. When connecting the voltage divider circuit directly to the input channel, this threshold might be exceeded and the sampling capacitor might have some residual charge from the previous reading. One way around this problem is to have an external charge reservoir capacitor, much larger than the sampling capacitor. When the sampling capacitor switches to a different channel and becomes essentially connected in parallel to the external capacitor, the latter charges up the sampling capacitor instantaneously.

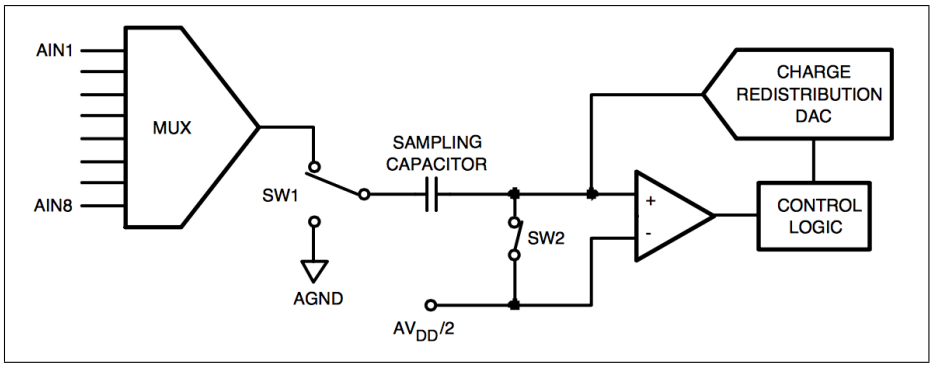

Figure 3.22: The internal structure of a multi-channel ADC (adapted from the ADC78H90 datasheet).

The op-amp from the preceding 1st order filter will act as a buffer to the external capacitor. This will reduce the impedance seen by the capacitor, which will keep the charge times short and enable faster sampling rates. Since op-amps are ideally not loaded with capacitive loads, a resistor is included before the capacitor [80]. This basically results in an RC filter being implemented in between the filter and the ADC, as illustrated in Figure 3.23. The addition of these conditioning circuits to the signal help to have more stable readings. This is not only attributed by the attenuation of high-frequency noise signals, but also by an improved performance of the ADC.

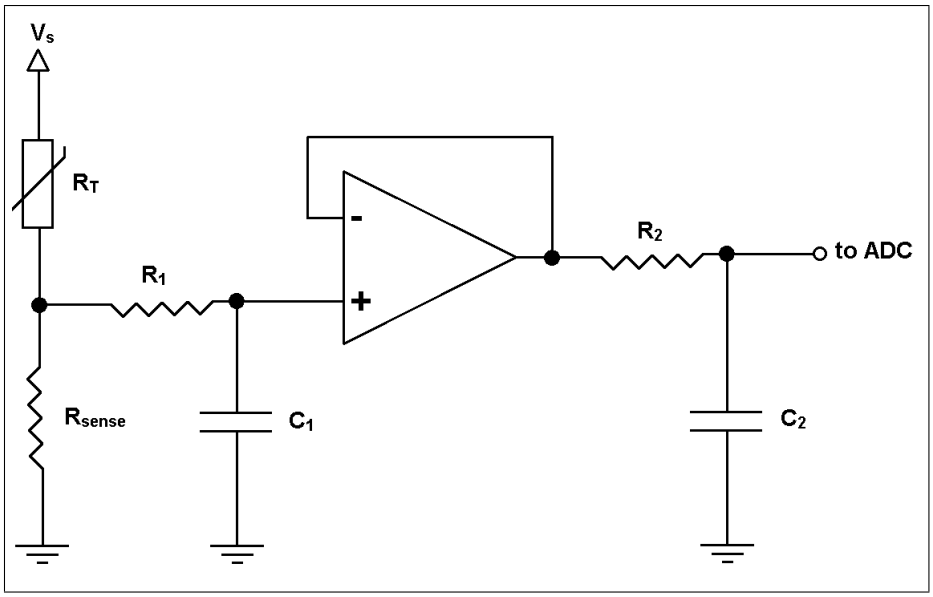

Figure 3.23: The signal conditioning circuitry leading to the ADC.

3.3.5 Saving to the memory card

The circuitry was required to support other auxiliary functions, such as saving to a memory card. The micro SD card is the smallest memory card available on the market. It utilises the SPI bus, with the respective pinouts illustrated in Figure 3.24. No intermediary circuitry is required for the microcontroller to be able to communicate with the memory card, given that the circuit operates within the required voltage range. SanDisk, Toshiba and Transcend define the operational voltage of their SD cards within the 2.7 V and 3.6 V range. Therefore, opting for a 3.3 V circuit voltage will help to reduce the circuit size and cost by avoiding the use of logic level shifters between the microcontroller and SD card.

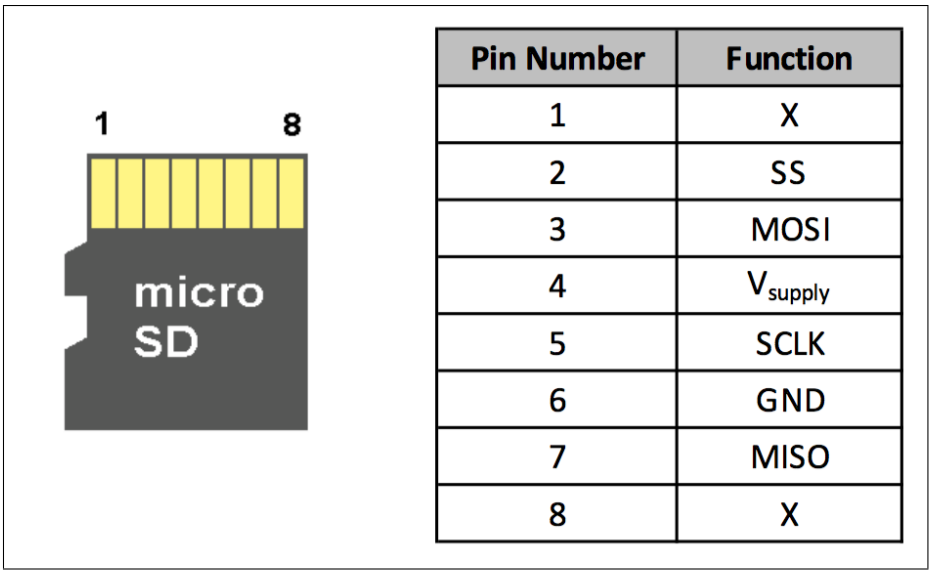

Pin Number	Function
1	X
2	SS
3	MOSI
4	V_{supply}
5	SCLK
6	GND
7	MISO
8	X

Figure 3.24: The SD card pinout configuration.

3.3.6 Wireless Data transmission

Since data logging onto a memory card will only provide data for analysis after a recording session, it is vital to have a means of evaluating the data in real-time while the device is in use. The best option for this is to have a means of wireless communication and avoid any further cabling in the system. There are various technologies that can be used for this purpose, including Wi-Fi, Bluetooth, cellular

data and radio frequency (RF) communication. Each of these methods have their strengths when compared to one another, but it is essential to find the one most suited for this application with regards to power consumption, range of communication, cost, and device compatibility. When considering cellular data and RF communication, there are immediate drawbacks that make them the least ideal choices. The former requires an active GSM connection which is costly to maintain, whereas the latter cannot be used to transmit data to other devices (PC, tablet, or smartphone) without any additional hardware on the receiving device's end.

On the other hand, both Bluetooth and Wi-Fi are standard in every device nowadays, and even though Wi-Fi was not originally designed for communication between devices, it can still provide such a function via Wi-Fi Direct. This enables peer-to-peer communication even when there isn't a network hub which both devices are connected to, enabling data transfer between devices just like Bluetooth. The main differences between the two are data transfer speeds, signal range and power consumption. Whereas Bluetooth loses the transfer speed and signal range battles, it is the more power efficient of the two and is the easiest to set up. As any other wearable gadget used in conjunction with a smart device, signal transmission ranges are generally quite small and the size of data transmitted can easily be handled with Bluetooth. It therefore makes sense to opt for Bluetooth in this case as well, with the added benefit of increasing the battery life of the device.

Bluetooth operates at 2.4 GHz, same as Wi-Fi, but differentiates from it in the way that the connection between devices is established. It uses a master/slave model, where one master device controls when to send or read data from the other slave devices it is connected to. Every Bluetooth device is identified by a unique 48-bit address, generally represented as a 12-digit hexadecimal value [81]. This address is used to pair devices together and establish a connection through which data can be transmitted. Nowadays, there are two main types of Bluetooth: Bluetooth Classic and BLE, both of which share the specifications previously described. The main difference is that Bluetooth Classic establishes a connection and is able to stream continuous data, whereas BLE is generally in sleep mode and activated when data is requested from the device. This is what enables BLE's low power

consumption, since it is designed for periodic data communication and goes into a low power idle mode when not transmitting data. For this reason, Bluetooth Classic is still the go-to communication protocol for audio streaming applications such as wireless headphones and speakers, since continuous data transmission is a must [82].

Considering that body temperature fluctuations are not very fast, the temperature data from the feet can be read and transmitted periodically. Without the need for continuous data streaming, BLE is more suited for this application as it consumes less power without impeding the frequency of data transfer. There are various BLE modules that were designed to enable microcontrollers with Bluetooth functionality, such as the HM-10 module depicted in Figure 3.25. This module houses the TI CC2541 System-On-Chip (SOC) solution, which has an integrated RF transceiver for BLE and proprietary 2.4 GHz applications [83]. Communication to the module is done via the universal asynchronous receiver/transmitter (UART) protocol, which enables serial communication using only two data lines. This protocol only allows two devices to communicate to one another, connecting the Transmit (Tx) pin from one device to the Receive (Rx) pin of the other, and vice-versa. As the name suggests, transmission is asynchronous and no clock signal is used to synchronise the transmission and reading of data at both devices. Instead, *Start* and *Stop* bits are added to the data being transmitted to let the receiver know that there is new data to be read and when it has been completely transmitted. The speed of transmission is defined by the set Baud Rate, and both devices need to be set up at the same setting to be able to communicate with one another.

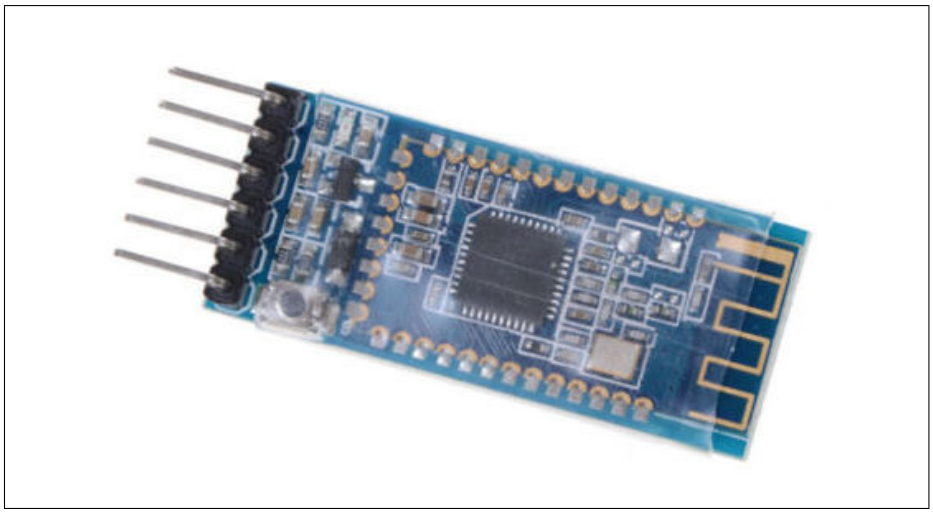

Figure 3.25: The HM-10 BLE module.

Whereas Bluetooth Classic would establish a connection between two Bluetooth devices and have data continuously sent between the two, BLE uses a different structure. The BLE protocol is a structure that is composed of three main blocks; the application, host, and controller as shown in Figure 3.26. Each block contains different layers with specific functions for data transmission over BLE. The physical layer (PHY) is the hardware that enables and defines the general parameters of the wireless data transmission. The Link Layer (LL) is composed of software and hardware, and interfaces directly with the hardware to control the type of communications between BLE devices. The Host Controller Interface (HCI) is the protocol that controls data communication between the Controller block and the Host, which is the core of the structure. This data is fed to the Logical Link Controller and Adaptation Protocol (L2CAP), encapsulating it into data packets for the upper layers. Similarly, it fragments data packets from the upper layers into raw data to be transmitted out via the lower layers of the stack. The Security Manager Protocol (SMP) manages the security of the data, encrypting and decrypting the packets. It also takes care in establishing the master and slave roles within a connection, once this is established. The Generic Attribute (GATT) Profile encases the Attribute Protocol (ATT), which is responsible for organising the data into attributes, that are identified by a Universally Unique ID (UUID) and have an assigned value and set of permissions. The GATT further organises these attributes, referred to as characteristics, into services, which are visible to the client to determine where data is

read from and written to. These characteristics not only contain a data value, but also have specific properties that define the possible functions to the client. A characteristics can be *broadcast*, *readable*, *writeable* and *notifiable*, whereby the client is notified by the server that new data is available to be read. There are standard services and characteristics identified by a 16-bit UUID, but BLE also provides the possibility of creating custom services identified by a 128-bit UUID. The final layer, the Generic Access Profile (GAP), provides an interface between the user and the entire stack structure, managing the connection for data transfer over BLE [84].

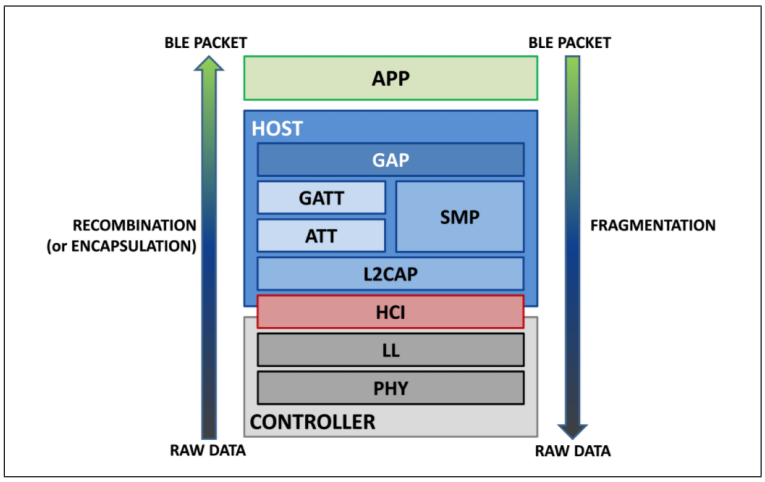

Figure 3.26: The BLE protocol stack structure, composed of the three main blocks: the Application (green), the Host (blue), and the Controller (grey) (adapted from [85]).

The second circuit prototype that was designed utilised BLE communication to transfer data wirelessly to the smart device. One of the predefined services was used in order to send the comma-separated data representing the sensor voltages and reading count. The Notify property was used so that the designed Android application would read the data as soon as it is available, processing it and then displaying it accordingly.

3.3.7 Board Prototypes

Throughout this project, there were two circuit designs that were done. Both of them supported the the previously discussed functions of reading sensor signals

and saving/transmitting the processed data. The main differences between the two were the size and weight of the design, and the level of signal conditioning incorporated in the circuit.

3.3.7.1 Prototype 1

In the first circuit design, certain component choices did not assist in keeping a small footprint. The ATMega328P chip was the 28-pin dual in-line package (DIP) type, which as can be seen in Figure 3.27, was one of the largest components on the PCB. The two other components with an even larger footprint were the 40-pin and 26-pin IDC connectors used to connect the sensors incorporated in the insole. These, along with all the other components within the circuit were fitted onto a PCB measuring 70 mm by 105 mm. The whole system was encased in a box 130 mm wide and 70 mm long, with a depth of 45 mm to also hold the battery underneath. The circuit was powered by a 7.4V 2400 mAh Li-ion battery, measuring 75 mm by 35 mm by 20 mm and weighing 110 grams. Even though these might seem small-scale, they were found to be quite detrimental to the system's portability when attached to a person's ankle.

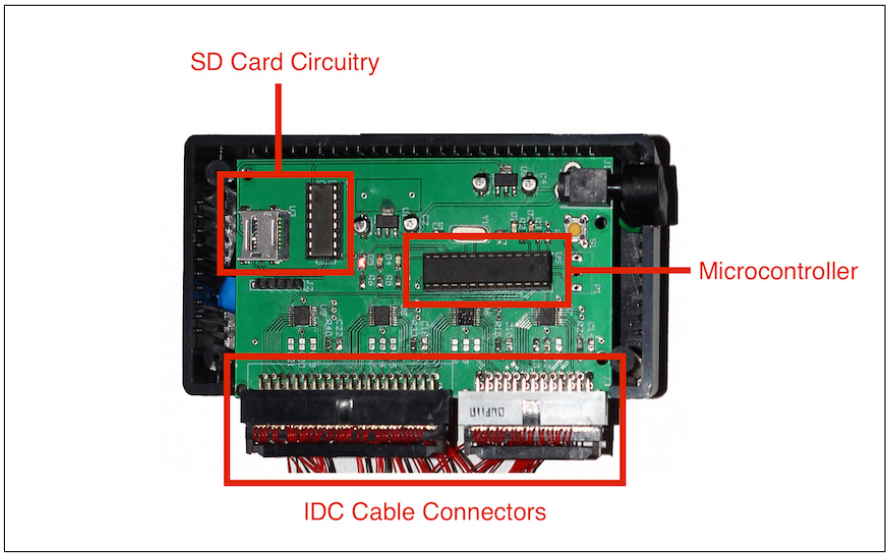

Figure 3.27: The first acquisition module design.

From a circuit design perspective, certain decisions had a negative impact

on both the size of the circuit as well as its performance. The majority of the circuit was operated at 5.0 V, with the only exception being the SD-card, which can only be operated at 3.3 V. This not only raised the need for an additional voltage regulator, but it also required a logic level shifter to scale down the SPI signals sent from the microcontroller. For this design, the filtering stage was omitted, and the voltage divider output was fed directly to the ADCs.

As mentioned earlier in Section 3.2.3, the first board was designed as a means of circuit evaluation and sensor testing. It proved useful in being able to capture data from the array of sensors when tested within a temperature chamber. Some dynamic testing was also done with the system to test out the various sensory platforms, but its weight and size proved that a re-design was imperative for testing on healthy subjects.

3.3.7.2 Prototype 2

In trying to rectify the shortcomings of the initial design, a second board prototype was designed. With the main aim of reducing the system's weight and size, a lot of the large components were replaced by more space saving alternatives. One of the main contributors to the weight of the system was the battery, and a smaller alternative had to be chosen. The majority of our portable devices nowadays are powered by 3.7 V batteries, which meant that the entire circuit would need to operate at 3.3 V. The advantages of opting for an operational voltage of 3.3 V rather than 5.0 V were two-fold. Firstly, it opens up the option for a lot of these smaller and lighter batteries that are available, and secondly, it would avoid the need for a logic level shifter for data transmission to the SD-card. However, with a smaller battery there would also be reduction in the system's battery life. A compromise had to be reached whereby trimming down the size of the battery did not result in an insufficient charge capacity. The most suitable option was a 3.7 V 1200 mAh Li-ion battery, which offered half the capacity at 45% the weight and 20% the size of the original battery. Another component that was reviewed for replacement was the sensors' IDC connector. A more compact solution was required, having denser connections but still

providing the same level of robustness. A similar type of board-to-cable connector was found, having 68 connections within the same length as the 40-pin connector that was used previously.

Within the circuit design, there were a few additional circuits that were incorporated to improve performance as well as ease of use. A charging circuit was included, making it possible to recharge the battery via a USB connection to the system rather than disconnecting the battery and charging it separately. Moreover, the filtering stage was implemented in this design so as to clean and buffer the signals before being fed to the ADCs. Even though there was an increase in the number of components with these added circuits, the overall size of the PCB was reduced. The newly designed 80 mm by 60 mm PCB was fit in a 95 mm by 70 mm by 25 mm 3D printed case shown in Figure 3.28. This was possible by opting for smaller IC packages where possible, and for better distribution of components on both sides of the PCB. In this design, the same microcontroller was used but selected the surface mount 32-pin TQFN package, which has a footprint approximately 3.5 times smaller than the through-hole equivalent used before.

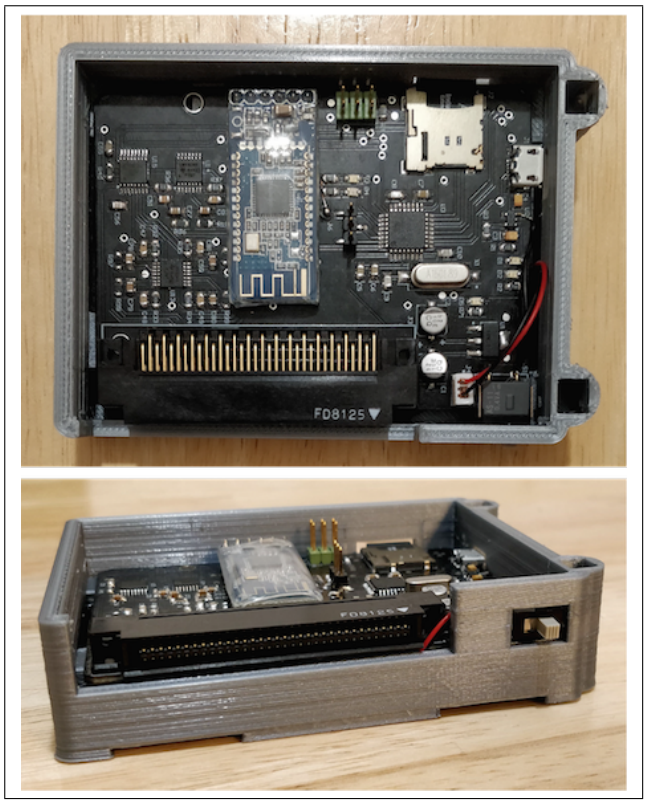

Figure 3.28: The second acquisition module design.

In order to improve battery life, a Bluetooth 4.0 dongle was used instead of the Bluetooth 2.0 used in the first design. As described earlier, this provided the option of using BLE, which consumes less power by suspending the connection when no data is being transmitted. The system was tested for battery life, and lasted well over 13 hours. This would provide a full day's usage on a single battery charge, which is ideal for a system designed to monitor the foot temperature throughout a person's day. Further testing was also done to validate the performance of the system as whole, which is outlined in Chapter 4.

3.4 Software

Any digital system requires not only hardware to function, but software to control functionality and provide a user interface. The system designed here is no different. There was embedded software programming of the microcontroller to be able to perform the desired functions within the system. In addition to that, graphic software was also designed to display the data being captured to the user for analysis.

3.4.1 Embedded Software

The ATMega328P can be programmed either in Assembly or in C, with the latter being the programming language of choice. The first circuit design was programmed using Arduino, since the MCU in the DIP format could easily be transferred from the Arduino board onto the designed PCB. In order to be able to do so, the microcontroller chip had to have the Arduino bootloader burnt into it. This is basically a small code that runs upon power up, which is responsible for deciding whether the processor should run the code stored in its FLASH memory or if it will be receiving new code for re-programming. It is very common to purchase the ATMega328P DIP with the Arduino bootloader readily burnt into it. Without the bootloader present, the microcontroller can only be programmed using a dedicated hardware programmer.

For the second designed circuit, using the ATMega328P in TQFP format, programming could not be done by swapping the IC between boards. Since the microcontroller would be soldered directly to the PCB, programming would need to be done slightly different. Firstly, the bootloader would need to be burnt into the MCU to then enable programming through universal asynchronous receiver/transmitter (UART). Even though some might argue that the use of a bootloader wastes resources from the microcontroller, it did not make much of a difference in this case. Not having a bootloader on the chip frees up only 0.5 kB from the 32 kB of FLASH memory, which in this case was not a limiting factor. Additionally, the slight delay caused by the bootloader running on power-up does not affect the performance of the system here.

The programming for the two boards was identical, except for a few changes in the selected pinouts depending on the board layout. The program utilised the SD library for interfacing with the memory card, but all the other functions were programmed manually at register level. This helps to have a more compact code and for it to run more efficiently. Within a single iteration of the whole program, data is read multiple times from every ADC and then fed to an average filter before being stored into the SD card and transmitted over Bluetooth. All these functions are managed by the microcontroller, but it is only able to provide raw data to the user. In order to understand this data in the context of foot temperature, other software was designed to present this data in a more meaningful way.

3.4.2 Graphic Software

One of the data representation tools that was designed was an Android application that could be run on a smartphone or tablet. The programme layout is shown in the flowchart in Figure 3.29. It utilises the data transmitted over BLE and translates it into temperature values. These temperatures are then represented superimposed over images of the two feet in the form of coloured spots, as shown in Figure 3.30. These coloured spots will vary in colour depending on the temperature value read by the respective sensor. The application has three main tabs; the one in

Figure 3.30(a) used to compare the temperatures at contralateral sites on the foot, and the other two, one of which is illustrated in Figure 3.30(b), used to monitor the temperatures of the left and right foot.

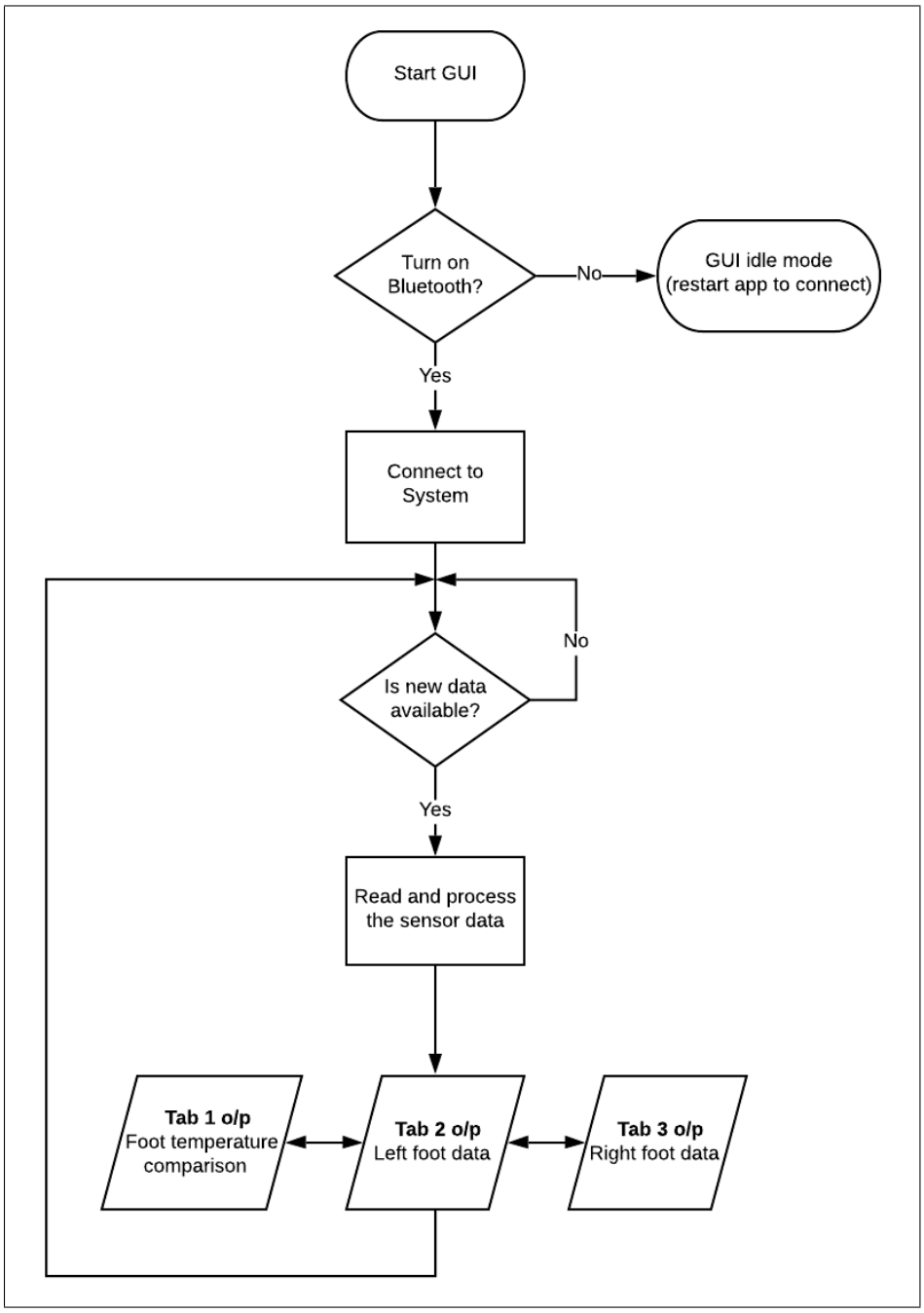

Figure 3.29: Flowchart illustrating the processes within the Android application.

This tool was mostly designed for real-time monitoring of the temperatures while the system is in use. It is a vital tool for the user to be able to monitor the

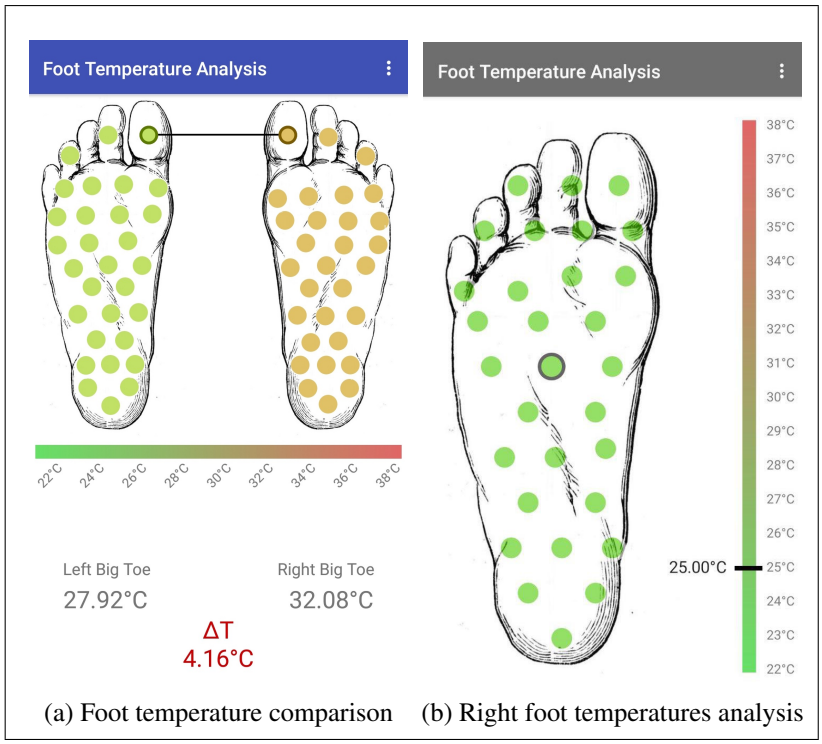

(a) Foot temperature comparison (b) Right foot temperatures analysis

Figure 3.30: Screenshots from the designed Android application: (a) The application tab where the temperature difference between contralateral sites on the feet can be measured; (b) The application tab where the right foot temperatures can be analysed.

temperatures of their feet during their day. Following instructions from their physician, they would know how to react if temperature high-spots are developed. The application was also deemed useful during data collection, as it could be used while the subjects were conducting the walk trials. It helped to identify any sensor breakages during the walk, and to also get a general idea of the range of temperatures being recorded across the subjects.

Since the temperature data is being presented as 30 discrete temperature spots, there was still the need to obtain a better thermal representation. For this reason, another tool was designed in Matlab, whereas the temperature data was interpolated and a temperature map is output. The data from the whole recording period is used to create an animation depicting the changes in temperature along the foot, as in Figure 3.31. This gives a clearer representation of the distribution of temperature along the sole of the foot, and how this changes over time. At this stage, no graphic user interface was designed for this tool. Loading of the data is done in-line through coding, which once run, produces the visual animation of the temperature maps.

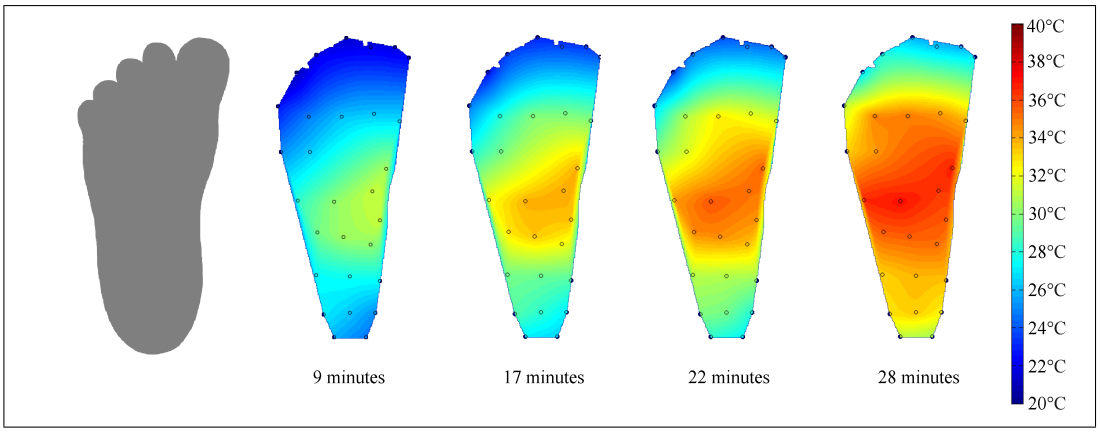

Figure 3.31: Snaps at different points in time of the output from the designed Matlab tool.

3.5 Summary

Once the hardware and the software design was finalised, the system was tested using various test setups. Chapter 4 will outline all the testing done on the separate components of the system, as well as the walking trials using healthy subjects conducted to validate the data captured by the system.

Chapter 4

Testing and Results

4.1 Introduction

The testing on the system was done systematically, making sure that the separate components making up the system performed correctly, before testing the system as a whole with healthy participants. It was required to:

1. Test the sensor performance using calibrated instruments to ensure correct temperature measurements.
2. Test the sensory platforms in dynamic environments to check their durability within the shoe environment and check the integrity of the measured temperatures.
3. Test the final system design in walk trials with healthy individuals to validate the recorded data and check the robustness of the system under real-life conditions.

All testing procedures and the results obtained are outlined in this chapter.

4.2 Sensor Testing

The sensors evaluation was done using the Heraeus Votsch VMT 04/35 climate chamber shown in Figure 4.1 (a). Temperatures within the chamber can be set from -40 °C to +180 °C, which covers the 15 °C to 50 °C temperature range required for testing. The temperature within the chamber was monitored using a calibrated Rotronic Hygropalm HP22 thermohygrometer as shown in Figure 4.1 (b).

(a) Climate chamber (b) Thermohygrometer

Figure 4.1: The hardware used for the static test setup: (a) the Heraeus Votsch VMT 04/35 climate chamber; (b) the Rotronic Hygropalm HP22 temperature and relative humidity (RH) meter

The sensors were tested while mounted on the insole as shown in Figure 4.2, since this made sure that the insole material did not have any negative effects on the sensor performance. Additionally, not only did it make it easier to have them placed on a uniform surface while in the chamber, but also guaranteed that all sensors had the same climatic exposure during testing. The data from the system was being logged onto an SD card and transmitted via Bluetooth to an Android device for monitoring during the testing period. The initial temperature was set to 15 °C, and increased in steps of 2.5 °C to a maximum of 50 °C. For temperatures closer to the body temperature, between 33 °C and 40 °C, the temperature was increased by 1 °C so as to have a denser array of measurements. The temperature within the chamber was left to settle for approximately 5 minutes before taking any sensor readings. A total of 100 sample readings were collected at every temperature setting.

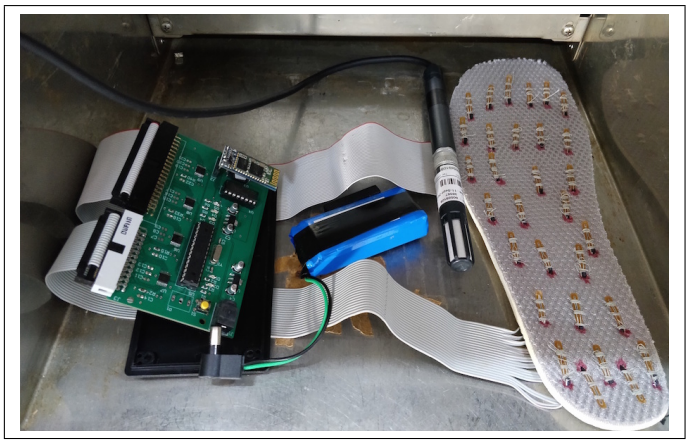

Figure 4.2: Placement of the system within the climate chamber, including the temperature/RH probe for climate monitoring.

From the recorded voltage readings, the resistance of the thermistor could be calculated. Knowing the exact temperature inside the climate chamber, the validity of the sensors could be assessed by comparing their resistance at a particular temperature with the data found in the sensors' datasheet. The assessment was done on the basis of correlation and limits of agreement (LoA) between the values defined by the datasheet and the results obtained from every sensor. Correlation was evaluated using the intraclass correlation coefficient (ICC), which is widely used in measuring the reproducibility of quantifiable measurements done by different methods or equipment [86]. The calculation gives a single measure r value between 0 and 1, with an ICC close to 1 signifying a high similarity between the two measurement methods. Koo and Li [86] gave the following guidelines for the interpretation of the ICC measures:

- $<$ 0.5 - poor reliability
- 0.5 to 0.75 - moderate reliability
- 0.75 to 0.9 - good reliability
- $>$ 0.9 - excellent reliability

On the other hand, the limits of agreement are estimated by the Bland-Altman plot. This is a scatter plot of the mean of the two measurement methods on

the X-axis and the difference between the measurements on the Y-axis. It visually represents the mean difference between the measurement methods, defined as the bias, and the 95% limits of agreement [87]. The latter are calculated as shown in Equation 4.1 below:

$$\text{LoA} = \text{Mean Difference} \pm (1.96 \times \text{Standard Deviation of differences}) \tag{4.1}$$

Good levels of agreement are represented by a low bias and a narrow LoA band. In practical terms, this means that the resistances measured from the sensors at specific temperatures should vary within a small range from the values defined in the datasheet.

25 ATC Semitec 103JT sensors were tested within the chamber, their resistance values calculated from the recorded voltage readings at varying levels of temperature. The ICC and LoA results are given in Table 4.1, listing the single measure *r* values and the mean difference with standard deviation, along with the lower boundary (LB) and upper boundary (UB) of the 95% Confidence Interval of each. The results for the full range of tested sensors can be found in Appendix D.

Table 4.1: Correlation and Level of Agreement results for worst (S_{14}-S_{15}) and best (S_{24}-S_{25}) performing thermistors.

Sensor #	**ICC**			**LoA**		
	Single Measure r	**95% CI**		**Mean Diff (± SD)**	**95% CI**	
		LB	**UB**		**LB**	**UB**
S_{14}	0.996	0.774	0.999	-0.269 (±0.148)	-0.560	0.022
S_{15}	0.997	0.765	0.999	-0.261 (±0.138)	-0.531	0.010
S_{24}	0.999	0.985	1.000	-0.132 (±0.126)	-0.379	0.114
S_{25}	0.999	0.974	1.0000	-0.149 (±0.123)	-0.390	0.092

When plotting the Bland-Altman plot for the thermistor sensors, it was found that the variance of the difference in resistance increased with an increasing mean resistance value. From Figure 4.3(a), it can be seen that the vertical spread of points for thermistor S1 is narrower towards lower mean resistance values than it is at the higher end of the range. When verifying the normal distribution of the differences in resistance, it was found that these are not normally distributed as the *P* value from the Shapiro-Wilk test was less than 0.05. Therefore, in order to assess the limits of agreement in the results, the natural logarithm of the data was used [87]. When plotting the Bland-Altman plot for the natural logarithm of the resistances for the thermistor S1, the vertical spread of differences is more uniform across the range of means as seen in Figure 4.3. The Bland-Altman plots for all the sensors can be found in Figures D.1 - D.25 in Appendix D.

From the obtained resistance value, the percentage difference from the target resistance value in the datasheet was calculated. Table 4.2 lists down the minimum and maximum percentage difference throughout the tested temperature range for best and worst performing sensors. The full data is included in Table D.2 in Appendix D.

Table 4.2: The maximum and minimum resistance percentage differences for four of the sensors under test.

Sensor #	Minimum % difference	Maximum % difference
S_1	0.23	4.80
S_2	1.49	5.68
S_3	1.77	6.28
S_4	0.93	4.99

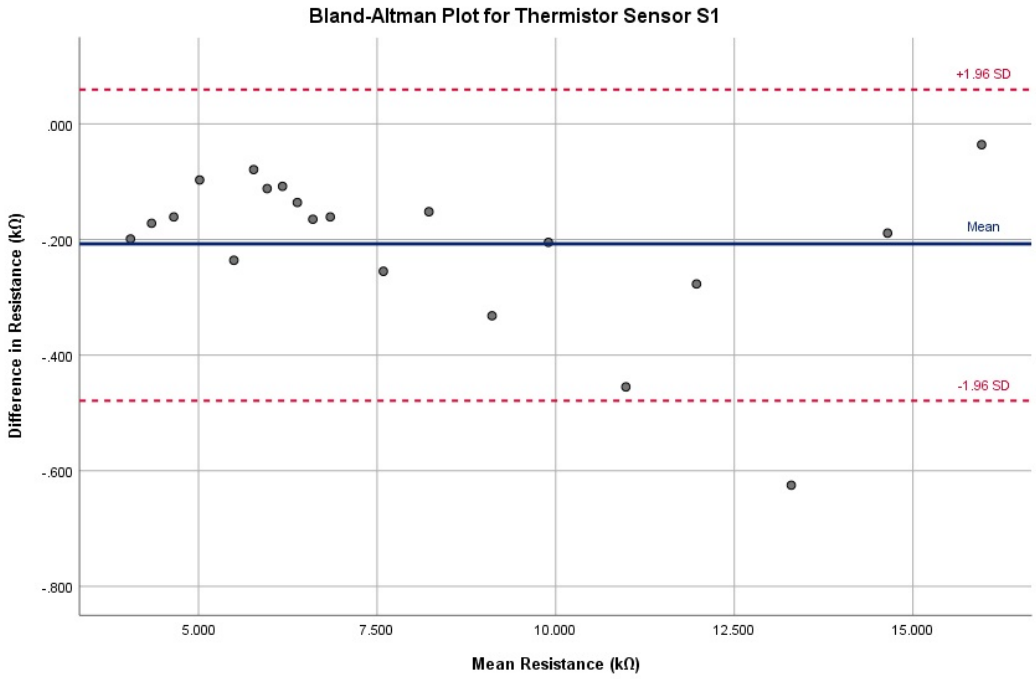

(a) Bland-Altman Plot for Resistance of S1

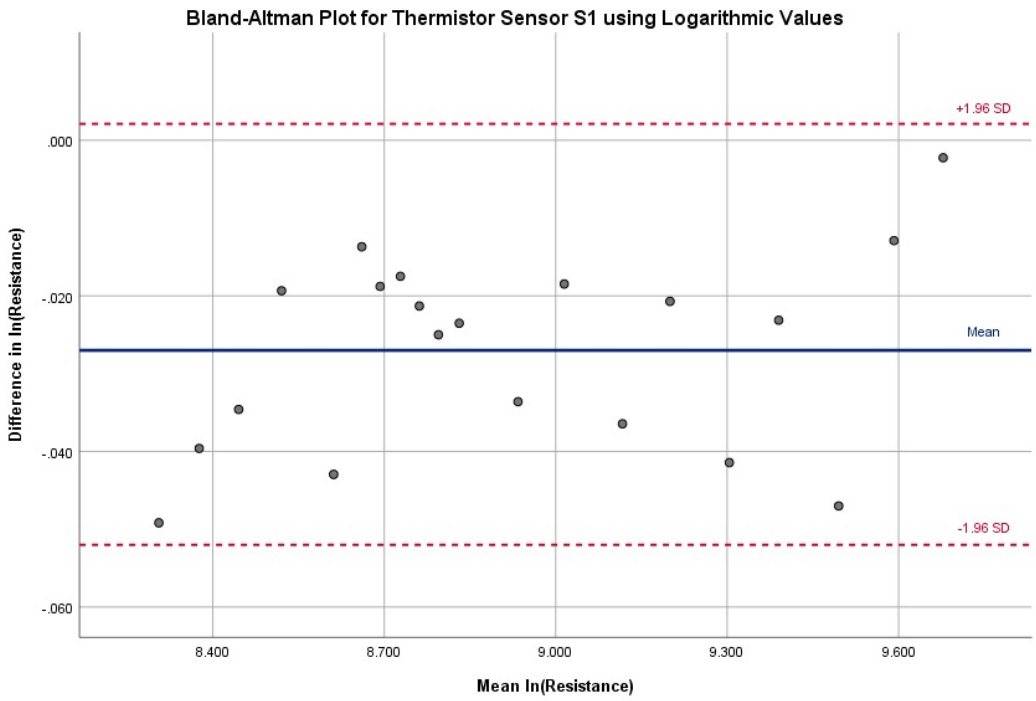

(b) Bland-Altman Plot for the natural logarithm of Resistance of S1

Figure 4.3: Bland-Altman Plots for Thermistor S1: (a) Plot using the resistance values of S1; (b) Plot using the natural logarithm of the resistance values of S1.

When comparing the temperature values measured by the sensors and the thermohygrometer, the differences vary across the range of temperatures of the test.

As seen in Table 4.3, the precision in temperature for four of the sensors under test varied from 0.01 °C (0.02%) up to 1.82 °C (5.76%). The full data is included in Table D.3 in Appendix D.

Table 4.3: The maximum and minimum temperature and temperature percentage differences for four of the sensors under test.

Sensor #	**Minimum Difference**		**Maximum Difference**	
	°C	**%**	**°C**	**%**
S_1	0.51	1.01	1.82	5.76
S_2	0.26	0.51	1.48	4.35
S_3	0.08	0.16	1.37	4.42
S_4	0.01	0.02	1.53	4.89

Since the data in tables 4.3 and D.3 illustrate the system's precision in measuring the absolute temperature within the chamber, it is also worth looking at how well the system quantifies a temperature change. By analysing the measured temperature differences between the steps of temperature elevations within the chamber, the system's ability in measuring a quantifiable temperature change can be assessed. Table 4.4 lists the measured temperature change ΔT (Equation 4.2) measured by the thermohygrometer and five of the sensors under test.

$$\Delta T = T_2 - T_1 \tag{4.2}$$

Where:

- $\mathbf{T_2}$ is the current chamber temperature
- $\mathbf{T_1}$ is the previously measured chamber temperature

Table 4.4: The temperature changes in the climate chamber as measured by the thermohygrometer and five of the sensors under test.

Chamber Temperature (°C)	**Measured Temperature Difference ΔT (°C)**					
	Meter	**S_1**	**S_2**	**S_3**	**S_4**	**S_5**
15.00	*Initial Chamber Temperature*					
17.50	2.50	2.52	2.51	2.52	2.49	2.55
20.00	2.40	2.61	2.64	2.61	2.64	2.58
22.50	2.60	2.56	2.58	2.55	2.57	2.58
25.00	2.30	2.51	2.53	2.52	2.49	2.58
27.50	2.60	2.64	2.64	2.64	2.65	2.60
30.00	2.30	2.48	2.48	2.47	2.47	2.48
33.00	2.70	2.74	2.73	2.75	2.71	2.80
34.00	1.10	1.04	1.07	1.04	1.10	1.05
35.00	0.90	0.88	0.90	0.87	0.89	0.88
36.00	0.90	0.93	0.90	0.95	0.91	0.95
37.00	1.00	0.93	0.93	0.93	0.91	0.93
38.00	0.90	0.82	0.86	0.81	0.81	0.80
39.00	0.90	0.84	0.84	0.84	0.85	0.85
40.00	0.80	0.86	0.89	0.86	0.82	0.85
42.50	2.50	2.23	2.13	2.23	2.25	2.23
45.00	2.50	2.19	2.22	2.24	2.25	2.25
47.50	2.30	1.88	2.02	1.83	1.89	2.02
50.00	2.20	2.02	1.98	2.02	1.98	2.02

4.3 Testing of Different Sensory Platform Form Factors

Once the sensor performance was assessed, the sensory platforms needed to be tested. Dynamic tests using the device in real-life conditions were required, testing the temperature measurement function as well as the physical durability of the sock/insole. The following subsections will outline the testing done on the designed sensory form factors described in Section 3.2.2, and how these performed. These tests not only provided temperature data collected by the respective sensory platforms, but they also served as an opportunity to assess the ergonomics of the system and how well the sensory platform can withstand the environment within the shoe.

4.3.1 Fabric Insole Form Factor

A single test subject was required to perform walks outdoors in the Maltese climate, while wearing the sensory fabric insole on the left foot with the first board prototype, as shown in Figure 4.4. The selected location for performing the test walks provided flat surfaces with no steep elevations. Additionally, in order to maintain a regular walking pace, a fitness tracker application running on a smartphone was used to monitor the walking speed.

Figure 4.4: The system prototype worn on the foot for dynamic testing.

Two separate walks were conducted using the sensory insole, averaging paces of 5.79 km/hr and 5.89 km/hr. Ambient conditions were comparable, since the walks were done within the same day, one late in the morning and the other one in the afternoon.

4.3.1.1 Walk 1

The first walk was approximately 30 minutes long, recording the temperatures across all areas of the foot, without any sensor breakages. The plot in Figure 4.5 illustrates temperature changes across all areas of the foot, with initial temperatures spanning from 18.91 °C to 28.98 °C and final temperatures between 25.98 °C and 37.07 °C. These recorded temperatures were categorised into five main areas of the foot, namely the arch, heel, lateral foot, metatarsal head (MTH), and toes. Table 4.5 lists the average initial and final temperatures, along with the overall temperature increase in these areas.

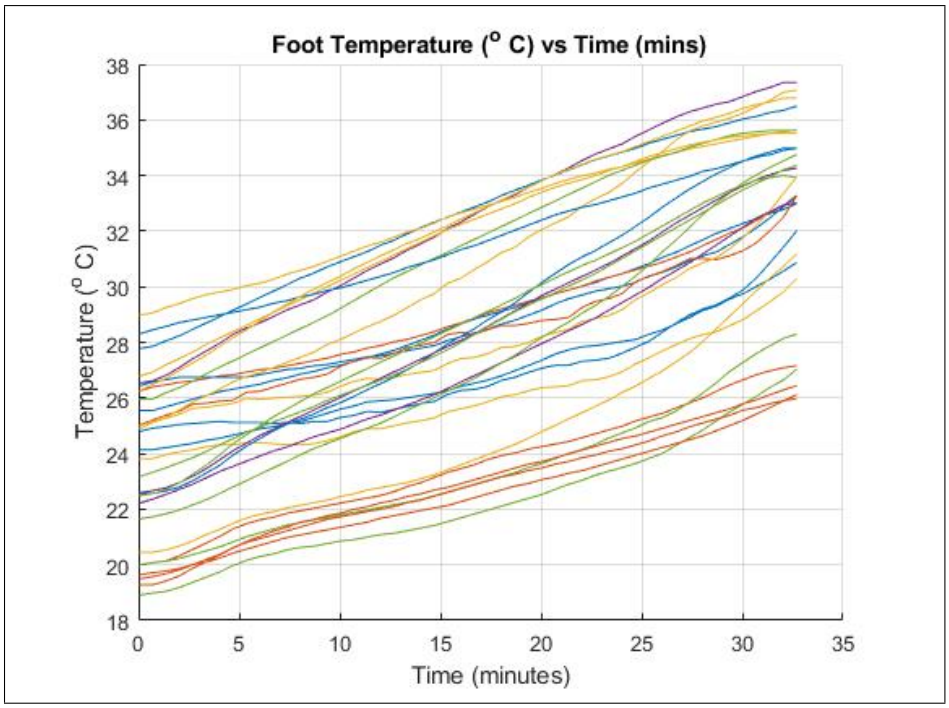

Figure 4.5: Plot of the temperatures recorded from the 30 insole sensors throughout the first walk.

Table 4.5: The average initial and final temperatures recorded at the 5 main areas of the foot, and their increase in temperature throughout the first walk.

Foot Area	Initial Temperature (°C)	Final Temperature (°C)	Temperature Increase(°C)
Arch	27.35	36.45	9.10
Heel	25.05	32.86	7.81
Lateral Foot	24.55	35.30	10.74
Metatarsal Heads	22.26	34.59	12.33
Toes	19.65	27.52	7.87

Using the designed Matlab tool, the temperature data was used to create an interpolated temperature map illustration to graphically represent the temperature elevations throughout the walk. The first and final frames of the animation are shown in Figure 4.6. These clearly show higher temperatures of the arch area when compared to the extremities of the foot.

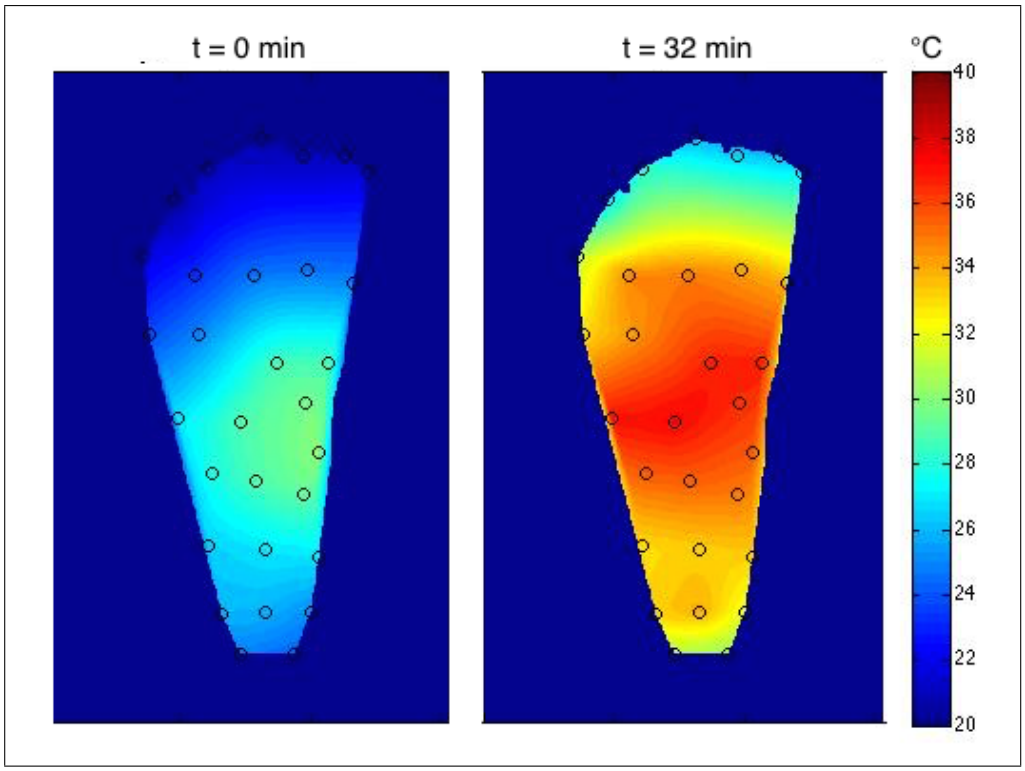

Figure 4.6: Interpolated temperature maps of the foot at the start and end of the first walk.

4.3.1.2 Walk 2

In order to investigate if the temperatures of the foot continue to develop further over a longer period of physical activity, the second walk was extended to one hour. In the plot in Figure 4.7, the temperatures can be seen to start plateauing beyond the 30-minute mark. Unfortunately, towards the middle of the walk, one of the sensors got disconnected due to wear and tear on the soldering connection. The readings from this sensor were omitted from any analysis done on the data.

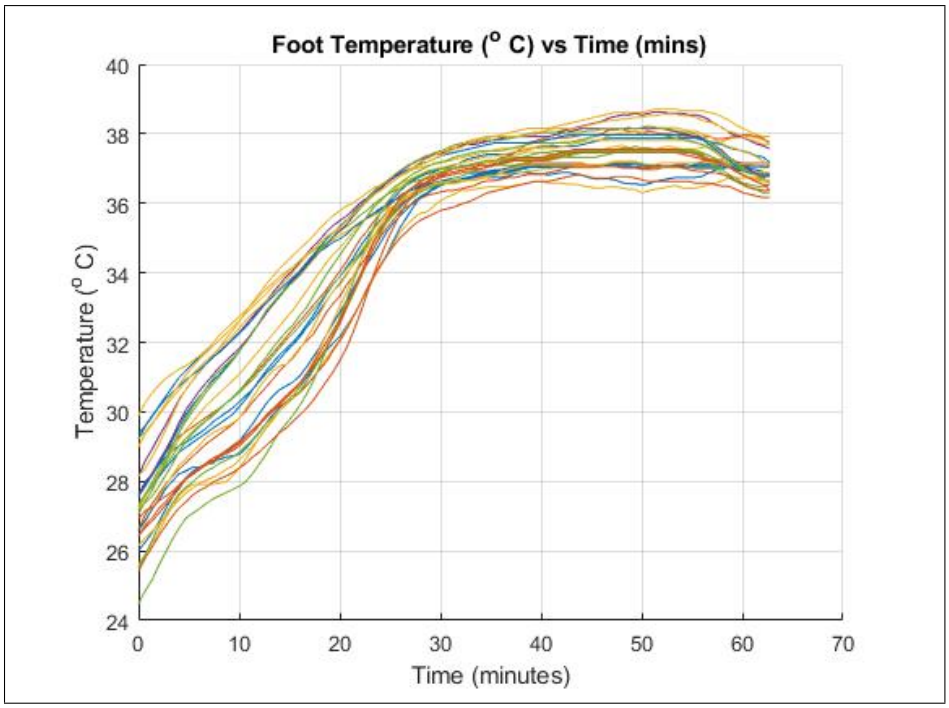

Figure 4.7: Plot of the temperatures recorded from the 29 insole sensors throughout the second walk.

Similar to before, the average temperatures for the same five areas of the foot were calculated. These are listed in Table 4.6, with the interpolated temperature maps shown in Figure 4.8.

Table 4.6: The average initial and final temperatures recorded at the 5 main areas of the foot, and their increase in temperature throughout the second walk.

Foot Area	Initial Temperature (°C)	Final Temperature (°C)	Temperature Increase(°C)
Arch	26.75	37.08	10.81
Heel	27.43	36.75	10.56
Lateral Foot	28.76	37.37	9.34
Metatarsal Heads	27.37	36.60	10.72
Toes	25.88	36.33	11.47

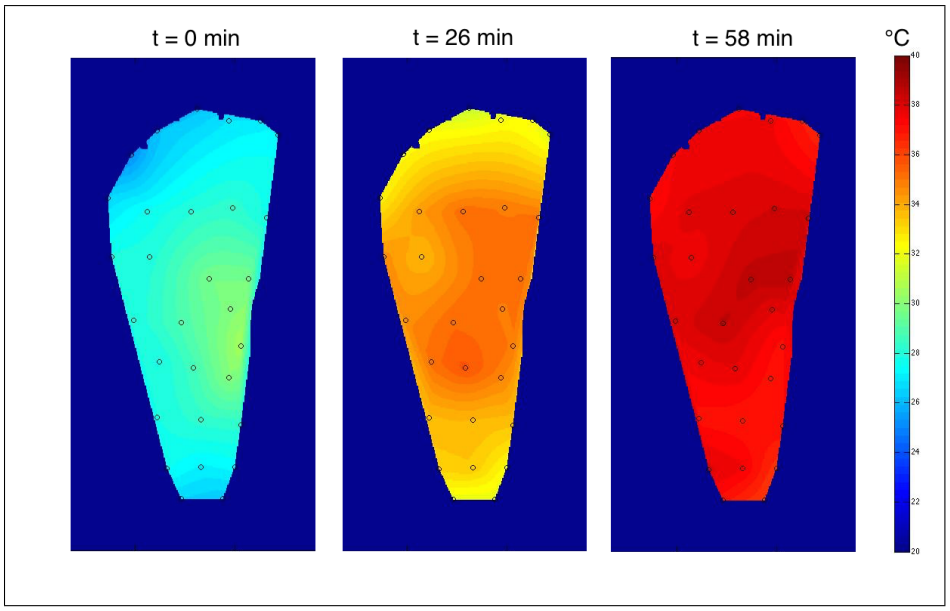

Figure 4.8: Interpolated temperature maps of the foot at the start, midway and end of the second walk.

4.3.2 Sock Form Factor

The sensory sock was also tested using the first board prototype as depicted in Figure 4.9. The same test subject as before wore the system on his left foot, and attempted to perform two one-hour walks. Unfortunately, both walks were cut short due to technical difficulties with excessive sensor breakages. The walks lasted approximately 40 minutes, averaging paces of 5.95 km/hr and 5.90 km/hr using the same walking route as before.

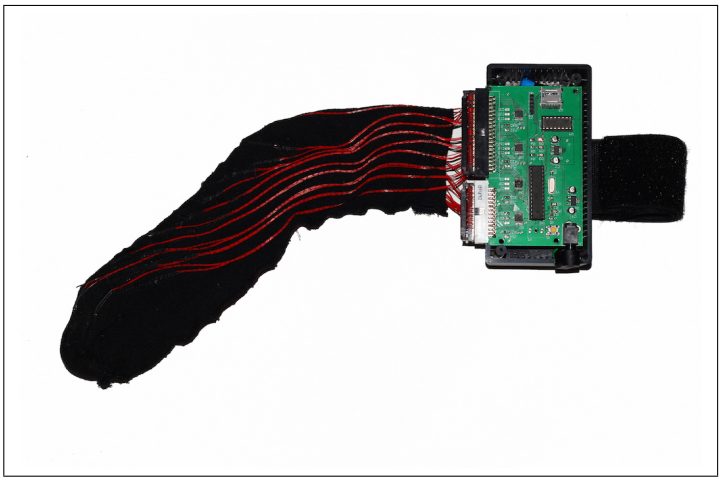

Figure 4.9: The sensory sock setup for dynamic testing.

The plots in Figures 4.10 (a) and (b) represent the data from both walks using the sensory sock, with data from the disconnected sensors omitted from the plot data. It is observable that some of the sensors were experiencing intermittent disconnections, more noticeable in the second walk. For these reasons, it was not feasible to extract the interpolation illustrations for the walks done with the sensory socks.

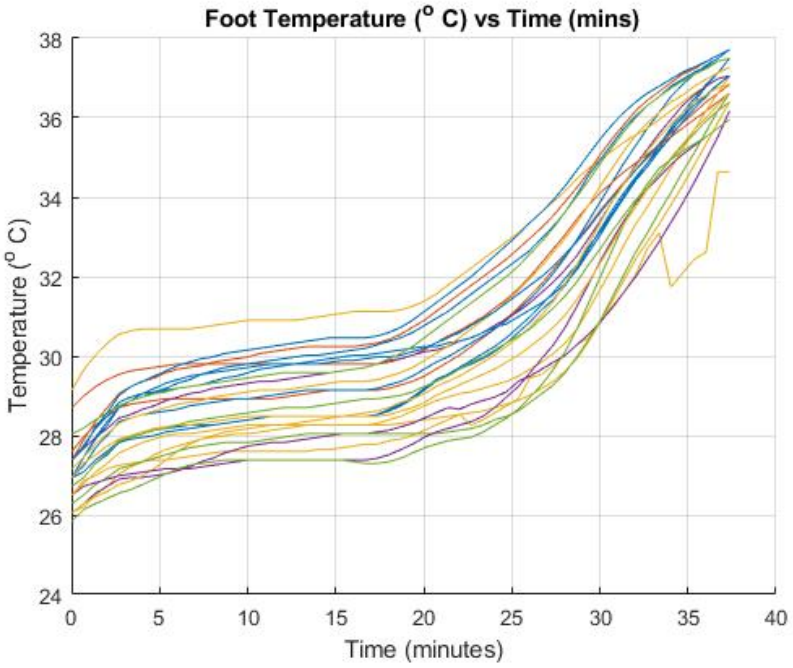

(a) Plot of the temperatures recorded from the sock sensors in the first walk.

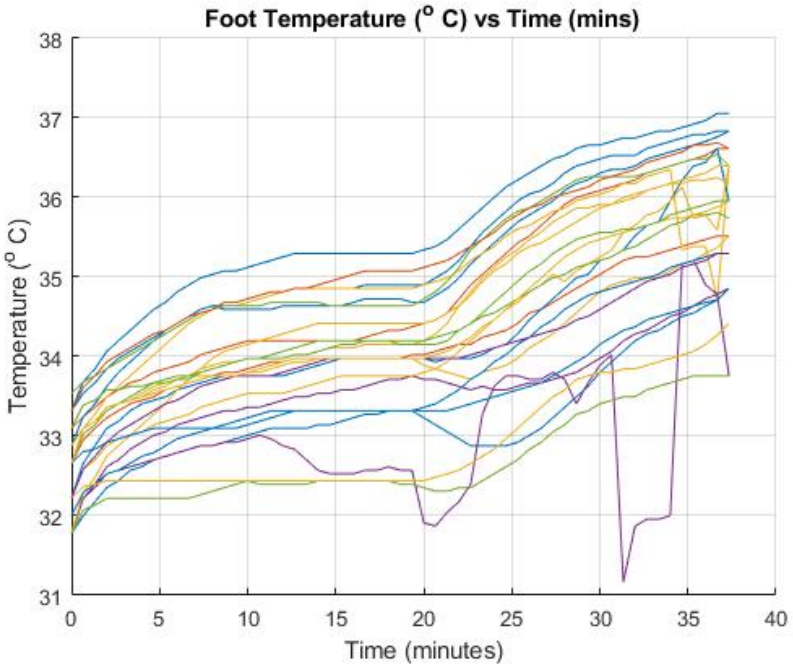

(b) Plot of the temperatures recorded from the sock sensors in the second walk.

Figure 4.10: Temperature plots of the walks using the sensory socks.

4.3.3 Sock-Insole Form Factor

The sensory sock-insole was tested using the second board prototype, which had an updated circuit design. This setup was first tested using a single subject and carrying out two test walks, similar to what was done with the previous sensor form factors. This preliminary testing was done with the sole aim of testing the robustness of the system and identify any general issues with the system design. A more comprehensive testing session was carried out to evaluate the validity of the temperature data collected. The testing was done in a controlled environment with 10 healthy subjects carrying out walk trials while wearing the system on both feet.

4.3.3.1 Preliminary Testing

Initial testing was done using a single module on the left foot, in line with what was done for the other sensory platform form factors. The walks were kept at a duration of one hour so as to make sure that foot temperature stability is reached. In order to have similar starting temperatures between the two walks, a 10 minute sitting period while wearing the system was done before starting the walk. This helped to make sure that the sensors would acclimatise to the resting foot temperatures before starting to record the rising foot temperatures during ambulation. The temperatures recorded throughout the two test walks are plotted as shown in Figure 4.11. It is worth noting that even though the same trail was used in both walks, with average paces of 5.97 km/hr and 5.98 km/hr for the first and second walk respectively, there was a drastic difference in the ambient temperature. The highest and lowest temperatures recorded by the meteorological office on the day of the first walk were 15 °C and 10°C whereas for the second walk they were 11 °C and 2°C (preliminary testing was done in the UK). This drop in temperature had an effect on the rate of temperature rise along the foot. This is clearly shown in the plots in Figure 4.11, where it can be seen that the extremities of the foot (toes and heel) took longer to warm up. The effects of ambient temperature on the in-shoe microclimate have been investigated in Mizzi's study [43]. It was shown that seasonal variations in temperature not only affect the in-shoe temperatures, but also the thermal kinetics during ambulation.

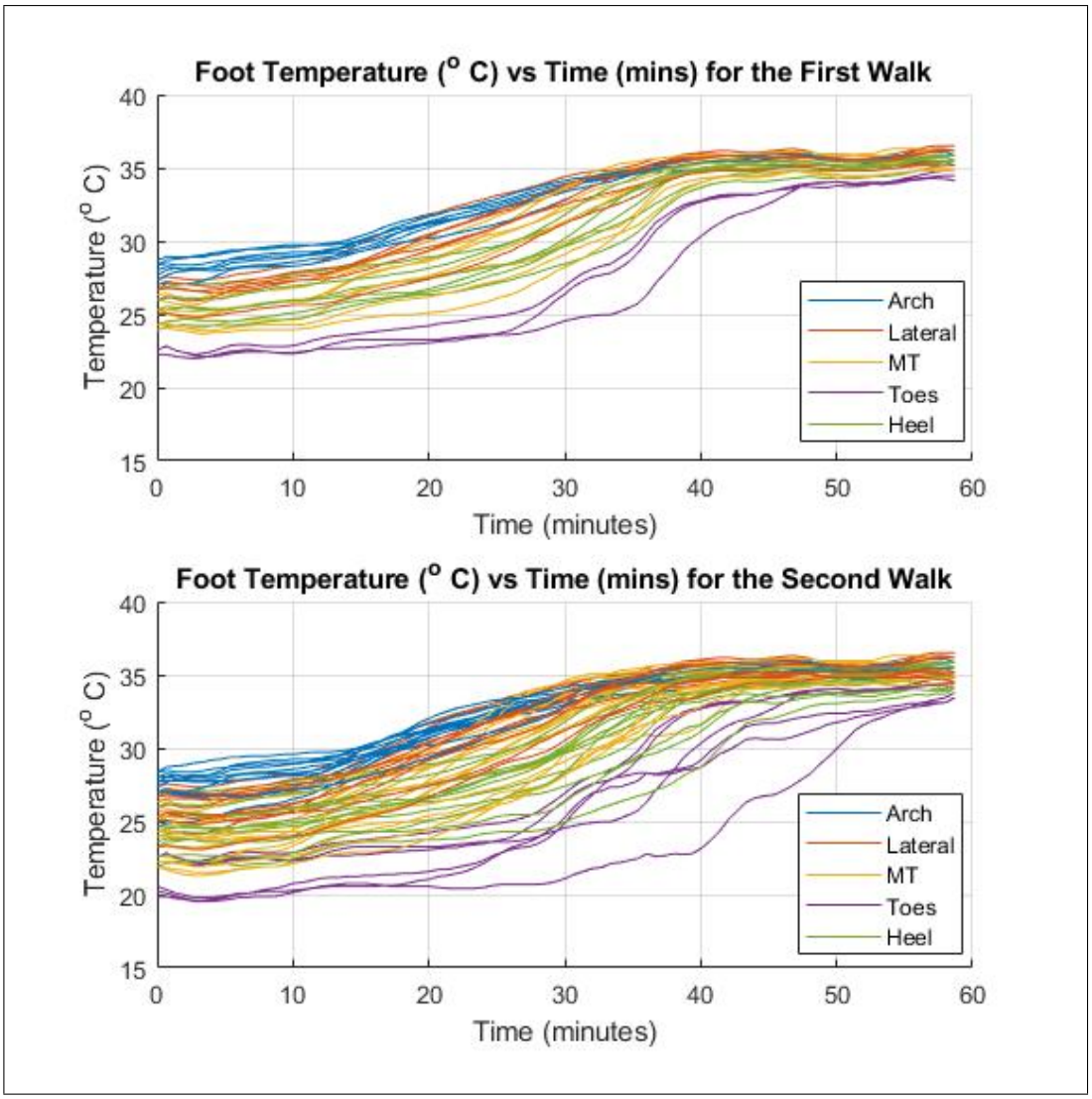

Figure 4.11: The temperature plots of both walks using the second prototype.

The average temperatures for the five main areas of the foot were calculated from the recorded data, and listed down in Table 4.7. This was done for both walks, extracting the initial and final temperatures of these areas, and by how much the temperature increased at the end of the walks.

Table 4.7: The average initial and final temperatures recorded at the five main areas of the foot, and their increase in temperature throughout the second walk.

Foot Area	Initial Temperature (°C)	Final Temperature (°C)	Temperature Increase(°C)
Walk 1			
Arch	27.93	36.07	8.15
Heel	25.20	35.89	10.69
Lateral Foot	26.38	35.89	9.51
Metatarsal Heads	25.10	35.46	10.35
Toes	22.48	34.70	12.22
Walk 2			
Arch	26.76	35.45	8.58
Heel	23.61	34.42	10.81
Lateral Foot	25.08	35.32	10.24
Metatarsal Heads	22.68	35.15	12.47
Toes	20.22	33.23	13.01

When generating the interpolated temperature maps shown in Figure 4.12, it can be seen that the temperatures at the extremities of the foot during the second walk are always lower than during the first walk. This highlighted the effect that ambient temperature has on the temperature distribution along the foot, and proved how vital it is to have testing done in a controlled environment.

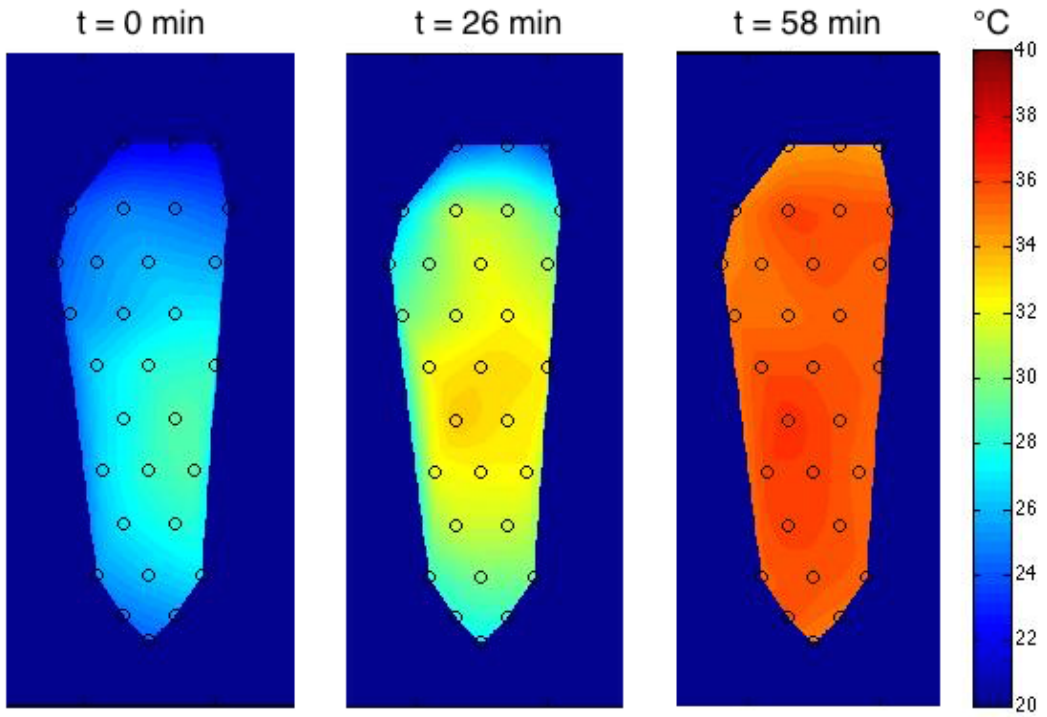

(a) Interpolated temperature maps of the foot for the first walk.

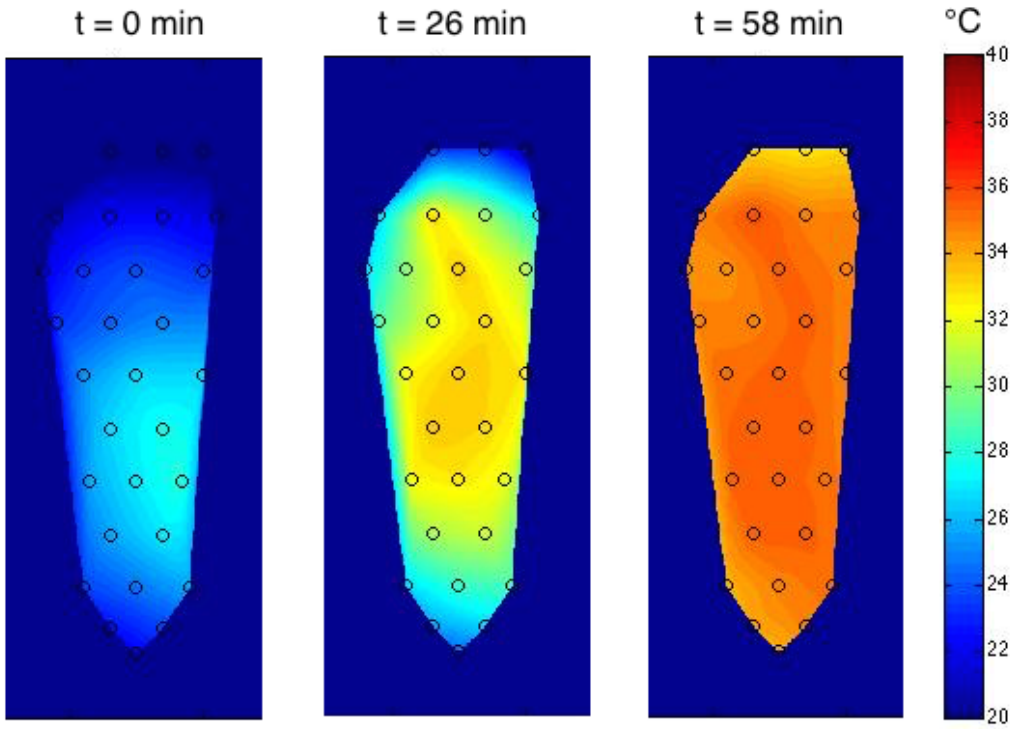

(b) Interpolated temperature maps of the foot for the second walk.

Figure 4.12: The interpolated temperature maps of the foot at the start, midway and end of both walks done using the second prototype.

4.3.3.2 Walk Trials

In order to avoid environmental factors from affecting the walking trials, these were done in the Biomechanics Lab at the Faculty of Health Sciences. The ambient temperature was set to 21 °C and monitored using a Testo (Hampshire, United Kingdom) 175H1 temperature and humidity monitor. The temperature monitor was kept close to the treadmill during the walk as shown in Figure 4.13. This ensured that the ambient temperature monitoring was done in close proximity to the area of the feet, recording any rise in temperature that might affect the in-shoe temperatures being recorded.

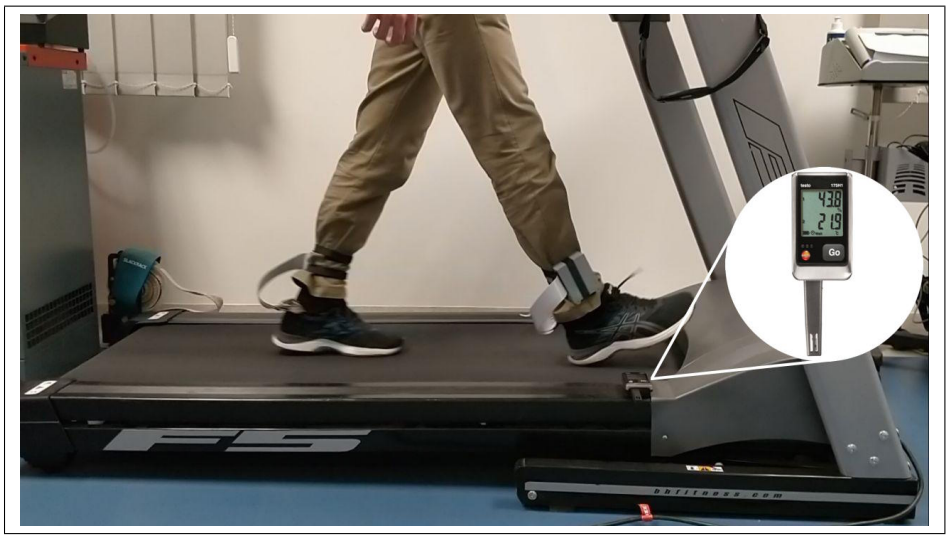

Figure 4.13: The setup used for the walk trials - subject wearing the system prototype and walking on a treadmill, with the Testo logger monitoring the ambient temperature.

A total of 10 healthy male test subjects were chosen for the study, having a mean age of 29 years (±5.4) with a mean height of 179.0 cm (±7.2) and a mean weight of 77.9 kg (±12.1). For the purposes of the system evaluation testing done here, females were excluded so as to have less variability within the test group. It was also vital in finding subjects with a similar shoe size, since a single sock-insole pair was available for testing. The criteria upon which the participants were chosen are listed in Table 4.8. The test protocol was explained to them, and then given a consent form to be signed before starting the recording session. This was in line with the ethics

approval that was granted by the University Research Ethic Committee.

Table 4.8: The list of criteria for the selection of study participants.

Inclusion	Exclusion
Male	Diabetes Mellitus
Over 18 years of age	Ulcerations (present or past)
Healthy	Foot deformities
Able to walk on treadmill for more than 30 minutes	Injuries hindering normal ambulation
Shoe size between 42-45	

Every subject was asked to bring a comfortable pair of shoes that they would normally use for walking or jogging. Before starting the recording session, they were asked to remove their shoes and socks, and sit for 10 minutes to allow their feet to cool down. Using the Flir E60 thermal camera, a thermographic image of the feet was taken before the sensory sock-insoles were worn. This was done so as to have a measure of the initial temperatures of the feet from another system for comparison. Once these were put on, the modules on both feet were switched on simultaneously to ensure that the recordings were in sync with each other. Similar to what was done during the validation testing of the second prototype, the first 10 minutes of recording were done with the subject sitting down. This was then following by 50 minutes of walking at a pace of 5 km/hr. Upon completion, the subjects sat down and the system was taken off before taking a second thermographic image of the feet to capture the foot temperatures at the end of the walk.

The temperatures recorded from both feet during the walk for Test Subject 1 are plotted in Figure 4.14. It can be seen that the temperatures of both feet follow a similar response, but the heel temperatures of the left foot rise at a slower rate than those on the right. This concurs with what is seen in the interpolated temperature maps in Figure 4.15, where the heel is clearly at a cooler temperature at the 58-minute mark.

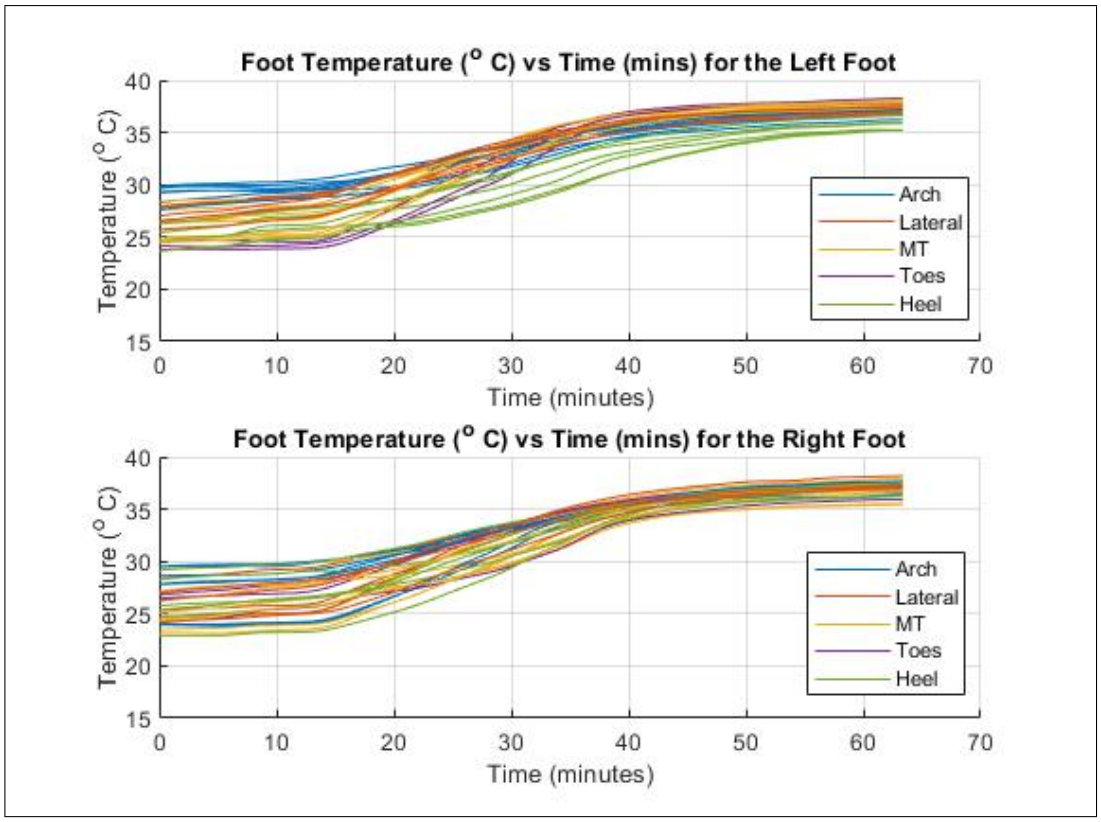

Figure 4.14: The temperature plots of both feet during the test walk of Test Subject 1.

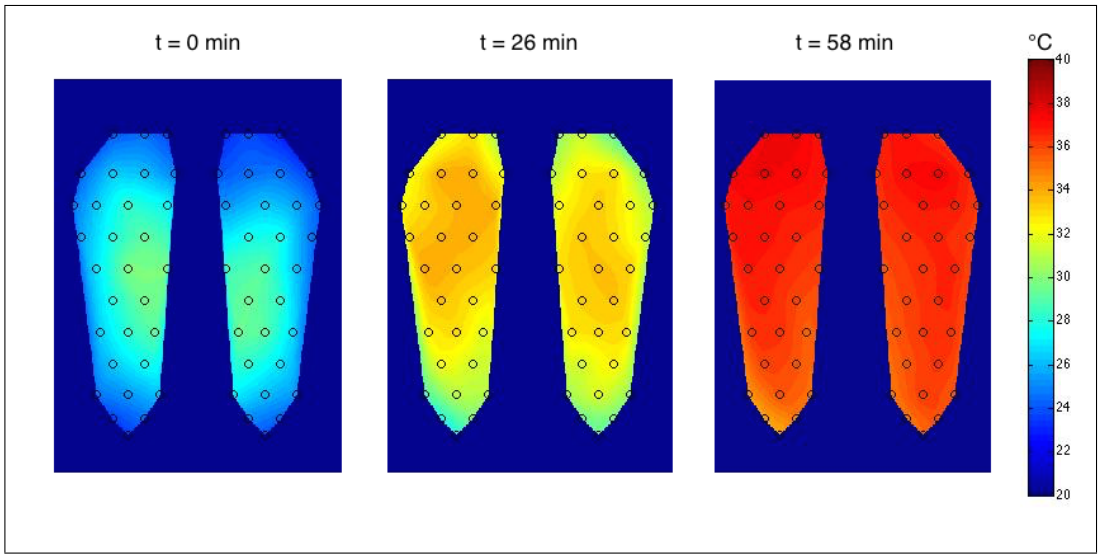

Figure 4.15: The interpolated temperature maps of the foot at the start, middle and end of the test walk of Test Subject 1.

The difference in temperatures between the two feet was extracted for the length of the walk, and represented in the plot in Figure 4.16. This was calculated from the temperatures recorded by contralateral sensors within the sensor matrices in

the sock-insoles. The temperature plots and difference in temperature plots for the other nine subject can be found in Figures D.26 - D.43 in Appendix D.

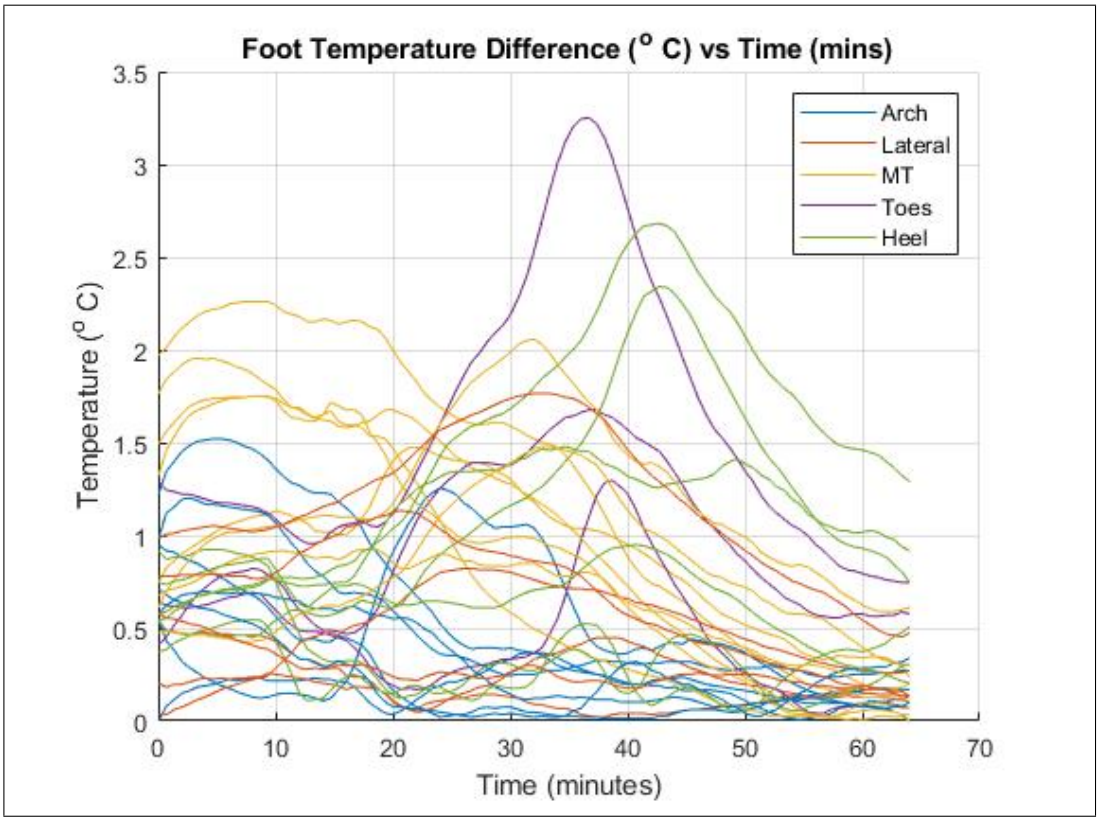

Figure 4.16: The difference in temperatures between the two feet throughout the test walk of Test Subject 1.

Since no other system could be used to compare and validate the results collected by the designed system, the temperatures recorded at the beginning and end of the walk was compared to the thermal data extracted from the thermal images taken by the IR camera. A total of 60 measurements points were placed on the thermal images captured during the recording sessions. These were placed roughly in the same locations along the feet where the sensors on the insole would have made contact, as shown in Figure 4.17. Table 4.9 shows the ICC results for the left foot and right foot temperatures at the start and the end of the walk. The actual recorded temperatures at these instances are also listed in Table D.4 in Appendix D.

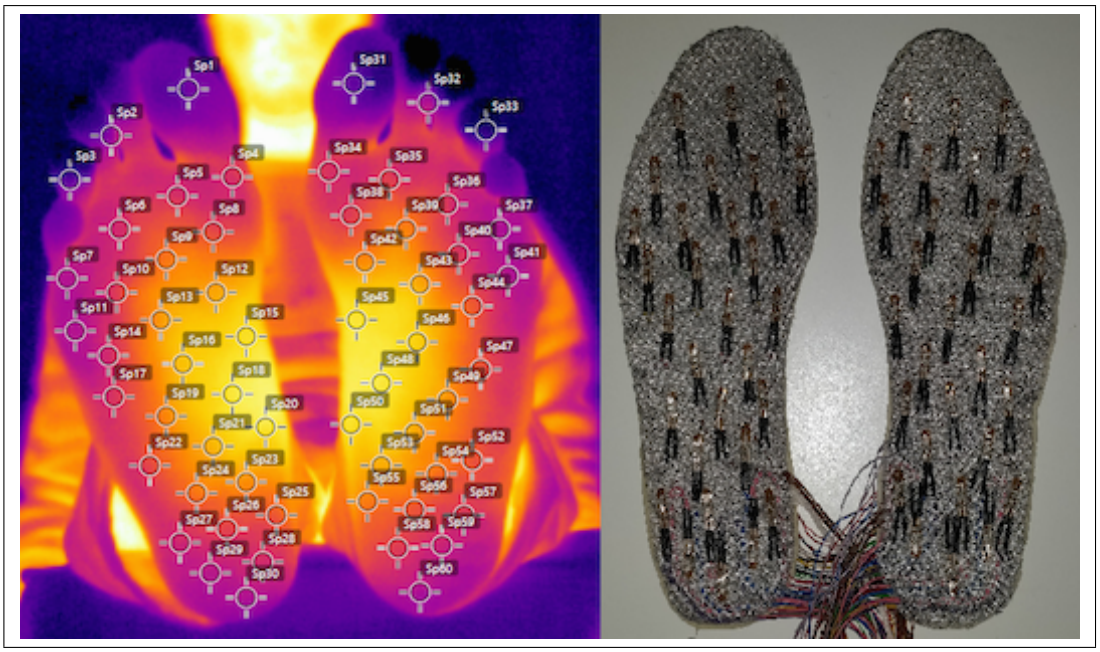

Figure 4.17: A comparison of the locations of the 60 spot measurements placed on the thermal image compared to the position of the sensors on the insoles.

Table 4.9: Correlation between the temperature recorded by the system and those extracted from the thermal images.

Temperatures	**ICC**		
	Single Measure r	**95% CI**	
		LB	**UB**
Left Foot (Start)	0.942	0.883	0.972
Right Foot (Start)	0.867	0.760	0.935
Left Foot (Finish)	0.766	0.565	0.881
Right Foot (Finish)	0.623	0.344	0.801

At the end of every test walk, feedback regarding the comfort of the system was collected from the test participants. They were asked to rate the comfort of the

sensory platform and the system as a whole, giving a score of 1 to 5, with a rating of 1 signifying 'very uncomfortable' and 5 meaning 'very comfortable'. For all the ten participants, the sock-insole was given a rating of 5, showing that there was no difference between the sensory sock-insole combination and regular socks without any incorporated sensory insole. With regards to the system as a whole, including the acquisition modules attached to both legs, the average rating across the participants was 4.

Chapter 5

Discussion

5.1 Sensor Testing

The first step in establishing whether the system would be able to measure temperature correctly was to ensure that the sensors themselves operate correctly. The datasheet provided by the manufacturer listed down the resistance values of the 103JT thermistor series for the range of operational temperatures at 1 °C intervals. The resistance tolerance was defined at $\pm 1\%$, whereas the tolerance for temperature varied across the range of temperatures; from ± 0.3 °C at 25 °C up to $\pm$ 1.8 °C at 125 °C.

The setup described in Section 4.2 was used to verify the operation of the sensors within the designed circuit. The thermistor resistance values obtained for the temperature range of the test were compared to the values defined in the datasheet. The reliability of the results can be considered as good to excellent [86], with the 95% confidence interval (CI) for the worst performing sensor falling between 0.765 and 0.999. This means that even though all sensors obtained single measure r values 0.995 or higher, indicating excellent reliability, there is still a 95% chance that the true value for ICC lies between the acquired lower and upper boundaries [86].

When analysing the resistance data and calculating the percentage deviation from the typical resistance values in the datasheet, it was found that the

measured resistances varied by more than the stated 1% in some cases. Certain sensors performed better than others, deviating from the ideal value by as low as 0.175% at specific temperatures. However, other sensors had percentage deviations of 1.84% at best. These percentage deviations varied with the set temperature within the chamber, with the higher end of deviations between 4-6%. This showed that the performance did vary between sensors, possibly due to manufacturing discrepancies, but there are other factors in play. Other components within the circuit, such as resistors and capacitors, will also deviate from their ideal values and in turn, affect the precision of the circuit output. Moreover, the temperature coefficients of the components within the circuit have an added affect on the results obtained since the entire circuitry is also exposed to the temperature changes imposed on the thermistors. An alternative approach to testing the thermistors would have been to measure the resistance directly without the use of any additional circuitry. This would have limited the sources of error from the measurements, at the expense of a less efficient test setup. In order to do so, multiple ohm-meters would be required to measure the resistance of all the thermistors, and the values would need to be recorded manually rather than logged automatically by the system.

When assessing the Bland-Altman plots for the tested sensors, all the sensors were found to have a negative bias in the region of -0.132 and -0.292. This means that all the sensors performed similarly to one another, but with values lower than those listed in the sensors' datasheet. However, there is a higher level of agreement at low resistance values, since the datapoints in the region of 5 - 7 kΩ are always about the calculated mean value. This means that at higher temperatures, there is a small discrepancy between the values of the sensors under test and the data stated in the datasheet. This follows from the non-linear relationship between resistance and temperature of the NTC thermistors, with higher resistance values at lower temperatures, and consequently bigger changes in resistance for small temperature changes. However, the temperature values recorded throughout the test walks was seen to lie between 20 °C and 37 °C, which translated to resistance values of 11.5 kΩ or lower, which are well within the obtained levels of agreement.

When analysing the precision in °C for measuring the absolute

temperature in the chamber, this varied by up to 1.8 °C at times, which is not ideal for an application where a temperature difference of 2.2 °C is significant. However, since the system is designed to measure temperature changes in the foot, and not to measure the absolute temperature to be compared to a set standard, it was worth looking into the system's ability to measure temperature change. By comparing the temperature changes measured by the temperature meter and the system, when altering the temperature in the chamber, the system's precision in measuring a temperature change was evaluated. It was found that at worst, the system can measure temperature changes to a precision of 0.47 °C, with the largest errors recorded towards the top end of the temperature range of operation, beyond the 42.5 °C mark. This precision level is acceptable for this application, with the system able to measure temperature changes well within the 2.2 °C range.

It is worth pointing out that during this testing stage, since the acquisition module was also placed within the temperature chamber, any component tolerances that vary with temperature had an effect on the collected results. The components used to build the circuit were not of the high precision type, and hence, are more prone to nominal value changes with temperature. Opting for high precision components could improve the stability and precision of the system across the range of operational temperatures. The effects of component quality was not investigated during this study, and is to be considered as part of the possible improvement to the system design in any future work.

5.2 Sensory Platform Testing

5.2.1 Sensory Insole Testing

During Walk 1, it was noted how the initial temperatures vary across the foot, and how these change throughout the walk. More importantly, as depicted in the interpolated temperature maps in Figure 4.6 of Section 4.3.1.1, the temperature distribution follows a butterfly pattern which has also been observed in various other

studies investigating foot skin temperatures [88], [89], [90]. The highest temperatures are located at the arch and the lowest temperatures are found towards the extremities such as the toes. From the data collected during Walk 1, the toes are seen to remain at a rather low temperature, averaging a temperature of 27.52 °C, when compared to the other areas of the foot with average temperatures higher than 32 °C.

In order to investigate how the temperatures continue to change along the foot sole, Walk 2 was extended to one hour. Even though one sensor failed during this extended walking activity, a more in-depth picture of the temperatures of the foot was acquired during this walk. The temperature plot in Figure 4.7 in Section 4.3.1.2 clearly shows that the foot temperatures eventually start to plateau towards the body temperature of 37 °C. This further increase in temperatures is also evident in the temperature maps of Figure 4.8, where it can be seen that the thermal distribution along the sole at the end of the walk is more uniform than what was previously observed after the 30 minute testing period of Walk 1.

From literature that was previously reviewed [91], the temperature trend was expected to follow an S-shape, started out at low initial temperatures and finally plateauing towards the body temperatures. Walk 1 clearly did not capture data for a long enough period to be able to observe these temperature trends. However, with an extended recording period, the temperatures were seen to plateau as expected. Since initial foot temperatures may vary depending on the subject's health condition as well any previous physical activity that was done, the full S-shape of the temperature trend maybe not be captured in full. Nevertheless, no signs of temperatures dips were noted, unlike some other studies [18], [19] that had issues with loss of contact between the skin and the sensors.

5.2.2 Sensory Sock Testing

The sensory sock was designed in order to provide a sensory platform that would keep the sensors as close as possible to the foot's skin during ambulation. Unfortunately, in trying to use thinner cable to avoid excess rigidity due to wiring, the

sensory sock experienced a lot of technical issues during testing. The thinner single-core cable that was used was too brittle to endure the movements and mechanical stresses under the foot. During the first walk, there were 5 sensors breakages whereas for the second walk 6 sensors were disconnected. Additionally, 2 sensors were having intermittent disconnections that were resulting in erratic temperature dips being recorded as seen in the plots in Figure 4.10 in Section 4.3.2. Given these issues, this sensor form factor was considered unsuccessful and no further testing was conducted.

If further work were to be pursued on the sensory sock, it may have been worthwhile to possibly reduce the number of sensors so as to be able to use slightly thicker cables for a more robust design. With the sensor count reduced, there would be less cables to run along the sock and would thus make the structure less rigid that what was previously designed. By opting for a design using a sensory insole placed inside a false-bottom sock, the main drawback is that there is an added sock layer between the skin and the sensors, whereas the sensory sock had direct contact between the skin and the sensors. By having a thin sock, the effects on the temperature readings should be negligible, but it would be best to have this tested. Even though this was not done in this study, it will be included in the future work to ascertain that the sock-insole design still provides the optimal temperature readings from the sensors.

5.2.3 Sensory Sock-Insole Testing

The final sensory form factor, fusing the sock and insole design into one, was successfully tested in the Preliminary Testing with two initial test walks using a single subject. The module, worn on the left foot, did not experience any sensor breakages and the temperatures from all 30 sensors were recorded. The results outlined in Section 4.3.3.1 show the recorded temperature variation in the foot during the two one-hour walks. The drop in ambient temperature between the two walks had its effects on the foot temperatures, with an average temperature difference of 1.75 °C at the beginning of the walk and 0.9 °C after one hour of walking. Climate conditions have been found to have an effect on the foot temperature [41], [43], and this proves that the

system was able to measure these effects on the foot.

This preliminary testing was vital in determining whether the re-designed circuitry and sensory platform was fit for testing with multiple healthy subjects. Ideally, the ambient temperature would have been comparable between the two walks so as to be able to analyse the stability in the performance of the system. The correlation between the two sets of data was poor, but this is understandable given the variability of ambient temperature. Nevertheless, no technical issues were noted and recording and transmission of the temperature data was continuous throughout both walks, with no modifications required prior to using the system in the walk trials.

5.3 Walk Trials with Healthy Subjects

The aims of carrying out the walk trials using multiple healthy subjects were twofold:

1. To test the robustness of the system and validate its performance over multiple test runs.
2. To check for consistency in collecting data from different healthy subjects.

Throughout the test walks, there were three instances where there was a sensor breakage or intermittent disconnection. In two of these cases, the same sensor failed in two consecutive test walks and this was due to inadequate repair between one testing session and the next. Ideally, the sensor was replaced rather than repaired, since the latter will result in a reduction of the fixed cable and hence greater strain on the soldering connection. In fact, once the sensor was replaced upon its second failure, no further issues were noted. From all other aspects, the system performed very well, with data being recorded and transmitted in full for all 10 subjects.

The ratings given by the study participants provided vital information in understanding what is deemed comfortable or uncomfortable for system user. The

rating of 5 for the insole comfort shows that there were no issues with the sensor and cabling under the participant's foot during the walk. However, there were some minor issues with the other system components. The feedback given by the subjects with regards to the comfort of the acquisition module and the respective wiring included:

- Concern with hitting the cables during walking.
- The acquisition module was strapped too tight and causing discomfort.
- The acquisition module was strapped too loose causing it to slip down the leg during walking.
- It is noticeable that there is a box attached to your leg during walking.

These issues highlighted possible improvements in the ergonomics of the system to make it more comfortable for the user.

From a performance perspective, the collected data was found to be in line with findings from other studies. The butterfly pattern in the temperature distribution of the foot [88], [89], [90] was more evident now that temperature data from both feet was recorded. The interpolated temperature maps illustrated in Figure 4.15 in Section 4.3.3.2 show higher temperatures in the arch area that spread out towards the extremities of the foot throughout the duration of the walk. When plotting the data from the same participant in Figure 4.14, the temperature trends from both feet follow on Cutajar et. al's [91] study on the analysis of in-shoe temperature data trends. In this particular test subject, the full S-shape is observed in the temperature trend, starting with a slow temperature increase across the foot until finally plateauing close to the 37 °C region.

When analysing the differences between the recorded temperatures from both feet, some dissimilarities are evident from the plots in Figure 4.14 as well as the interpolated temperature maps in Figure 4.15. The plots show that the heel temperatures on the left foot experienced slower rates of temperature increase throughout the walk. On the other hand, when analysing the interpolated temperature maps, the toes on the left foot seem to be at higher temperatures at all three depicted

intervals. Furthermore, when calculating the temperature differences throughout the entire walk, the biggest differences in temperatures were also recorded at the toes and heel. This was also the case in Test Subject 7 and Test Subject 10. Given that these discrepancies have been noted mostly at the areas that experience the biggest changes in temperature throughout the walk, it could be that the insole within the left sock was pushed back when putting on the shoe. If this were the case, the sensors supposedly recording toe temperatures would be recording temperature closer to the metatarsal region, which would explain the higher toe temperatures on the left foot. Additionally, the sensors at the other end of the insole would be measuring temperatures from an area of the heel further from the arch of the foot when compared to the right foot. This would explain the peaks depicted in the plot in Figure 4.16 of Section 4.3.3.2. The misalignment in the sensors positions between the two feet caused temperature differences greater than 2.2 °C mid-way through the walk, which eventually went down to below 1.5 °C once the temperatures in the foot stabilised. The fact that this issue was also noted in some of the other subjects highlighted the fact that, even though the sensory insole was encapsulated within the sock to help maintain sensor contact, initial sock-insole alignment still needs be ensured.

When analysing the data from the other participants, other temperature patterns were noted. In Test Subject 2, 3, 4, 8, and 9, the temperature plots on both feet are clustered tightly together, especially after 30 minutes of walking. Looking at their respective temperature difference plots, any peak differences in temperature occur before the 30 minute mark until eventually settling down to values below 1 °C. It is worth pointing out that in Test Subject 8, one of the heel sensors was recording differences of up to 4.5 °C according to the plot in Figure D.39. This was due to a sensor breakage at the left heel, and as seen in the respective temperature plot in Figure D.38, there is a sensor recording a constant value from before the 20-minute mark - this signifies a sensor breakage. The results collected from these test subjects proved that the system designed here was recording temperature values from both feet with discrepancies within 1 °C, which is to be expected from healthy subjects.

Of course, given the novelty of the system designed as part of this study, there was no other device that could be used to capture similar data and compare their

performance. The only comparison that could be done was using an IR camera and comparing temperatures at the beginning and end of the walks, before and after the sensory sock-insoles were worn by the subjects. It is worth pointing out that there were some shortcomings in this method. Firstly, there is always a time gap between the capture of the thermal image and the readings from the designed system. At the start of the walk, the image is taken at least 2 minutes before the first readings by the system can be recorded. This is the approximate time taken to put on the sensory socks and shoes on both feet and start recording. Since the system is put on one side at a time, the side on which the sock-insole is put on first might record slightly higher temperatures since the foot may start warming up slightly. On the other hand, when taking the thermal image at the end of the walk, the issue is that the feet start to cool down. Once the walk is finished, the subject is asked to sit down and the shoes and sensory sock-insoles are removed one side at a time. This means that there is once again a time delay between the final readings recorded by the system and the time at which the thermal photo is taken. Since the feet will be warm following the ambulation period, a greater temperature gradient is present between the feet and ambient than at the beginning of the walk. This may cause more rapid temperature fluctuations in the feet and result in a thermal image that is not reliably depicting the temperature of the feet at the same instance of the last system reading. This is clearly evident in the correlation results for the temperatures recorded by the system and those extracted from the thermal images listed in Section 4.3.3.2. These were found to be good to excellent [86] at the start of the walk, where foot temperatures may not have varied significantly when wearing the system. However, at the end of the walk, the correlation was found to be moderate to good for the left foot and varying between poor and good for the right foot.

Chapter 6

Conclusion

6.1 Summary of Works

The aim of the work was to design a system that is capable of providing a denser measurement method of the temperatures of the feet during ambulation. As seen in Chapter 2, various multi-sensor systems have been designed [16], [18], [19], [22], some of which monitor up to 7 points along the foot. The system designed here went beyond measuring specific points but consisted of an array of 30 sensors that was used to reproduce interpolated temperature maps of the soles of the feet. Various sensory platforms were tested throughout the development process of the system, with the chosen design providing consistent sensor contact without hindering comfort or ease of use.

The designed system was able to be used outdoor for extended periods of operation without any issues. This was one of the main aims of the study, to have a portable device that can monitor a person's foot temperature without hindering their day-to-day activities. The study participants that used the device reported no difference between the sensory sock-insole and any other regular sock, however pointing out some further improvements to be done in the ergonomics of the acquisition module and its connectivity.

No such system has been found in the literature, and the results obtained here gave an insight on the variations of the temperatures along the foot during ambulation beyond single temperature values. The temperature data collected throughout the walk followed trends that were previously seen in other studies [88], [91]. Additionally, the designed software provided interpolated thermographic images obtained from the sensor array that mimicked thermal images and video from an IR camera.

6.2 Current Limitations and Future Works

Even though the system designed proved effective in measuring the temperatures of the feet during ambulation, the testing procedure can be made more robust to have a stronger basis of comparison for its performance. Firstly, it would be ideal to have multiple sensory sock-insoles of varying sizes so as to have one less constraint of subject selection. Other than that, a better size fitting of the sock-insole might avoid issues with insole movement and the respective sensor alignment during testing. Additionally, having more than a single pair of sensory sock-insoles will also reduce sensory degradation due to extensive use; something which was not tested in this study. With regards to thermal imagery, shortening the gap between putting on/taking off the system and capturing the IR image might result in more consistent results between the two systems. Moreover, it would be ideal to have the thermal camera set up on a tripod and maintain a constant distance between the camera and the feet to have consistency in the method.

Since the system was designed with the final aim of assisting people suffering from DFU, testing on diabetic patients would need to be done. This of course would require a medical practitioner to assess the test subjects, before and after the testing. This is necessary to make sure that there are no signs of ulcerations or skin damage prior to testing, and to then ensure that the system did not cause any damage to the skin on patients' feet. The data recorded from these walk trials would then be analysed and compared to studies that have also investigated the foot

temperatures within the diabetic population.

Other than improvements in the testing protocol used during the walk trials, further testing and development can be done on this system to continue to improve it. As previously mentioned, no testing on sensor degradation was done during this project. The main concern with the sensors was the durability of the connection, making sure that the cabling would endure the conditions within the foot during walking. Other approaches to sensor-wire connectivity, such as crimping, can be explored and tested, with particular attention given to the risk of injury when these types of connection are located under the foot. Moreover, the performance of the sensors themselves can vary over long periods of operation, and this must be tested to establish the period of operation that the sensors can be deemed to operate up to the specification. Systems found on the market, such as the Siren sensory socks [22], ship out new sensory socks every 6 months to ensure that the users have a continuous supply of operational and calibrated sensor platforms.

From a system design point of view, the feedback given by the test subjects suggests that making the acquisition module smaller would greatly improve the comfort of the system. This is possible by opting for even smaller component packages to be able to reduce the size of the PCB even further. There will obviously be a limit as to how small the module can be without reducing functionality of the system. Also, even though the sensor connector was reduced in size when designing the second board prototype, the same amount of cables were still present and found to affect some of the subjects. In order to solve this issue, the placement of the acquisition module may need to be closer to the sock so as to have shorter cabling, or else use the same thin cable in the insole up to the acquisition module, omitting the ribbon cable altogether.

While testing the system on both feet, one of the most critical issues was to make sure that the acquisition modules were switched on simultaneously. Failure to do so would have caused discrepancies in the readings between the two feet due to a time delay introduced between respective readings recorded by each module. The best way to avoid this is to have a timestamp with every reading, whereby even if the

two modules were switched on at different times, the data can still be matched up by checking when a particular reading was recorded. This solution can be implemented with the addition of a real-time clock chip in the circuit design.

Finally, in order to make the system more complete and easier to use, it would be ideal to include the data representation outputs done in Matlab within the Android application. The addition of the interpolated temperature maps would give a clearer idea of the temperature distributions along the foot, going one step ahead of the single temperature spots currently in use. Moreover, by having the data plots available on the application, it would enable the user to look back at the temperature data during system use, since currently only data in real-time can be displayed.

6.3 Conclusion

With the possible improvements in mind, the current design of the system still reached the initial requirements at the beginning of the design process: to have a portable system able to acquire dense temperature recordings from both feet over a prolonged period of time. The representation of that data is done on two software platforms, each with their own level of detail. The Android application is able to represent the real-time data that is transmitted over Bluetooth from the acquisition module. It displays the foot temperatures from the 30 separate sensors on each foot, as well as checking for temperature differences between the two feet. Additionally, a more in-depth analysis can be done by extracting the data logged onto the SD card. The temperature trends for the duration of the walks can be extracted and animated illustrations of interpolated temperature maps can be produced to visually assess the temperature changes in the feet during ambulation.

Further work is required to fine-tune this system, but its novelty and potential could make it a useful tool for both clinicians as well as patients themselves.

Appendices

Appendix A

PCB insoles component layout

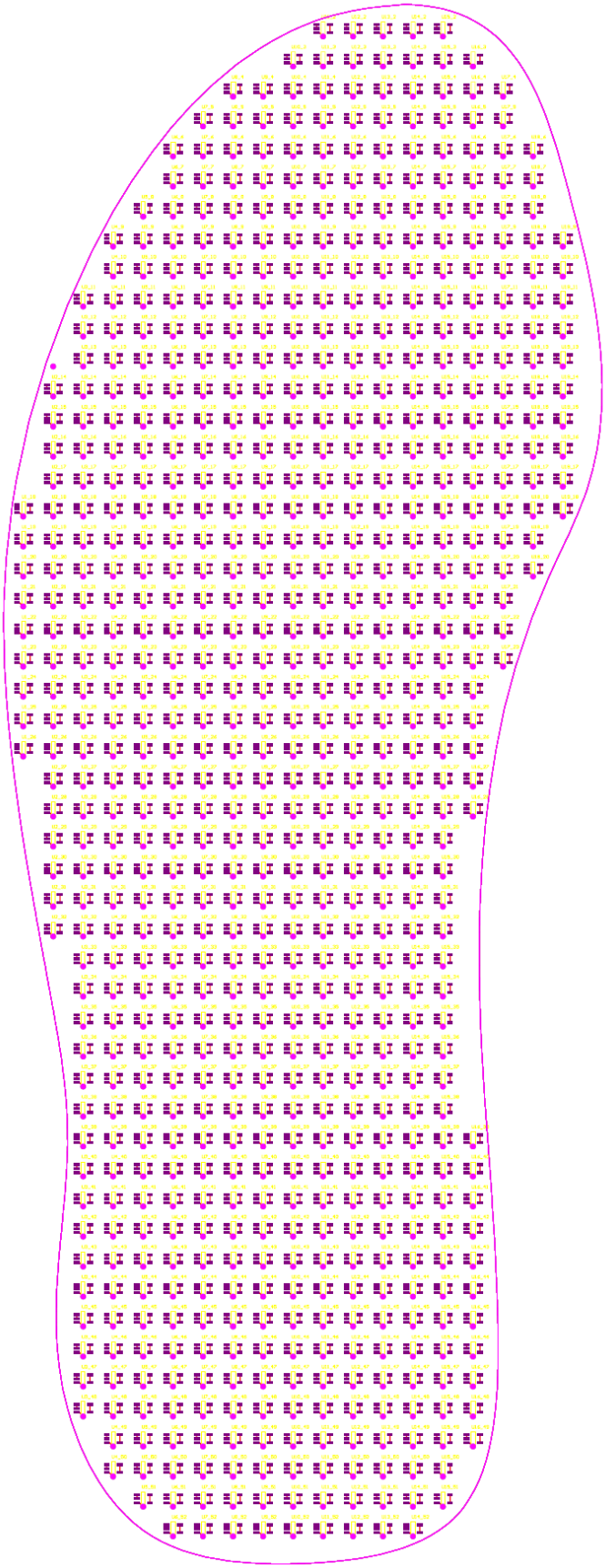

Figure A.1: Component layout for the sensory PCB insole using LMT86 analogue sensors.

Figure A.2: Component layout for the sensory PCB insole using MCP9808 digital sensors.

Appendix B

Board Prototype 1 Circuit Diagrams

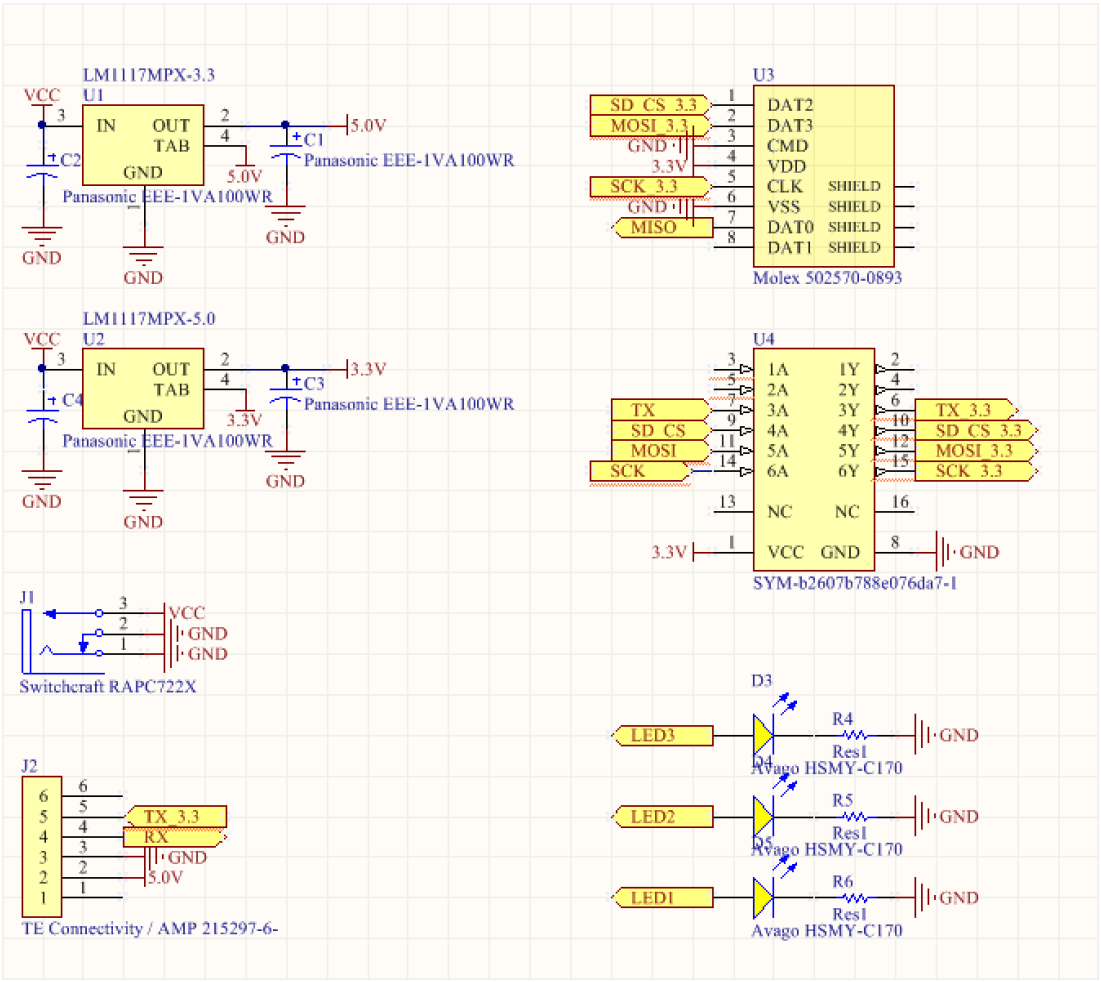

Figure B.1: Schematic diagrams of the voltage regulator circuits (U1,U2), the connectivity of the SD-card connector (U3), voltage level shifter (U4), LED circuits (D3-D5) and connector pinouts (J1, J2).

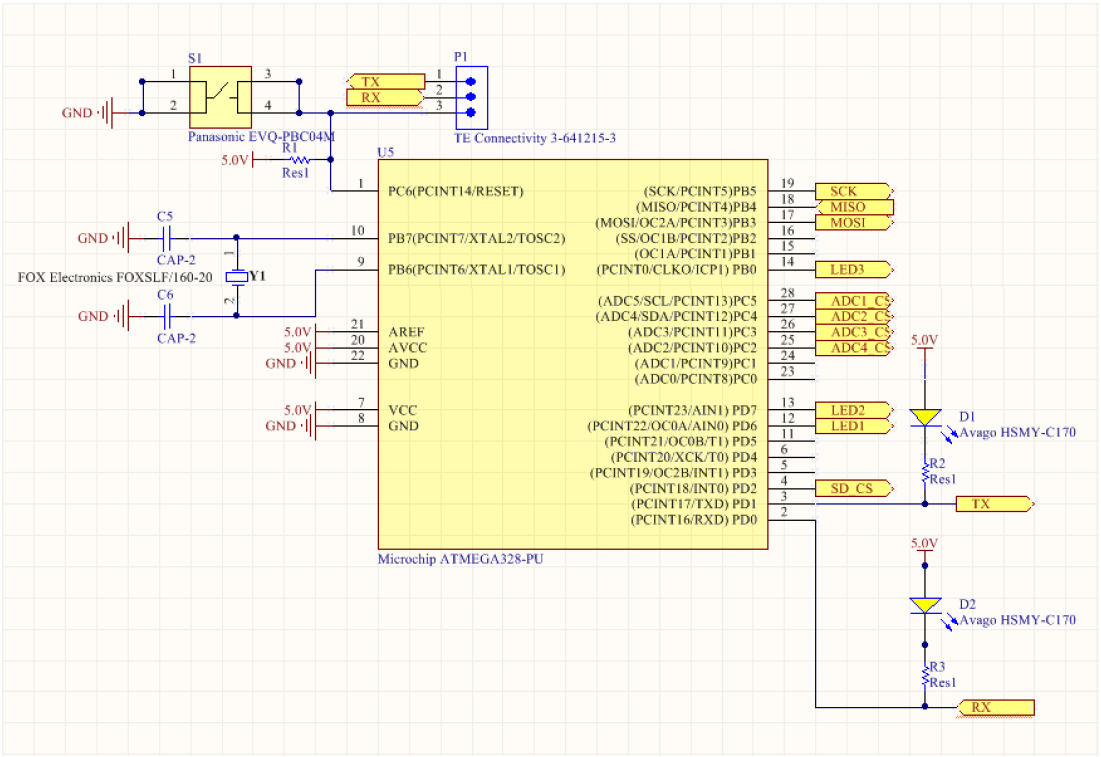

Figure B.2: Schematic diagram of the microcontroller (U5).

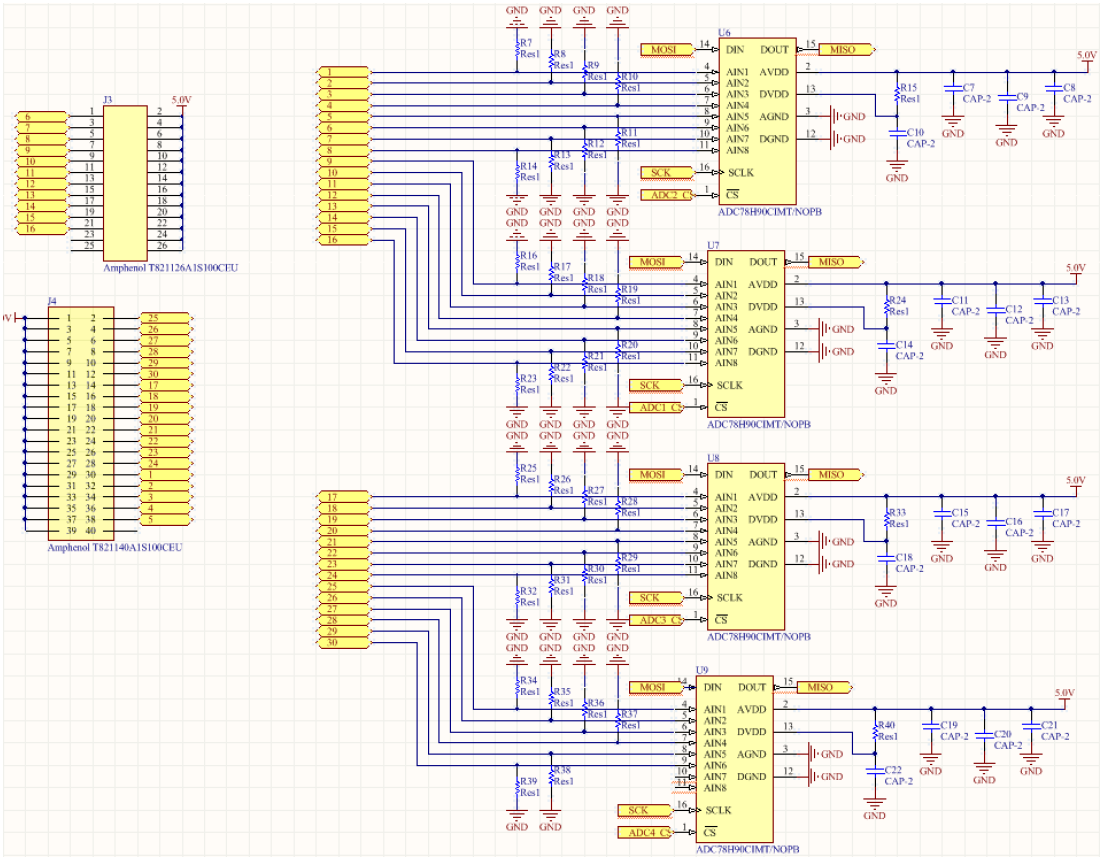

Figure B.3: Schematic diagrams of the ADCs (U6-U9) and the sensor connector pinouts (J3, J4).

Appendix C

Board Prototype 2 Circuit Diagrams

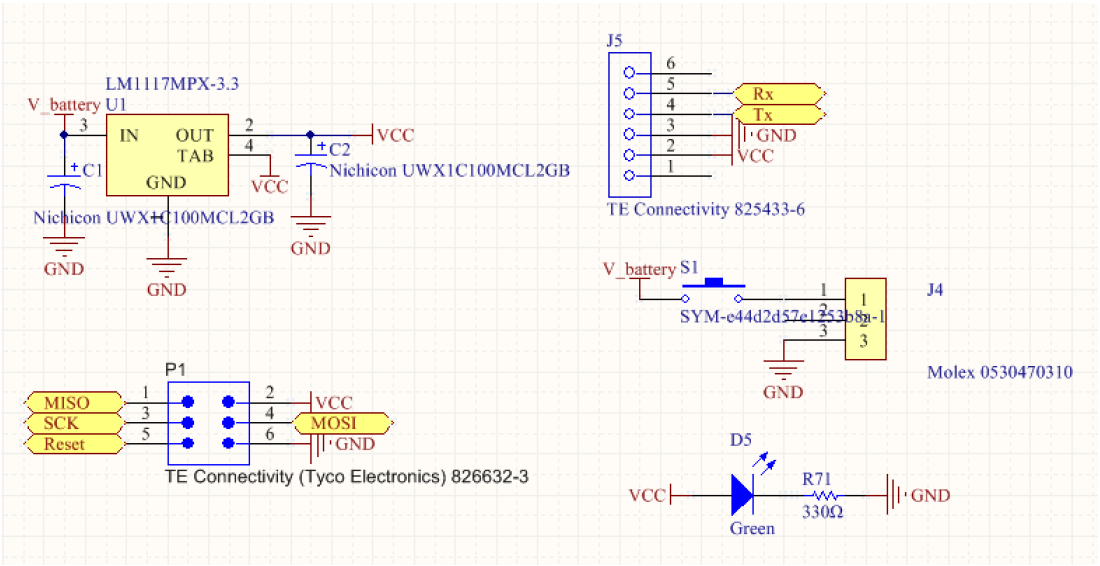

Figure C.1: Schematic diagrams of the voltage regulator circuit (U1), the ICSP connector pinout (P1), LED circuit (D5) and connector pinouts (J4, J5).

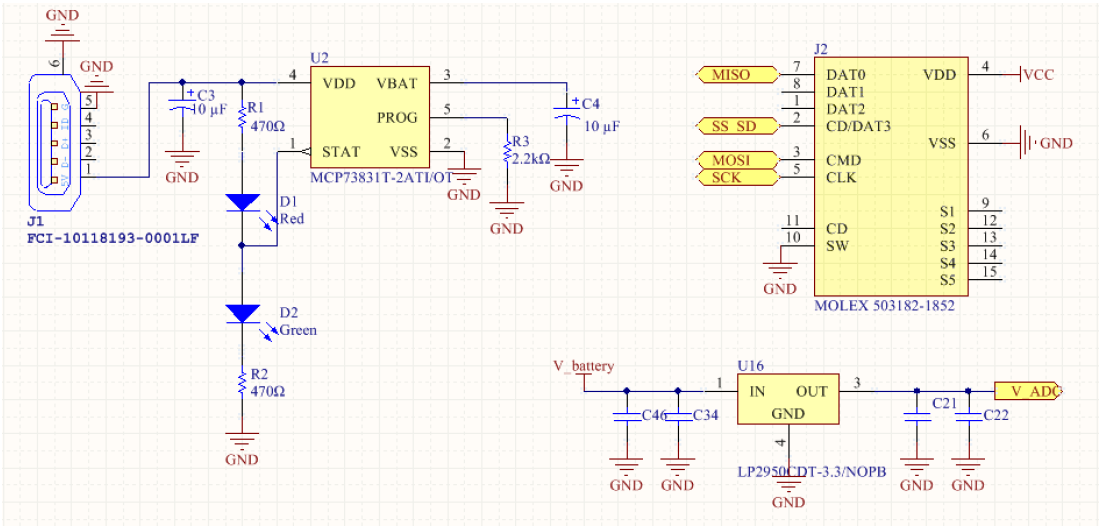

Figure C.2: Schematic diagrams of the battery charging circuit (U2), the SD-card connector (J2) and ADC votlage regulator circuit (U16).

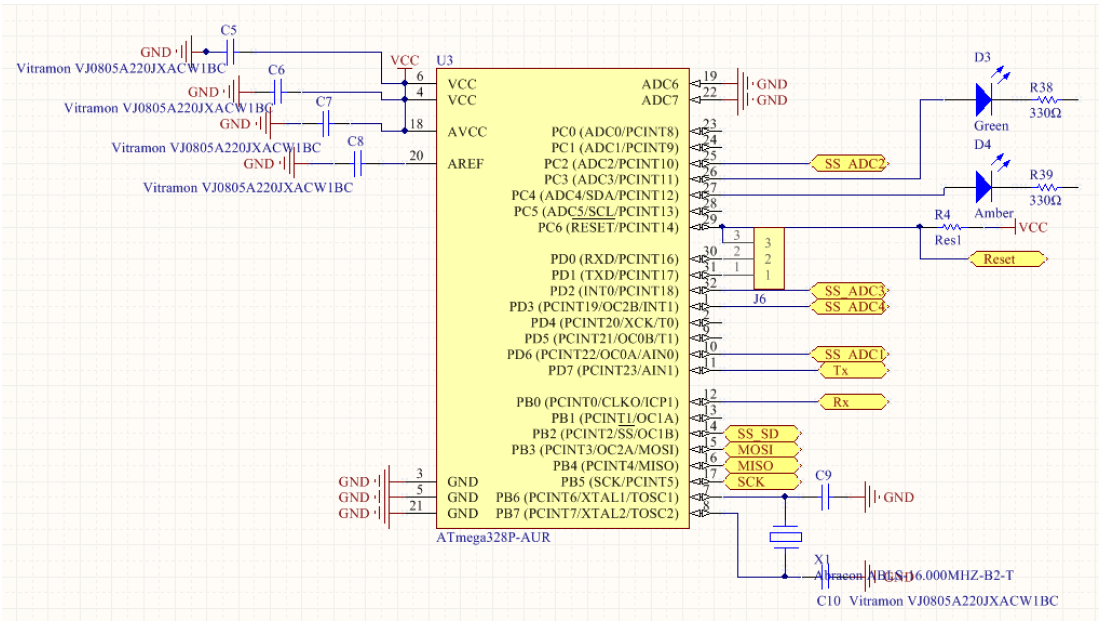

Figure C.3: Schematic diagram of the microcontroller (U3).

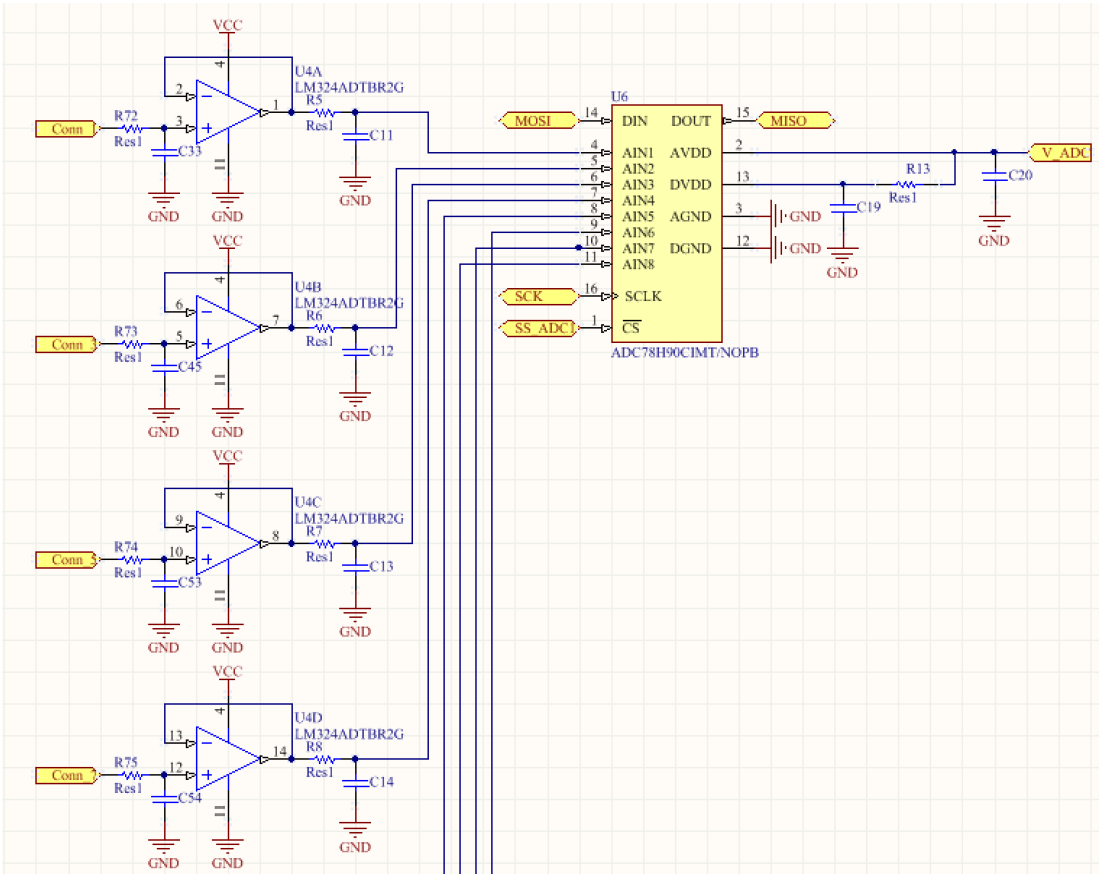

Figure C.4: Schematic diagram of one of the ADCs (U6) connected to the signal conditioning circuitry for four of the sensors.

Appendix D

Results

Table D.1: Correlation and Level of Agreement results for all thermistor sensors.

Sensor	ICC			LoA		
	Single Measure r	95% CI		Mean Diff (± SD)	95% CI	
		LB	UB		LB	UB
S_1	0.998	0.908	0.999	-0.208 (±0.136)	-0.474	0.059
S_2	0.996	0.839	0.999	-0.267 (±0.169)	-0.600	0.065
S_3	0.995	0.847	0.999	-0.292 (±0.201)	-0.686	0.103
S_4	0.997	0.831	0.999	-0.244 (±0.142)	-0.522	0.035
S_5	0.997	0.900	0.999	-0.232 (±0.160)	-0.547	0.082
S_6	0.997	0.907	0.999	-0.232 (±0.165)	-0.555	0.091

Continued on next page

Table D.1 – continued from previous page

Sensor	ICC			LoA		
	Single Measure r	95% CI		Mean Diff (± SD)	95% CI	
		LB	UB		LB	UB
S_7	0.995	0.817	0.999	-0.286 (±0.181)	-0.642	0.069
S_8	0.995	0.807	0.999	-0.286 (±0.176)	-0.631	0.060
S_9	0.997	0.901	0.999	-0.222 (±0.149)	-0.514	0.070
S_{10}	0.997	0.898	0.999	-0.230 (±0.156)	-0.536	0.076
S_{11}	0.996	0.913	0.999	-0.243 (±0.183)	-0.601	0.116
S_{12}	0.999	0.985	1.000	-0.132 (±0.126)	-0.379	0.114
S_{13}	0.997	0.857	0.999	-0.233 (±0.140)	-0.507	0.042
S_{14}	0.996	0.774	0.999	-0.269 (±0.148)	-0.560	0.022
S_{15}	0.997	0.765	0.999	-0.261 (±0.138)	-0.531	0.010
S_{16}	0.997	0.866	0.999	-0.221 (±0.131)	-0.478	0.036
S_{17}	0.997	0.899	0.999	-0.219 (±0.144)	-0.501	0.064

Continued on next page

Table D.1 – continued from previous page

Sensor	ICC			LoA		
	Single Measure r	95% CI		Mean Diff (± SD)	95% CI	
		LB	UB		LB	UB
S_{18}	0.996	0.832	0.999	-0.268 (±0.167)	-0.595	0.058
S_{19}	0.997	0.887	0.999	-0.226 (±0.146)	-0.512	0.060
S_{20}	0.997	0.868	0.999	-0.222 (±0.133)	-0.483	0.039
S_{21}	0.998	0.970	1.000	-0.157 (±0.128)	-0.407	0.094
S_{22}	0.998	0.949	1.000	-0.176 (±0.127)	-0.424	0.073
S_{23}	0.998	0.969	1.000	-0.158 (±0.127)	-0.407	0.092
S_{24}	0.998	0.956	1.000	-0.170 (±0.128)	-0.421	0.080
S_{25}	0.999	0.974	1.0000	-0.149 (±0.123)	-0.390	0.092

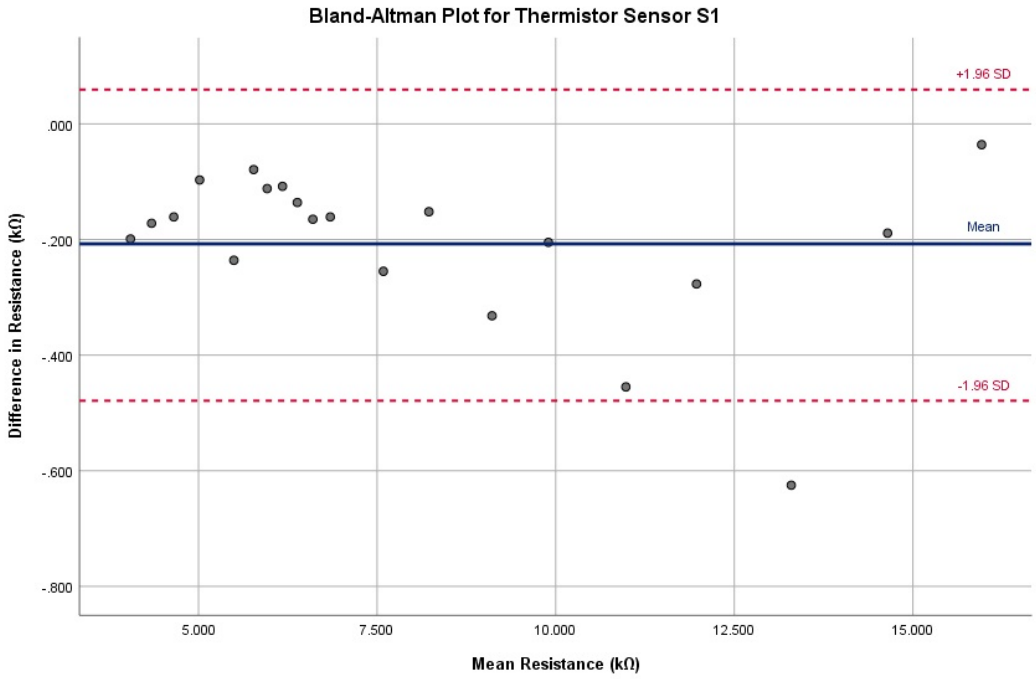

(a) Bland-Altman Plot for Resistance of S1

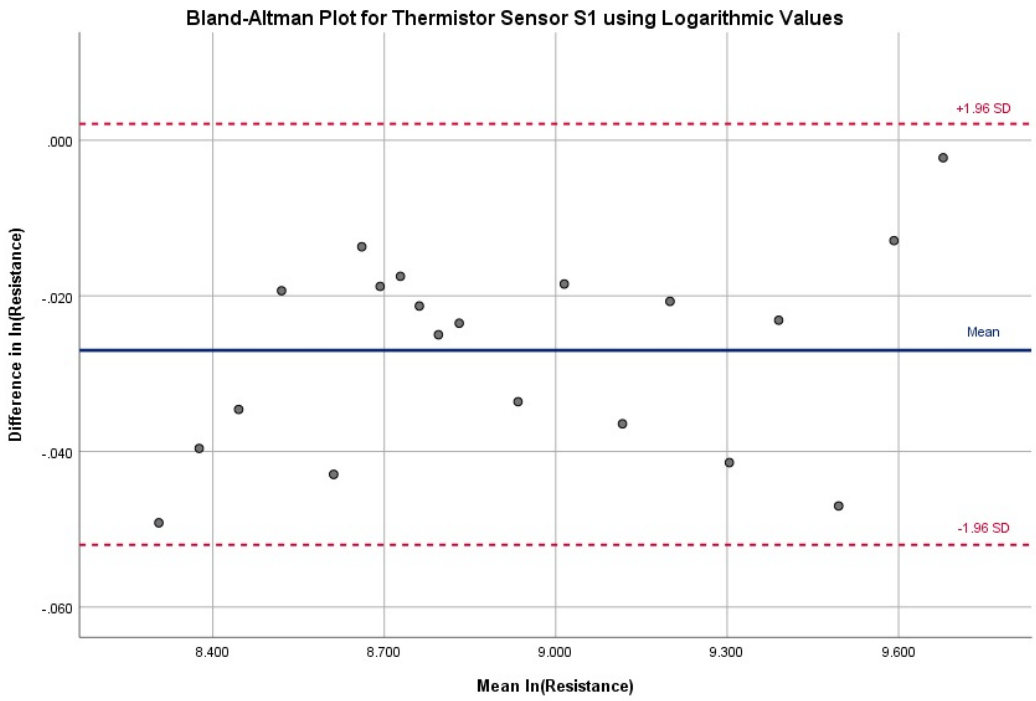

(b) Bland-Altman Plot for the natural logarithm of Resistance of S1

Figure D.1: Bland-Altman Plots for Thermistor S1: (a) Plot using the resistance values of S1; (b) Plot using the natural logarithm of the resistance values of S1.

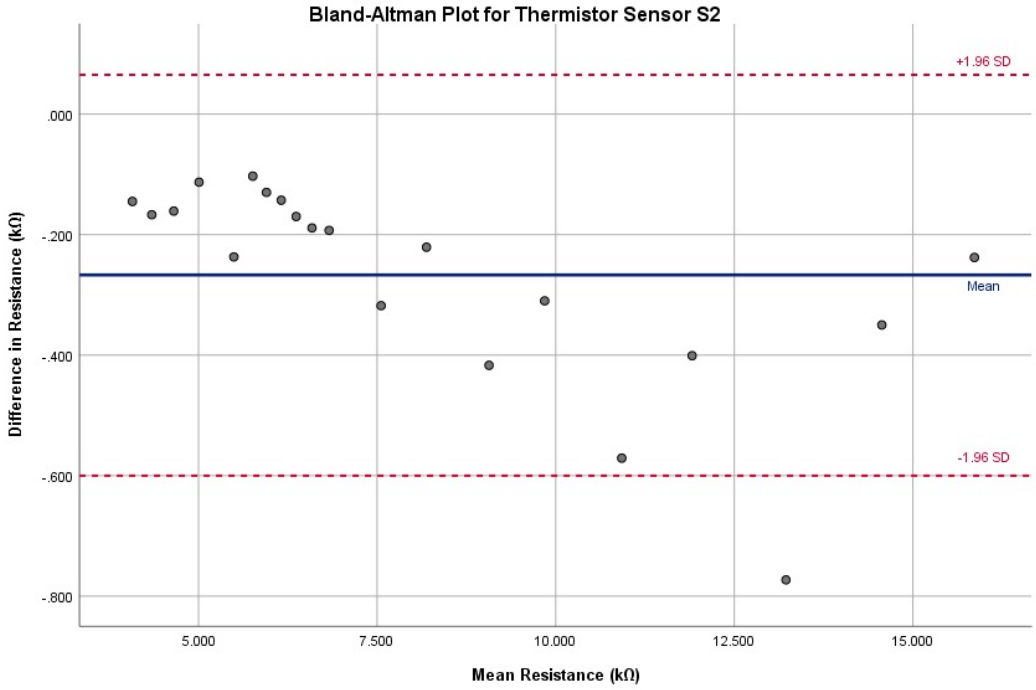

(a) Bland-Altman Plot for Resistance of S2

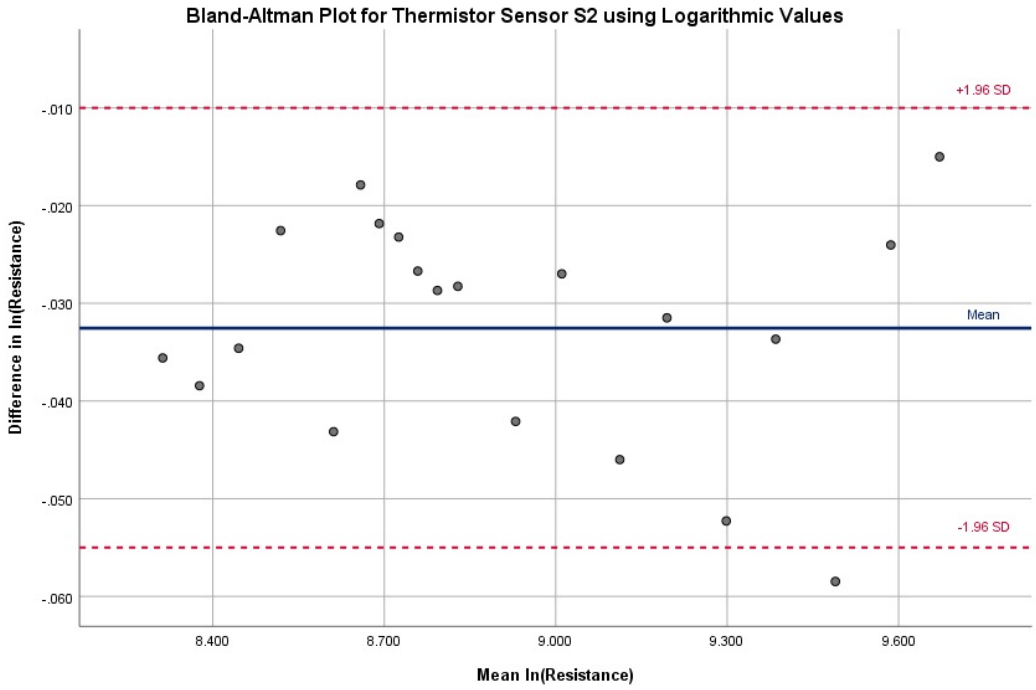

(b) Bland-Altman Plot for the natural logarithm of Resistance of S2

Figure D.2: Bland-Altman Plots for Thermistor S2: (a) Plot using the resistance values of S2; (b) Plot using the natural logarithm of the resistance values of S2.

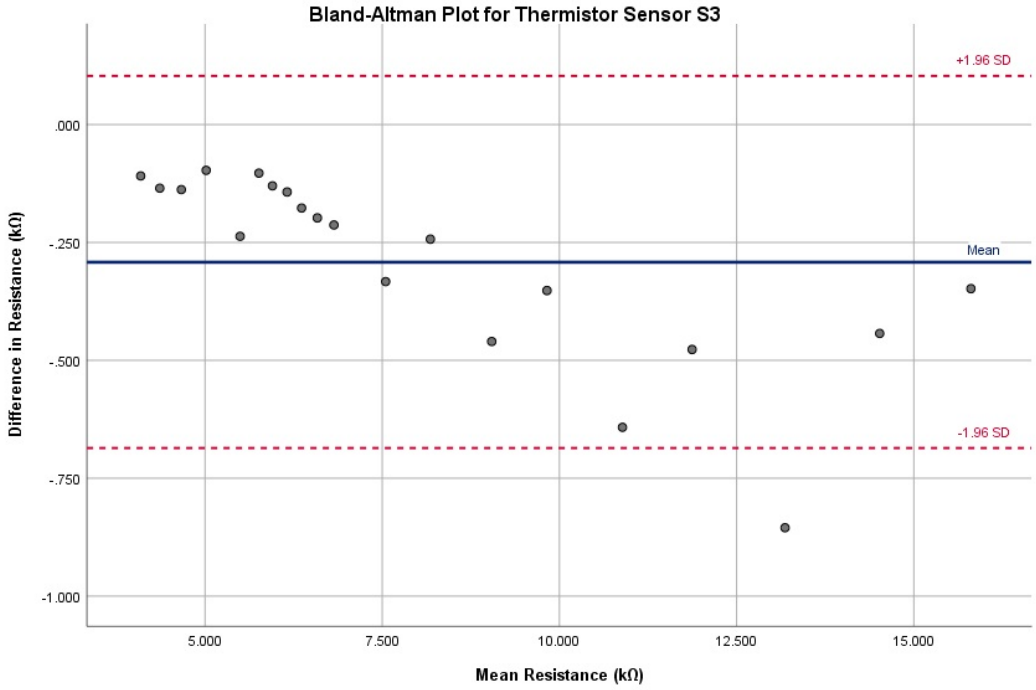

(a) Bland-Altman Plot for Resistance of S3

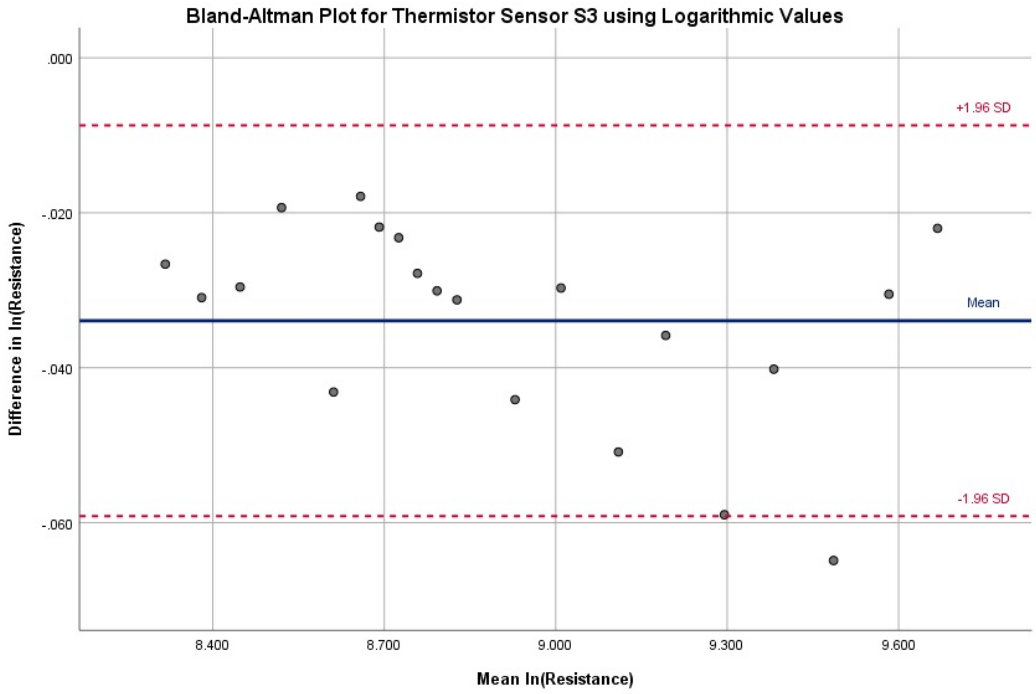

(b) Bland-Altman Plot for the natural logarithm of Resistance of S3

Figure D.3: Bland-Altman Plots for Thermistor S3: (a) Plot using the resistance values of S3; (b) Plot using the natural logarithm of the resistance values of S3.

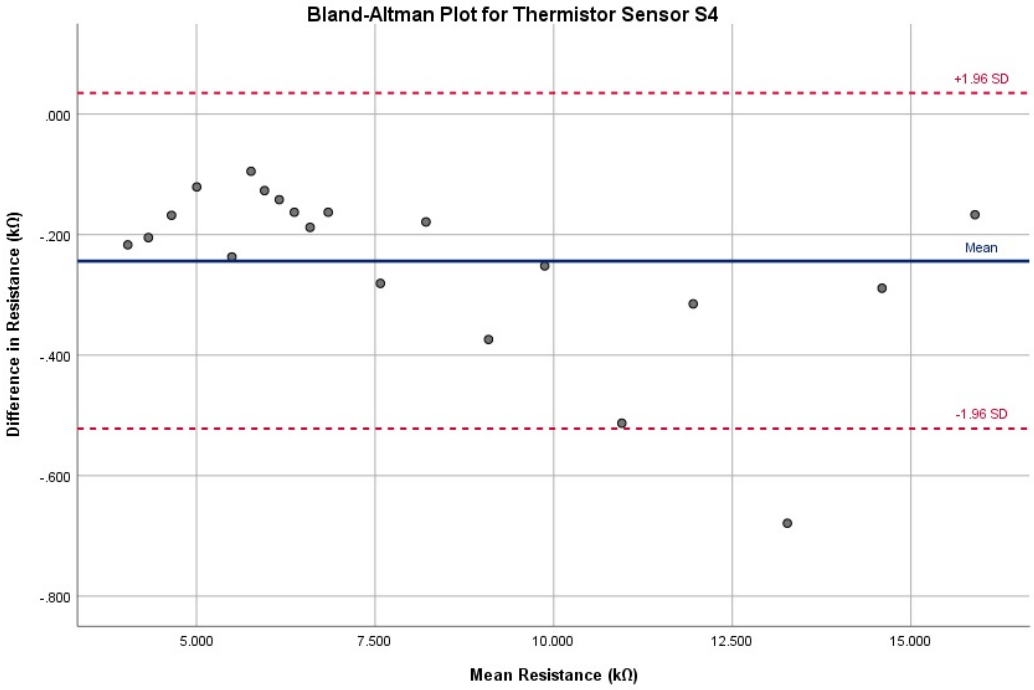

(a) Bland-Altman Plot for Resistance of S4

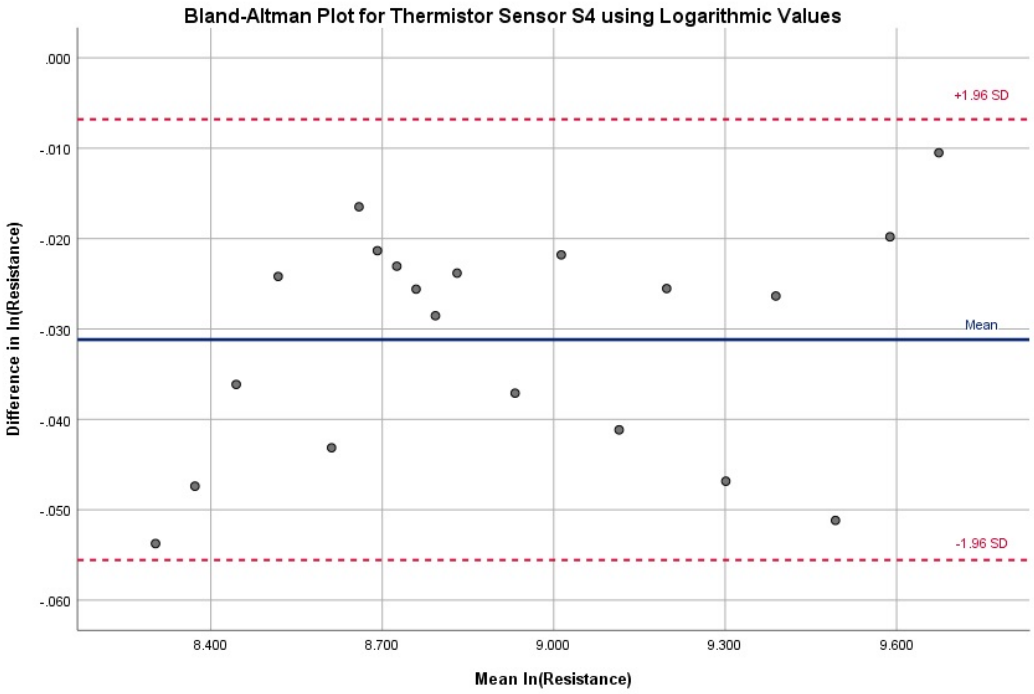

(b) Bland-Altman Plot for the natural logarithm of Resistance of S4

Figure D.4: Bland-Altman Plots for Thermistor S4: (a) Plot using the resistance values of S4; (b) Plot using the natural logarithm of the resistance values of S4.

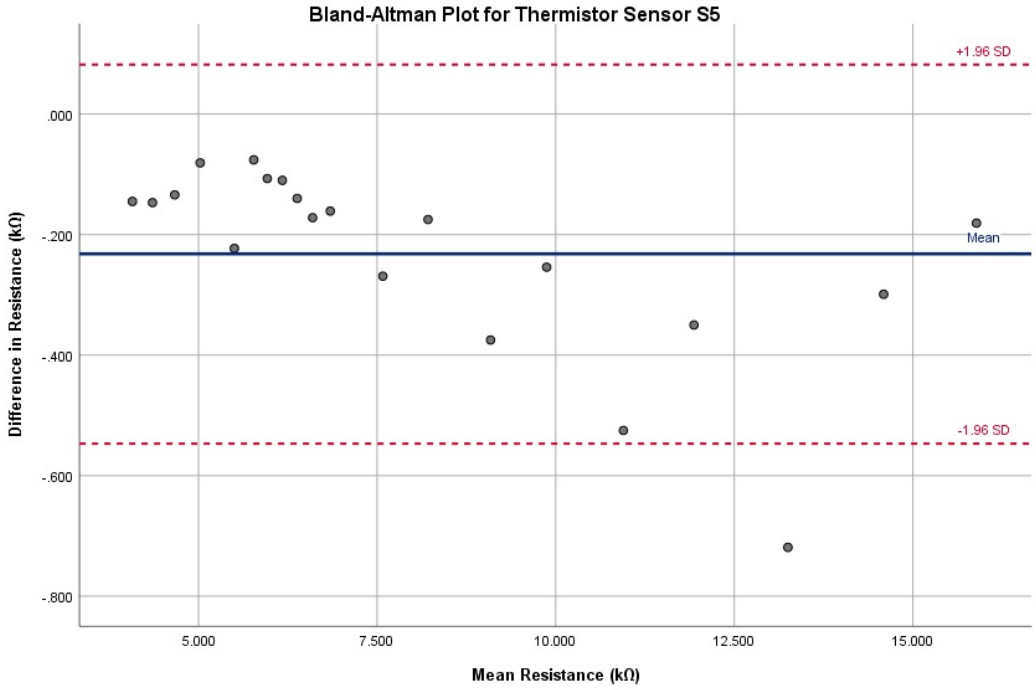

(a) Bland-Altman Plot for Resistance of S5

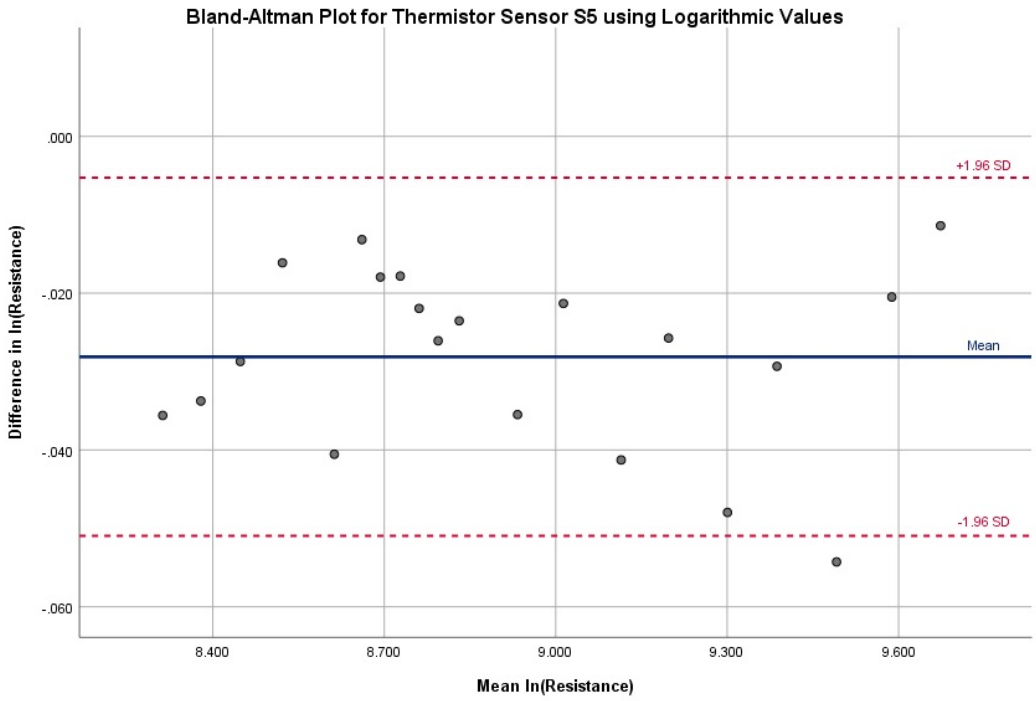

(b) Bland-Altman Plot for the natural logarithm of Resistance of S5

Figure D.5: Bland-Altman Plots for Thermistor S5: (a) Plot using the resistance values of S5; (b) Plot using the natural logarithm of the resistance values of S5.

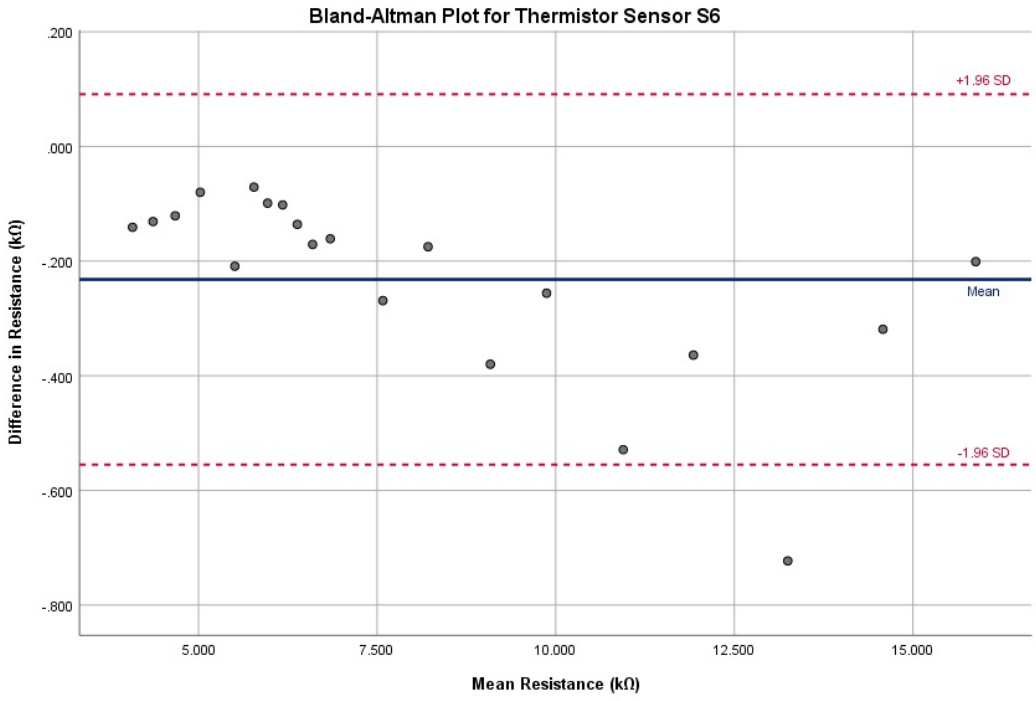

(a) Bland-Altman Plot for Resistance of S6

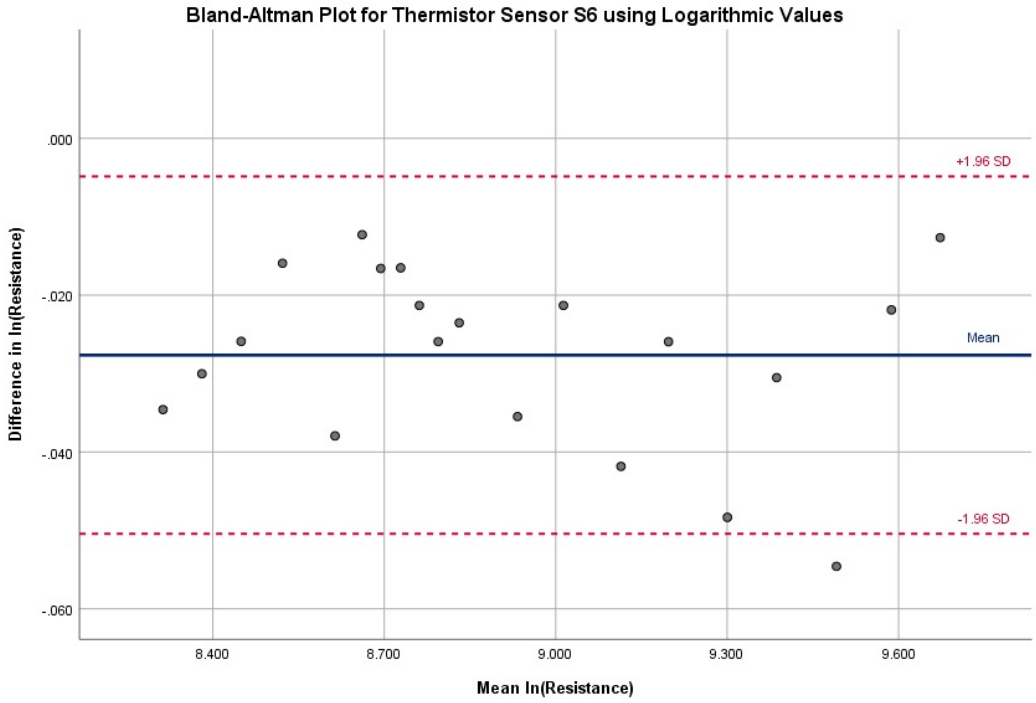

(b) Bland-Altman Plot for the natural logarithm of Resistance of S6

Figure D.6: Bland-Altman Plots for Thermistor S6: (a) Plot using the resistance values of S6; (b) Plot using the natural logarithm of the resistance values of S6.

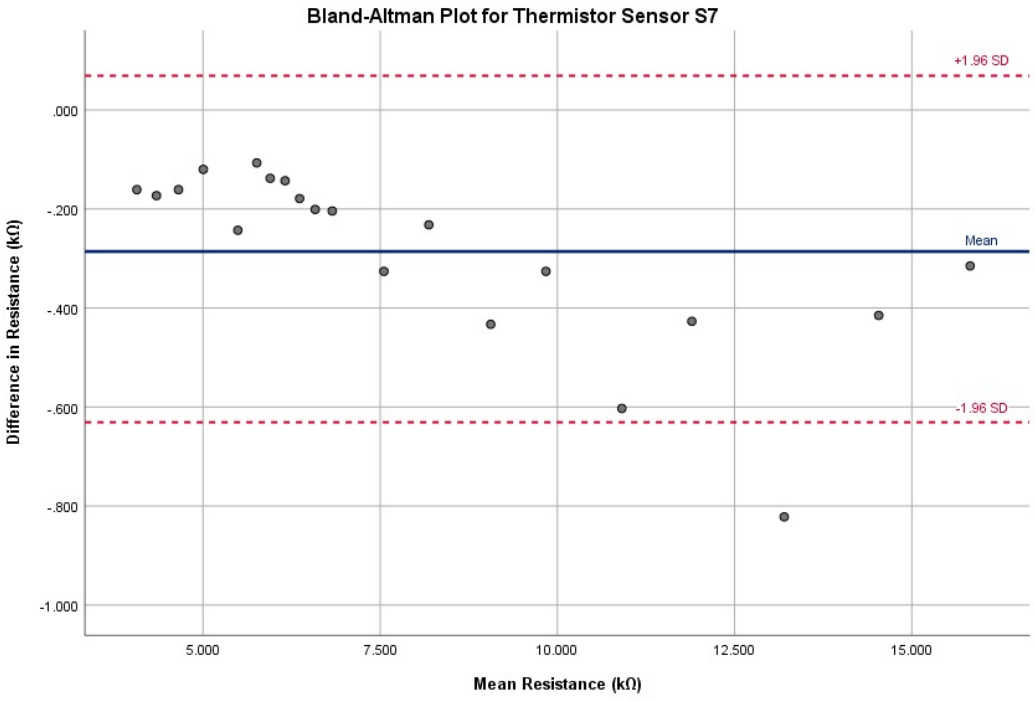

(a) Bland-Altman Plot for Resistance of S7

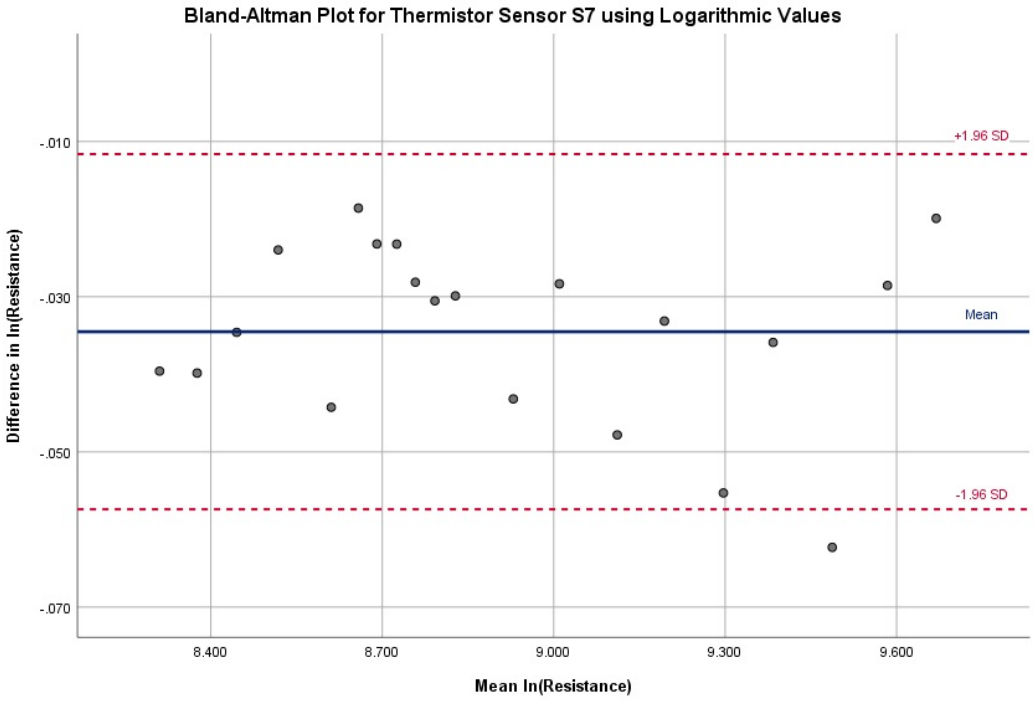

(b) Bland-Altman Plot for the natural logarithm of Resistance of S7

Figure D.7: Bland-Altman Plots for Thermistor S7: (a) Plot using the resistance values of S7; (b) Plot using the natural logarithm of the resistance values of S7.

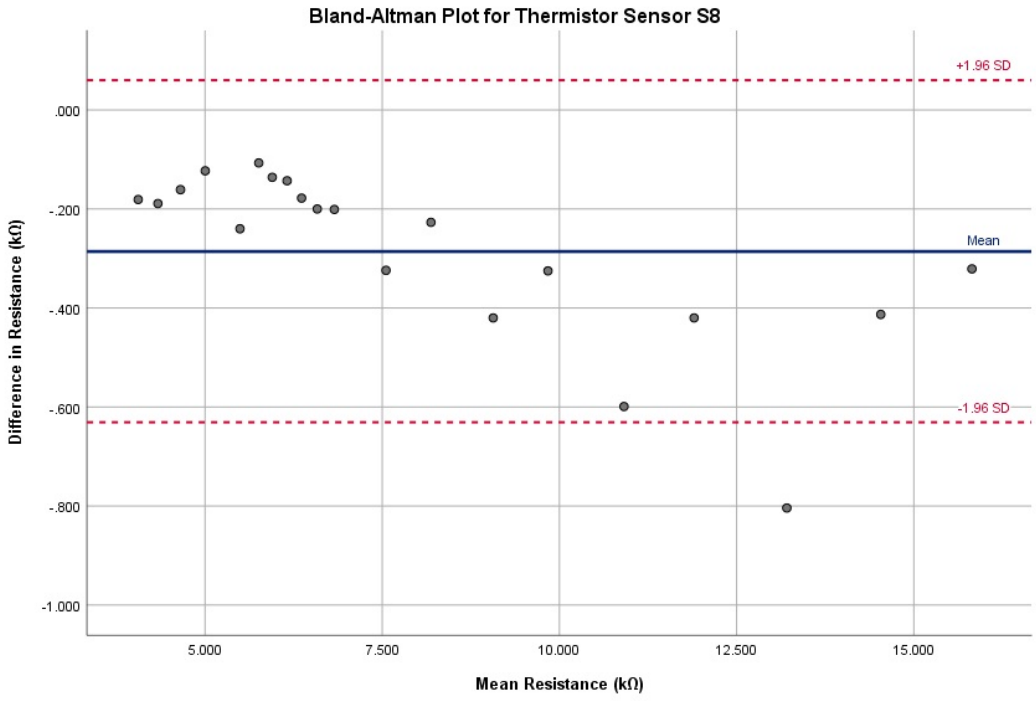

(a) Bland-Altman Plot for Resistance of S8

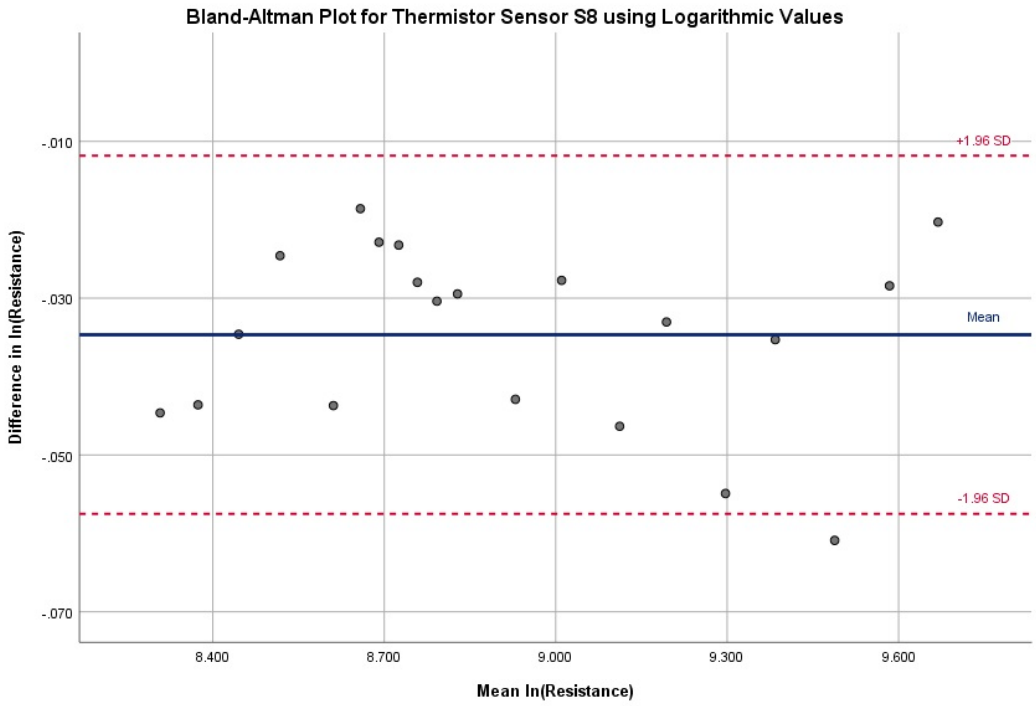

(b) Bland-Altman Plot for the natural logarithm of Resistance of S8

Figure D.8: Bland-Altman Plots for Thermistor S8: (a) Plot using the resistance values of S8; (b) Plot using the natural logarithm of the resistance values of S8.

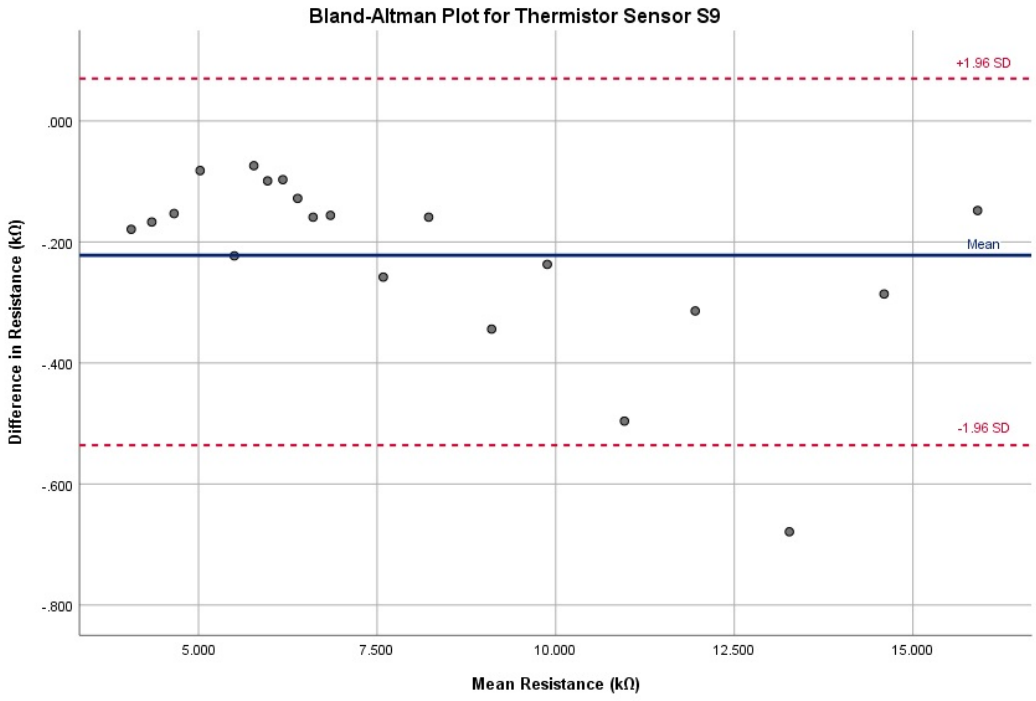

(a) Bland-Altman Plot for Resistance of S9

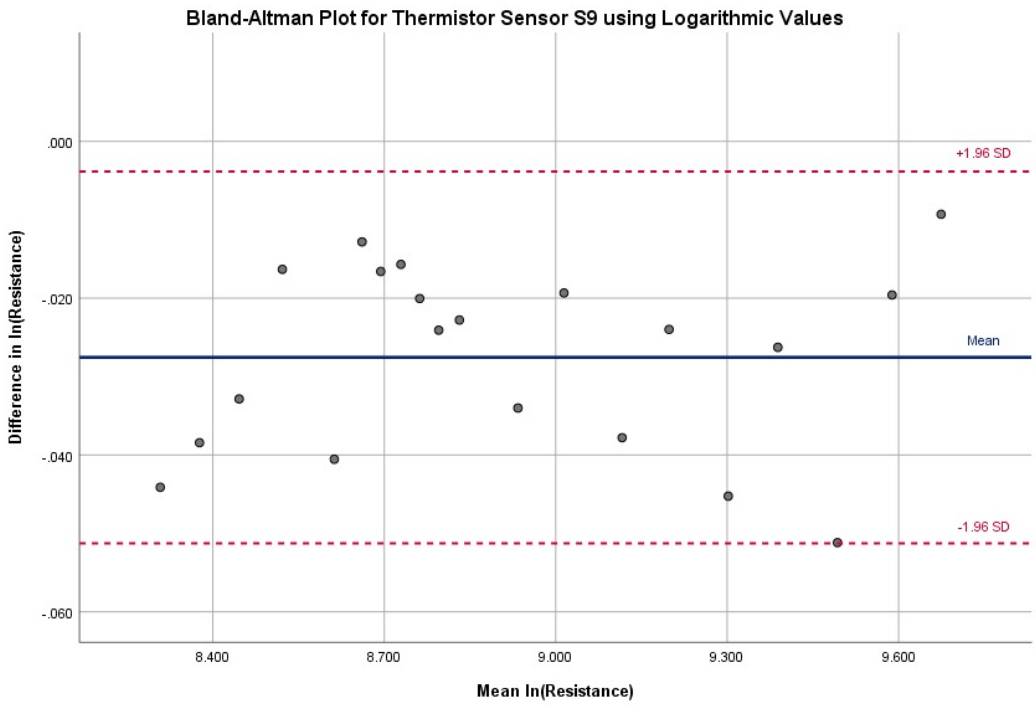

(b) Bland-Altman Plot for the natural logarithm of Resistance of S9

Figure D.9: Bland-Altman Plots for Thermistor S9: (a) Plot using the resistance values of S9; (b) Plot using the natural logarithm of the resistance values of S9.

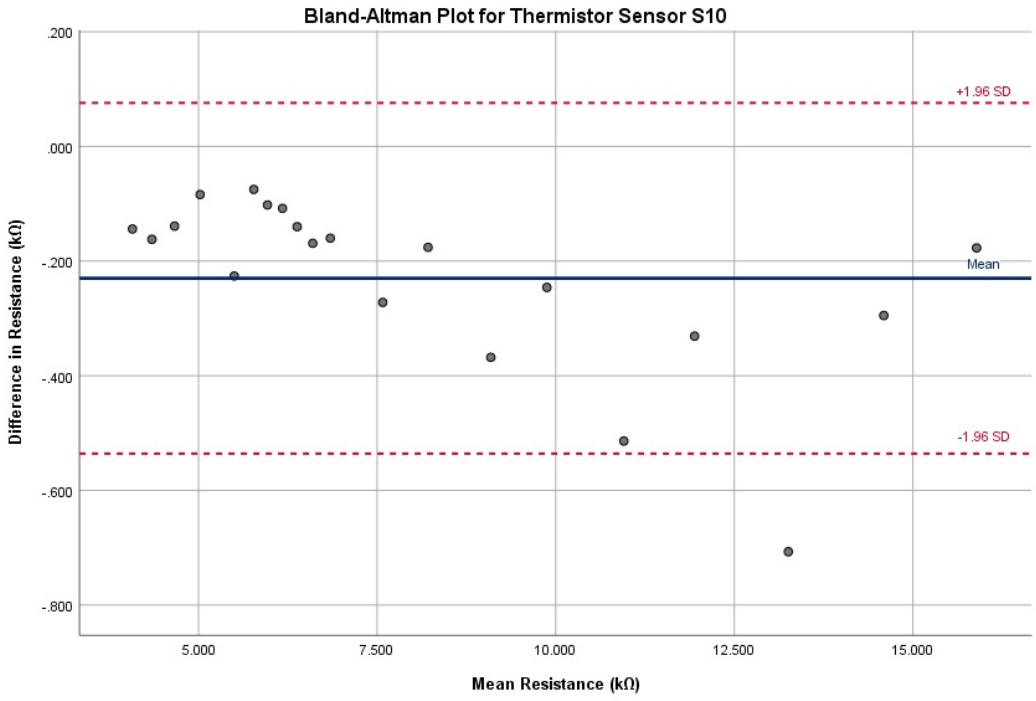

(a) Bland-Altman Plot for Resistance of S10

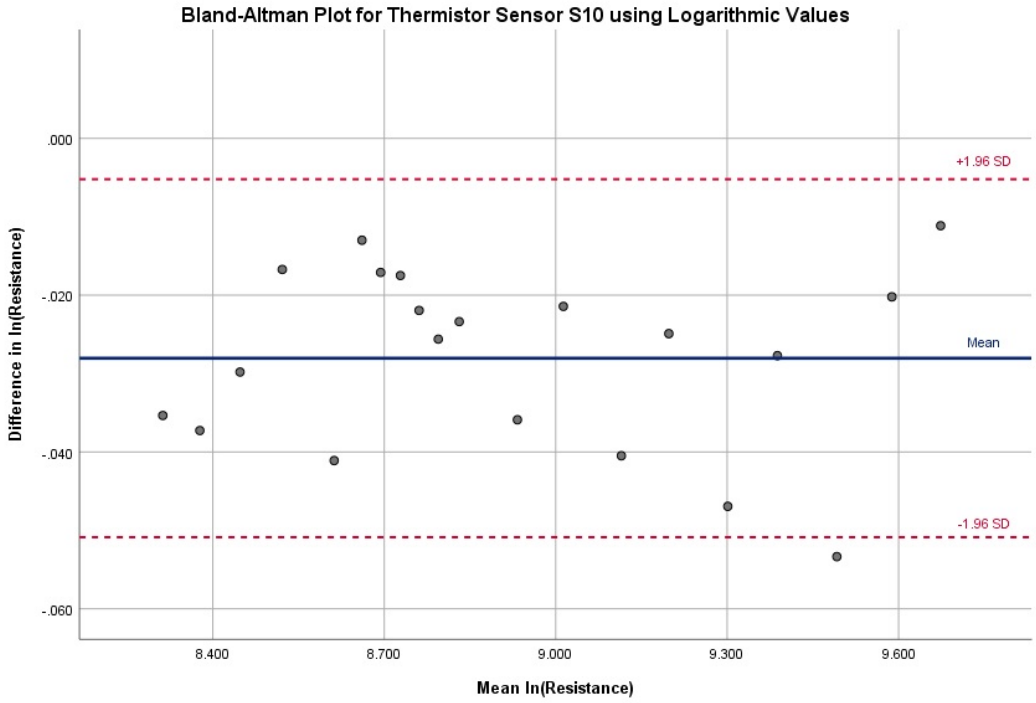

(b) Bland-Altman Plot for the natural logarithm of Resistance of S10

Figure D.10: Bland-Altman Plots for Thermistor S10: (a) Plot using the resistance values of S10; (b) Plot using the natural logarithm of the resistance values of S10.

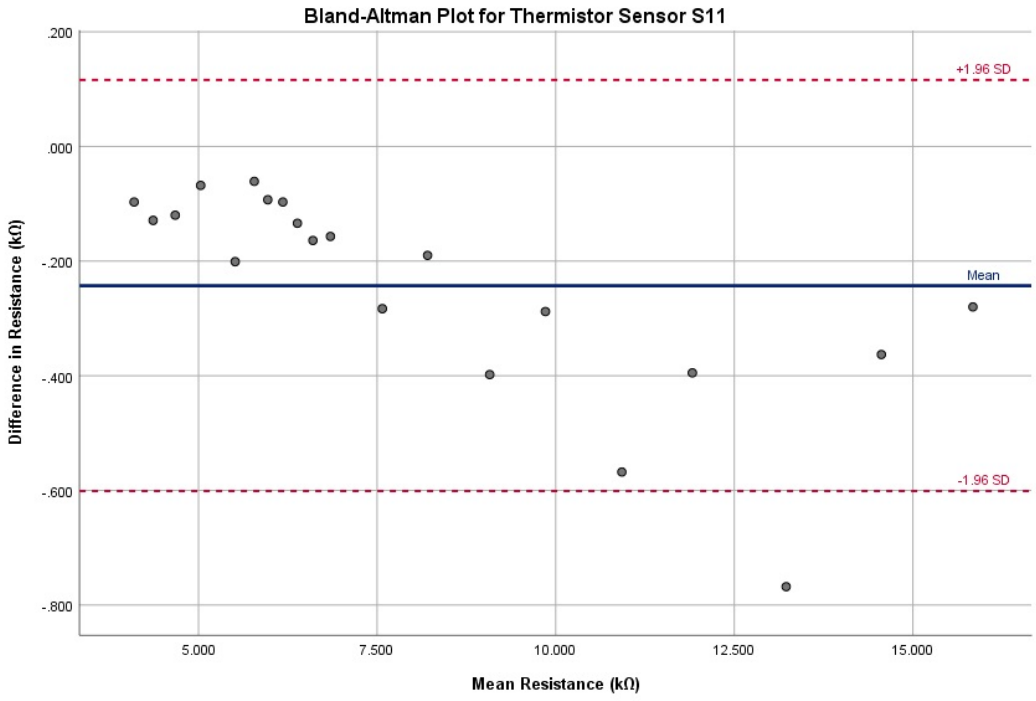

(a) Bland-Altman Plot for Resistance of S11

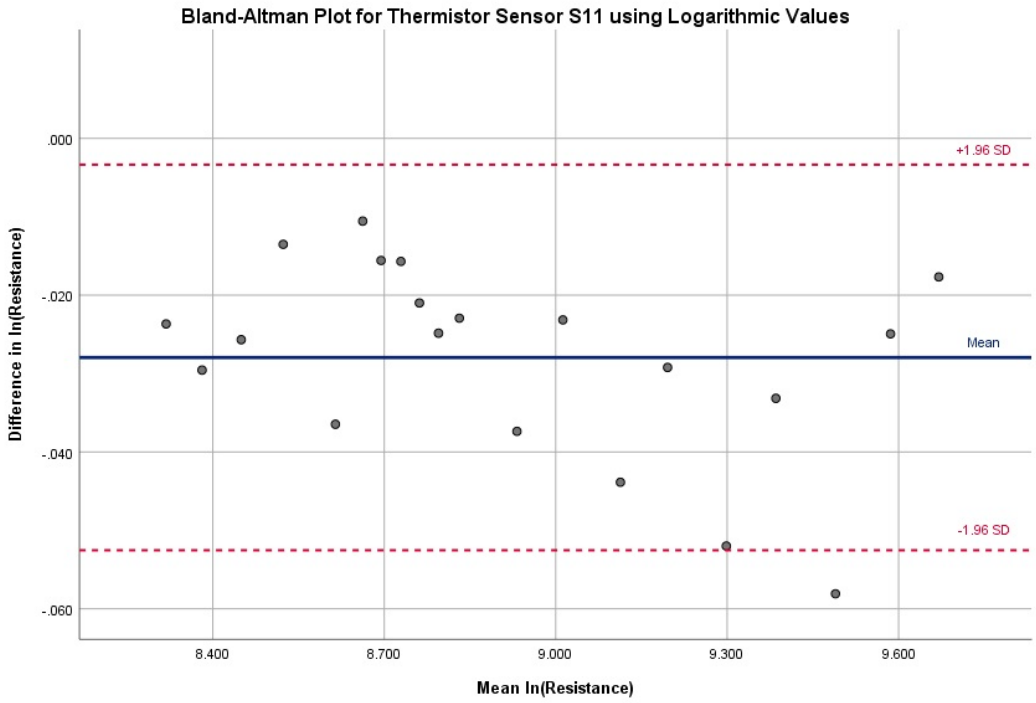

(b) Bland-Altman Plot for the natural logarithm of Resistance of S11

Figure D.11: Bland-Altman Plots for Thermistor S11: (a) Plot using the resistance values of S11; (b) Plot using the natural logarithm of the resistance values of S11.

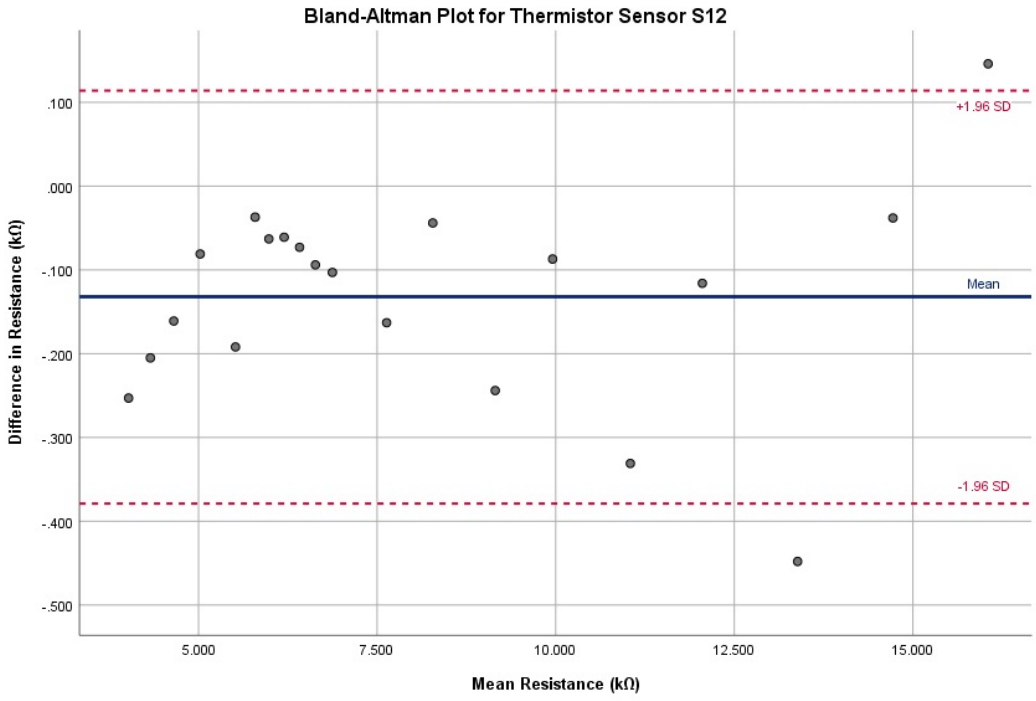

(a) Bland-Altman Plot for Resistance of S12

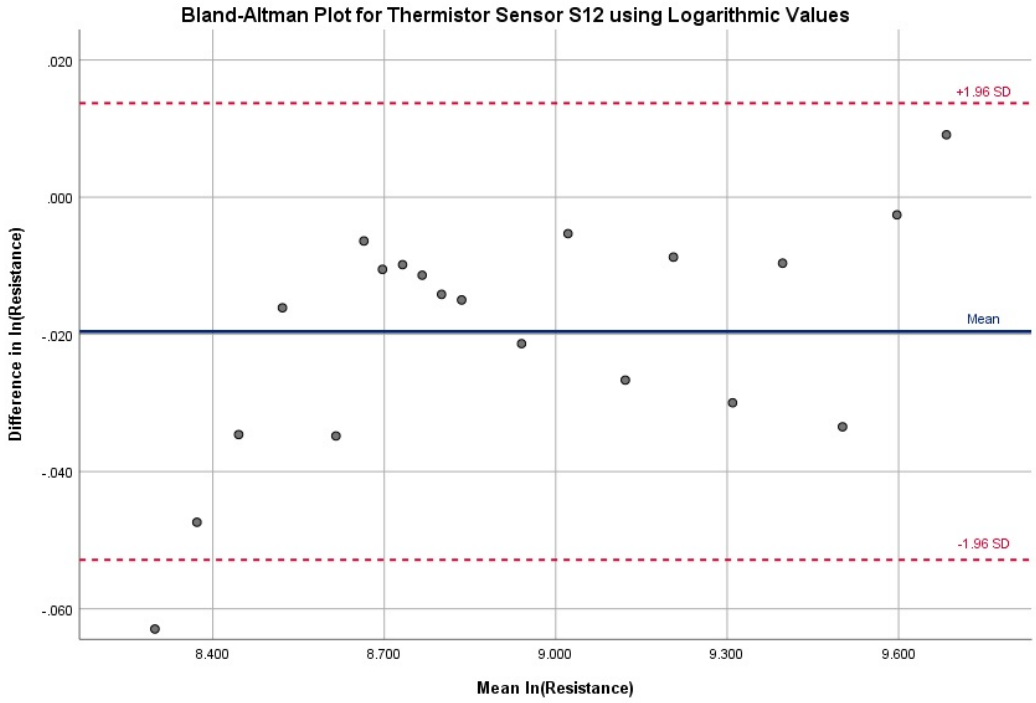

(b) Bland-Altman Plot for the natural logarithm of Resistance of S12

Figure D.12: Bland-Altman Plots for Thermistor S12: (a) Plot using the resistance values of S12; (b) Plot using the natural logarithm of the resistance values of S12.

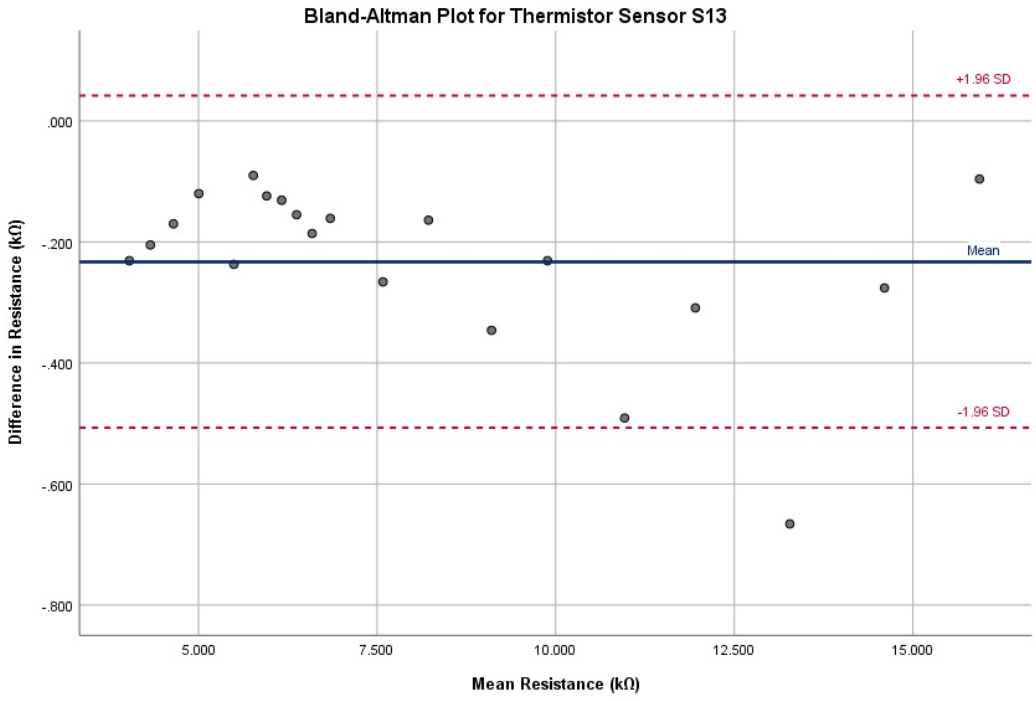

(a) Bland-Altman Plot for Resistance of S13

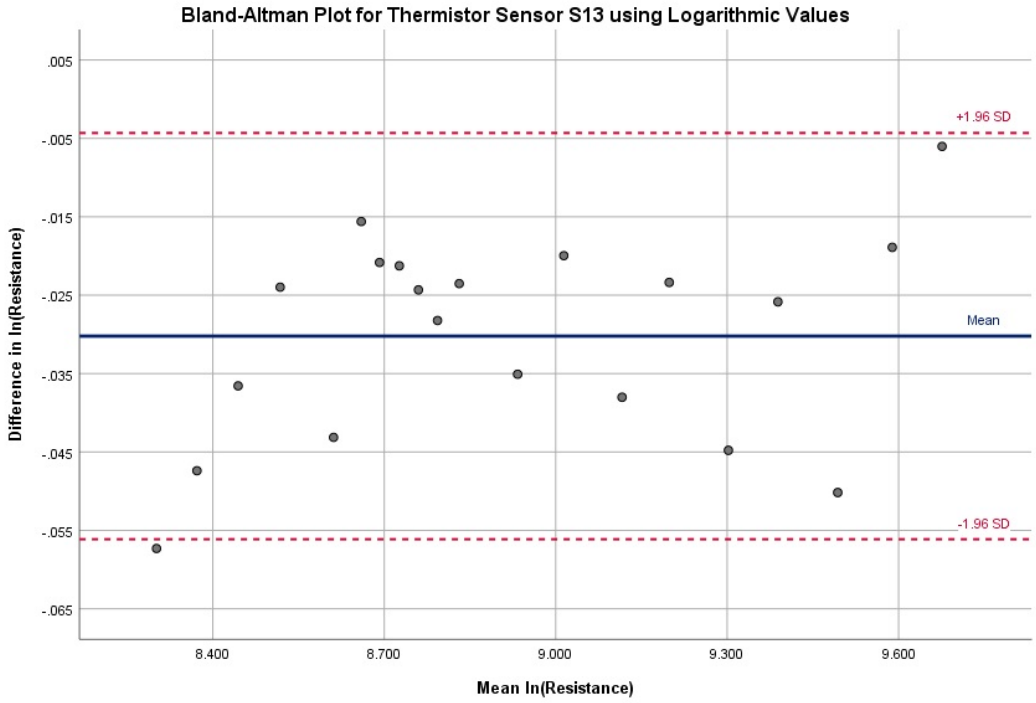

(b) Bland-Altman Plot for the natural logarithm of Resistance of S13

Figure D.13: Bland-Altman Plots for Thermistor S13: (a) Plot using the resistance values of S13; (b) Plot using the natural logarithm of the resistance values of S13.

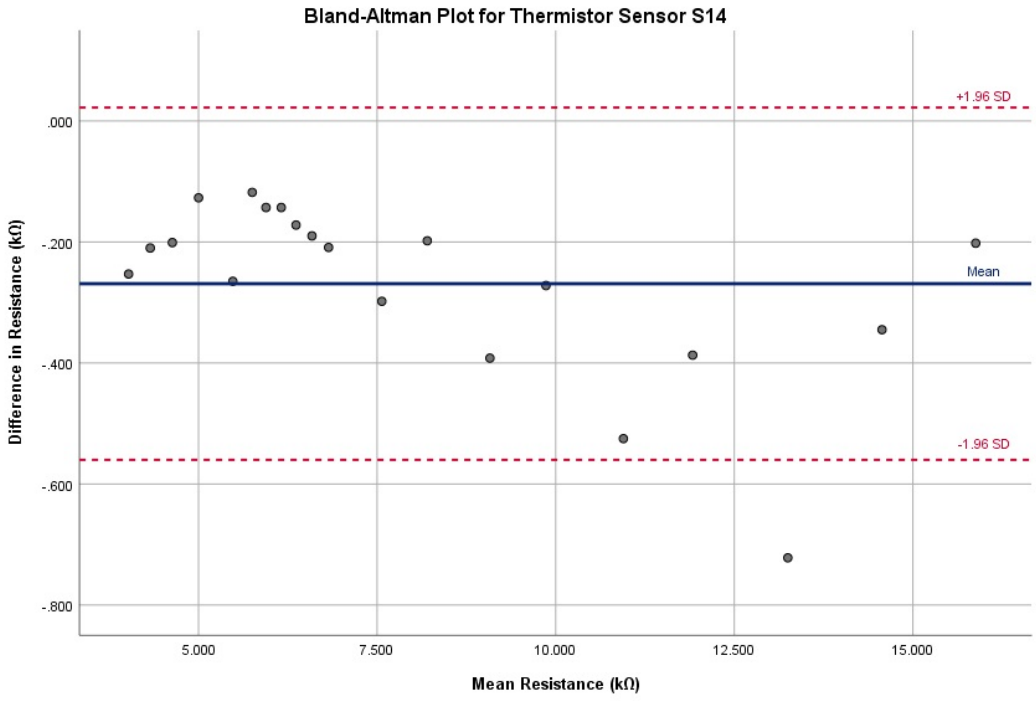

(a) Bland-Altman Plot for Resistance of S14

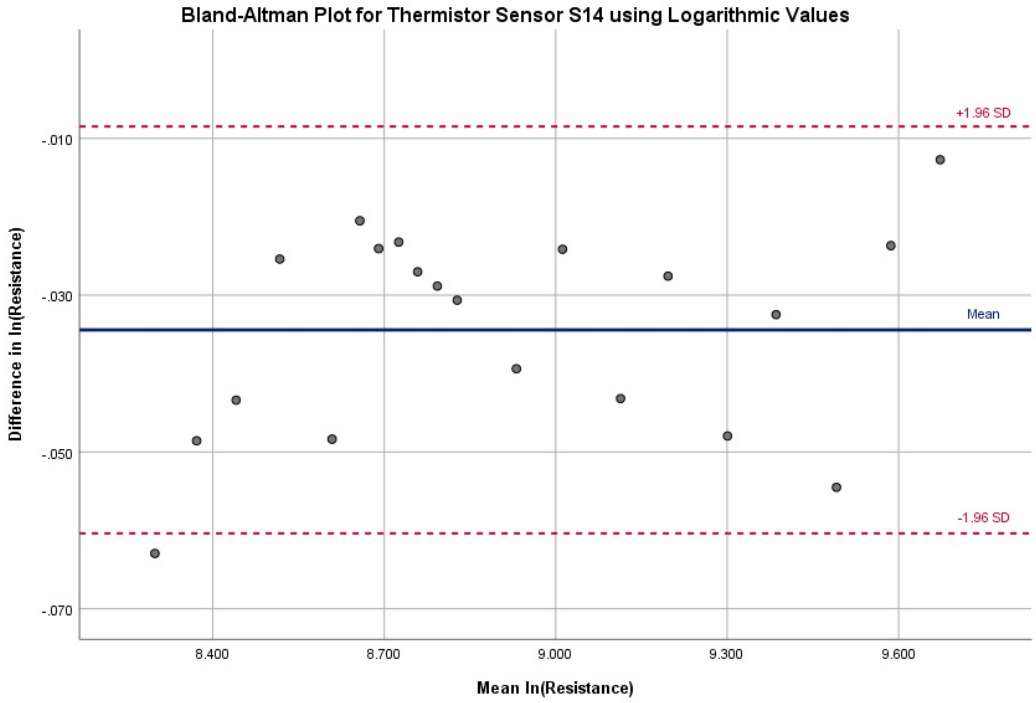

(b) Bland-Altman Plot for the natural logarithm of Resistance of S14

Figure D.14: Bland-Altman Plots for Thermistor S14: (a) Plot using the resistance values of S14; (b) Plot using the natural logarithm of the resistance values of S14.

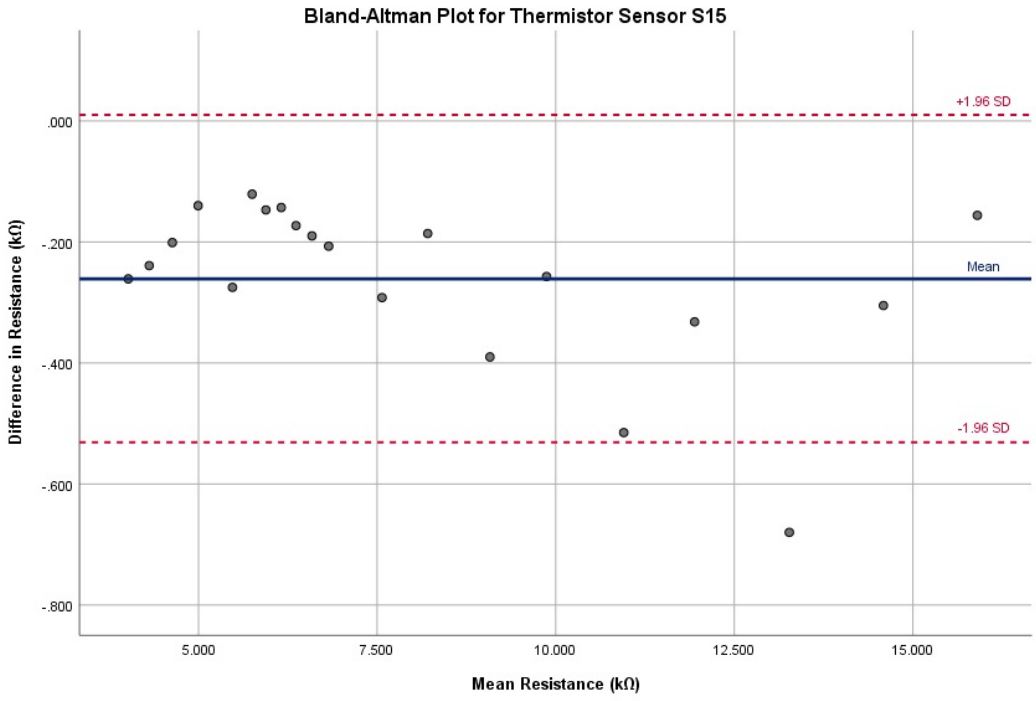

(a) Bland-Altman Plot for Resistance of S15

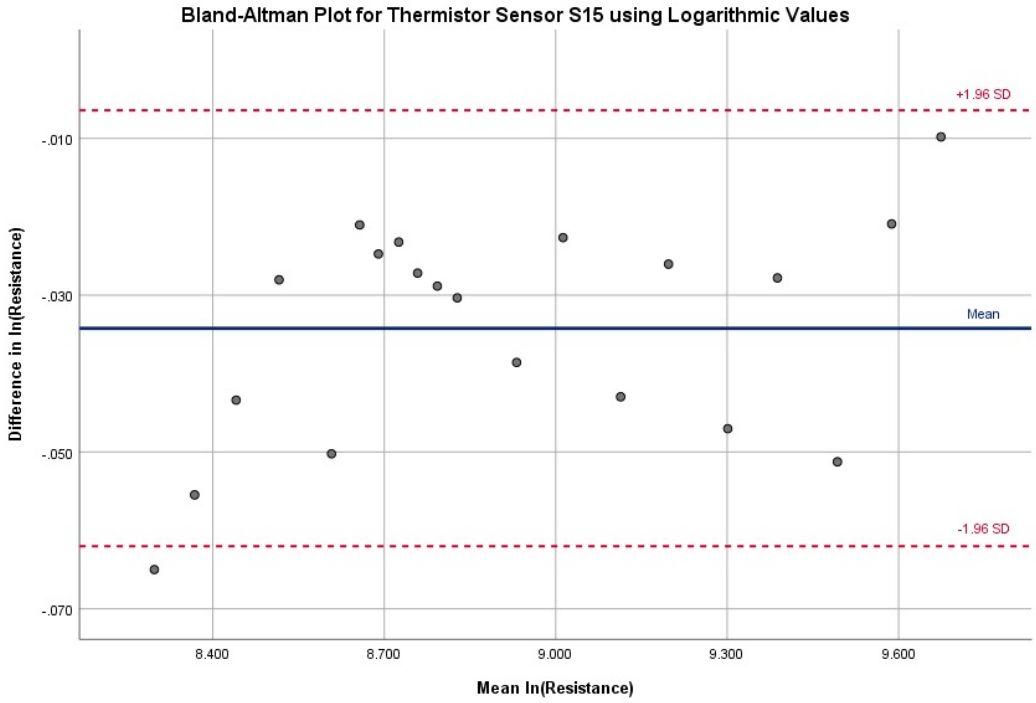

(b) Bland-Altman Plot for the natural logarithm of Resistance of S15

Figure D.15: Bland-Altman Plots for Thermistor S15: (a) Plot using the resistance values of S15; (b) Plot using the natural logarithm of the resistance values of S15.

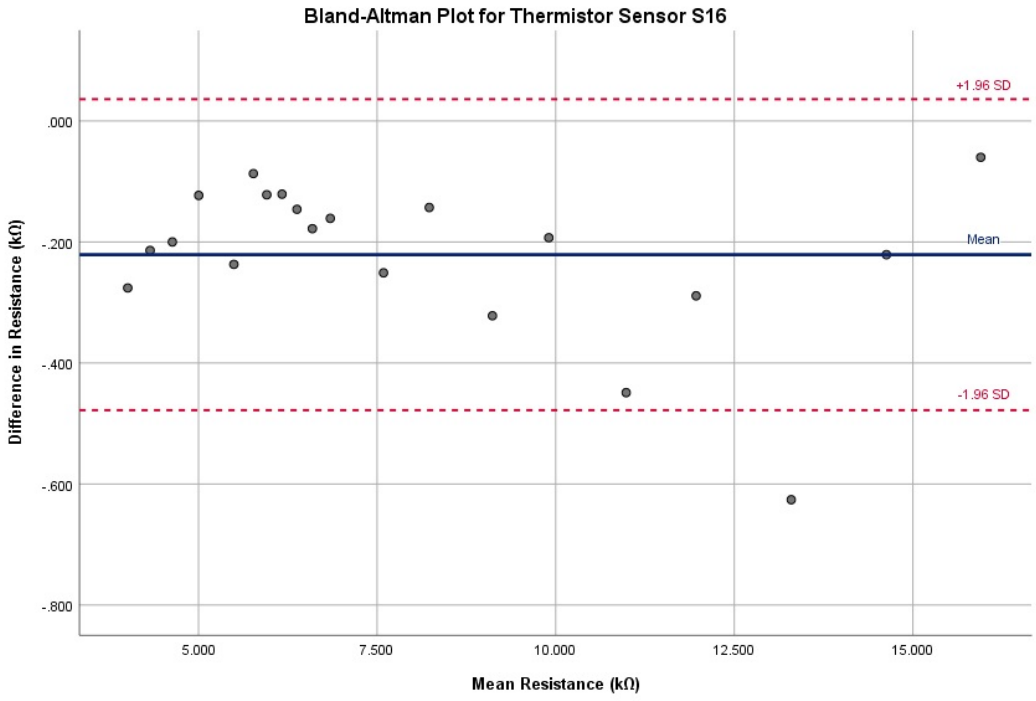

(a) Bland-Altman Plot for Resistance of S16

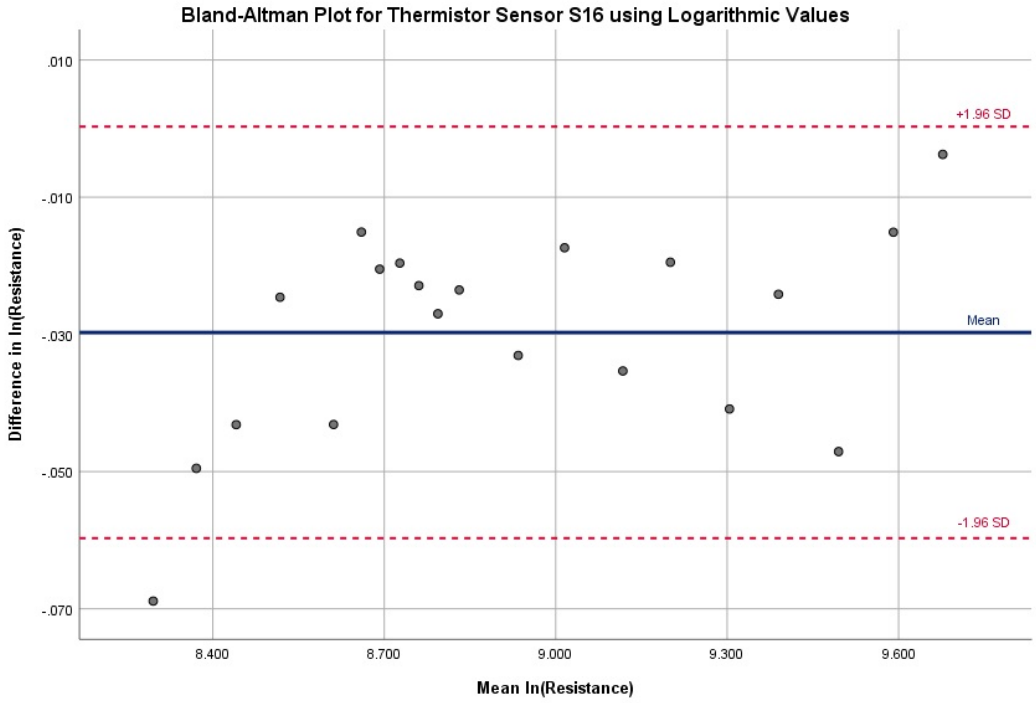

(b) Bland-Altman Plot for the natural logarithm of Resistance of S16

Figure D.16: Bland-Altman Plots for Thermistor S16: (a) Plot using the resistance values of S16; (b) Plot using the natural logarithm of the resistance values of S16.

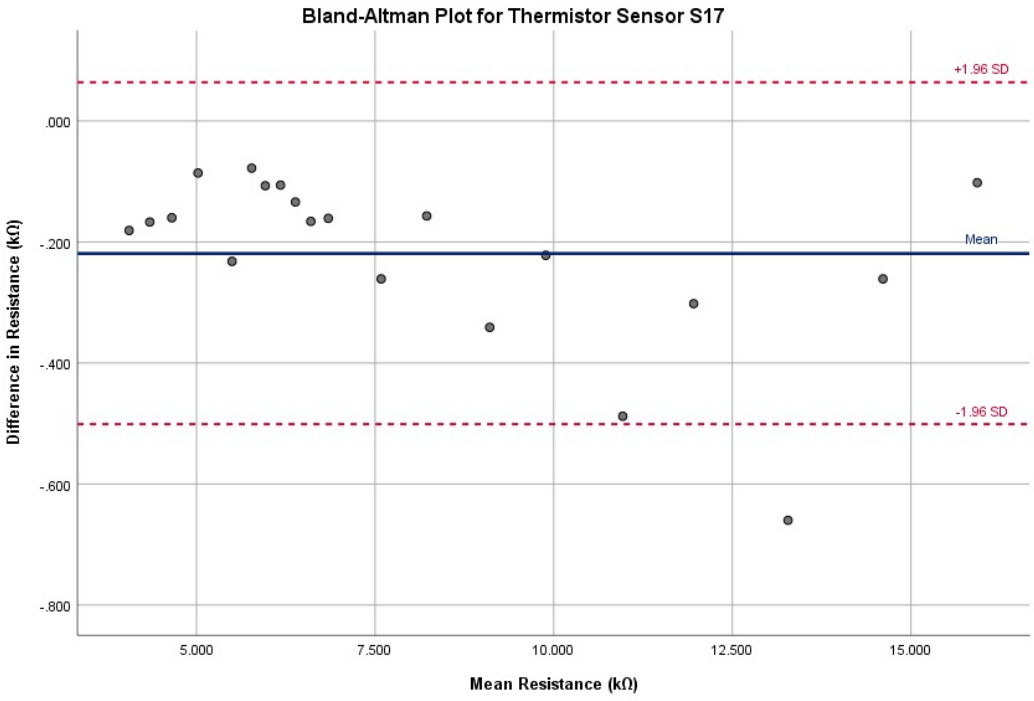

(a) Bland-Altman Plot for Resistance of S17

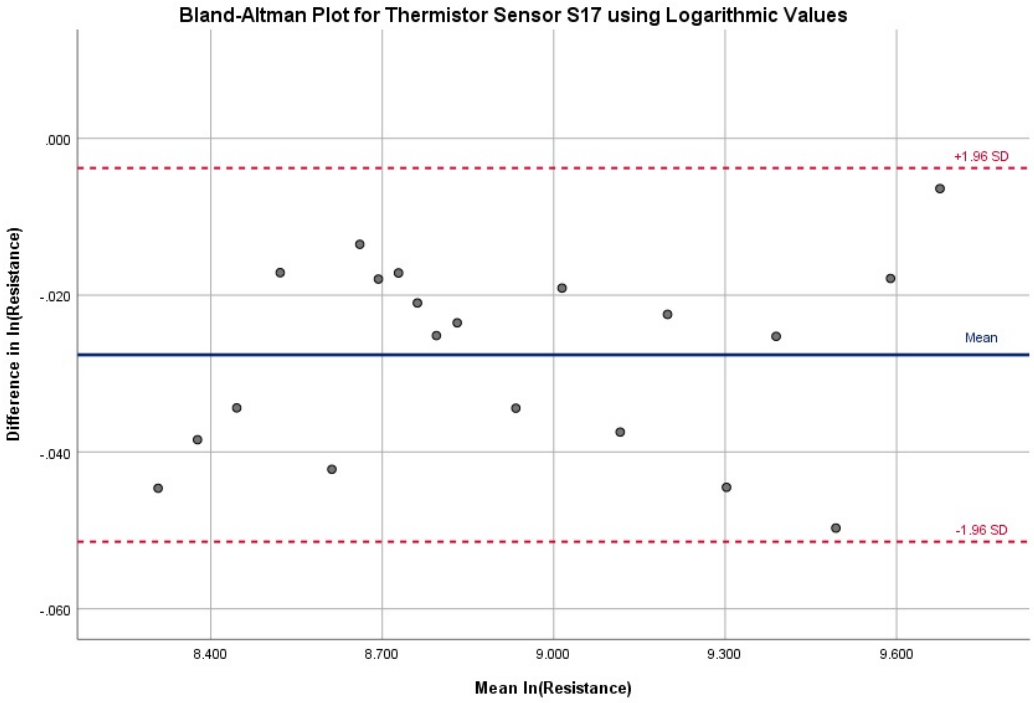

(b) Bland-Altman Plot for the natural logarithm of Resistance of S17

Figure D.17: Bland-Altman Plots for Thermistor S17: (a) Plot using the resistance values of S17; (b) Plot using the natural logarithm of the resistance values of S17.

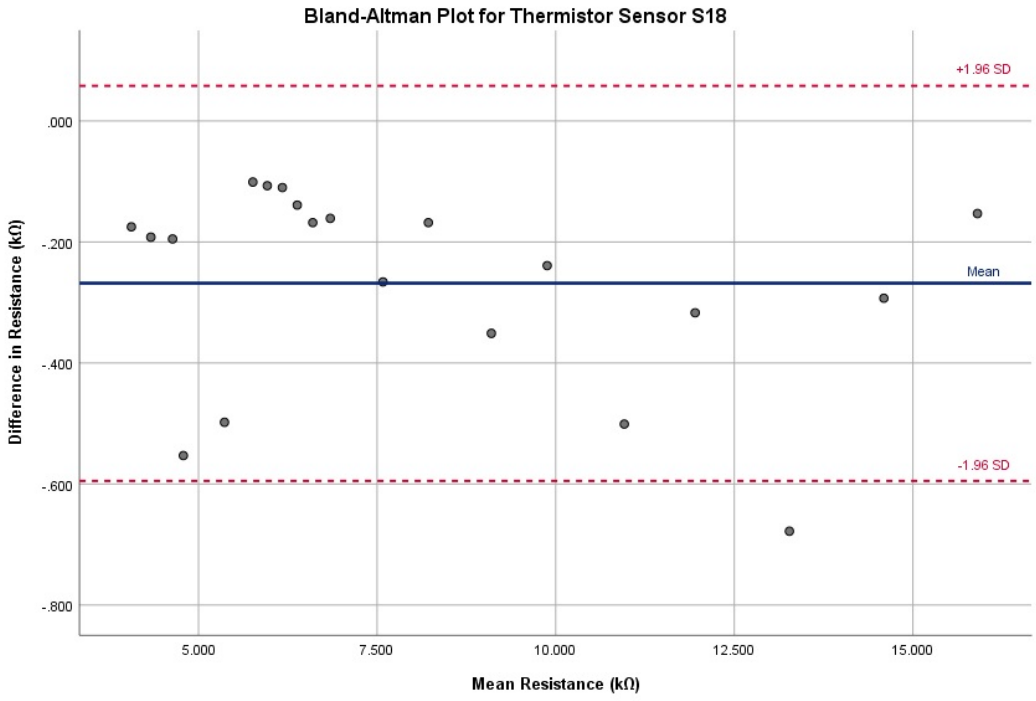

(a) Bland-Altman Plot for Resistance of S18

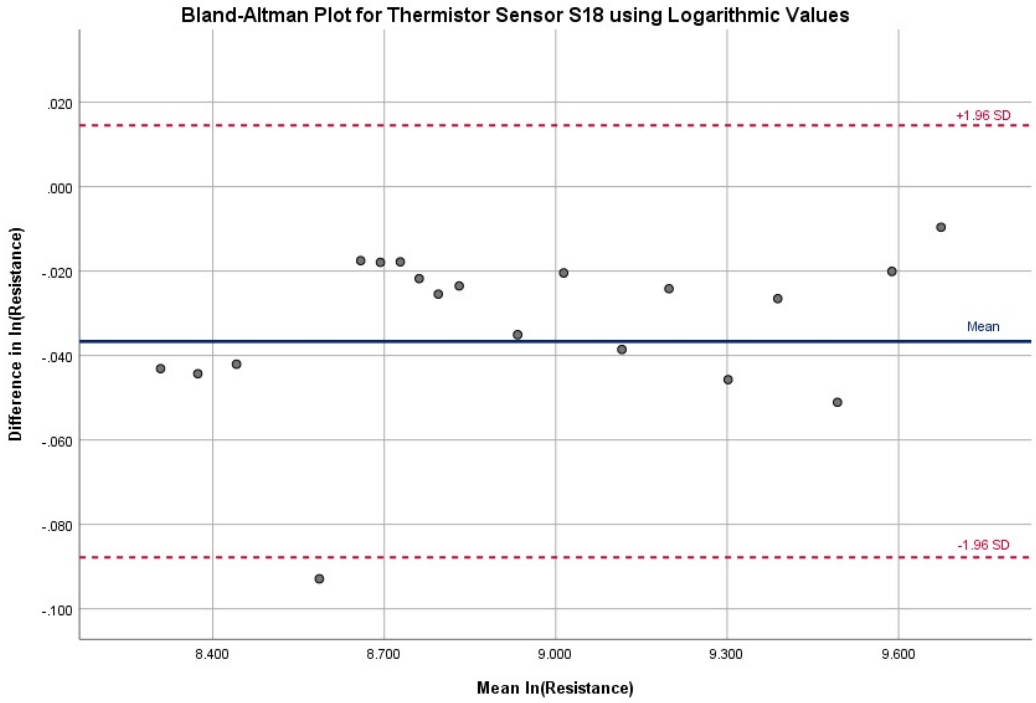

(b) Bland-Altman Plot for the natural logarithm of Resistance of S18

Figure D.18: Bland-Altman Plots for Thermistor S18: (a) Plot using the resistance values of S18; (b) Plot using the natural logarithm of the resistance values of S18.

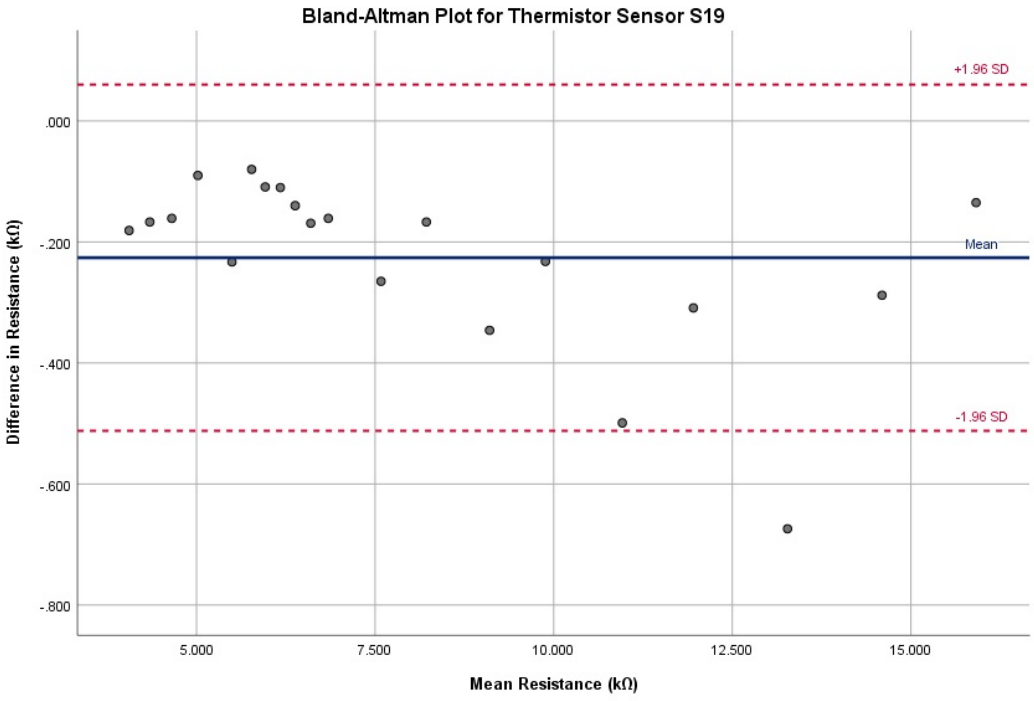

(a) Bland-Altman Plot for Resistance of S19

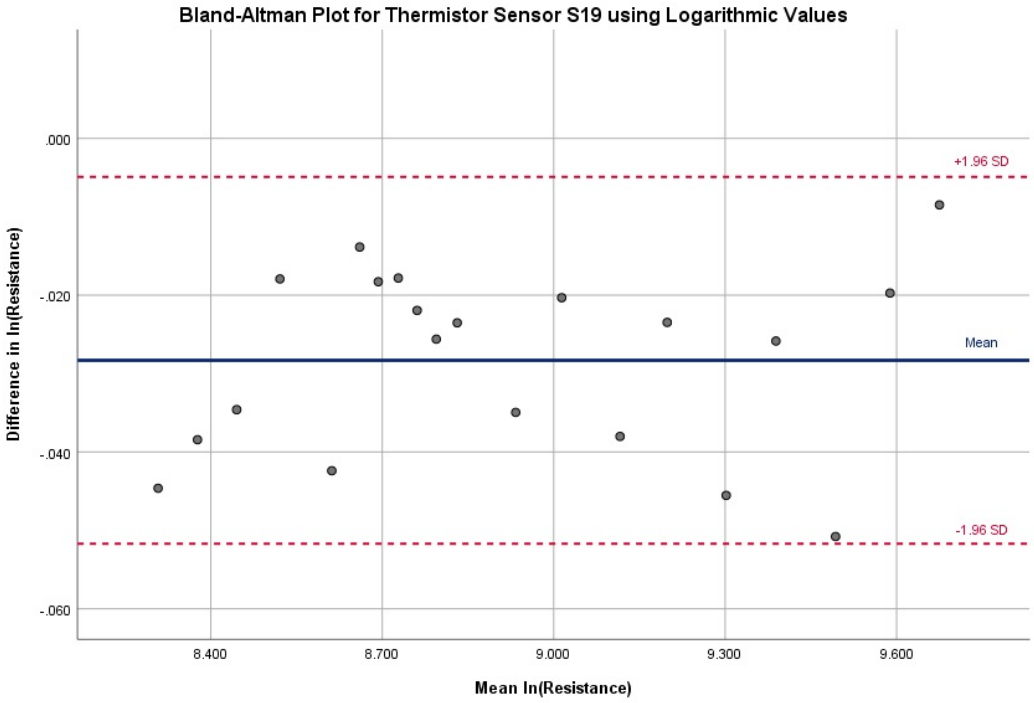

(b) Bland-Altman Plot for the natural logarithm of Resistance of S19

Figure D.19: Bland-Altman Plots for Thermistor S19: (a) Plot using the resistance values of S19; (b) Plot using the natural logarithm of the resistance values of S19.

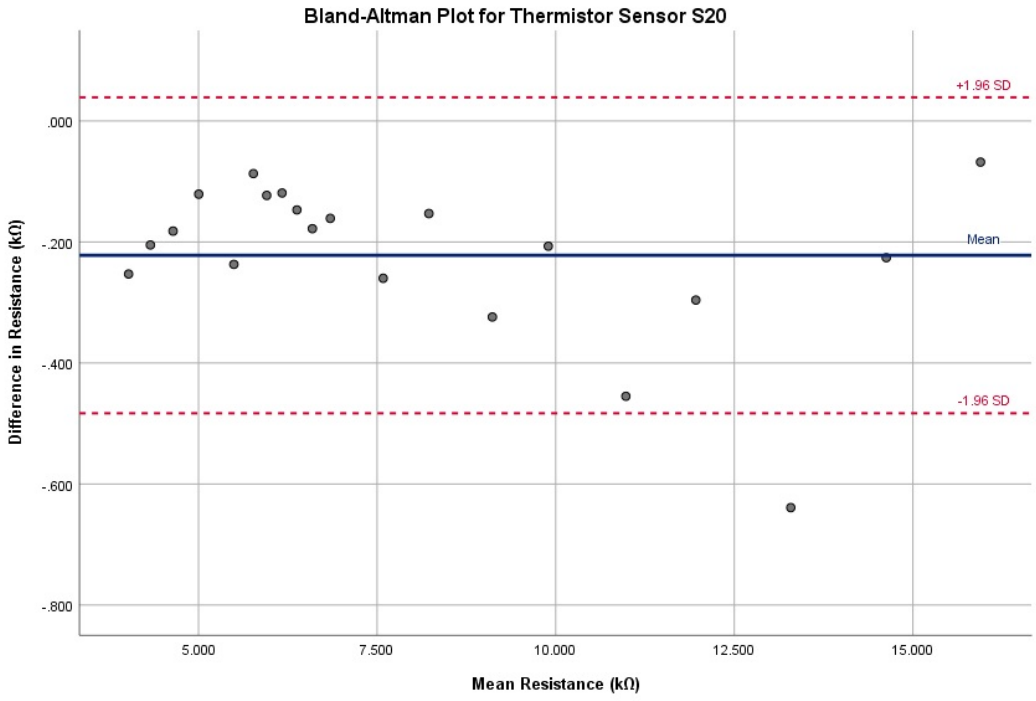

(a) Bland-Altman Plot for Resistance of S20

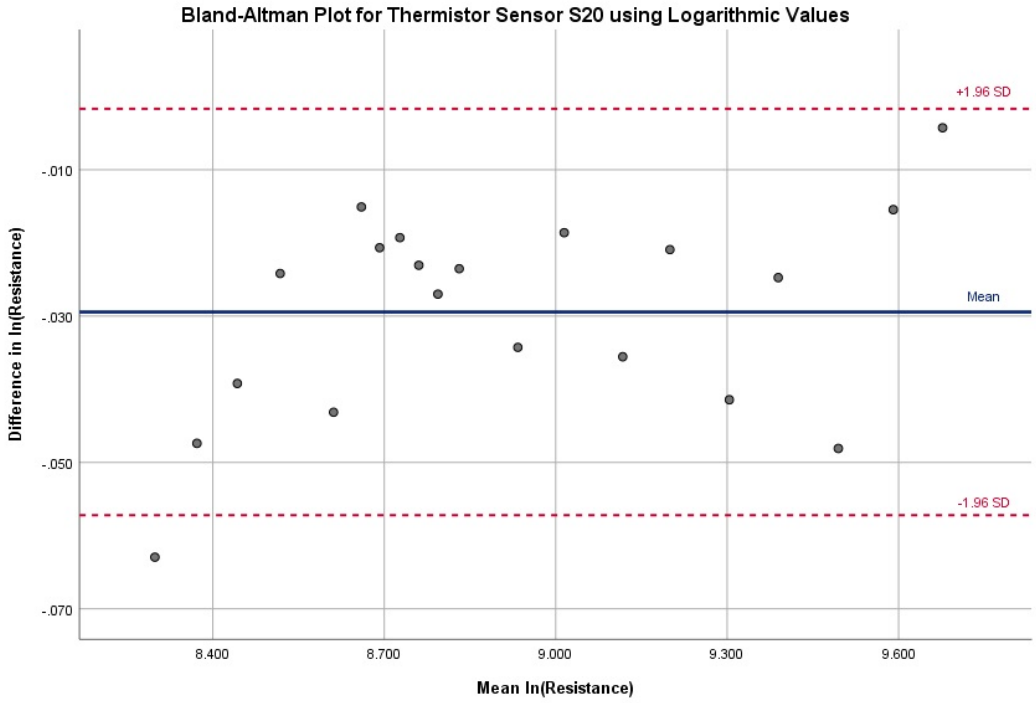

(b) Bland-Altman Plot for the natural logarithm of Resistance of S20

Figure D.20: Bland-Altman Plots for Thermistor S20: (a) Plot using the resistance values of S20; (b) Plot using the natural logarithm of the resistance values of S20.

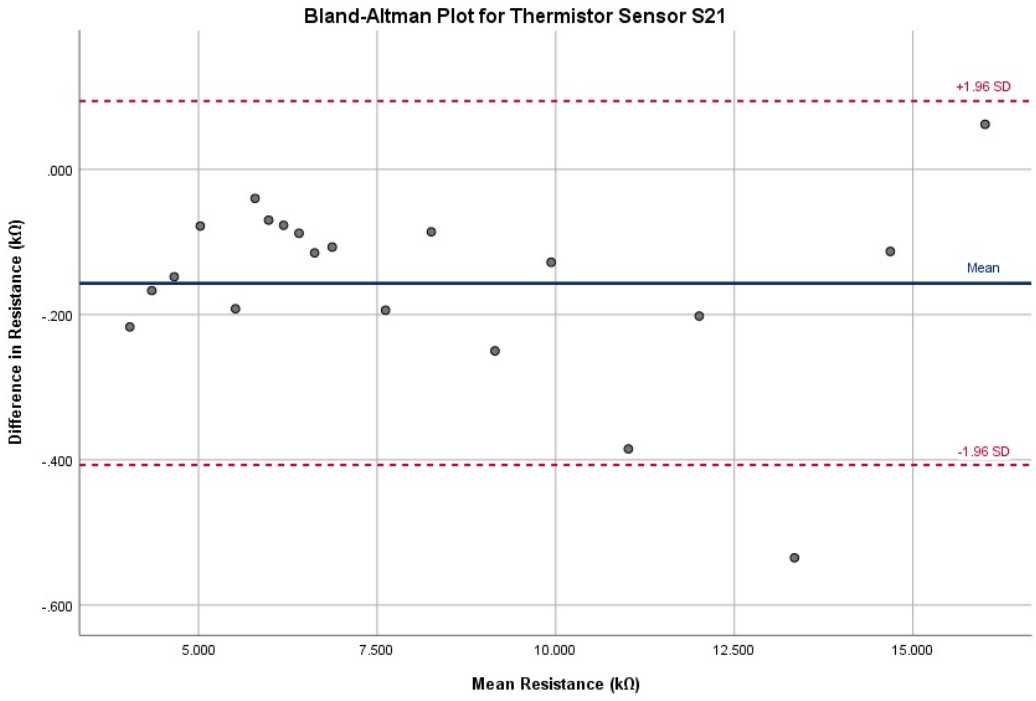

(a) Bland-Altman Plot for Resistance of S21

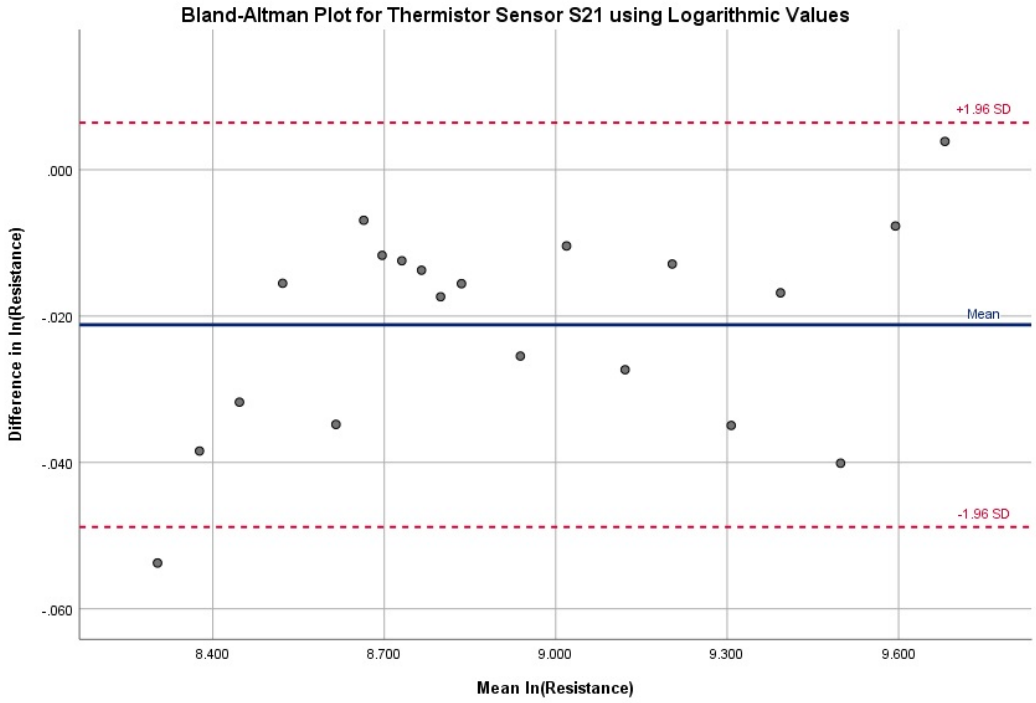

(b) Bland-Altman Plot for the natural logarithm of Resistance of S21

Figure D.21: Bland-Altman Plots for Thermistor S21: (a) Plot using the resistance values of S21; (b) Plot using the natural logarithm of the resistance values of S21.

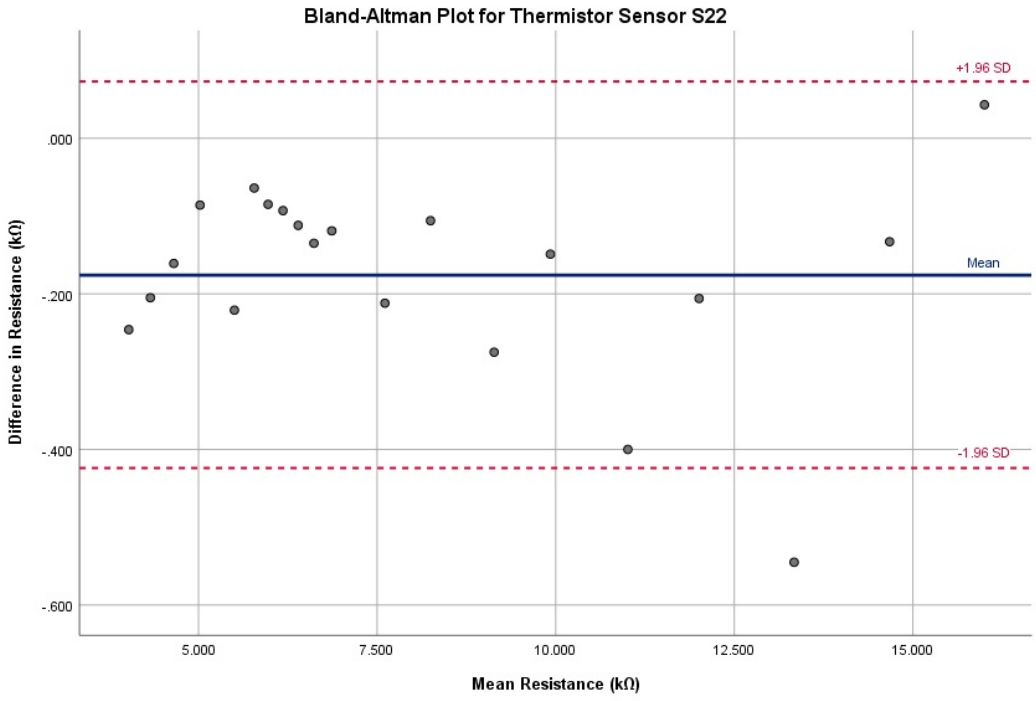

(a) Bland-Altman Plot for Resistance of S22

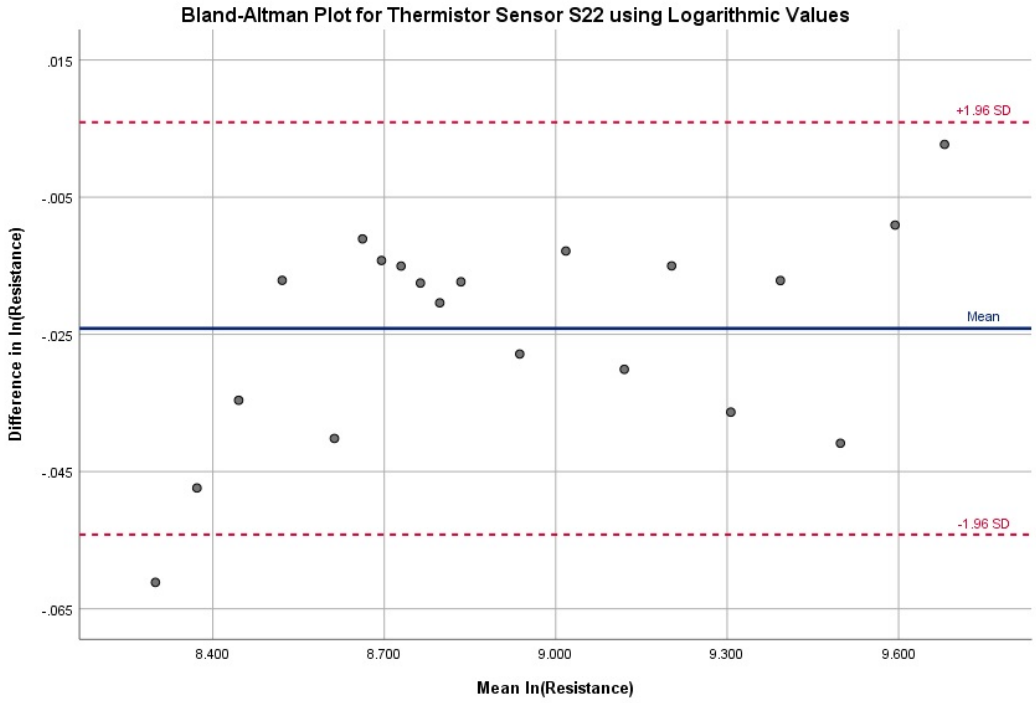

(b) Bland-Altman Plot for the natural logarithm of Resistance of S22

Figure D.22: Bland-Altman Plots for Thermistor S22: (a) Plot using the resistance values of S22; (b) Plot using the natural logarithm of the resistance values of S22.

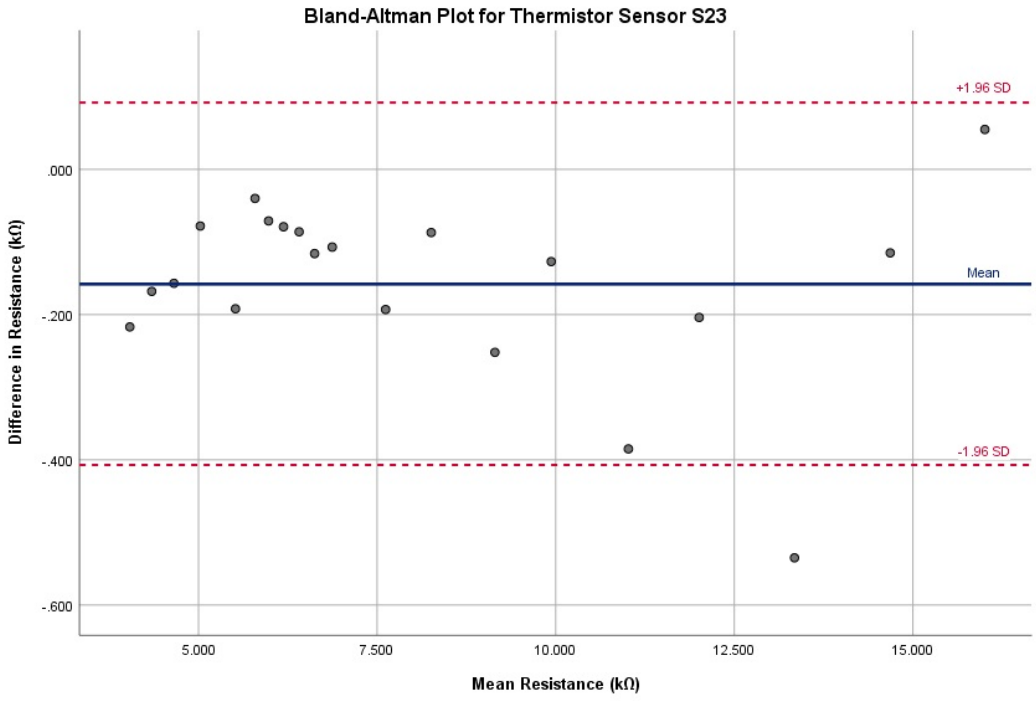

(a) Bland-Altman Plot for Resistance of S23

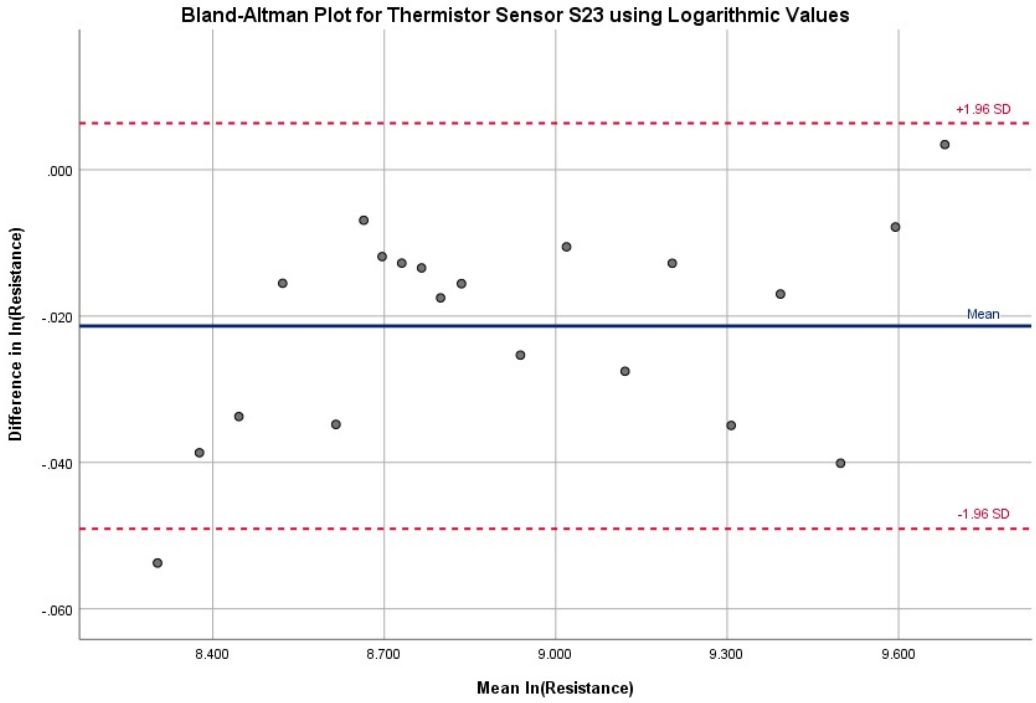

(b) Bland-Altman Plot for the natural logarithm of Resistance of S23

Figure D.23: Bland-Altman Plots for Thermistor S23: (a) Plot using the resistance values of S23; (b) Plot using the natural logarithm of the resistance values of S23.

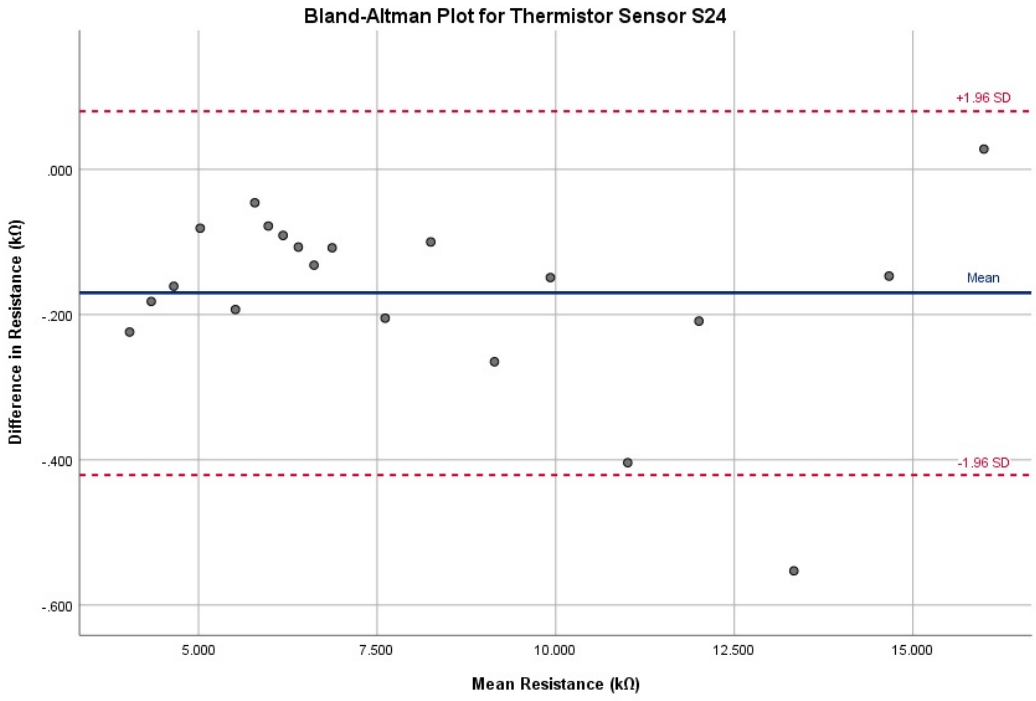

(a) Bland-Altman Plot for Resistance of S24

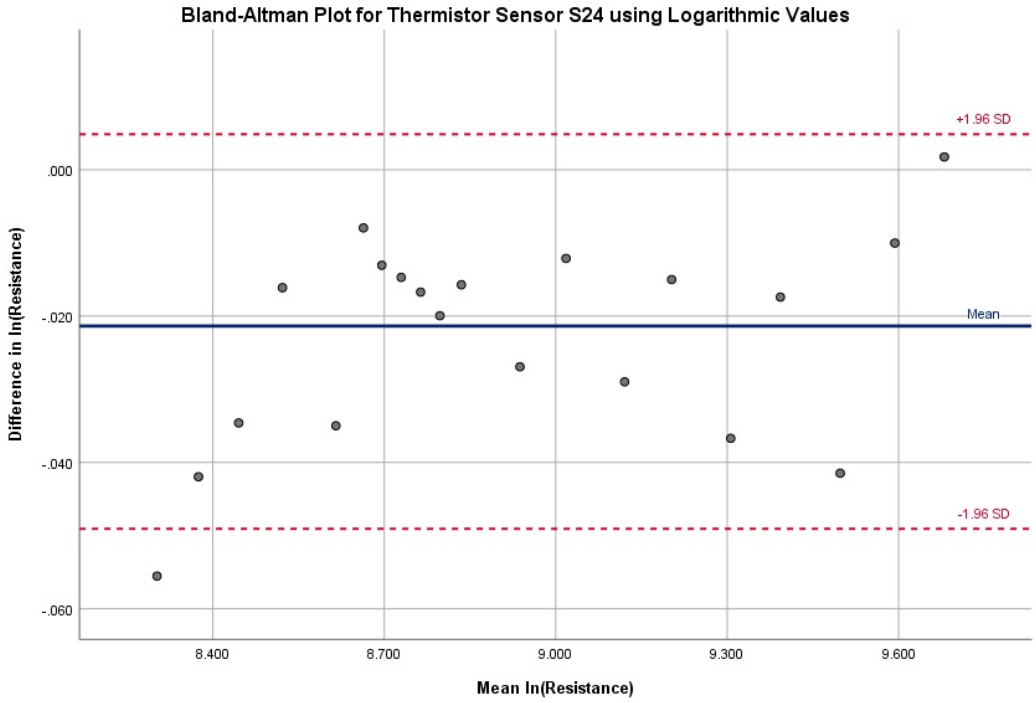

(b) Bland-Altman Plot for the natural logarithm of Resistance of S24

Figure D.24: Bland-Altman Plots for Thermistor S24: (a) Plot using the resistance values of S24; (b) Plot using the natural logarithm of the resistance values of S24.

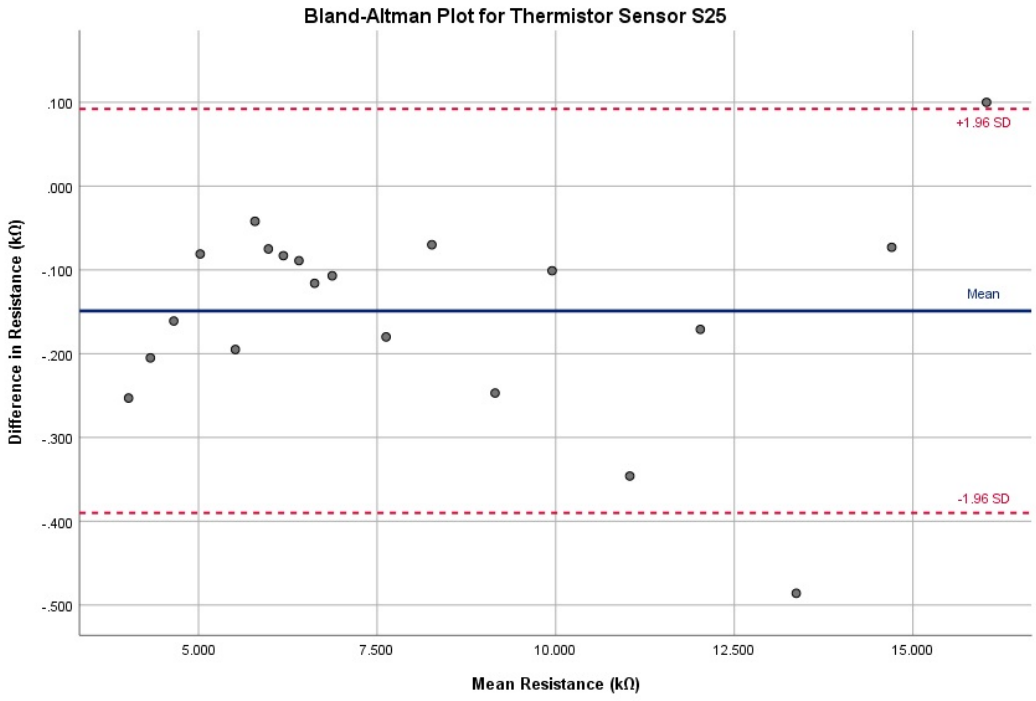

(a) Bland-Altman Plot for Resistance of S25

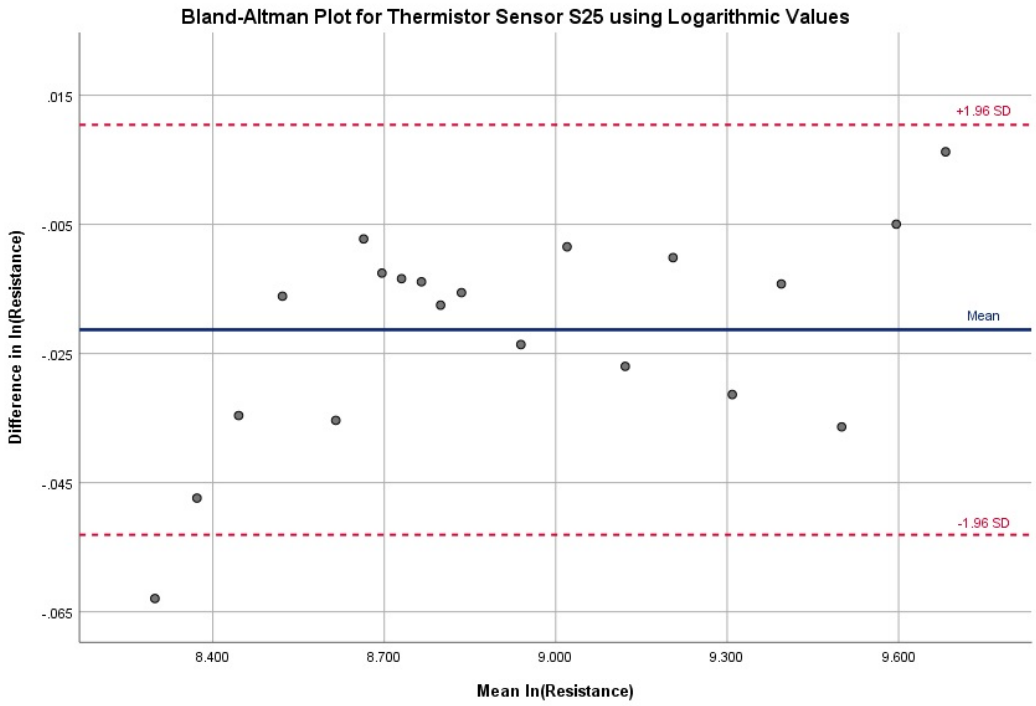

(b) Bland-Altman Plot for the natural logarithm of Resistance of S25

Figure D.25: Bland-Altman Plots for Thermistor S25: (a) Plot using the resistance values of S25; (b) Plot using the natural logarithm of the resistance values of S25.

Table D.2: The maximum and minimum resistance percentage differences for the sensors under test.

Sensor #	Minimum % difference	Maximum % difference
S_1	0.23	4.80
S_2	1.49	5.68
S_3	1.77	6.28
S_4	0.93	4.99
S_5	1.13	5.28
S_6	1.22	5.31
S_7	1.84	6.04
S_8	1.84	5.91
S_9	1.05	5.23
S_{10}	1.11	5.19
S_{11}	1.05	5.64
S_{12}	0.26	6.10
S_{13}	0.60	5.57
S_{14}	1.26	6.10
S_{15}	0.98	6.29
S_{16}	0.38	6.66
S_{17}	0.64	4.85
S_{18}	0.96	6.92
S_{19}	0.84	4.95
S_{20}	0.43	6.10
S_{21}	0.39	5.23
S_{22}	0.27	5.93
S_{23}	0.34	5.23
S_{24}	0.18	5.40
S_{25}	0.50	6.10

Table D.3: The maximum and minimum temperature and temperature percentage differences for the sensors under test.

Sensor #	Minimum Difference		Maximum Difference	
	°C	%	°C	%
S_1	0.51	1.01	1.82	5.76
S_2	0.26	0.51	1.48	4.35
S_3	0.08	0.16	1.37	4.42
S_4	0.01	0.02	1.53	4.89
S_5	0.69	1.36	1.59	4.41
S_6	0.63	1.23	1.70	5.02
S_7	0.53	1.05	1.64	5.02
S_8	0.33	0.66	1.64	5.29
S_9	0.29	0.58	1.60	5.03
S_{10}	0.29	0.58	1.60	5.03
S_{11}	0.42	0.82	1.79	5.56
S_{12}	0.38	0.74	1.72	5.54
S_{13}	0.30	0.60	1.60	5.02
S_{14}	0.30	0.58	1.65	5.36
S_{15}	0.11	0.22	1.58	4.98
S_{16}	0.06	0.12	1.52	4.84
S_{17}	0.31	0.61	1.60	5.02
S_{18}	0.56	1.09	1.82	5.63
S_{19}	0.43	0.85	1.73	5.27
S_{20}	0.35	0.68	1.60	4.96
S_{21}	0.32	0.63	1.60	5.02
S_{22}	0.34	0.68	1.53	4.47
S_{23}	0.15	0.29	1.67	5.46

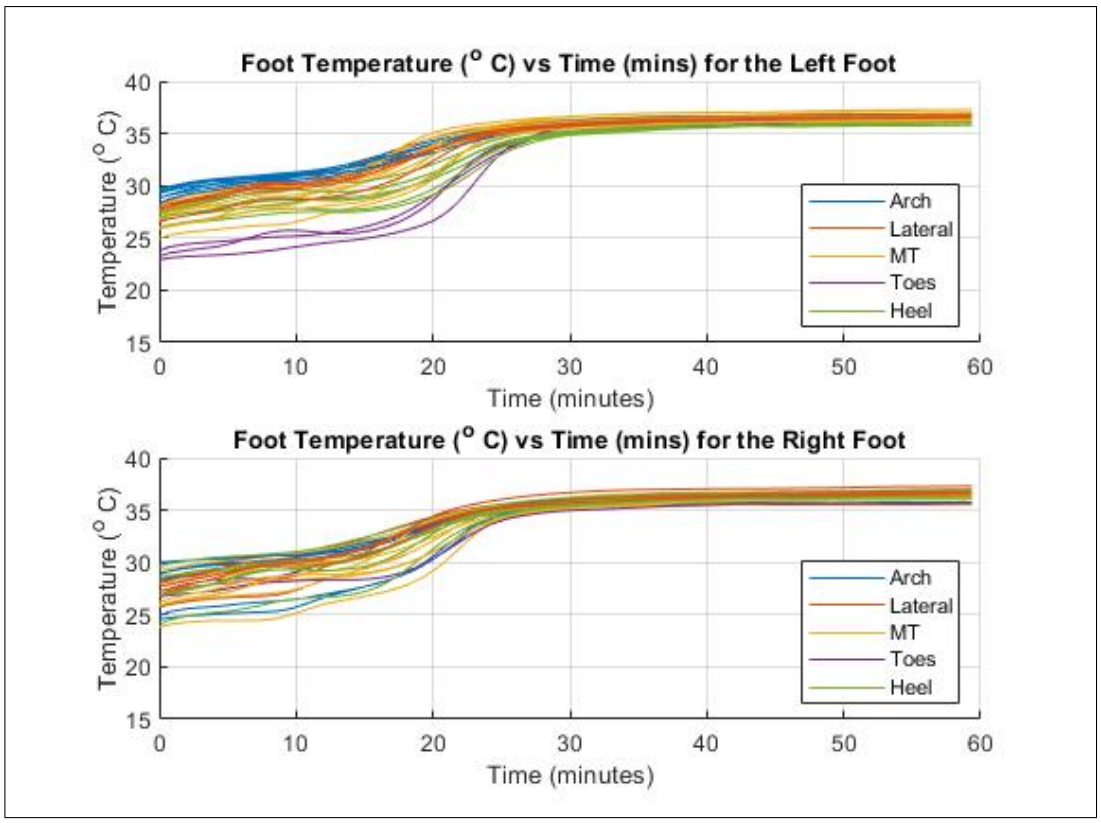

Figure D.26: The temperature plots of both feet during the test walk of Test Subject 2.

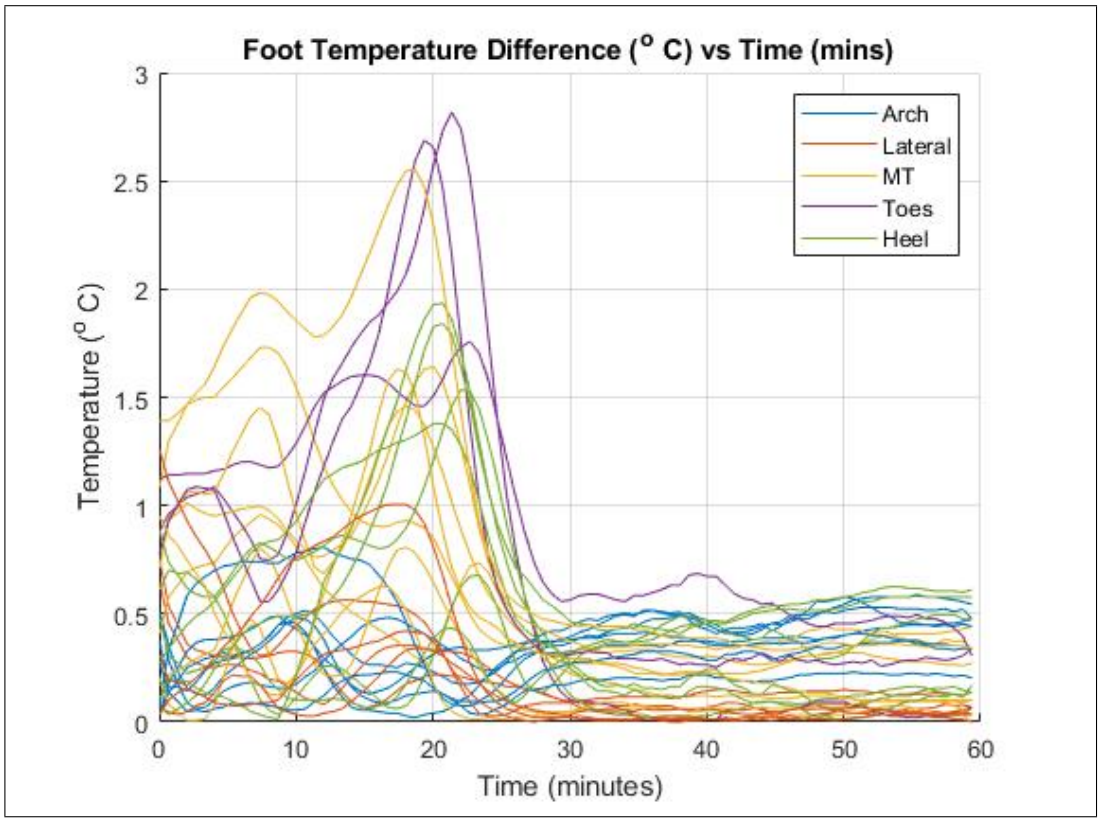

Figure D.27: The difference in temperatures between the two feet throughout the test walk of Test Subject 2.

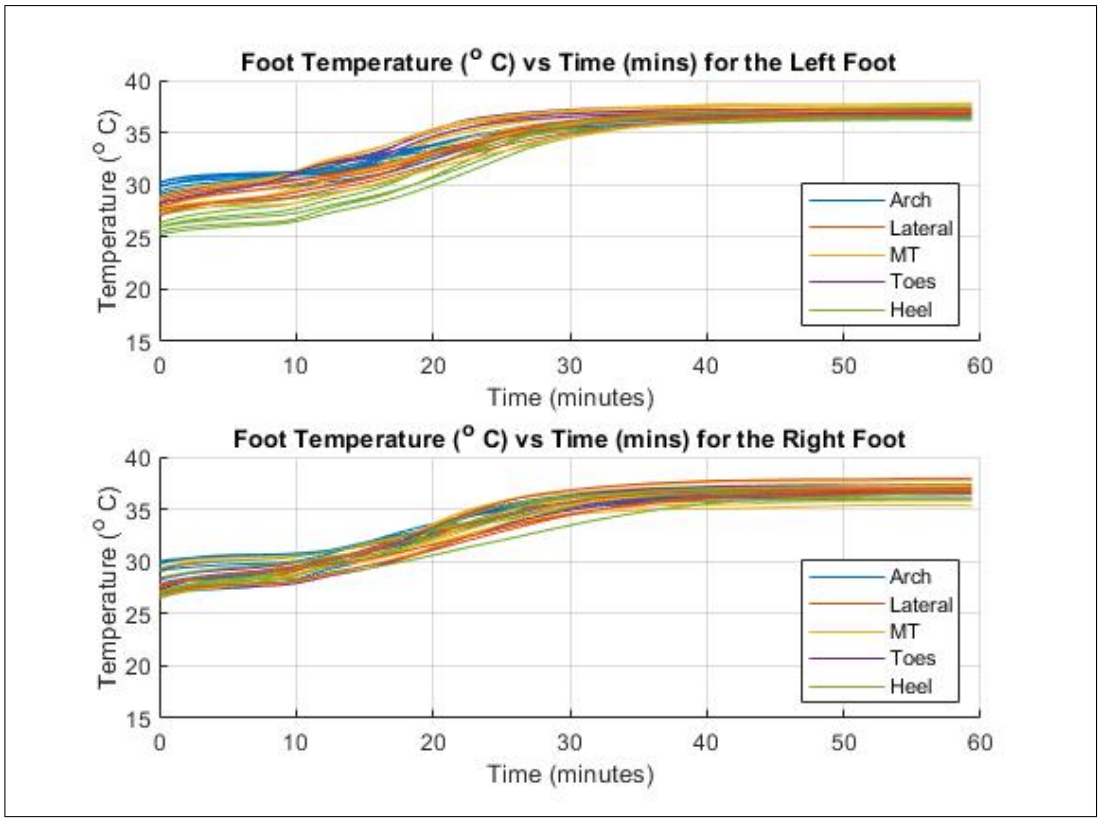

Figure D.28: The temperature plots of both feet during the test walk of Test Subject 3.

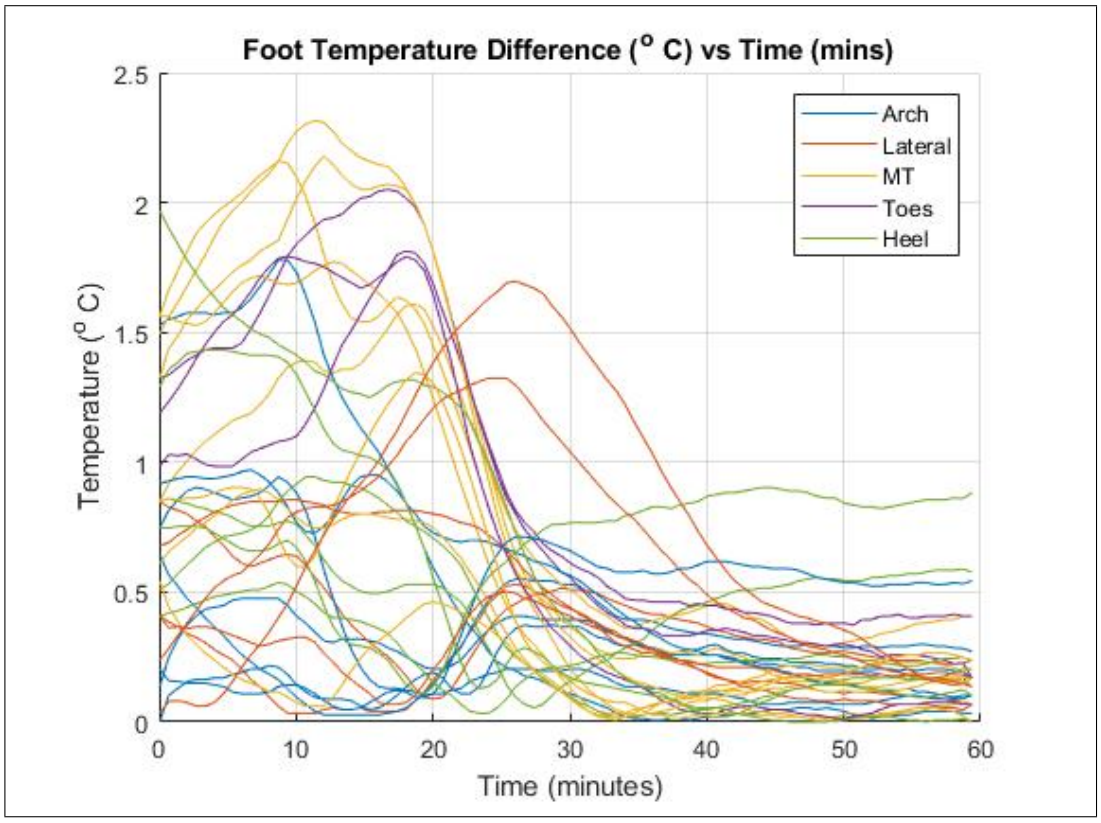

Figure D.29: The difference in temperatures between the two feet throughout the test walk of Test Subject 3.

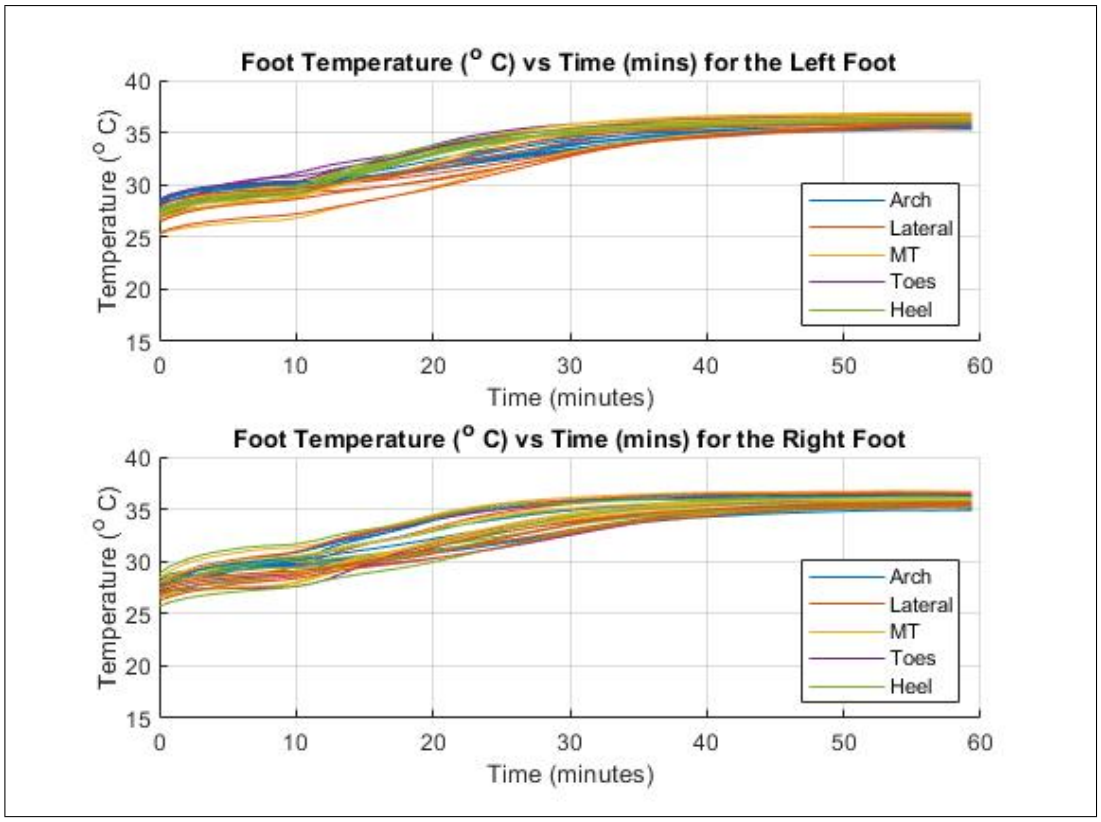

Figure D.30: The temperature plots of both feet during the test walk of Test Subject 4.

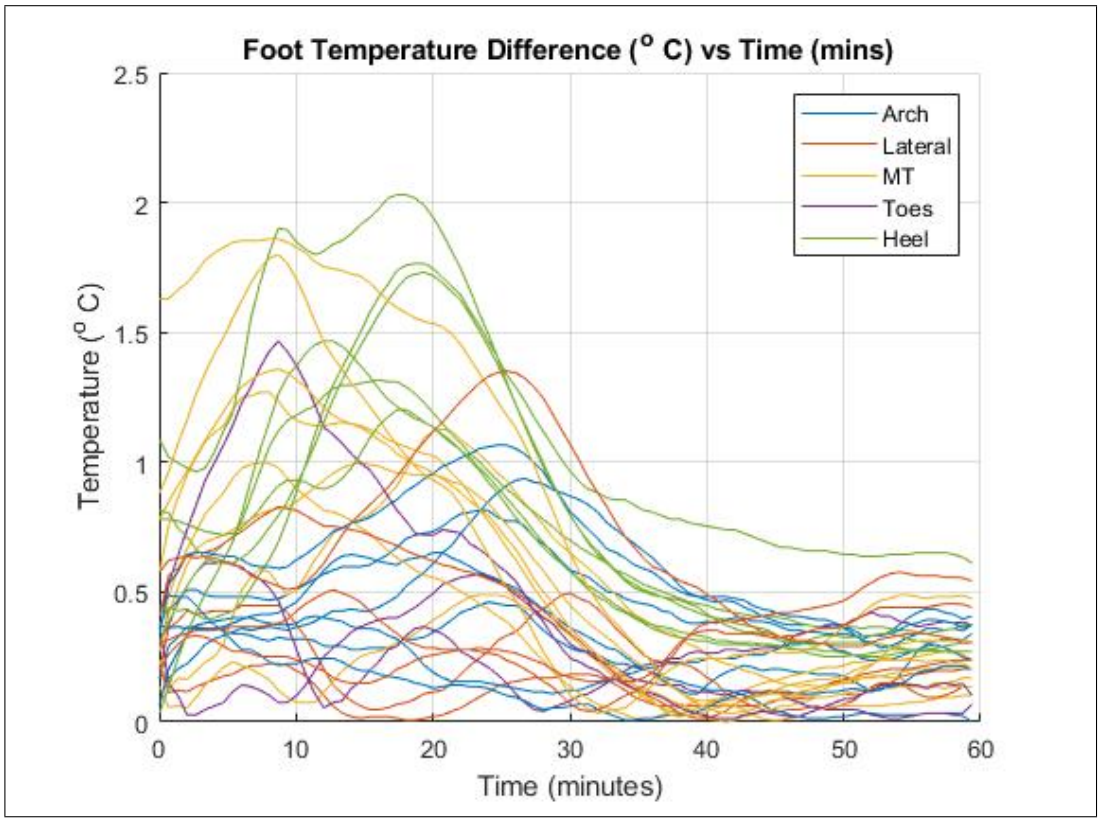

Figure D.31: The difference in temperatures between the two feet throughout the test walk of Test Subject 4.

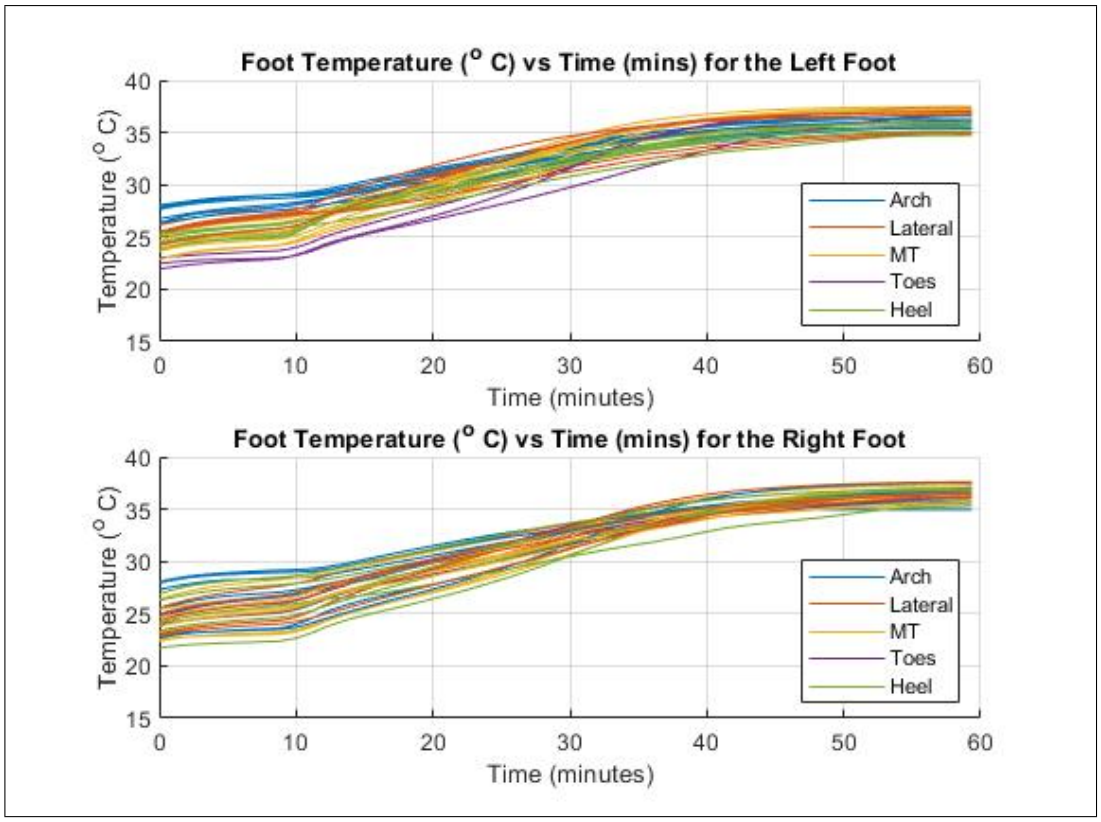

Figure D.32: The temperature plots of both feet during the test walk of Test Subject 5.

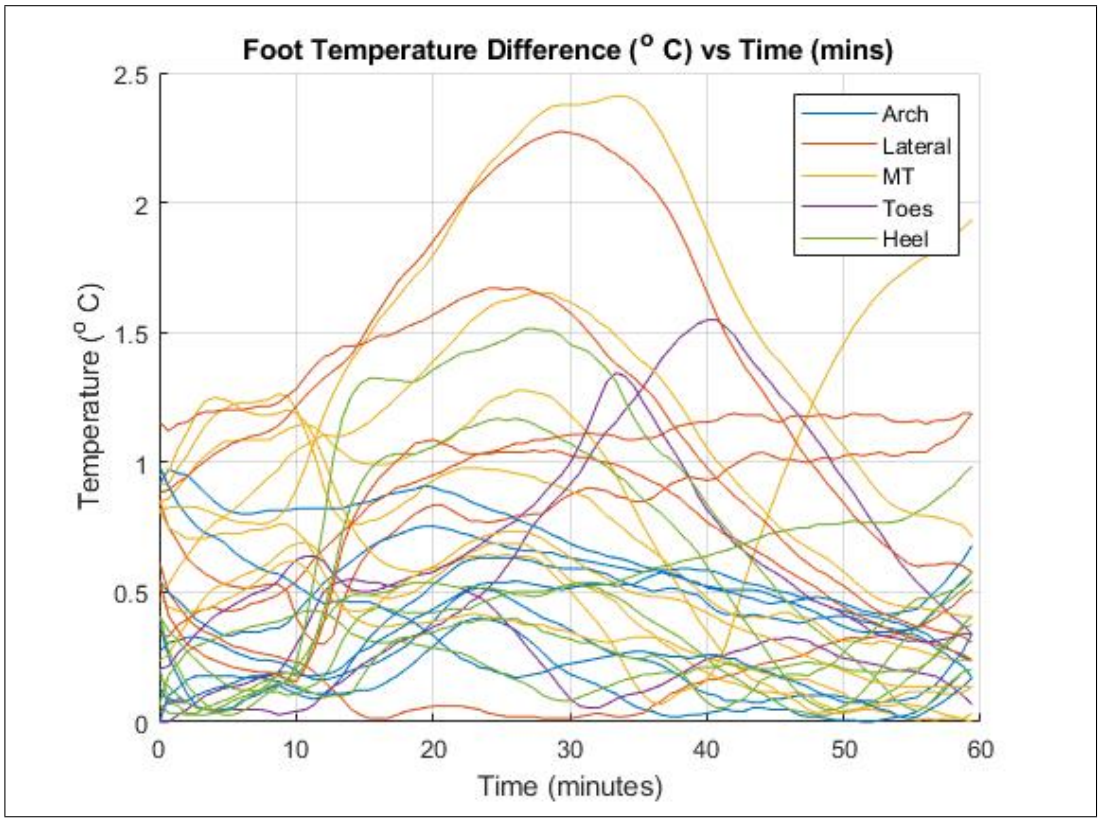

Figure D.33: The difference in temperatures between the two feet throughout the test walk of Test Subject 5.

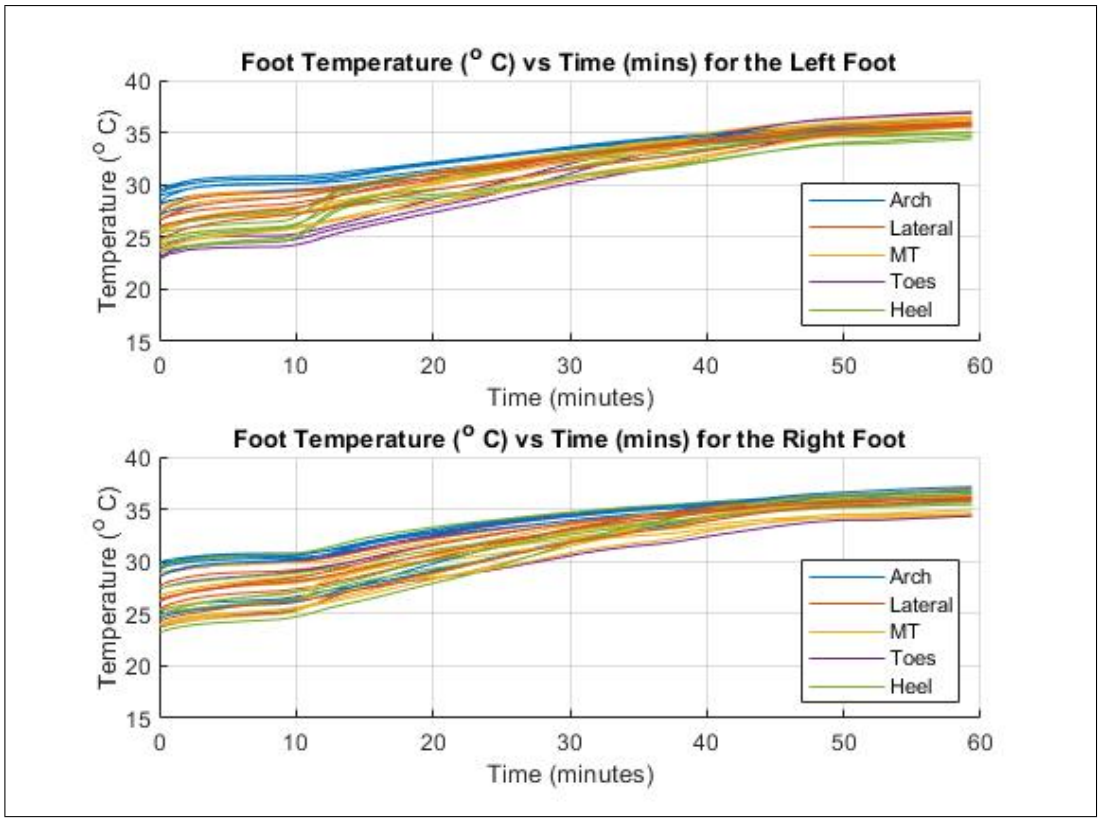

Figure D.34: The temperature plots of both feet during the test walk of Test Subject 6.

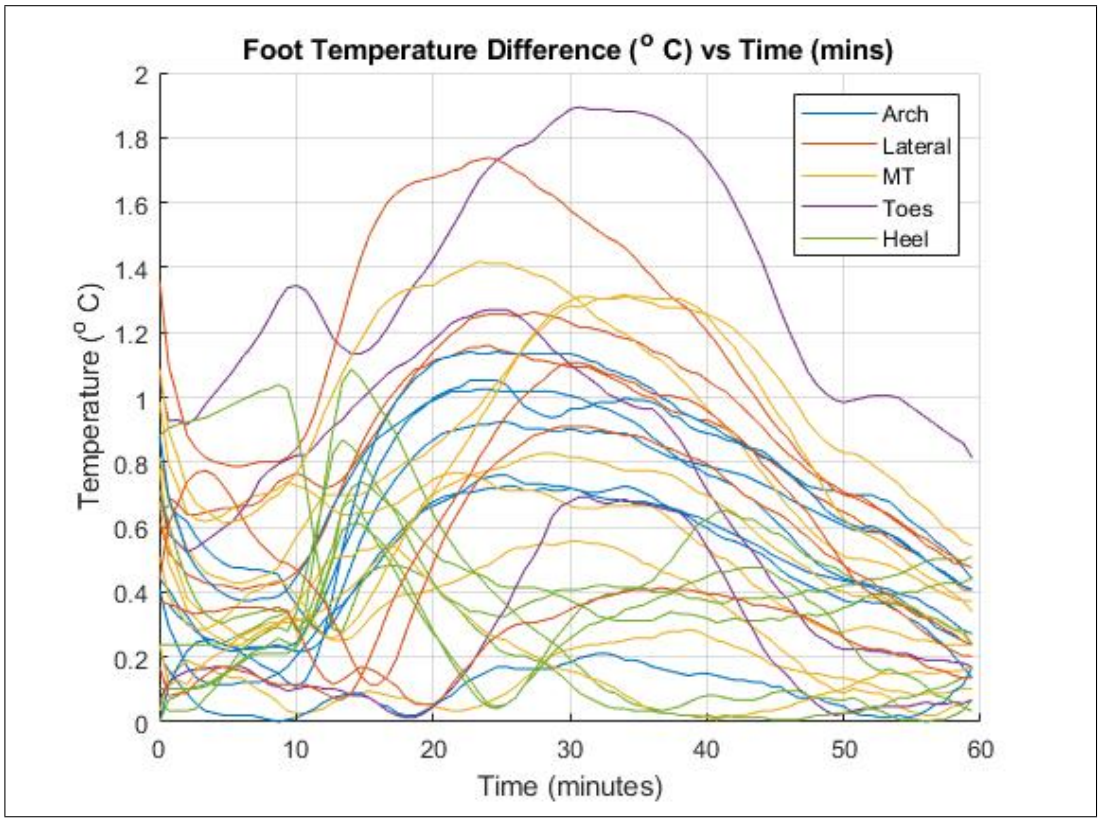

Figure D.35: The difference in temperatures between the two feet throughout the test walk of Test Subject 6.

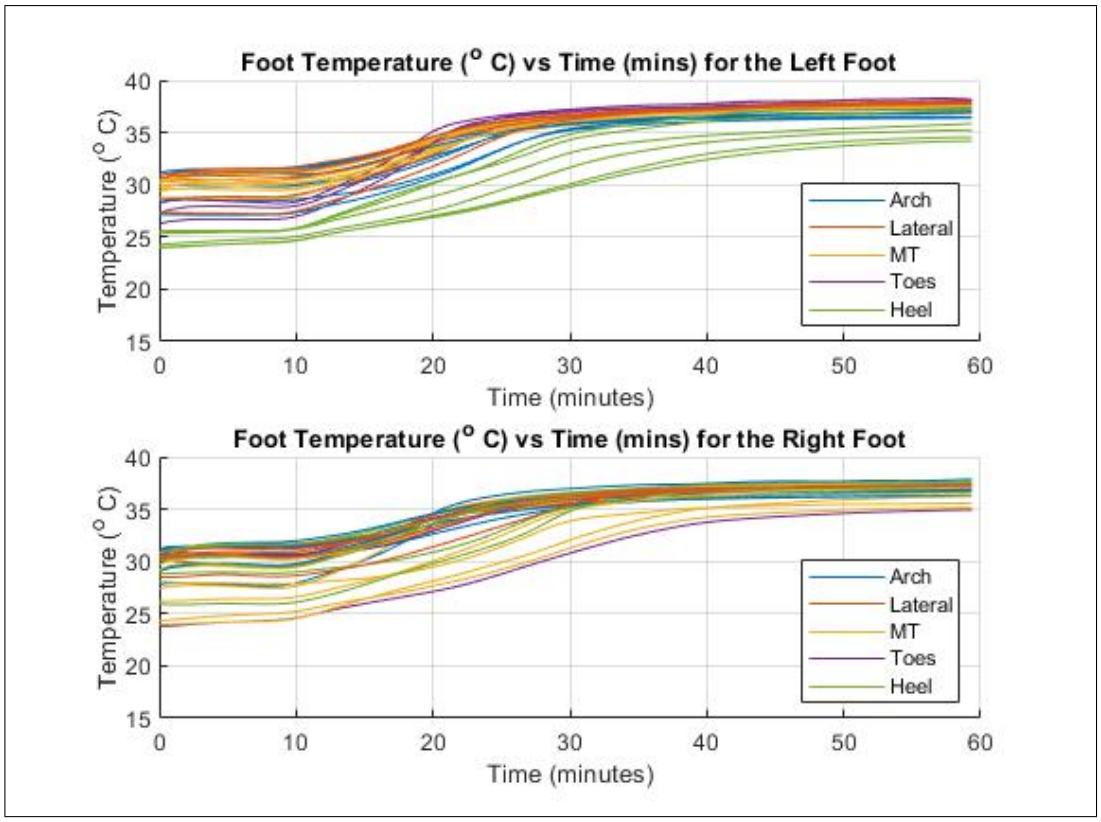

Figure D.36: The temperature plots of both feet during the test walk of Test Subject 7.

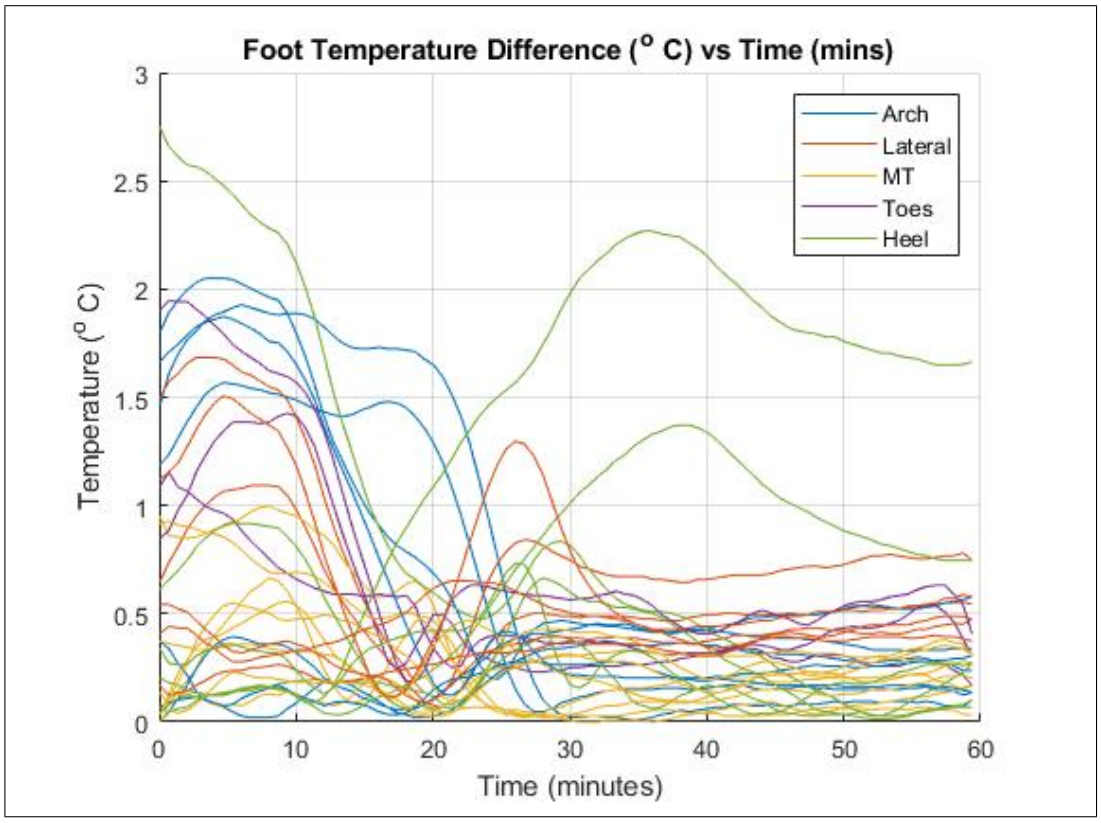

Figure D.37: The difference in temperatures between the two feet throughout the test walk of Test Subject 7.

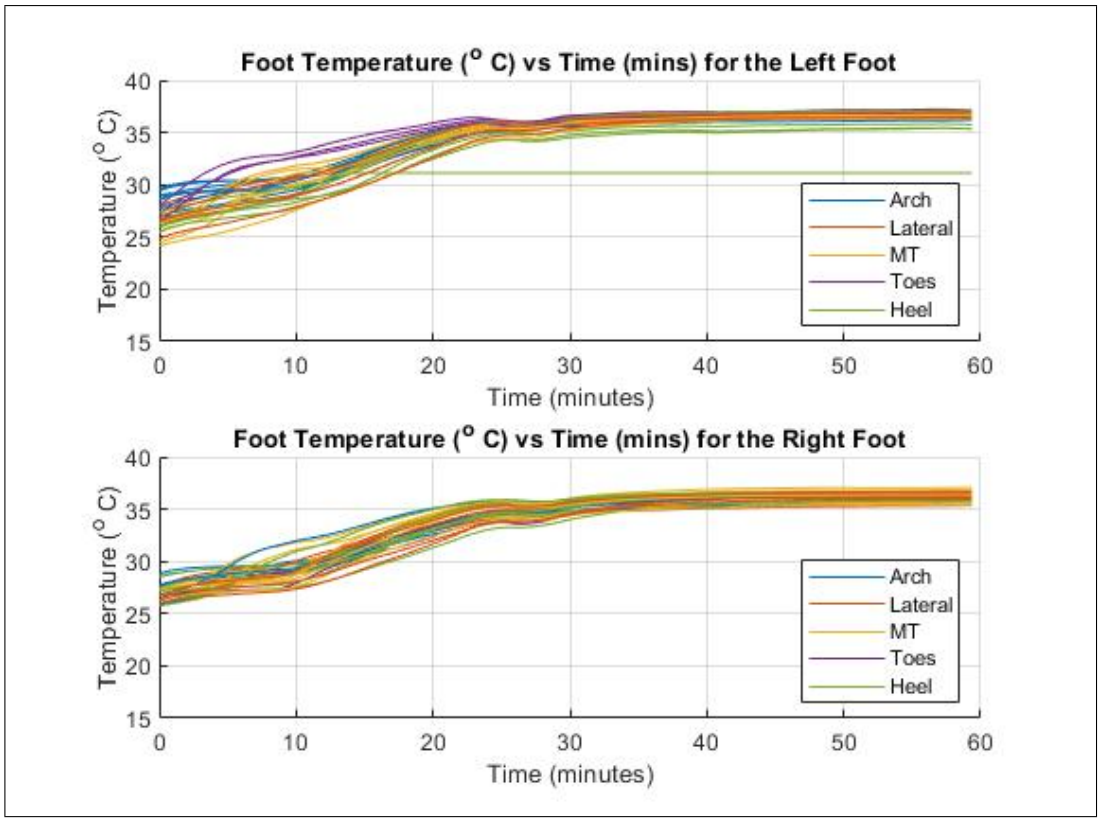

Figure D.38: The temperature plots of both feet during the test walk of Test Subject 8.

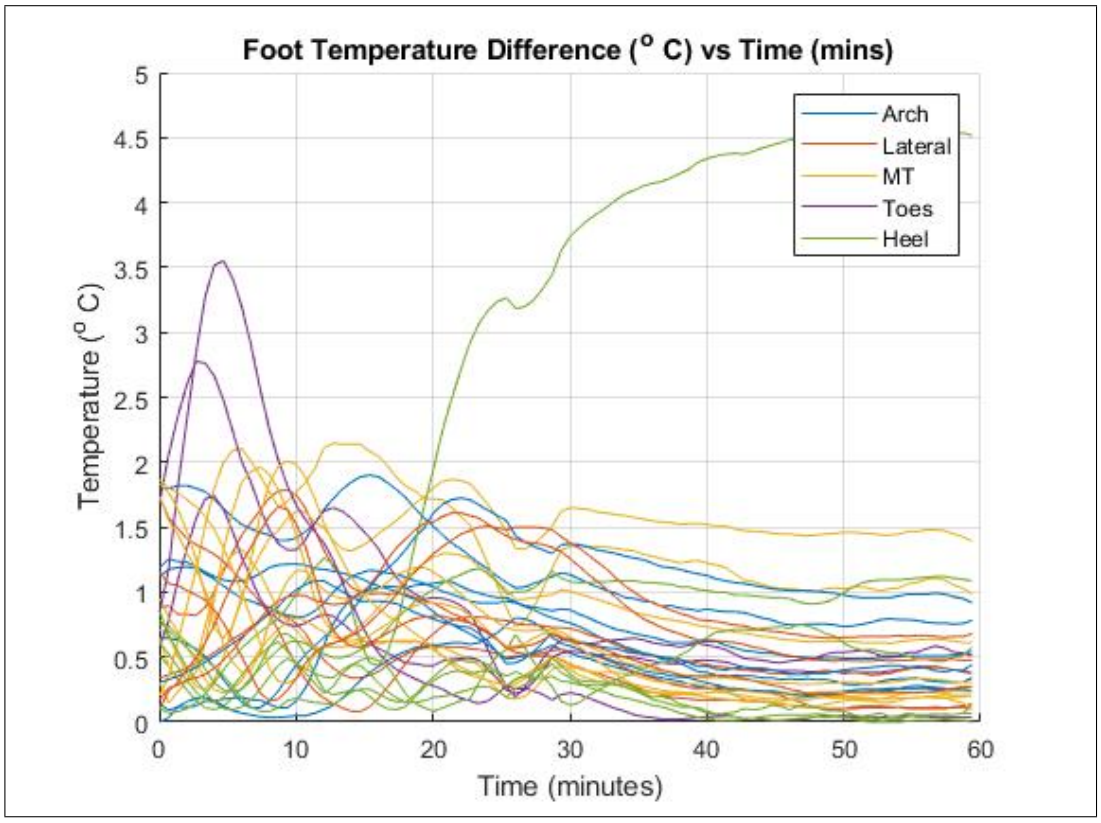

Figure D.39: The difference in temperatures between the two feet throughout the test walk of Test Subject 8.

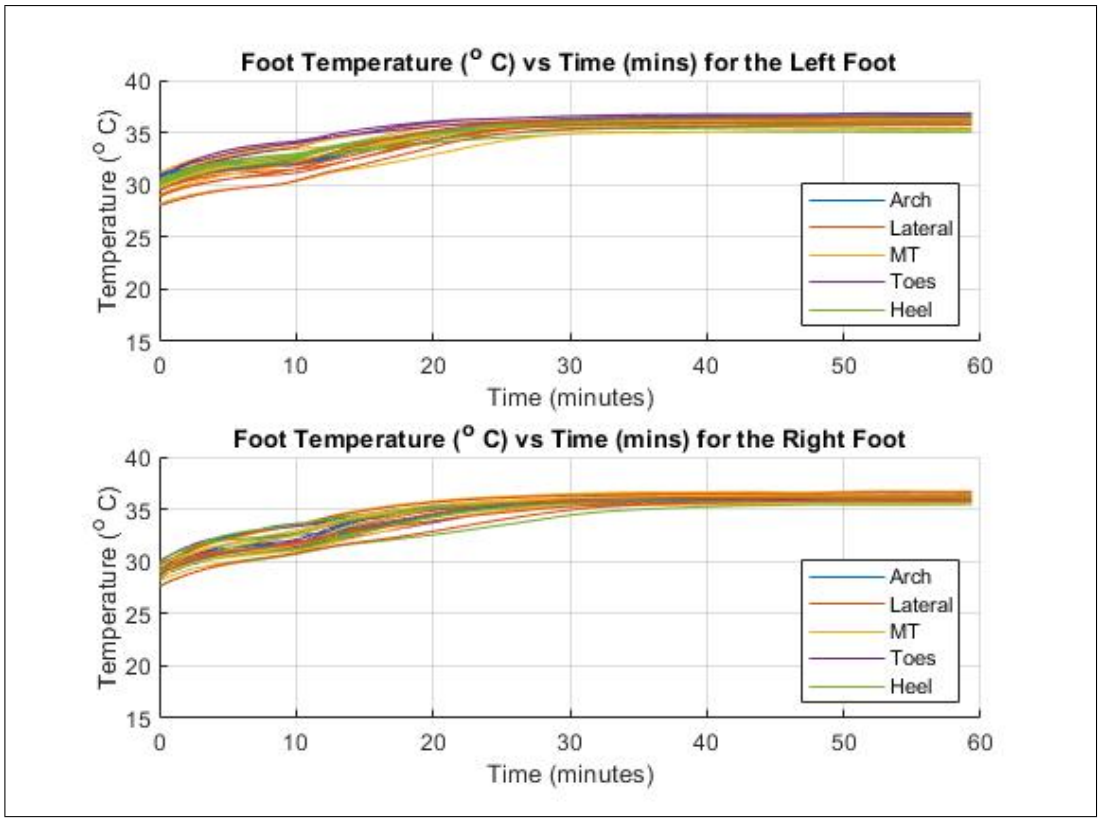

Figure D.40: The temperature plots of both feet during the test walk of Test Subject 9.

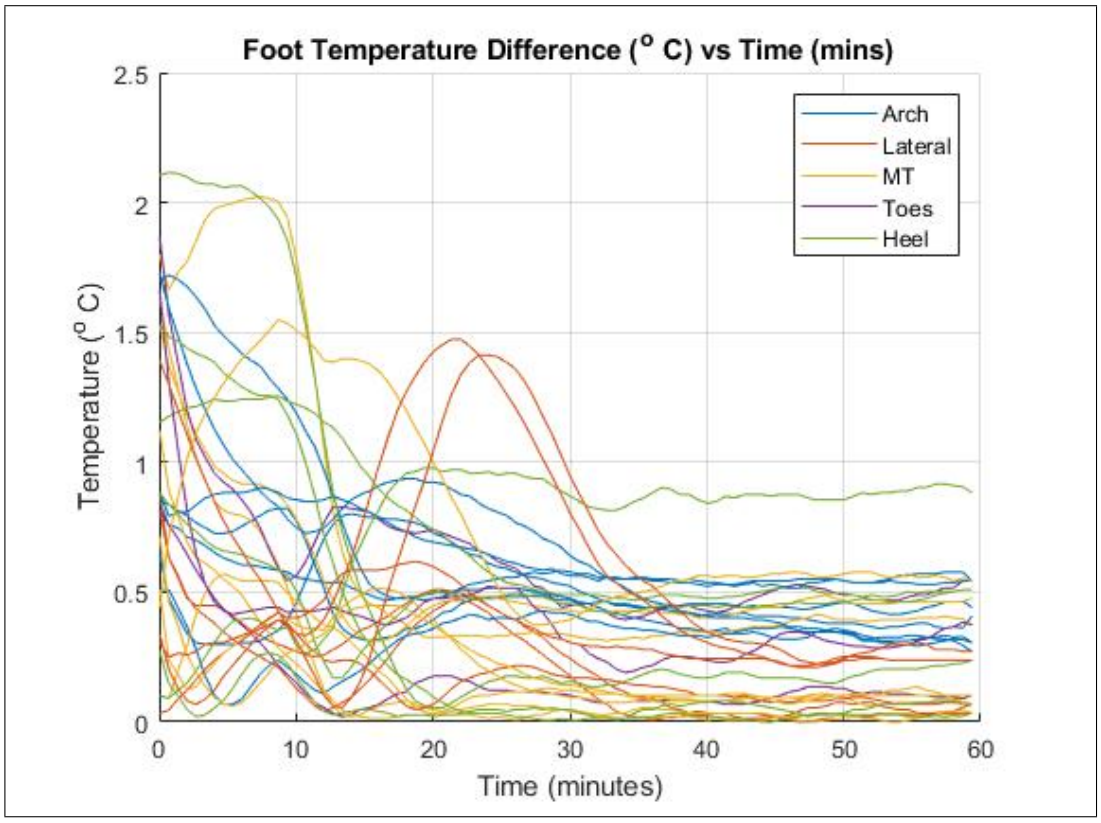

Figure D.41: The difference in temperatures between the two feet throughout the test walk of Test Subject 9.

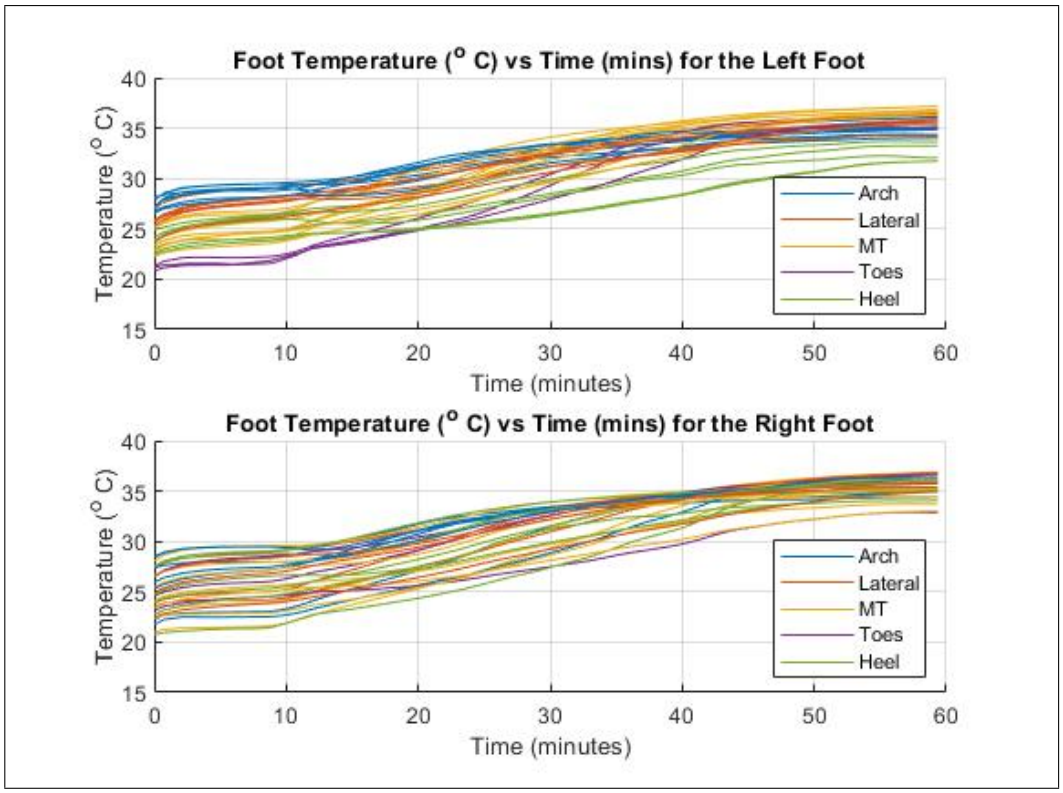

Figure D.42: The temperature plots of both feet during the test walk of Test Subject 10.

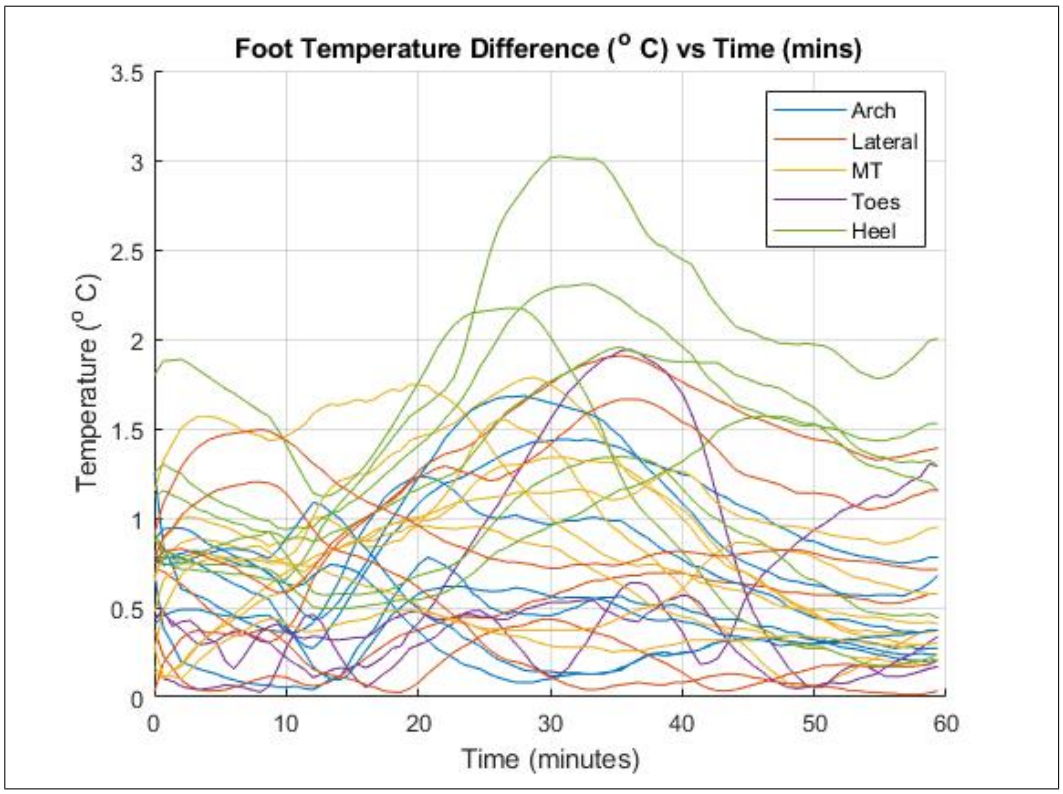

Figure D.43: The difference in temperatures between the two feet throughout the test walk of Test Subject 10.

Table D.4: Temperature data for Test Subject 1 for left and right foot at the start and end of the trial walk [A = Arch, H = Heel, MT = Metatarsal, L = Lateral, T = Toe].

Foot Location	Temperature (°C)			
	Start of Walk		End of Walk	
	System	IR Camera	System	IR Camera
Left A1	28.48	27.50	35.54	35.30
Left A2	29.16	30.90	35.30	34.70
Left A3	28.95	30.00	35.71	35.60
Left A4	28.85	31.00	35.47	35.20
Left A5	28.41	30.80	34.89	35.00
Left A6	27.39	28.40	35.16	35.30
Left A7	26.85	28.60	35.06	35.00
Left H1	25.59	27.10	34.52	34.50
Left H2	24.64	26.00	34.65	35.10
Left H3	24.13	25.30	34.11	33.50
Left H4	24.13	25.40	34.32	34.40
Left H5	23.18	24.90	33.81	33.80
Left H6	23.11	24.10	33.74	33.80
Left L1	27.12	28.40	35.13	35.30
Left L2	24.98	26.10	34.93	34.50
Left L3	26.10	25.90	34.99	34.60
Left L4	26.92	27.70	34.86	34.90
Left L5	25.76	26.10	34.86	34.70

Continued on next page

Table D.4 – continued from previous page

Foot Location	Temperature (°C)			
	Start of Walk		End of Walk	
	System	IR Camera	System	IR Camera
Left L6	25.63	26.60	34.52	35.00
Left MT1	24.57	25.30	34.18	35.10
Left MT2	25.46	25.60	34.45	35.30
Left MT3	25.83	25.40	34.25	34.70
Left MT4	23.83	24.20	34.62	34.40
Left MT5	26.92	25.40	34.55	34.50
Left MT6	27.59	27.10	35.13	35.50
Left MT7	25.76	25.30	35.13	35.00
Left MT8	24.13	24.30	34.18	33.90
Left T1	23.59	22.50	34.32	34.10
Left T2	24.27	24.30	33.47	34.00
Left T3	23.89	22.20	33.94	34.30
Right A1	27.25	28.20	34.99	34.50
Right A2	28.17	30.60	35.16	34.40
Right A3	28.37	29.30	35.23	34.90
Right A4	28.85	31.00	35.50	34.60
Right A5	28.95	30.90	34.99	34.80
Right A6	28.34	28.90	34.79	34.60
Right A7	27.56	27.50	34.59	34.40

Continued on next page

Table D.4 – continued from previous page

Foot Location	Temperature (°C)			
	Start of Walk		End of Walk	
	System	IR Camera	System	IR Camera
Right H1	26.51	26.10	34.42	34.30
Right H2	25.39	25.60	33.91	34.50
Right H3	24.71	25.10	34.45	34.10
Right H4	24.51	25.10	33.67	33.80
Right H5	23.72	24.40	34.32	33.80
Right H6	23.66	24.20	34.01	33.40
Right L1	27.15	27.70	34.82	34.90
Right L2	24.00	25.10	34.38	34.30
Right L3	25.32	25.30	34.89	34.20
Right L4	27.46	27.20	34.62	34.50
Right L5	25.96	25.70	34.79	34.40
Right L6	26.20	26.80	34.38	34.30
Right MT1	23.83	25.10	34.18	34.80
Right MT2	24.13	25.20	34.42	34.80
Right MT3	24.34	25.10	34.48	34.60
Right MT4	23.22	24.30	34.35	34.10
Right MT5	24.95	25.70	34.18	34.40
Right MT6	25.83	26.80	34.65	34.80
Right MT7	25.08	25.50	35.13	34.50
Right MT8	23.66	24.30	34.48	34.10

Continued on next page

Table D.4 – continued from previous page

Foot Location	Temperature (°C)			
	Start of Walk		End of Walk	
	System	IR Camera	System	IR Camera
Right T1	22.94	22.90	34.25	34.00
Right T2	23.86	23.50	33.40	33.50
Right T3	22.60	22.50	34.18	33.90

Bibliography

[1] F. Aguiree, A. Brown, N. H. Cho, G. Dahlquist, S. Dodd, T. Dunning, M. Hirst, C. Hwang, D. Magliano, C. Patterson, C. Scott, J. Shaw, G. Soltesz, J. Usher-Smith, and D. Whiting, *IDF Diabetes Atlas.* 6th ed. International Diabetes Federation, 2013.

[2] G. Katona, I. Aganovic, V. Vuskan, and Z. Skrabalo, "National diabetes programme in Malta: Phase I and II Final Report.", 1983.

[3] D. of Health Information and Research, "European Health Examination Survey 2010 – Pilot Study.", 2010.

[4] *Gangrene*. [Online]. Available: `https://www.diabetes.co.uk/diabetes-complications/gangrene-and-diabetes.html` (visited on 12/02/2019).

[5] A. J. Boulton, "Management of Diabetic Peripheral Neuropathy.", *Clinical diabetes*, vol. 23, pp. 9–15, 1 2005.

[6] American Diabetes Association, "Clinical practice recommendations 2009.", *Diabetes care*, vol. 32, pp. 1–98, 2009.

[7] L. A. Lavery, K. R. Higgins, D. R. Lanctot, G. P. Constantinides, R. G. Zamorano, K. A. Athanasiou, D. G. Armstrong, and C. M. Agrawal, "Preventing diabetic foot ulcer recurrence in high-risk patients: Use of temperature monitoring as a self-assessment tool.", *Diabetes care*, vol. 30, pp. 14–20, 1 2007.

[8] R. M. M. W. J. Jeffcoate and E. M. Fletcher, "The description and classification of diabetic foot lesions.", *Diabetes Med.*, vol. 10, pp. 676–679, 1993.

[9] L. A. Lavery, K. R. Higgins, D. R. Lanctot, G. P. Constantinides, R. G. Zamorano, D. G. Armstrong, K. A. Athanasiou, and C. M. Agrawal, "Home monitoring of foot skin temperatures to prevent ulceration.", *Diabetes care*, vol. 27, pp. 2642–2647, 11 2004.

[10] D. G. Armstrong, L. A. Lavery, P. J. Liswood, W. F. Todd, and J. A. Tredwell, "Infrared dermal thermometry for the high-risk diabetic foot.", *Physical therapy*, vol. 77, pp. 169–175, 2 1997.

[11] R. M. Saalfeld, K. S. M. Purim, and S. Kusma, "Impact of Diabetic Foot and others Comorbidities on the Quality of Life of Diabetic Patients Monitored at a Specialized Outpatient Clinic", *International Journal of Nursing*, vol. 6, pp. 107–116, 2019.

[12] M. Kerr, E. Barron, P. Chadwick, T. Evans, W. M. Kong, G. Rayman, M. Sutton-Smith, G. Todd, B. Young, and W. J. Jeffcoate, "The cost of diabetic foot ulcers and amputations to the National Health Service in England", *Diabetic Medicine*, vol. 36, pp. 995–1002, 2019.

[13] V. J. Houghton, V. M. Bower, and D. C. Chant, "Is an increase in skin temperature predictive of neuropathic foot ulceration in people with diabetes? A systematic review and meta-analysis", *Journal of Foot and Ankle Research*, vol. 6, 2013.

[14] D. G. Armstrong, K. Holtz-Neiderer, C. Wendel, M. J. Mohler, H. R. Kimbriel, and L. A. Lavery, "Skin temperature monitoring reduces the risk for diabetic foot ulceration in high-risk patients.", *The american journal of medicine*, vol. 120, pp. 1042–1046, 12 2007.

[15] A. Gatt, C. Formosa, K. Cassar, K. P. Camilleri, C. D. Raffaele, A. Mizzi, C. Azzopardi, S. Mizzi, O. Falzon, S. Cristina, and N. Chockalingam, "Thermographic Patterns of the Upper and Lower Limbs: Baseline Data.", *International Journal of Vascular Medicine*, 2015.

[16] R. E. Morley, Jr., E. J. Richter, J. W. Klaesner, K. S. Maluf, and M. J. Mueller, "In-shoe multisensory data acquisition system.", *IEEE transaction on biomedical engineering*, vol. 48, pp. 815–820, 7 2001.

[17] K. S. Maluf, R. E. Morley Jr, E. J. Richter, J. W. Klaesner, and M. J. Mueller, "Monitoring in-shoe plantar pressures, temperature, and humidity: Reliability and validity of measures from a portable device.", *Archives of physical medicine and rehabilitation*, vol. 82, pp. 1119–1127, 2001.

[18] P. N. Reddy, G. Cooperb, A. Weightmanb, E. Hodson-Tolea, and N. Reevesa, "An in-shoe temperature measurement system for studying diabetic foot ulceration etiology: Preliminary results with healthy participants.", in *Procedia cirp 49*, 2016, pp. 153–156.

[19] J. J. Sandoval-Palomares, J. Yáñez-Mendiola, A. Gómez-Espinosa, and J. M. López-Vela, "Portable system for monitoring the microclimate in the footwear-foot interface.", *Sensors*, vol. 16, 1059 2016.

[20] J. Coates, A. Chipperfield, and G. Clough, "Wearable multimodal skin sensing for the diabetic foot.", *Electronics*, vol. 5, 45 2016.

[21] R. Morovati and I. Maclean, "Development of Foot Temperature Measuring Device for Diabetes.", *Journal of Medical Devices*, vol. 10, 2016.

[22] A. M. Reyzelman, K. Koelewyn, M. Murphy, X. Shen, E. Yu, R. Pillai, J. Fu, H. J. Scholten, and R. Ma, "Continuous Temperature-Monitoring Socks for Home Use in Patients With Diabetes: Observational Study.", *Journal of Medical Internet Research*, vol. 20, 2018.

[23] P. Arezes, M. M. Neves, S. Teixeira, C. P. Leao, and J. Cunha, "Testing thermal comfort of trekking boots: An objective and subjective evaluation", *Applied ergonomics*, vol. 44, no. 4, pp. 557–565, 2013.

[24] P. Hofer, M. Hasler, G. Fauland, T. Bechtold, and W. Nachbauer, "Microclimate in ski boots-temperature, relative humidity, and water absorption", *Applied ergonomics*, vol. 45, no. 3, pp. 515–520, 2014.

[25] C. Garcia-Hernandez, E. J. Sanchez-Alvarez, and J.-L. Huertas-Talon, "Foot model for tracking temperature of safety boot insoles: Application to different insole materials in firefighter boots", *International journal of occupational safety and ergonomics*, vol. 22, no. 1, pp. 12–19, 2016.

[26] R. T. Murff, D. G. Armstrong, D. Lanctot, L. A. Lavery, and K. A. Athanasiou, "How effective is manual palpation in detecting subtle temperature differences?", *Clinics in podiatric medicine and surgery*, vol. 15, pp. 151–154, 1 1998.

[27] H. T. Bergtholdt and P. W. Brand, "Temperature assessment and plantar inflammation.", *Leprosy review*, vol. 47, pp. 211–219, 3 1976.

[28] R. M. Stess, P. C. Sisney, K. M. Moss, P. M. Graf, K. S. Louie, G. A. Gooding, and C. Grunfeld, "Use of liquid crystal thermography in the evaluation of the diabetic foot.", *Diabetes care*, vol. 9, pp. 267–272, 3 1986.

[29] E. J. Boyko, J. H. Ahroni, V. Stensel, R. C. Forsberg, and D. R. D. D. G. Smith, "A prospective study of risk factors for diabetic foot ulcer. the seattle diabetic foot study.", *Diabetes care*, vol. 22, pp. 1034–1042, 7 1999.

[30] P. C. Sun, H. D. Lin, S. H. Jao, Y. C. Ku, R. C. Chan, and C. K. Cheng, "Relationship of skin temperature to sympathetic dysfunction in diabetic at-risk feet.", *Diabetes research and clinical practice*, vol. 73, pp. 41–46, 1 2006.

[31] M. POPOVICI and E. BUDESCU, "Aspects of thermodynamics in sports footwear",

[32] J. J. van Netten, J. G. van Baal, C. Liu, F. van Der Heijden, and S. A. Bus, *Infrared thermal imaging for automated detection of diabetic foot complications*, 2013.

[33] S. Bagavathiappan, J. Philip, T. Jayakumar, B. Raj, P. N. S. Rao, M. Varalakshmi, and V. Mohan, "Correlation between plantar foot temperature and diabetic neuropathy: A case study by using an infrared thermal imaging technique", *Journal of diabetes science and technology*, vol. 4, no. 6, pp. 1386–1392, 2010.

[34] 2015. [Online]. Available: `https://www.grainger.com/content/qt-370-infrared-thermometers`.

[35] L. C. Rogers and R. G. Frykberg, "A Guide To Early Intervention For The Charcot Foot.", *Podiatry Today*, vol. 21, pp. 66–72, 8 2008.

[36] K. Roback, M. Johansson, and A. Starkhammar, “Feasibility of a thermographic method for early detection of foot disorders in diabetes.”, *Diabetes technology and therapeutics*, vol. 11, pp. 663–667, 10 2009.

[37] R. G. Frykberg, A. Tallis, and E. Tierney, “Diabetic foot self examination with the tempstattm as an integral component of a comprehensive prevention program.”, *The journal of diabetic foot complications*, vol. 1, no. 3, pp. 13–18, 2 2009.

[38] [Online]. Available: `https://www.amazon.com/Metatarsal-Pads-Cushions-Designed-Brison/dp/B00BSEEP44` (visited on 04/29/2017).

[39] R. G. Frykberg, I. L. Gordon, A. M. Reyzelman, S. M. Cazzell, R. H. Fitzgerald, G. M. Rothenberg, J. D. Bloom, B. J. Petersen, D. R. Linders, A. Nouvong, and B. Najafi, “Feasibility and Efficacy of a Smart Mat Technology to Predict Development of Diabetic Plantar Ulcers.”, *Diabetes Care*, vol. 40, pp. 973–980, 2017.

[40] P. B. Kang, S. N. Hoffman, E. Krimitsos, and S. B. Rutkove, “Ambulatory foot temperature measurement: A new technique in polyneuropathy evaluation.”, *Muscle and nerve*, vol. 27, pp. 737–742, 6 2003.

[41] P. Foltyński, P. Ładyżyński, J. M. Wójcicki, M. Brandl, J. Grabner, K. Migalska-musiał, M. Molik1, S. Sabalińska, and A. Ciechanowska, “Continuous monitoring of feet temperature using a data logger with wireless communication.”, *Biocybernetics and biomedical engineering*, vol. 32, pp. 59–64, 4 2012.

[42] Y. Shimazaki and M. Murata, “Effect of gait on formation of thermal environment inside footwear.”, *Applied ergonomics*, vol. 49, pp. 55–62, 2015.

[43] S. Mizzi, “The influence of seasonal variation on in-shoe temperature and relative humidity during moderate excercise in a maltese population: Implications for diabetic foot ulceration”, PhD, Canterbury Christ Church University, 2016.

[44] [Online]. Available: `https://www.instrumart.com/assets/tc4000_ds.pdf` (visited on 04/29/2017).

[45] S. B. Rutkove, R. Nie, T. Mitsa, and R. A. Nardin, “A methodology for the real-time measurement of distal extremity temperature.”, *Physiological measurement*, vol. 28, pp. 1421–1428, 2007.

[46] D. Rosenbaum, S. Hautmann, M. Gold, and L. Claes, “Effects of walking speed on plantar pressure patterns and hindfoot angular motion.”, *Gait and posture*, vol. 2, pp. 191–197, 3 1994.

[47] E. Eils, S. Nolte, M. Tewes, L. Thorwesten, K. Völker, and D. Rosenbaum, “Modified pressure distribution patterns in walking following reduction of plantar sensation.”, *Journal of biomechanics*, vol. 35, pp. 1307–1313, 10 2002.

[48] G. Borg, “Psychophysical scaling with applications in physical work and the perception of exertion”, *Scandinavian journal of work, environment & health*, pp. 55–58, 1990.

[49] Z. O. Abu-Faraj, G. F. Harris, J. H. Abler, and J. J. Wertsch, “A Holter-type, microprocessor-based, rehabilitation instrument for acquisition and storage of plantar pressure data.”, *Journal of Rehabilitation Research and Development*, vol. 34, pp. 187–194, 2 1997.

[50] S. C. Walker, P. A. Helm, and L. A. Lavery, “Gait pattern alteration by functional sensory substitution in healthy subjects and in diabetic subjects with peripheral neuropathy.”, *Archives of physical medicine and rehabilitation*, vol. 78, pp. 853–856, 8 1997.

[51] Z. Pataky, L. Faravel, J. Da Silva, and J. P. Assal, “A new ambulatory foot pressure device for patients with sensory impairment. a system for continuous measurement of plantar pressure and a feed-back alarm.”, *Journal of biomechanics*, vol. 33, pp. 1135–1138, 9 2000.

[52] P. Brown, in *Quick reference to wound care.* Jones and Bartlett Publishers, 2009.

[53] N. Tentolouris, C. Voulgari, S. Liatis, I. Eleftheriadou, K. Makrilakis, K. Marinou, and N. Katsilambros, “Moisture status of the skin of the feet assessed by the visual test neuropad correlates with foot ulceration in diabetes.”, *Diabetes care*, vol. 33, pp. 1112–1114, 5 2010.

[54] M. Klaassen, D. J. Schipper, and M. A. Masen, “Influence of the relative humidity and the temperature on the in-vivo friction behaviour of human skin.”, *Biotribology*, vol. 6, pp. 21–28, 2016.

[55] I. Atmaca and A. Yigit, “Predicting the effect of relative humidity on skin temperature and skin wettedness.”, *Journal of thermal biology*, vol. 31, pp. 442–452, 5 2006.

[56] N. K. Veijgen, E. van der Heigen, and M. A. Masen, “A multivariable model for predicting the frictional behaviour and hydration of the human skin.”, *Skin research and technology*, vol. 19, pp. 330–338, 3 2013.

[57] C. P. Hendriks and S. E. Franklin, “Influence of surface roughness, material and climate conditions on the friction of human skin.”, *Tribology letters*, vol. 37, pp. 361–373, 2 2010.

[58] S. Baird, C. M. Skinner, S. Trail, and J. S. Frankis, “Anhydrosis in the diabetic foot: A comparison of two urea creams.”, *The diabetic foot journal*, vol. 6, pp. 122–136, 3 2003.

[59] D. Ziegler, “Diagnosis and treatment of diabetic autonomic neuropathy.”, *Current diabetes reports*, vol. 1, pp. 216–227, 3 2001.

[60] C. R. Harding, A. Watkinson, A. V. Rawlings, and I. R. Scott, “Dry skin, moisturization and corneodesmolysis.”, *International journal of cosmetic science*, vol. 22, pp. 21–52, 1 2000.

[61] B. Najafi, H. Mohseni, G. S. Grewal, T. K. Talal, R. A. Menzies, and D. G. Armstrong, “An Optical-Fiber-Based Smart Textile (Smart Socks) to Manage Biomechanical Risk Factors Associated With Diabetic Foot Amputation.”, *Journal of Diabetes Science and Technology*, vol. 11, pp. 668–677, 2017.

[62] *FBG Principle*. [Online]. Available: `https://www.fbgs.com/technology/fbg-principle` (visited on 12/19/2018).

[63] *Siren Care*. [Online]. Available: `https://siren.care` (visited on 12/24/2018).

[64] *Diabetes Daily - Siren Diabetic Smart Socks to Protect Your Feet*. [Online]. Available: https://www.diabetesdaily.com/blog/siren-diabetic-smart-socks-to-protect-your-feet-536891/ (visited on 12/26/2018).

[65] F. Leens, "An Introduction to i2C and SPI Protocols.", *IEEE Instrumentation and Measurement Magazine*, vol. 12, pp. 8–13, 1 2009.

[66] *Thermocouple image*. [Online]. Available: http://media.rs-online.com/t_large/F3630294-01.jpg (visited on 10/21/2017).

[67] *Thermistor image*. [Online]. Available: https://www.ametherm.com/wp-content/uploads/2017/04/Polymer-PPTC-Thermistor-300.png (visited on 10/21/2017).

[68] *RTD image*. [Online]. Available: https://www.omega.com/Temperature/images/F1500_F2000_F4000_l.jpg (visited on 10/21/2017).

[69] *Digital IC sensor image*. [Online]. Available: https://www.ti.com/content/dam/ticom/images/products/ic/sensing-products/chips/lmt84-chip-shot-pp422.png (visited on 10/21/2017).

[70] *Thermocouples operating principles*. [Online]. Available: https://www.msm.cam.ac.uk/utc/thermocouple/pages/ThermocouplesOperatingPrinciples.html (visited on 04/29/2017).

[71] *What is a Thermocouple*. [Online]. Available: http://www.thermocoupleinfo.com (visited on 04/29/2017).

[72] *What are you sensing? Pros and cons of four temperature sensor types.* [Online]. Available: https://e2e.ti.com/blogs_/b/analogwire/archive/2015/08/26/what-are-you-sensing-pros-and-cons-of-four-temperature-sensor-types (visited on 10/21/2017).

[73] *What is a Thermistor and how does it work*. [Online]. Available: http://www.omega.com/prodinfo/thermistor.html (visited on 04/30/2017).

[74] *Thermistor vs RTD Temperature Measurement Accuracy – Application Note*. [Online]. Available: https://www.bapihvac.com/application-note/thermistor-vs-rtd-temperature-measurement-accuracy-application-note/ (visited on 11/07/2017).

[75] *Introduction to Pt100 RTD Temperature Sensors*. [Online]. Available: http://www.omega.com/prodinfo/rtd.html (visited on 04/30/2017).

[76] *RTD Specifications*. [Online]. Available: https://www.omega.com/Temperature/pdf/RTDSpecs_Ref.pdf (visited on 11/07/2017).

[77] *Temperature Sensor Basics*. [Online]. Available: http://www.ni.com/white-paper/53184/en/ (visited on 05/01/2017).

[78] *Digital Temperature Sensors*. [Online]. Available: http://www.electronicdesign.com/boards/digital-temperature-sensors (visited on 05/01/2017).

[79] *Voltage Dividers*. [Online]. Available: https://dlb.sa.edu.au/rehsmoodle/file.php/466/kpsec.freeuk.com/vdivider.htm (visited on 10/15/2019).

[80] 2013. [Online]. Available: https://www.analog.com/en/technical-articles/adc-drivers-filters-single-ended-buffer.html.

[81] *Bluetooth Basics*. [Online]. Available: https://learn.sparkfun.com/tutorials/bluetooth-basics/all (visited on 09/23/2019).

[82] *Bluetooth Classic vs Bluetooth low energy*. [Online]. Available: https://www.plugintoiot.com/bluetoothclassic-vs-bluetoothlowenergy/ (visited on 09/24/2019).

[83] *CC2541 Datasheet*. [Online]. Available: http://www.ti.com/lit/ds/symlink/cc2541.pdf (visited on 09/24/2019).

[84] J. Tosi, F. Taffoni, M. Santacatterina, R. Sannino, and D. Formica, "Performance Evaluation of Bluetooth Low Energy: A Systematic Review", *Sensors*, vol. 17, 2017.

[85] K. Townsend, C. Cufi, and R. Davidson, *Getting Started with Bluetooth Low Energy: Tools and Techniques for Low-Power Networking*. O'Reilly Media, Inc., 2014.

[86] T. K. Koo and M. Y. Li, "A Guideline of Selecting and Reporting Intraclass Correlation Coefficients for Reliability Research.", *Journal of Chiropractic Medicine*, vol. 15, pp. 155–163, 2016.

[87] D. Giavarina, "Understanding Bland Altman analysis.", *Biochemia Medica*, vol. 25, pp. 141–151, 2015.

[88] A. W. Chan, I. A. MacFarlane, and D. R. Bowsher, "Contact Thermography of Painful Diabetic Neuropathic Foot.", *Diabetes Care*, vol. 14, pp. 918–922, 10 1991.

[89] D. Hernandez-Contreras, H. Peregrina-Barreto, J. Rangel-Magdaleno, J. Gonzalez-Bernal, and L. Altamirano-Robles, "A quantitative index for classification of plantar thermal changes in the diabetic foot.", *Infrared Physics and Technology*, vol. 81, pp. 242–249, 2017.

[90] B. G. Sudha, V. Umadevi, J. M. Shivaram, M. Y. Sikkandar, A. A. Amoudi, and H. C. Chaluvanarayana, "Statistical Analysis of Surface Temperature Distribution Pattern in Plantar Foot of Healthy and Diabetic Subjects using Thermography.", in *International Conference on Communication and Signal Processing*, 2018.

[91] L. Cutajar, O. Falzon, A. Mizzi, I. Swaine, K. Springett, and S. Mizzi, *A Novel Method to Determine Dynamic Temperature Trends Applied to In-Shoe Temperature Data During Walking.* 2018.